IAEA
International Atomic Energy Agency

IAEA TECDOC SERIES

No. 2075

Assessing Technical and Economic Aspects of Nuclear Hydrogen Production for Near Term Deployment

ASSESSING TECHNICAL AND ECONOMIC ASPECTS OF NUCLEAR HYDROGEN PRODUCTION FOR NEAR TERM DEPLOYMENT

The following States are Members of the International Atomic Energy Agency:

AFGHANISTAN
ALBANIA
ALGERIA
ANGOLA
ANTIGUA AND BARBUDA
ARGENTINA
ARMENIA
AUSTRALIA
AUSTRIA
AZERBAIJAN
BAHAMAS
BAHRAIN
BANGLADESH
BARBADOS
BELARUS
BELGIUM
BELIZE
BENIN
BOLIVIA, PLURINATIONAL STATE OF
BOSNIA AND HERZEGOVINA
BOTSWANA
BRAZIL
BRUNEI DARUSSALAM
BULGARIA
BURKINA FASO
BURUNDI
CABO VERDE
CAMBODIA
CAMEROON
CANADA
CENTRAL AFRICAN REPUBLIC
CHAD
CHILE
CHINA
COLOMBIA
COMOROS
CONGO
COSTA RICA
CÔTE D'IVOIRE
CROATIA
CUBA
CYPRUS
CZECH REPUBLIC
DEMOCRATIC REPUBLIC OF THE CONGO
DENMARK
DJIBOUTI
DOMINICA
DOMINICAN REPUBLIC
ECUADOR
EGYPT
EL SALVADOR
ERITREA
ESTONIA
ESWATINI
ETHIOPIA
FIJI
FINLAND
FRANCE
GABON
GAMBIA
GEORGIA
GERMANY
GHANA
GREECE
GRENADA
GUATEMALA
GUINEA
GUYANA
HAITI
HOLY SEE
HONDURAS
HUNGARY
ICELAND
INDIA
INDONESIA
IRAN, ISLAMIC REPUBLIC OF
IRAQ
IRELAND
ISRAEL
ITALY
JAMAICA
JAPAN
JORDAN
KAZAKHSTAN
KENYA
KOREA, REPUBLIC OF
KUWAIT
KYRGYZSTAN
LAO PEOPLE'S DEMOCRATIC REPUBLIC
LATVIA
LEBANON
LESOTHO
LIBERIA
LIBYA
LIECHTENSTEIN
LITHUANIA
LUXEMBOURG
MADAGASCAR
MALAWI
MALAYSIA
MALI
MALTA
MARSHALL ISLANDS
MAURITANIA
MAURITIUS
MEXICO
MONACO
MONGOLIA
MONTENEGRO
MOROCCO
MOZAMBIQUE
MYANMAR
NAMIBIA
NEPAL
NETHERLANDS, KINGDOM OF THE
NEW ZEALAND
NICARAGUA
NIGER
NIGERIA
NORTH MACEDONIA
NORWAY
OMAN
PAKISTAN
PALAU
PANAMA
PAPUA NEW GUINEA
PARAGUAY
PERU
PHILIPPINES
POLAND
PORTUGAL
QATAR
REPUBLIC OF MOLDOVA
ROMANIA
RUSSIAN FEDERATION
RWANDA
SAINT KITTS AND NEVIS
SAINT LUCIA
SAINT VINCENT AND THE GRENADINES
SAMOA
SAN MARINO
SAUDI ARABIA
SENEGAL
SERBIA
SEYCHELLES
SIERRA LEONE
SINGAPORE
SLOVAKIA
SLOVENIA
SOUTH AFRICA
SPAIN
SRI LANKA
SUDAN
SWEDEN
SWITZERLAND
SYRIAN ARAB REPUBLIC
TAJIKISTAN
THAILAND
TOGO
TONGA
TRINIDAD AND TOBAGO
TUNISIA
TÜRKİYE
TURKMENISTAN
UGANDA
UKRAINE
UNITED ARAB EMIRATES
UNITED KINGDOM OF GREAT BRITAIN AND NORTHERN IRELAND
UNITED REPUBLIC OF TANZANIA
UNITED STATES OF AMERICA
URUGUAY
UZBEKISTAN
VANUATU
VENEZUELA, BOLIVARIAN REPUBLIC OF
VIET NAM
YEMEN
ZAMBIA
ZIMBABWE

The Agency's Statute was approved on 23 October 1956 by the Conference on the Statute of the IAEA held at United Nations Headquarters, New York; it entered into force on 29 July 1957. The Headquarters of the Agency are situated in Vienna. Its principal objective is "to accelerate and enlarge the contribution of atomic energy to peace, health and prosperity throughout the world''.

IAEA-TECDOC-2075

ASSESSING TECHNICAL AND ECONOMIC ASPECTS OF NUCLEAR HYDROGEN PRODUCTION FOR NEAR TERM DEPLOYMENT

INTERNATIONAL ATOMIC ENERGY AGENCY
VIENNA, 2024

COPYRIGHT NOTICE

For further information on this publication, please contact:

Nuclear Power Technology Development Section
International Atomic Energy Agency
Vienna International Centre
PO Box 100
1400 Vienna, Austria
Email: Official.Mail@iaea.org

Printed by the IAEA in Austria
November 2024
https://doi.org/10.61092/iaea.8uf6-pfqz

IAEA Library Cataloguing in Publication Data

Names: International Atomic Energy Agency.
Title: Assessing technical and economic aspects of nuclear hydrogen production for near term deployment / International Atomic Energy Agency.
Description: Vienna : International Atomic Energy Agency, 2024. | Series: IAEA TECDOC series, ISSN 1011-4289 ; no. 2075 | Includes bibliographical references.
Identifiers: IAEAL 24-01724 | ISBN 978-92-0-134824-1 (paperback : alk. paper) | ISBN 978-92-0-134924-8 (pdf)
Subjects: LCSH: Hydrogen as fuel. | Hydrogen as fuel — Economic aspects. | Hydrogen industry. | Nuclear energy.

FOREWORD

The hydrogen economy concept is gaining more and more interest and developing around the world. In addition to around 60 million tonnes of hydrogen consumed annually worldwide today — mainly as feedstock by petroleum and chemical industries — hydrogen is increasingly being used as fuel in the transport sector and its use for power generation is widely anticipated. More than 95% of the hydrogen used today is produced from fossil fuels (i.e. oil, gas and coal) and involves adverse effects such as resource depletion and environmental impacts due to the emission of greenhouse gases.

The strong and growing interest of Member States in a potential future role for hydrogen in national energy economies, including production from nuclear energy, prompted the IAEA to continue the work of a previous coordinated research project, entitled Examining the Technoeconomics of Nuclear Hydrogen Production and Benchmark Analysis of the IAEA HEEP Software, by launching a new project in 2018 entitled Assessing Technical and Economic Aspects of Nuclear Hydrogen Production for Near-term Deployment. These projects included information exchange on the status and challenges of hydrogen production from nuclear energy, an assessment of techno-economic aspects of production and the development, updates and benchmarking of an analytical tool to assist Member States in such an assessment. In the scope of these projects, hydrogen produced using nuclear energy was referred to as nuclear hydrogen.

This publication documents the results of the 2018 coordinated research project. For this project, the near term was the interval of a decade. The project resulted in a platform for information exchange among ten Member States. The project assessed technical and economic aspects of nuclear hydrogen production, which included case studies of various scenarios, comparing hydrogen produced with nuclear energy with hydrogen produced using conventional and renewable options and improving the understanding of the practical challenges involved. On the basis of the participants' suggestions, in 2022 the IAEA launched an activity to develop a roadmap for hydrogen deployment from nuclear energy. The project also helped in releasing a new version of the IAEA Hydrogen Economic Evaluation Program which allows a cost assessment of various options for nuclear hydrogen production.

This publication is based on the contributions provided by the experts listed at the end of the publication. The IAEA officer responsible for this publication was A. Constantin of the Division of Nuclear Power.

EDITORIAL NOTE

This publication has been prepared from the original material as submitted by the contributors and has not been edited by the editorial staff of the IAEA. The views expressed remain the responsibility of the contributors and do not necessarily represent the views of the IAEA or its Member States.

Guidance and recommendations provided here in relation to identified good practices represent expert opinion but are not made on the basis of a consensus of all Member States.

Neither the IAEA nor its Member States assume any responsibility for consequences which may arise from the use of this publication. This publication does not address questions of responsibility, legal or otherwise, for acts or omissions on the part of any person.

The use of particular designations of countries or territories does not imply any judgement by the publisher, the IAEA, as to the legal status of such countries or territories, of their authorities and institutions or of the delimitation of their boundaries.

The mention of names of specific companies or products (whether or not indicated as registered) does not imply any intention to infringe proprietary rights, nor should it be construed as an endorsement or recommendation on the part of the IAEA.

The authors are responsible for having obtained the necessary permission for the IAEA to reproduce, translate or use material from sources already protected by copyrights.

The IAEA has no responsibility for the persistence or accuracy of URLs for external or third party Internet web sites referred to in this publication and does not guarantee that any content on such web sites is, or will remain, accurate or appropriate.

CONTENTS

1. INTRODUCTION

1.1. BACKGROUND

The majority of the hydrogen used presently is produced from fossil resources (primarily natural gas, but also oil and coal), which results in carbon dioxide emissions. Nuclear energy has the potential to replace fossil fuels for supplying a forecasted large increase in the demand of hydrogen with low or zero carbon dioxide emissions. One of the IAEA's statutory objectives is to "seek to accelerate and enlarge the contribution of atomic energy to peace, health and prosperity throughout the world". This objective may be achieved also through hydrogen production from nuclear energy.

There are currently several demonstration projects worldwide ongoing and planned for the production of hydrogen using operational nuclear power plants, as well as developments considering advanced reactor technologies for hydrogen production. Additionally, various hydrogen generation options are considered for being coupled with the nuclear component: conventional electrolysis, high temperature steam electrolysis, thermochemical cycles but also steam methane reforming, the latter one in the view of lowering the fossil fuel component of hydrogen production through the use of nuclear reactors to provide the necessary energy input for the process.

Currently several Member States have their national roadmaps for hydrogen generation, while just a few of them include the option of nuclear hydrogen production. The process of coupling different technologies brings various challenges, both from the technical and economic perspectives. Also, as hydrogen can pose additional hazards in the vicinity of a nuclear power plant, further research activities and tests should be conducted to understand the nature and the possibility of safe coupling of nuclear power plant with hydrogen production plant.

The IAEA CRP titled "Assessing Technical and Economic Aspects of Nuclear Hydrogen Production for Near-term Deployment" addressed the issues expected for the potential upscaling of nuclear hydrogen production technologies and opportunities for maturity of currently under development.

It also tackled the techno-economics and safety considerations, based on the specific cases of participant Member States: Algeria, Argentina, China, Greece, India, Japan, Russian Federation, Saudi Arabia, Türkiye, and the United States of America. This continued the successful completion of the previous CRP on Examining the Techno-Economics of Nuclear Hydrogen Production and Benchmark Analysis of the IAEA HEEP Software and benefited from extensive experience of the participating Member States' experts.

1.2. OBJECTIVE

The objective of this publication is to present the outcomes and results achieved by participants to the IAEA CRP "Assessing Technical and Economic Aspects of Nuclear Hydrogen Production for Near-term Deployment" and make them available to all Member States, scientists, decision makers, and specialists interested in hydrogen production using nuclear energy and related topics of relevant technologies.

1.3. SCOPE

The scope of this publication is to deliver an understanding towards the development of hydrogen production using nuclear energy aiming to accelerate deployment of large-scale nuclear hydrogen production projects by proper realization of the concerns and challenges such projects face.

1.4. STRUCTURE

The publication is structured in the following sections:

- Section 1 is the introductory one of the publication, covering the motivation, objectives, scope and structure of the CRP.
- Section 2 describes the hydrogen production routes available and how nuclear energy can support hydrogen production through the integration of various coupled nuclear reactors, including the high temperature reactors, with hydrogen production facilities, illustrated with the study conducted by USA. The use of multi-criteria assessment for the evaluation of different options of nuclear hydrogen production is illustrated in this section. The approach is considered in the study developed by Russian Federation.
- Section 3 details the studies conducted by India, Japan, Türkiye and Argentina, investigating hydrogen production through thermochemical cycles, hybrid cycles and respectively gasification of solid fuels, with the energy provided by nuclear reactors. India and Japan studied the sulphur-iodine (S-I) cycle and research and development (R&D) was conducted for elucidating relevant aspects, such as the kinetics of the chemical steps involved, installations and materials, at laboratory scale. Türkiye investigated the hybrid cycles. A critical evaluation of the technical alternatives for upscaling the indirect-heating gasification reactors to a more commercial phase was carried out by Argentina.
- Section 4 includes the studies conducted by Algeria and Greece on the potential for small modular reactors for hydrogen production, looking also at hydrogen storage and transportation aspects and at hydrogen produced with hybrid energy systems.
- Section 5 details on the techno-economic assessment of hydrogen production using nuclear energy, with case studies conducted by Algeria, Türkiye and Russian Federation.
- Section 6 presents the conclusions and recommendations derived from the work conducted in the CRP.
- An Appendix that covers in brief the contributions of each contract and agreement of the CRP.

2. EVOLUTION AND ASSESSMENT OF NUCLEAR HYDROGEN PRODUCTION ROUTES

Energy has always been the driving force behind economic and social developments in the history of humanity. The sources have evolved, and each new energy source has given fresh impulse to societal, technological, and economic changes. Nowadays, energy occupies a fundamental position in all human activities and its demand is increasing exponentially worldwide.

Currently, fossil fuels are supporting the majority of the world's energy needs. However, the ever-increasing energy demand is putting a lot of pressure on the hydrocarbon reserves with the risks of shortage becoming a reality in a few decades. In addition to this problem, the exploitation of hydrocarbons including their production, transportation, and utilization all negatively impact the environment. Moreover, current energy resources do not adequately meet the needs of remote areas. This is the case of islands in the middle of the seas or the oases in the middle of the deserts. The growing concerns about the rapid decreasing of the hydrocarbon reserves and the fear of the disastrous effects on the environment have led to the active search for alternative energy solutions. Renewable technologies are experiencing rapid development, particularly for wind and solar photovoltaic energy, reaching the industrial maturity and the energy market competitiveness. However renewable energy sources suffer from intrinsic disadvantages. They are seasonal and have a diluted and intermittent character. There is also a disparity in energy supply and demand. To overcome these obstacles, there is need for sources of high energy density, that can be stored for long periods and certainly transported over long distances. Among these options, hydrogen is gaining an increasing consideration as a clean energy carrier. It can also be used in mobile and stationary applications.

New concepts resorting to hydrogen technologies have emerged and offer the possibility of efficient and viable large penetration of renewable energy sources and successful energy transition. These new concepts have revived interest in hydrogen as a multipurpose product that can be used as an energy vector, an alternative fuel, a chemical feedstock, and a storage medium.

Nonetheless, there are still challenges associated with new technologies for clean and efficient hydrogen production.

2.1. HYDROGEN PRODUCTION ROUTES (CENTRE DE DÉVELOPPEMENT DES ENERGIES RENOUVELABLES, ALGERIA)

Hydrogen is a common element in the universe, but it is found on earth mainly in combination with other elements. As hydrogen has multiple uses, including as feedstock in the chemical industry or as fuel, it is then necessary to find sustainable ways to produce it. As shown in

FIG. *1*, the production methods vary based on the nature of the feedstock, the process involved, and the energy used for the process [1].

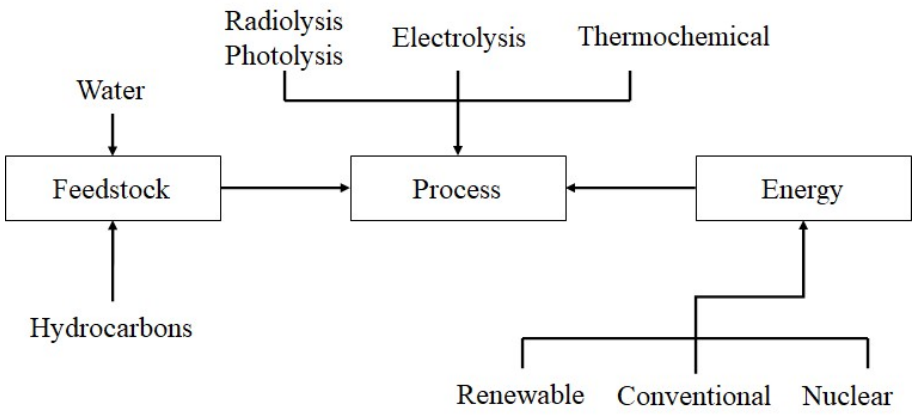

FIG. 1. Hydrogen production – feedstocks, energy sources and processes.

The energy sources can be hydrocarbons, nuclear or renewables.

Currently, the most used process for hydrogen production is steam methane reforming. However, this process brings in the challenges associated with feedstock sustainability and CO_2 emissions.

2.1.1. Water electrolysis

Electrolysis has been reliably used to generate high quality hydrogen since the mid-19th century.

Electrolysis is based on the reverse process of that occurring in a fuel cell. By breaking the molecule of water into hydrogen and oxygen, the involved electrical energy is converted into chemical energy. For example, hydrogen could benefit on the use of nuclear energy for its production. During low demand, the excess of nuclear-based electricity can be converted, through electrolysis, into hydrogen for storage to be used at a later time; while during high demand, the hydrogen can be converted back, through a fuel cell, into electricity.

At low temperatures, two types of cells are currently used: alkaline electrolysis cells, and proton exchange membrane (PEM) cells. The alkaline cells can use cheaper, non-noble metal catalysts for their electrodes, while the PEM cells have higher efficiencies.

Alkaline electrolysis has become a well matured technology for hydrogen production up to the megawatt range and is a worldwide commercialized technology. The electrolysis cell consists of two electrodes: an anode, and a cathode, that are immersed into an electrolyte. The electrolyte, an aqueous solution (around 30% KOH), ensures the ion (OH^-) flow from the anode side to the cathode side. A membrane is used to separate the anode side from the cathode side. This membrane should allow the flow of ions (OH^-) but not the flow of electrons.

The PEM electrolysis uses a thin membrane (20–300 μm thick) that provides high proton conductivity, low gas crossover, compact system design and high-pressure operation. Capable of operating at higher current density and possibly lower operation cost than the alkaline electrolysis cells, the PEM cell technology is in full expansion.

High temperature electrolysis uses a solid oxide electrolysis cell (SOEC).

Figure 2 shows the schematic of the operating principle of an alkaline, PEM and solid oxide water electrolysis, respectively.

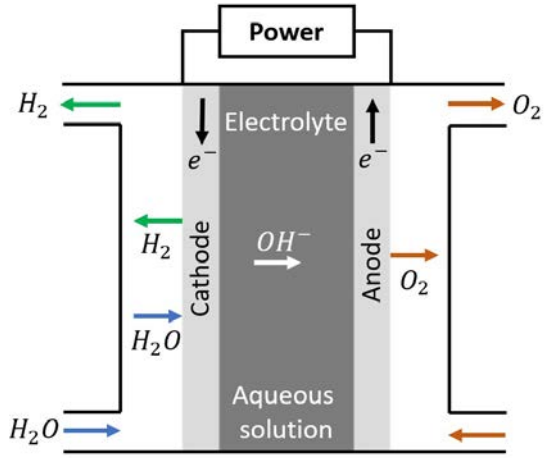

(a) Alkaline electrolysis cell (40–90°C)

Anode: $2OH^- \rightarrow H_2O + \frac{1}{2} O_2 + 2e^-$

Cathode: $H_2O + 2e^- \rightarrow H_2 + O^{2-}$

Total reaction: $H_2O \rightarrow H_2 + \frac{1}{2} O_2$

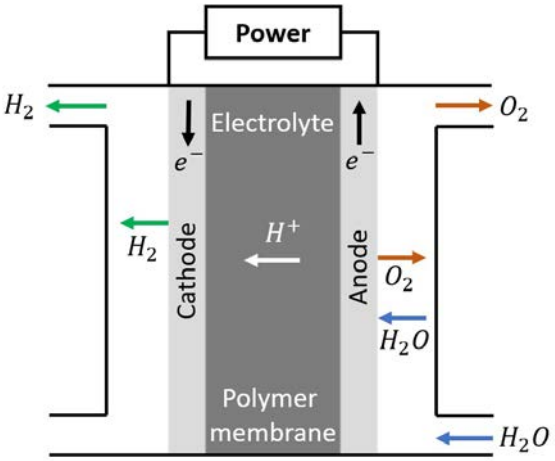

(b) PEM electrolysis cell (20–100°C)

Anode: $H_2O \rightarrow 2H^+ + \frac{1}{2} O_2 + 2e^-$

Cathode: $2H^+ + 2e^- \rightarrow H_2$

Total reaction: $H_2O \rightarrow H_2 + \frac{1}{2} O_2$

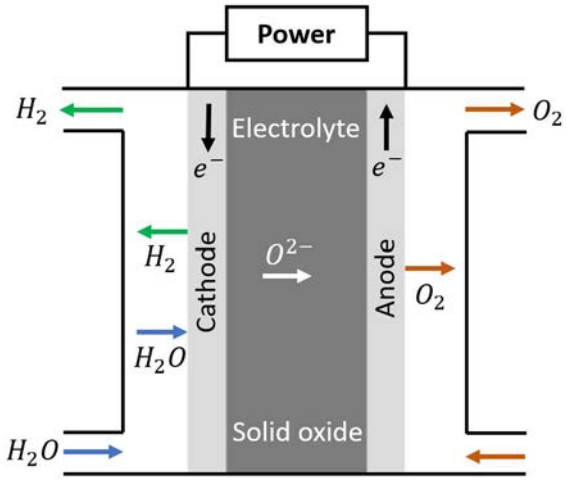

(c) Solid oxide electrolysis cell

Anode: $O^{2-} \rightarrow \frac{1}{2} O_2 + 2e^-$

Cathode: $H_2O + 2e^- \rightarrow H_2 + O^{2-}$

Total reaction: $H_2O \rightarrow H_2 + \frac{1}{2} O_2$

FIG. 2. Schematic representation of different types of electrolysis cells: (a) Alkaline electrolysis cell; (b) PEM cell and (c) SOEC.

2.1.1.1. Low temperature electrolysis

There are two main types of electrolysers operating at low temperatures: alkaline and PEM. The electrolyte of the alkaline electrolyser is an alkaline aqueous solution, commonly a 25% to 30% potassium hydroxide aqueous solution. The operating temperature could go up to 90°C and the pressure up to 30 bars. Though affected by corrosion, low current density, and high-power consumption, alkaline electrolysers are widely used in commercial applications [2].

For the PEM type, the electrolyte is an acid membrane, specifically a layer of Nafion, a branded name for a sulfonated tetrafluoroethylene-based fluoropolymer copolymer. This membrane plays the role of electrolyte and of a gas separator. The operating temperature is limited by the temperature tolerated by the electrolyte membrane, which is in the order of 100°C.

The PEM electrolysers offer many advantages over alkaline electrolysers. Indeed, besides being more compact, PEM electrolysers offer the ability of operating at high pressure, consuming less power and producing high purity hydrogen [3–5]. Moreover, they can also be coupled directly to an intermittent renewable source of electricity [6].

Theoretically, the energy required for water electrolysis is given by the change in the enthalpy ΔH of the following reaction:

$$H_2O\ (l) + \Delta H\ (237.2\ kJ/mol + 48.6\ kJ/mole) \rightarrow H_2\ (g) + (1/2)\ O_2\ (g)$$

where 237.2 kJ/mole is in the form of electricity and 48.6 kJ/mole is heat energy at standard conditions.

A source of electrical energy and some heat is required for electrolysis. Depending on the technology and the operating conditions, the energy required for the production of 1 m^3 of hydrogen varies roughly from 4 kWh to 6 kWh.

Table 1 lists the specifications of an alkaline and PEM electrolyser (based on data from [7]).

TABLE 1. SPECIFICATIONS OF ALKALINE AND PEM ELECTROLYSERS

Specifications	**Alkaline electrolysis**	**PEM electrolysis**
Cell temperature (°C)	60–80	50–80
Cell pressure (bar)	<30	<30
Current density (mA/cm^2)	0.2–0.4	0.6–2.0
Cell voltage (V)	1.8–2.4	1.8–2.2
Power density (mW/cm^2)	<1	<4.4
Voltage efficiency (%)	62–82	67–82
Specific energy consumption, stack (kWh N/m^3)	4.2–5.9	4.2–5.6
Lower partial load range (%)	20–40	0–10
Cell area (m^2)	>4	<0.03
H_2 production rate, stack-system (m^3/h)	<760	<10
Lifetime stack (h)	<90 000	<20 000
Lifetime system (a)	20–30	10–20
Degradation rate (mV/h)	<3	<14

Several empirical and semi-empirical models that allow the determination of the electrolyser's performance have been developed [8–16]. These allow the determination of the electrolyser's efficiency, and the specific energy of production under different operating conditions.

2.1.1.2. High temperature steam electrolysis

The high temperature steam electrolysis (or high temperature electrolysis) typically operates from 800–1000°C using water in the form of steam. The SOECs are attractive because they can convert electrical energy into chemical energy, producing hydrogen with high efficiency.

Contrary to the alkaline electrolyser and the PEM electrolyser, the electrolyte of the solid oxide cell is a solid oxygen ion conducting ceramic membrane. This is a membrane that plays the role of both an electrolyte, and a gas separator; high temperature is necessary to ensure ionic conduction in the membrane [17–19]. The standard SOEC has oxygen transporting solid state yttria or scandia stabilized zirconia (YSZ, ScSZ) electrode. Recently both oxygen ion transport and proton conducting SOEC have been developed to operate in the range 550–850°C.

High temperature electrolysis requires energy in the form of heat and electricity. It is well suited for systems operating at a high temperature such as solar concentrating systems and a high temperature nuclear reactor [20, 21], but also for light water reactors in connection with heat recuperators.

Though not as well developed as the low temperature electrolysis technologies, high temperature electrolysis technology has, because of its higher chemical reaction rate and lower electrical energy requirement, a more attractive potential for large-scale hydrogen production [22].

Water electrolysis occurs according to the following reaction:

$$H_2O\ (\text{steam}) \rightarrow H_2\ (g) + (1/2)\ O_2\ (g)$$

ΔH is the reaction enthalpy. As expressed in the relation reported below, this reaction enthalpy takes two forms: an electrical energy form which is related to Gibbs free energy (ΔG), and a thermal form which is related to the product of the reaction temperature (T) and the change of entropy (ΔS):

$$\Delta H = \Delta G + T\Delta S \tag{1}$$

The enthalpy and entropy of each species (water, oxygen, and hydrogen) entering in the electrolysis reaction are given by.

$$\Delta H_i = \Delta H_{0,i} + \int_{T_0}^{T} C_{p_i} dT \tag{2}$$

$$\Delta S_i = \Delta S_{0,i} + \int_{T_0}^{T} \frac{C_{Pi}}{T}\, dT \tag{3}$$

where C_{pi}, the specific heat at constant pressure of species i, is usually expressed as:

$$C_{Pi} = a_{0i} + a_{1i}\, T + a_{2i}\, T^2 + a_{3i}\, T^3 + a_{4i}\, T^4 \tag{4}$$

Using the different values of the factors in Eq. (4), reported in Ref. [23], and the initial values of the enthalpy and entropy of formation, the enthalpy ΔH_i and entropy ΔS_i of the different species (water, hydrogen and oxygen) are evaluated using the following equations [24, 25]:

$$\Delta H = \Delta H_{H_2} + \frac{1}{2}\Delta H_{O_2} - \Delta H_{H_2O} \quad (5)$$

$$\Delta S = \Delta S_{H_2} + \frac{1}{2}\Delta S_{O_2} - \Delta S_{H_2O} \quad (6)$$

$$\Delta G = \Delta H - T\Delta S \quad (7)$$

The evolutions of the relative contribution of electricity, expressed by $\Delta G/\Delta H$, and of heat, expressed by $T\Delta S/\Delta H$, with temperature are reported in Figure 3.

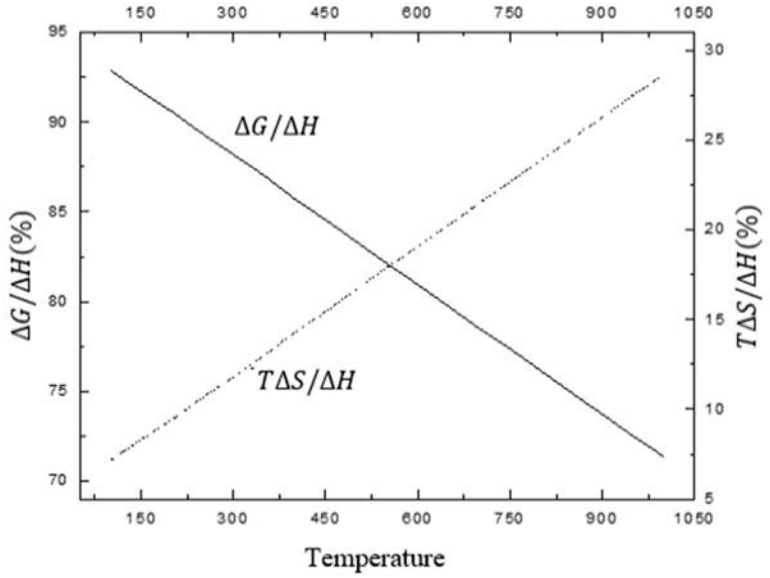

FIG. 3. Evolution of the ratios $\Delta G/\Delta H$ and $T\Delta S/\Delta H$ with temperature.

Figure 3 shows that the value of $T\Delta S/\Delta H$ more than quadruples when the electrolysis temperature goes from 100°C to 1000°C. On the other hand, and over the same temperature interval, $\Delta G/\Delta H$ drops from 93% to 71%. The fraction of thermal energy contributing to the electrolysis of water is function of the electrolysis temperature (T), the change in entropy (ΔS), and the change in Gibbs free energy (ΔG) [26, 27].

2.1.2. Thermochemical cycles

Thermochemical cycles produce hydrogen based on a sequence of chemical reactions, where the net reaction is the hydrogen and oxygen production by splitting water at a much lower temperature than the direct thermal decomposition of water [28] (thermolysis of water requires temperatures in excess of 2 200°C). There are more than 100 thermochemical water splitting cycles that have been identified. However, some cycles which operate below 900°C have received more attention and were developed and demonstrated for small scale level hydrogen production. These cycles are listed in Table 2, and include Mark 1, Fe-Cl UT-3, hybrid copper-chlorine (Cu-Cl) cycle, sulphur family, Westinghouse, Mark 13, and manganese oxide-based cycles.

TABLE 2. THERMOCHEMICAL-HYBRID WATER-SPLITTING CYCLES BELOW 900°C

Thermo-chemical cycle	Reactions involved
Mark 1	$CaBr_2 + 2H_2O \rightarrow Ca(OH)_2 + 2HBr$ $2HBr + Hg \rightarrow HgBr_2 + H_2$ (180–200°C) $HgBr_2 + Ca(OH)_2 \rightarrow CaBr_2 + HgO + H_2O$ (180–200°C) $HgO \rightarrow Hg + 1/2O_2$ (630°C)
Fe-Cl cycle	$3FeCl_2 + 4H_2O \rightarrow Fe_3O_4 + 6HCl + H_2$ (650–700°C) $Fe_3O_4 + 8HCl \rightarrow FeCl_2 + 2FeCl_3 + 4H_2O$ (200–300°C) $2FeCl_3 \rightarrow 2FeCl_2 + Cl_2$ (280–320°C) $Cl_2 + H_2O \rightarrow 2HCl + 1/2O_2$ (600–700°C)
UT-3 cycle	$CaBr_2(s) + H_2O(g) \rightarrow CaO + 2HBr(g)$ (700–760°C) $CaO(s) + Br_2(g) \rightarrow CaBr_2(s) + 0.5O_2(g)$ (500–600°C) $Fe_3O_4(s) + 8HBr(g) \rightarrow 3FeBr_2(s) + 4H_2O(g) + Br_2(g)$ (200–300°C) $3FeBr_2(s) + 4H_2O(g) \rightarrow Fe_3O_4(s) + 6HBr(g) + H_2(g)$ (550–650 °C)
Hybrid Cu-Cl cycle	$2Cu(s) + 2HCl(g) \rightarrow H2 + 2CuCl(s)$ (425°C) $4CuCl(s) \rightarrow 2Cu(s) + 2CuCl_2(s)$ (electrochemical) $2CuCl_2(s) + H_2O \rightarrow Cu_2OCl_2(s) + 2HCl(g)$ (325°C) $Cu_2OCl_2(s) \rightarrow 2CuCl(s) + 1/2O_2$ (550°C)
Sulphur family	H_2SO_4-$H_2O \rightarrow H_2SO_4 + H_2O$ (330°C) $H_2SO_4 \rightarrow H_2O + SO_3$ (350–700°C) $SO_3 \rightarrow SO_2 + 1/2O_2$ (>800°C) $H_2SO_4(aq.) \rightarrow H_2O + SO_2 + 1/2O_2 \quad \Delta H_o = 371$ kJ
Westinghouse Cycle (Mark 11)	$2H_2O + SO_2 \rightarrow H_2SO_4 + H_2$ (80°C) (electrolysis) $2H_2O + xI_2 + SO_2 \rightarrow H_2SO_4 + 2HI_x$ (100°C) (Bunsen) $2HI_x \rightarrow xI_2 + H_2$ (300–500°C)
Mark 13	$2H_2O + Br_2 + SO_2 \rightarrow H_2SO_4 + 2HBr$ (27°C) $2HBr \rightarrow H_2 + Br_2$ (100°C) (electrolysis)
Mn(II)/Mn(III) oxide-based cycle	$2Mn_3O_4 + 3Na_2CO_3 \rightarrow 4NaMnO_2(s) + 2MnO + Na_2CO_3 + 2CO_2(g)$ (850°C) $2MnO + Na_2CO_3 + H_2O(g) \rightarrow 2NaMnO_2(s) + CO_2(g) + H_2(g)$ (850°C) $6NaMnO_2(s) + ayH_2O(l) + (3+b)\ CO_2(g) \rightarrow 3Na_2CO_3(aq) + aH_xMnO_2 \cdot yH_2O(s) + bMnCO_3 + cMn_3O_4$ (400°C) $aH_xMnO_2 \cdot yH_2O(s) + bMnCO_3 \rightarrow (2 - c)\ Mn_3O_4(s) + ayH_2O(g) + bCO_2(g) + 0.5O_2(g)$ (850°C) where $a + b + 3c = 6$ and $(4 - x) \cdot a + 2b + 8c = 18$

The most promising thermochemical cycles for the water splitting are the S-I cycle and the Westinghouse hybrid sulphur (HyS) cycle (Fig. 4).

The S-I cycle consists of three main reactions:

- The Bunsen reaction where water, sulphur dioxide, and iodine react to form sulfuric acid and hydrogen iodide;
- The decomposition of sulfuric acid into oxygen, sulphur dioxide, and water;
- The decomposition of hydrogen iodide into iodine and hydrogen.

Sulphur and iodine are recycled in the process.

The HyS cycle eliminates iodine and has two reactions:

- The decomposition of sulfuric acid;
- The electrolysis reaction of water and sulphur dioxide into hydrogen and sulfuric acid.

Both the S-I and HyS cycles are potentially promising options for water splitting cycles.

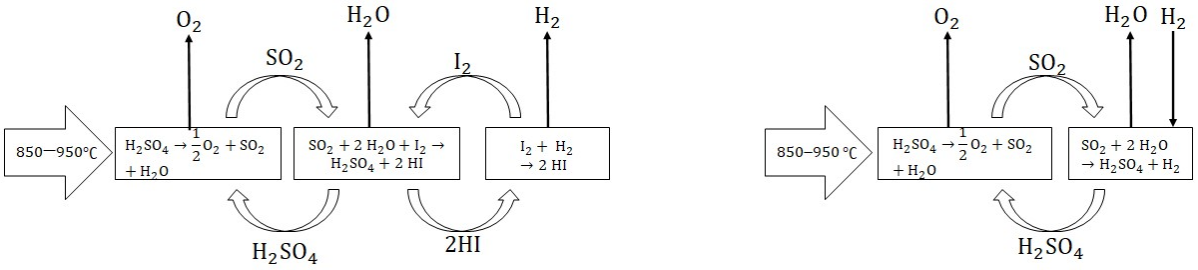

S-I cycle

$H_2SO_4 \rightarrow \frac{1}{2}O_2 + SO_2 + H_2O$

$SO_2 + 2\,H_2O + I_2 \rightarrow H_2SO_4 + 2\,HI$

$I_2 + H_2 \rightarrow 2\,HI$

HyS cycle

$H_2SO_4 \rightarrow \frac{1}{2}O_2 + SO_2 + H_2O$

$SO_2 + 2\,H_2O \rightarrow H_2SO_4 + H_2$

FIG. 4. Sulphur–iodine and hybrid sulphur cycles for water splitting to produce hydrogen.

2.1.3. Energy sources for hydrogen production

Hydrogen can be produced from different energy sources. In the present work, the study is limited to the hydrogen produced using nuclear and solar energy.

2.1.3.1. Nuclear energy for hydrogen production

The production of hydrogen using nuclear energy has been investigated in various studies [29, 30]. Nuclear-based hydrogen production is expected to offer the nuclear energy sector the opportunity to widen its field of applications and expand. It is under consideration for development in many countries and several projects have already been proposed [31]. The hydrogen produced using nuclear energy would be without greenhouse gases emissions [32].

Any nuclear reactor technology can be coupled with a hydrogen production plant [33]. The nuclear plant supplies the energy needed for the hydrogen production, in the form of heat, electricity or both [34].

The coupling of nuclear reactors with hydrogen production units has been studied (e.g. in Ref. [35]). The nuclear reactor heat is interfaced to the hydrogen production plant through a power conversion system generating electricity and in some cases through heat exchanger units [36, 37]. The energy requirements (electrical and/or thermal) of the hydrogen production process should be met by the available nuclear reactor. Conventional water-cooled reactors are well suited for low temperature electrolysis hydrogen production, as well as high temperature electrolysis with heat recuperators, while high temperature nuclear reactors are more effective for high temperature electrolysis, and thermochemical cycles. In the case of high temperature reactors, the intermediate heat exchangers, particularly those made of nickel based super alloys, have to be used. Table 3 presents the outlet temperature that could be reached by selected nuclear technologies.

TABLE 3. STEAM TEMPERATURE FOR DIFFERENT NUCLEAR REACTORS TECHNOLOGIES

Technology	Temperature, °C
Very high temperature reactor	1000
Gas cooled fast reactor	850
Sodium cooled fast reactor	550
Liquid metal cooled reactor	550
Water-cooled reactor	320

Recent advances in reactor technology, in particular small modular reactors, have offered the opportunities to some countries to further engage in the development of programmes for hydrogen production using nuclear energy. Small modular reactors, through their particular features, offer a more flexible opportunity for nuclear based hydrogen production.

2.1.3.2. Solar-based technologies for hydrogen production

There are different solar technologies, based on the nature of the conversion of the solar electromagnetic radiation into useful energy. The most used solar technologies are:

— Solar photovoltaic (PV) technology, with the conversion of the electromagnetic solar radiation into electricity;
— Concentrating solar technology (solar parabolic trough, solar central receiver, dish), with the conversion of the electromagnetic solar radiation into heat;
— Concentrating photovoltaic (CPV) technology, that is a combination of photovoltaic technology and concentrating solar technologies with the production of both heat and electricity.

The main characteristics of these technologies are reported in Table 4.

TABLE 4. SOLAR BASED TECHNOLOGIES FOR ENERGY

Technology	Form of energy	Temperature, °C
Solar PV	Electricity	–
CPV	Electricity + heat	Depends on concentrator
Solar parabolic trough	Heat	300–400
Solar central receiver system	Heat	800–1000
Dish	Heat	1000

Hydrogen production through solar PV technology is based on the use of a PV system coupled with an electrolyser. Many studies have been carried out on PV-electrolysis systems [38–40], indicating these systems as simple and attractive options for hydrogen production, since the technology is mature and offers flexibility and modularity [41, 42]. Technological breakthroughs greatly improved the efficiency of the PV cells (currently up to 40%, with the multi-junction PV cells) and reduced the associated costs, making solar PV electricity production cost competitive with conventional electricity production.

Concentrating solar PV based technology for hydrogen production represents a combination of both the solar PV method and the thermal method. This system is particularly important in processes, such as high temperature electrolysis, where both heat and electricity are needed or could be used. The main components of a concentrating PV system are the optical reflector, the PV module, the heat transfer system, and the tracking system. Secondary optical reflectors are sometimes fitted in some of the concentrating PV systems. The optical reflector concentrates and reflects solar radiation onto the PV module where it is converted into

electricity. The heat transfer fluid is used not only to cool the PV module but also to collect the generated heat that could be used for different applications [43, 44]. The cooling of the solar cells leads to an increase in the PV cells efficiency and thus to an improvement in the efficiency of the overall system. For an efficient collection of the solar energy, the tracking system is used to follow the sun movement.

There are different concentrating PV systems, based on the PV cell technology, the nature of the heat transfer fluid and the shape of the solar concentrating system [43, 45–47].

Studies on hydrogen production by water electrolysis using concentrating solar PV systems have already been performed (e.g. Ref. [48]).

Based on its high specific electrical energy generation coefficient and the possibility of using the generated heat, it has been shown [26, 49, 50] that solar concentrating PV systems can not only increase the efficiency of the system but also reduce the electrical energy required for electrolysis. An advantage over conventional flat solar PV system is that concentration increases the solar energy irradiance incident on the solar cells, leading then to a much higher electrical energy production. Moreover, with the availability of thermal energy, the part of energy required in the form of electricity diminishes leading to a reduction in the cost of hydrogen production.

In the case of thermal and concentrating solar technology for hydrogen production, the electromagnetic energy of the solar radiation is first converted into thermal energy. Flat reflectors and concentrators are used to focus the solar radiation on a receiver where the conversion occurs. There are three main concentrating solar technologies: the parabolic trough and Fresnel mirror technologies, the solar tower technology, and the parabolic dishes. The concentration can reach 100 suns with parabolic troughs, 5 000 suns with solar towers, as well as 10 000 suns with parabolic dishes.

Parabolic trough technology is the most developed solar technology and has reached the industrial maturity. These cylindric parabolic-shaped concentrators focus the solar radiation on a tube located on the focal line and containing a heat transfer fluid that could be water or synthetic oil. The heat transfer fluid can reach temperatures of about 400°C [51].

Solar towers consist of a set of flat mirrors, called heliostats, laid out so as to concentrate solar radiation on a receiver located at the top of a tower [52]. Heat is generated at the receiver and transmitted by means of a heat transfer fluid which is often a molten salt. Although it is less developed than the parabolic through technology, it has been argued that the solar tower technology offers better prospects [53].

Parabolic concentrators gathers solar radiation on a focal point. Solar towers and parabolic concentrators produce temperatures up to 1600°C [54]. Thermal solar systems provide higher conversion efficiency than PV systems. These systems can provide either thermal heat or electricity, or both [55]. A thermodynamic unit is though necessary to generate electricity. These systems can then be used in conjunction with low temperature as well as high temperature electrolysers. Because of this, these systems are the subject of intense research activity [56].

2.1.3.3. Hybrid system for hydrogen production

The reliance on renewable energy sources to address the climate change goals has set in motion the energy transition and started shaping up the future of the energy. This situation has led to a massive introduction of renewable energy in the energy mix. However, as the renewable energy sources are site specific, and of low capacity and fluctuating nature, serious challenges emerged hindering the energy transition and negatively affecting the energy system performance. Among the measures under consideration to overcome these challenges, there is the option of energy systems integration in hybrid systems. These hybrid systems offer increased flexibility, efficiency and reliability.

Nuclear-renewable hybrid energy systems are among the hybrid energy systems that have attracted a lot of attention [57–60]. In these systems, nuclear and renewable energy complement each other: nuclear helps overcome the renewable intermittence and the fluctuating nature while renewables help to save on the nuclear fuel and increase the time for fuel replacement. Moreover, a nuclear-renewable hybrid energy system offers the opportunity for clean energy, increased efficiency of energy conversion, increased profitability, optimized system reliability, and stability in energy supply. The development of small modular reactors has also offered the possibility of nuclear-renewable hybrid system design and scaling options.

Numerous renewable energy sources can be coupled in different modes to a nuclear unit in a nuclear-renewable hybrid energy system [60]. Wind, solar and geothermal energies are among the renewable energy sources that are considered mostly. Nuclear-solar hybrid energy systems for hydrogen production includes several subsystems, the main ones being:

- A nuclear reactor. Depending on the configuration, its generated heat is used either for electricity generation in the power generation unit, hydrogen production in the high temperature electrolysis unit, or both.
- One or more solar technologies, such as PV, concentrated solar power (CSP), central receiver systems, etc., for electricity (solar PV) or for heat generation (CSP, central receiver systems, etc.) or both (CPV). Depending on the configuration, the generated heat is used either for electricity generation in the power generation unit, hydrogen production in the high temperature electrolysis unit or both.
- A thermodynamic unit (a steam generator and a power generation unit) to generate electricity using heat produced by the nuclear reactor or the solar unit.
- A hydrogen production unit.

There are numerous configurations or coupling options of the hybrid system, depending on the technical specifications, the economic constraints, and the local solar resources. Among these configurations, there are:

- Solar PV – pressurized water reactor (PWR) – conventional electrolysis. In this hybrid system the PWR generates part of the electrical energy required by the conventional electrolysis system. The other fraction of the electrical energy required by the electrolysis system is provided by the solar PV field.
- Solar CPV – PWR – high temperature steam electrolysis (HTSE). In this hybrid system, the PWR generates part of the electrical energy required by the electrolysis system. The solar concentrating PV field provides the other fraction of the electrical energy and also the heat required by the electrolysis at high temperature. Using CPV allows high

specific electrical energy generation coefficient and collecting the heat leads to PV cell cooling, thus improving the PV system efficiency.

— Solar PV – high temperature gas cooled reactor (HTGR) – HTSE. In this hybrid system, the HTGR is used to provide the heat (for steam generation) required by the HTSE unit. The solar PV field provides part of the electrical energy for the HTSE. The remaining part of the electrical energy needed is provided by the HTGR.
— CSP (solar parabolic trough, central receiver systems, dish) – PWR – HTSE. In this configuration, CSP systems that produce heat at high temperatures are considered. These systems could be parabolic troughs, central receiver system, or dishes. The CSP provides the heat needed by the HTSE while the PWR provides, through the power generation unit, the electrical energy needed by the HTSE.
— CSP (solar parabolic trough, central receiver systems, dish) – HTGR – HTSE system. In this configuration, both the nuclear and the solar systems can produce high temperature steam. Two operational options are possible in this case:

  - The CSP provides the heat needed for steam generation to be fed into the HTSE while the HTGR provides, through the power generation unit, the electrical energy required for the HTSE. The HTGR provides extra heat for steam generation when necessary.
  - The CSP provides, through the power generation unit, the electrical energy needed by the HTSE; while the HTGR provides the necessary heat for the HTSE and also, through the power generation unit, any extra electrical energy needed.

2.2. MULTI-CRITERIA ASSESSMENT OF HYDROGEN PRODUCTION PROCESSES (NATIONAL RESEARCH CENTER KURCHATOV INSTITUTE, RUSSIAN FEDERATION)

This section presents the details of the multi-criteria assessment of hydrogen production process.

2.2.1. Multi-criteria assessment approach

The multi-criteria assessment approach is an effective tool for the evaluation of different options of hydrogen production using nuclear energy. The approach is to consider different aspects of the options, defined by the set of criteria grouped in several areas of assessment, in accordance with the common aspect. It is used to establish a rating of the assessed option, select the best option and optimize options characteristics. However, the multi-criteria assessment has to address challenges such as: selection of adequate criteria set, establishing a clear interpretation of each criterion, correctly determining the criteria weights (importance), ensuring a correct processing of data obtained from a group of experts (if group averaging is applied), correct evaluation of criteria values, and selection of the convolution method. Every criterion is characterized by the following parameters:

— Value of the criterion, which has to be determined based on option characteristics;
— Range of actual or possible values (min … max) and suitable unit;
— Preference direction of value variation (the more the better or the less the better);
— Weight or importance of criterion in the multi-criteria assessment (%).

The assessment for each option is performed using the convolution method and the outcome consists in the rating of options. The metrics related to the group of ideal point methods are used for this assessment [61]. The convolution method is briefly described as it follows. There are m alternatives options (i = 1, ..., m) and n criteria k_j (j = 1, ..., n) characterizing options. The following steps are considered:

— *Step 1*. Form an ideal option $\{k_1^+ \dots k_n^+\}$, where k_j^+ is the most preferred criterion value among all options (ideal), i.e. $k_j^+=\max(k_j^i)$, if preference of the option increases with increasing criterion value; or, conversely, $k_j^+=\min(k_j^i)$, if preference of the option increases with decreasing criterion value.

— *Step 2*. Form a worst option $\{k_1^- \dots k_n^-\}$, where k_j^- is the least preferred criterion value among all options (worst), i.e. $k_j^-=\min(k_j^i)$, if preference of the option increases with increasing criterion value; or, conversely, $k_j^-=\max(k_j^i)$, if preference of the option increases with decreasing criterion value.

— *Step 3.* Transition from physical units of measurement to relative is made in accordance with the normalization procedure described by the following expressions:

$$d_j^i = \frac{\left(k_j^i - k_j^-\right)}{\left(k_j^+ - k_j^-\right)} \tag{8}$$

$$d_j^i = \frac{\left(k_j^+ - k_j^i\right)}{\left(k_j^+ - k_j^-\right)} \tag{9}$$

After normalization all criteria values vary in the interval [0,1] in relative units. For expression (8), the closer the d_j^i value is to 1, the closer the option is to the ideal. Thus, all values of an ideal option are equal to one, and those of the worst are zero. And vice versa for expression (9).

— *Step 4*. Further, the distance to each option from the worst is determined by the expression (10):

$$L_i^p = \left[\sum_{j=1}^{n}\left(w_j \cdot d_j^i\right)^p\right]^{\frac{1}{p}} \tag{10}$$

where w_j – is a weight of j-criterion. Following four metrics are proposed to be used for present multi-criteria assessment:

- If p=1 and expression (8) is used for normalization, the result is a metric *«Lp1-»*, which corresponds to the weighted sum of normalized criteria, and also to the path length along the coordinate axes from the point in the multidimensional space of criteria values corresponding to the present option to the worst point.
- If p=2 and expression (8) is used for normalization, the result is a metric *«Lp2-»*, which corresponds to the Euclidean distance from the point in the multidimensional space of criteria values corresponding to the present option to the worst point.
- If p=2 and expression (9) is used for normalization, the result is a metric *«Lp2+»*, which corresponds to the Euclidean distance from the point in the multidimensional space of criteria values corresponding to the present option to the ideal point.
- The metric is a combination of (8) and (9) determined by the expression (11):

$$Lp2\text{-}» / («Lp2\text{-}» + «Lp2+») \quad (11)$$

— *Step 5.* Thus, the calculation of these metrics for all options gets aggregated values, based on which considered options are ranked.

2.2.2. List of criteria for multi-criteria assessment of hydrogen production options using nuclear energy

Due to the competition with other energy sources, especially the renewables, some NPPs around the world may face challenges to stay economically viable. Nuclear operators need to update their operational and business plans in order to meet this challenge. Increasing revenue by generating other products, other than power, is one option. Nuclear power plants have the ability to produce hydrogen, which can be utilized as clean, storable energy or to enable the decarbonization of many industries, including the transportation sector. Despite this opportunity with certain benefits, integrating hydrogen production with existing NPPs is not a trivial endeavor. Due to the numerous subsystem components, complicated interconnections, and interdependencies between them, the system that represents the combined operation of a NPP and hydrogen production plant is extremely complex. The stakeholders, which might have conflicting goals among them, are another factor contributing to the system's complexity. In order to guarantee the effective design, deployment, and operation of the coupled system, this complexity gives rise to numerous relationships and uncertainties that need to be taken into account during system design and development stage.

One of the evaluation options that captures the complexity and the various dimensions of hydrogen production using nuclear energy is the multi-criteria assessment. One of the most important steps in the multi-criteria assessment is choosing acceptable and pertinent criteria. The criteria have to precisely depict the possible consequences of every option that has been narrowed down and enable a suitable assessment and comparison with the alternative choices. For comparative multi-criteria assessment of hydrogen production with the use of nuclear energy, a set of 14 criteria grouped in four areas: economic, technical, impact on environment, and safety, is proposed. However, the list of criteria proposed is not an exhaustive one and it might be expanded to include additional refinement in the assessment. For example, it can include:

— Policy and regulatory support, as government rules and policies can influence and support the economic viability and sustainability of hydrogen production and utilization. Financial incentives, carbon pricing, research funding, and regulatory frameworks are examples of supportive policies that can stimulate investment, foster innovation, and establish a favorable business climate for hydrogen production.
— Infrastructure compatibility and plant integration, as the economic viability and sustainability of hydrogen production are significantly influenced by the current energy infrastructure (this applies, for example, when hydrogen production is envisaged using the existing NPPs). Transporting and distributing hydrogen can be made less expensive by being compatible with the infrastructure already in place, such as distribution networks, storage spaces, and pipelines. For hydrogen production and utilization to be successfully integrated into the energy system, infrastructure have to be expanded or adapted.

However, only the criteria described below were used for the work conducted in the framework of the IAEA CRP “Assessing Technical and Economic Aspects of Nuclear Hydrogen

Production for Near-term Deployment", considering they can enable hydrogen produced using nuclear energy to be a key player in the next decade to achieve decarbonization of various sectors. In addition, the findings from the on-going pilot projects on hydrogen production using existing NPPs can bring valuable insights on which criteria are of most significance.

The systems selected to illustrate the multi-criteria assessment comprise already available technologies (both for the nuclear reactor and for the hydrogen generating plant), as well as technologies that are still under development but envisaged to be used in the next decade for hydrogen production using nuclear energy. The criteria established for the assessment described below are considered relevant for the technologies currently available, as well as for the ones that have potential to be used in the future.

The economic indicators include the following:

— *Capital cost* (USD). This refers to the capital cost of one unit of facility that is minimum necessary for the realization of technology. The absolute value of the capital cost is proposed to be used for multi-criteria assessment considering near-term deployment of hydrogen production; assuming that, exactly absolute value (instead of specific value) of investments will determine the attractiveness for near-term projects. Criteria values for options were determined according to Tables 5 and 6.
— *Cost of hydrogen* (USD/kg). This is the unit cost of hydrogen at the outlet of the generating plant.
— *Multi-productivity*. This is the number of different products transferred to external consumer (e.g. hydrogen, electricity, thermal energy).

The technical indicators include the following:

— *Technology readiness level* (TRL). This is a value representing the maturity of the coupled technology, determined as the minimum value between the TRL of the technology for producing the energy needed and the TRL of the hydrogen production plant. The range of possible values is [1..9].
— *Weight and size characteristics of equipment*. This is a value representing an expert comparative assessment of weight and size characteristics of the biggest module or overall amount of equipment. The range of possible values is [1…5].
— *Initial thermal energy consumption* (kWh/kg H_2). This is the specific amount of the initial thermal energy (considering all involved sources) consumed by hydrogen production (FIG. 5).

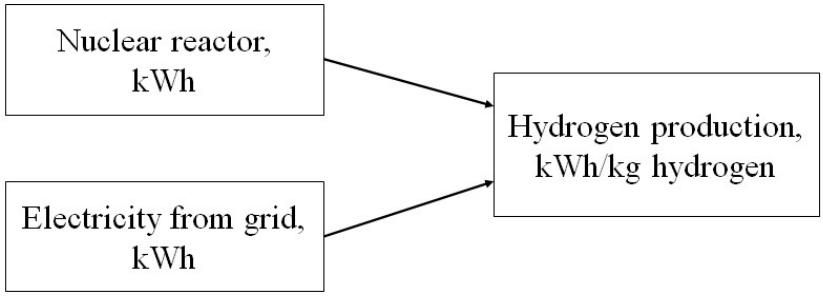

FIG. 5. Scheme for calculating the initial consumption of thermal energy.

The indicators related to the impact on environment include the following:

- *Greenhouse gas emissions (GHG)* (g eq.CO_2/kg H_2). This indicator refers to the specific GHG emissions considering the life cycle of the energy source and hydrogen generating plant.
- *Hydrocarbon consumption* (MJ/kg H_2). This indicator refers to the specific consumption of any hydrocarbon feedstock in the process (natural gas in the context of this assessment).
- *Consumption of natural uranium* (kg/kWh). This is the specific consumption of natural uranium.
- *Water consumption* (m^3/kg H_2). This is the specific consumption of water for energy generation and operation of the hydrogen production plant.

The safety indicators include the following:

- *Explosive and flammable substances*. This value indicates the presence of large quantities of explosive and flammable substances on the site (hydrogen and natural gas in the context of this assessment).
- *Radioactive materials* (relative units). This reflects the presence of large quantities of radioactive materials on the site (relative mass of core for nuclear reactor is used in a context of this multi-criteria assessment).
- *Maximum process temperature* (ºC). This is the maximum process temperature of all equipment on the site.
- *Maximum process pressure* (MPa). This is the maximum process pressure of all equipment on the site.

2.2.3. Evaluation of criteria values for the selected options

The initial data used to calculate the criteria values are as follows:

- The efficiency of generation of external (grid) electricity is taken equal to 35%, approximately as for PWR;
- GHG emissions for the NPP is taken equal to 10 g eq.CO_2/kWh, based on studies for the entire life cycle GHG-emissions for different nuclear power plants;
- CO_2 emissions for steam methane reforming process is taken equal to 6 kg/kg hydrogen;
- Content of U-235 in natural uranium is taken equal to 0.711%;
- Specific consumption of natural uranium for PWR is taken equal to ~18 g/MWh.

Data sources and methods, including calculations performed using the techno-economic models developed and the assessments derived from expert opinion, for the evaluation of criteria values for the selected options are summarized in Table 5.

TABLE 5. SOURCES AND METHODS FOR EVALUATION OF CRITERIA VALUES FOR SELECTED OPTIONS

Area of assessment	ID	Criterion	Option 1 HTGR-200 +Steam reforming	Option 2 MHR-T +Steam reforming	Option 3 MHR-T +HTSE	Option 4 HTGR-200 +Steam reforming+ Carbon capture	Option 5 PWR electricity +PEM
Economic indicators	E1	Capital cost	[62]	[63]+calc.	[63]+calc.	[62]	[62]
	E2	Cost of hydrogen	Calculated	Calculated	Calculated	Calculated	Calculated
	E3	Multi-productivity	- Heat - H_2	- Heat - Electricity - H_2	- Heat - Electricity - H_2	- Heat - H_2	- H_2
Technical indicators	T1	TRL	Expert evaluation	Expert evaluation	Expert evaluation	Expert evaluation	Expert evaluation
	T2	Weight and size characteristics of equipment	Expert evaluation	Expert evaluation	Expert evaluation	Expert evaluation	Expert evaluation
	T3	Initial thermal energy consumption	Calculated	Calculated	Calculated	Calculated	Calculated
Impact on environment indicators	I1	GHG emissions	[64]+calc.	[64]+calc.	[64]+calc.	[64]+calc.	[64]+calc.
	I2	Hydrocarbon consumption (gas)	[62]	[63]	-	[62]	-
	I3	Consumption of natural uranium	Calculated	Calculated	Calculated	Calculated	Calculated
	I4	Water consumption	[62]	[63]	[63]	[62]	[65]
Safety indicators	S1	Explosive and flammable substances	- H_2 - natural gas	- H_2 - natural gas	- H_2	- H_2 - natural gas	- H_2
	S2	Radioactive materials	[62]+calc.	[63]	[63]	[62]+calc.	-
	S3	Maximum coolant temperature	[66]	[66]	[66]	[66]	[65]
	S4	Maximum process pressure	[66]	[66]	[66]	[66]	[65]

The matrix for multi-criteria assessment containing the criteria values evaluated for the selected options is presented in Table 6.

TABLE 6. MATRIX OF CRITERIA VALUES

ID	Unit	Direction of preference	HTGR-200 +Steam reforming	MHR-T +Steam reforming	MHR-T +HTSE	HTGR-200 +Steam reforming +Carbon capture	PWR electricity +PEM	Worst value	Best value
E1	Million USD	-1	769	1 061	835	961	30	1061	30
E2	USD/kgH_2	-1	1.28	0.96	1.98	1.45	5.79	5.79	0.96
E3	Score	1	2	3	3	2	1	1	3
T1	Score	1	6	5	4	6	8	1	9
T2	Score	1	3	1	1	2	5	1	5
T3	kWh/kg H_2	-1	21.5	20.3	90.8	22.4	156.0	156.0	20.0
I1	g eq.CO_2/kg H_2	-1	6215	6203	908	224	1560	6215	224
I2	m^3/kg H_2	-1	4.02	3.17	0	4.02	0	4.02	0
I3	kg/t H_2	-1	0.19	0.18	0.79	0.20	1.00	1.00	0.18
I4	m^3/kg H_2	-1	0.018	0.018	0.035	0.018	0.010	0.030	0.010
S1	Score	-1	2	2	1	2	1	2	0
S2	Relative units	-1	1	3	3	1	0	3	0
S3	ºC	-1	850	950	950	850	80	950	80
S4	MPa	-1	5.0	7.5	7.5	5.0	3.5	8.0	4.0

2.2.4. Determination of criteria weights

The selection of the criteria weights has a significant impact on the correctness of the findings produced by applying multi-criteria assessment. In general, as the number of criteria increases, the accuracy of the expert rating decreases.

The following three variants of the criteria weight sets were simulated in the frame of this multi-criteria assessment and are presented in Table 7:

— *EW*: This equals the total weights of criteria;
— *W1*: The set of weights for the target of the assessment is to select the option of hydrogen production for near-term deployment;
— *W2*: The set of weights for the target of the assessment is to select the option of hydrogen production for near-term deployment, with greater importance of the impact on the environment.

TABLE 7. VARIANTS OF THE CRITERIA WEIGHTS SETS

EW		*W1*		*W2*		
Total weight of criterion	**Set value of area weight**	**Set value of criterion weight**	**Total weight of criterion**	**Set value of area weight**	**Set value of criterion weight**	**Total weight of criterion**
7.1%	2	4	14.8%	2	4	12.7%
7.1%		4	14.8%		4	12.7%
7.1%		1	3.7%		1	3.2%
7.1%	2	2	16.7%	2	2	14.3%
7.1%		1	8.3%		1	7.1%
7.1%		1	8.3%		1	7.1%
7.1%	1	4	6.1%	2	4	10.4%
7.1%		4	6.1%		4	10.4%
7.1%		2	3.0%		2	5.2%
7.1%		1	1.5%		1	2.6%
7.1%	1	3	5.6%	1	3	4.8%
7.1%		3	5.6%		3	4.8%
7.1%		2	3.7%		2	3.2%
7.1%		1	1.9%		1	1.6%

2.2.5. Results and conclusions of multi-criteria assessment of hydrogen production options

The resulted ranks of the considered hydrogen production options calculated using the four convolution metrics are presented in Table 8.

TABLE 8. RESULT RANKS OF THE OPTIONS FOR DIFFERENT SETS OF WEIGHTS AND DIFFERENT CONVOLUTION METRICS

Set of weights	**Metric**	**Option of hydrogen production using nuclear energy**				
		HTGR-200 +Steam methane reforming	**MHR-T +Steam methane reforming**	**MHR-T +HTSE**	**HTGR-200 +Steam methane reforming+ Carbon capture**	**PWR electricity +PEM**
EW	*Lp1-*	3	5	4	2	1
	Lp2-	3	4	5	2	1
	Lp2+	3	5	4	2	1
	Lp2-/(Lp2- + Lp2+)	3	5	4	2	1
W1	*Lp1-*	3	5	4	2	1
	Lp2-	2	4	5	3	1
	Lp2+	1	5	4	3	2
	Lp2-/(Lp2- + Lp2+)	2	5	4	3	1
W2	*Lp1-*	4	5	3	2	1
	Lp2-	4	5	3	2	1
	Lp2+	4	5	2	3	1
	Lp2-/(Lp2- + Lp2+)	4	5	3	2	1

As it can be seen from Table 8, based on the considered sets of weights corresponding to choosing an option for near-term deployment, the most preferred option is electrolysis that

takes its energy from an operating NPP. This is a consequence of the fact that this option has the best indicators in safety, as well as the highest TRL, and the lowest capital cost (the weights of the last two criteria are among the largest); this compensates even the contribution of the highest unit cost of hydrogen that is typical for this option.

The next ranked option is the HTGR-200 coupled with a steam methane reforming process. Moreover, for the case of weights set with greater importance of the impact on environment (*W2*) the option with CO_2 capture is preferable. Also in this case, the MGR-T with HTSE option takes the third rank due to high weights for the impact on environment.

The MGR-T with steam methane reforming option obtained an overall low rank, as it has the worst values for the indicators of TRL and capital cost, as well as for the indicators in the areas of safety and impact on environment compared to other options. This is also due to the large unit power and the lack of CO_2 capture option. But given the low unit cost of hydrogen, this option may be attractive in the long term if large-scale hydrogen production is required, provided the project is successfully developed and CO_2 capture is provided.

The proposed approach to multi-criteria assessment can be used to compare various options for hydrogen production using nuclear energy, considering the adequate assignment of weighting factors in accordance with the purpose of the comparative assessment. Using the proposed multi-criteria assessment matrix, it is possible to analyse the prospects of considered options and identify indicators that have the greatest impact on results of assessment. For the assessment of considered options in the long-term perspective, the matrix of multi-criteria assessment could be modified, for example the values for TRL and impact on environmental indicators, as well as weights of some criteria that are expected to evolve in time.

2.3. ASSESSMENT OF COMPATIBLE NUCLEAR REACTOR TECHNOLOGIES (UNIVERSITY OF PURDUE, UNITED STATES OF AMERICA)

The current LWRs (PWRs and BWRs) as well as various designs of small modular reactors, supercritical water reactors, high temperature gas cooled reactors, and fast breeder reactors were considered for hydrogen production in a study developed by University of Purdue, USA, in the framework of the IAEA CRP “Assessing Technical and Economic Aspects of Nuclear Hydrogen Production for Near-term Deployment”.

In the study, the following relevant data was collected:

- Nuclear power plant data: heat and operational characteristics of LWRs (PWRs, BWRs), PHWRs, supercritical water reactor (SCWR), various SMRs, liquid metal cooled reactors, fast breeder reactors (FBR), advanced gas reactors (AGRs) and HTGRs;
- Data and characteristics of hydrogen production processes: steam methane reforming, low temperature electrolysis, high temperature electrolysis, and thermo-chemical cycles (S-I cycle, CuCl cycle, and MnO cycle).

The characteristics for each hydrogen production process were then matched with those of the reactors. Based on appropriate matching of temperatures, heat flux, and power, the coupled systems were developed as integrated nuclear hydrogen production systems (INHPS). The energy transfer through intermediate heat exchanger or electrical supply units were designed for each INHPS. Operating models were developed for each INHPS that enabled computation

of the hydrogen generation as function of the system parameters. The following reactor analysis tools were used in the study:

- Integral system safety and risk analysis (first principle-based analysis);
- Hydrogen production systems – ASPEN PLUS;
- Economic analysis H2A, HEEP.

Some of the relevant characteristics of the typical currently operating reactors and some future planned reactors are listed in Table 9. In addition to these, new advanced reactors are currently under development such as VHTR that can operate at very high temperatures, up to 1000°C.

TABLE 9. CHARACTERISTICS OF CURRENT OPERATING AND OF SOME ADVANCED REACTOR DESIGNS (ADAPTED FROM [67])

Characteristic	**BWR**	**PWR**	**PHWR**	**HTGR**	**AGR**	**FBR**	**SMR**	**SCWR**
Reference design manufacturer	GE	WE	AECL	GA	NNC	Novatomic	NuScale	Canada SCWR
Primary coolant	H_2O	H_2O	D_2O	He	CO_2	Liq. Na	H_2O	H_2O
Secondary coolant	-	H_2O	H_2O	H_2O	H_2O	Na/H_2O	H_2O	-
Thermal energy (MWt)	3100	3600	1993	891	1480	1591	160	2540
Net electricity (MWe)	1015	1204	600	350	610	650	50.0	1273
Efficiency (%)	32.7	33.4	30.1	39.3	41.2	40.9	31.52	50.10
Heat exchanger	-	U Tube Steam generator	U Tube Steam generator	Helical Coil	Helical Coil	Helical Coil	Helical Coil	-
Primary pressure (MPa)	7.17	15.5	10	4.9	4.3	0.1	12.7	25
Core inlet temp. (°C)	278	286	267	318	334	395	263.9	350
Core outlet temp. (°C)	288	324	310	741	635	545	318.9	625
Secondary pressure	-	5.7	4.7	17.2	16.0	0.1/17.7	3.4	-
Secondary inlet temp. (°C)	-	224	187	188	156	345/235	149	-
Secondary outlet temp. (°C)	-	273	260	513	541	525/487	307	-

GE- General Electric, AECL – Atomic Energy Canada Limited, GA- General Atomics, NNC- National Nuclear Corp. WE- Westinghouse Electric.

The operating temperature ranges for the advanced reactors designs, including VHTR, SCWR, molten salt reactor (MSR), gas cooled fast reactor (GFR), sodium cooled fast reactor (SFR), lead cooled fast reactor (LFR), are identified in Table 10.

TABLE 10. OUTLET TEMPERATURE IN ADVANCED REACTOR DESIGNS UNDER DEVELOPMENT

Neutron spectrum	Reactor type	Maximum core outlet temperature (°C)
Thermal	VHTR	~1000
	SCWR	600
	MSR	650
Fast	GFR	950
	SFR	650
	LFR	650–800

2.3.1. Coupling of hydrogen plant and nuclear reactor

Many process heat plants could be coupled to a nuclear reactor. A nuclear reactor could be used to drive a steam reforming plant, a coal gasification facility, or an electrolysis plant. These processes have an inherently low efficiency. Most thermochemical cycles are purely thermodynamic, and thus have higher thermodynamic efficiency. The ideal heat source for a thermochemical cycle is either a high temperature nuclear reactor or a solar thermal array. Gas cooled reactors produce large amounts of heat at high temperature (>750°C). In Fig. 6, the possible combination of nuclear plant and the hydrogen production processes are shown with overlapping temperature ranges. The key to the coupling between a nuclear reactor and a thermochemical hydrogen generation plant is the intermediate heat exchanger (IHX). In addition to providing heat to the chemical plant, the IHX serves several other purposes:

— Isolation of the chemical plant from the NPP;
— Exclusion, or, at the very least, limitation of radioactive contamination;
— Prevention of the undesired ingress of corrosive chemical reactants to the nuclear facility;
— Conventional design and maintenance of the heat utilization system.

Ultimately, the IHX acts as both an interface and an isolation device between the thermochemical plant and the nuclear reactor.

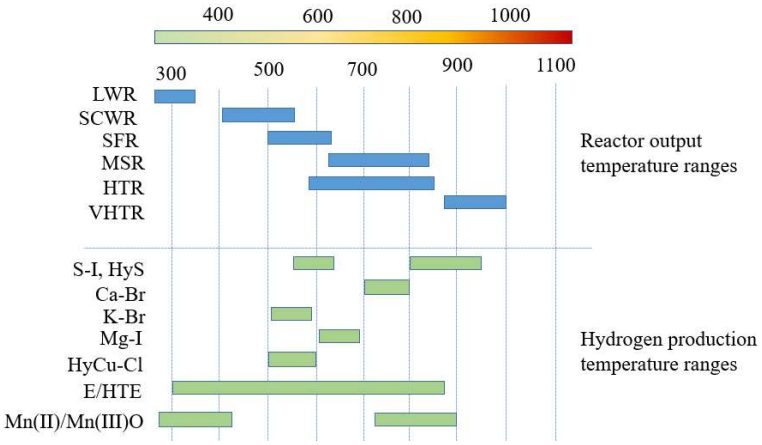

FIG. 6. Nuclear plant temperature ranges overlapping temperature for hydrogen production method.

This direct coupling is illustrated in Fig. 7. A more generalized view, including cogeneration and a general chemical process facility (e.g., a steam reforming or desalination plant), is illustrated in Fig. 8.

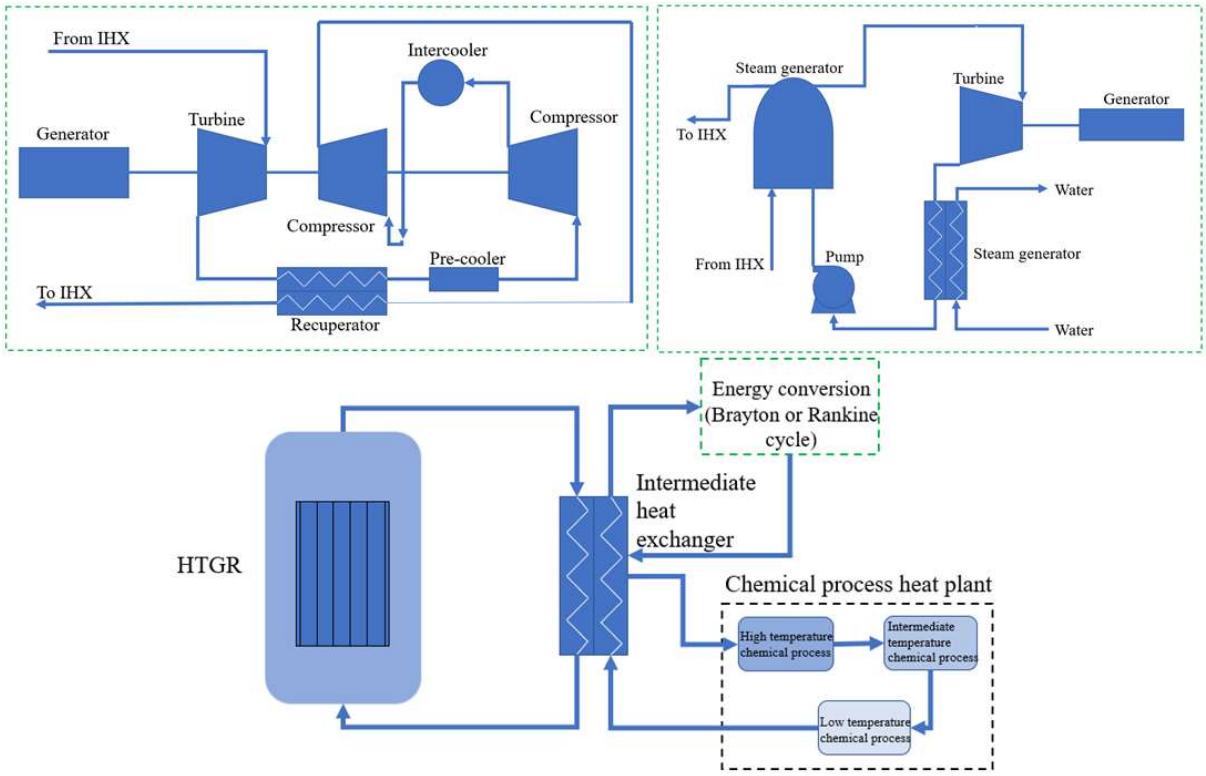

FIG. 8

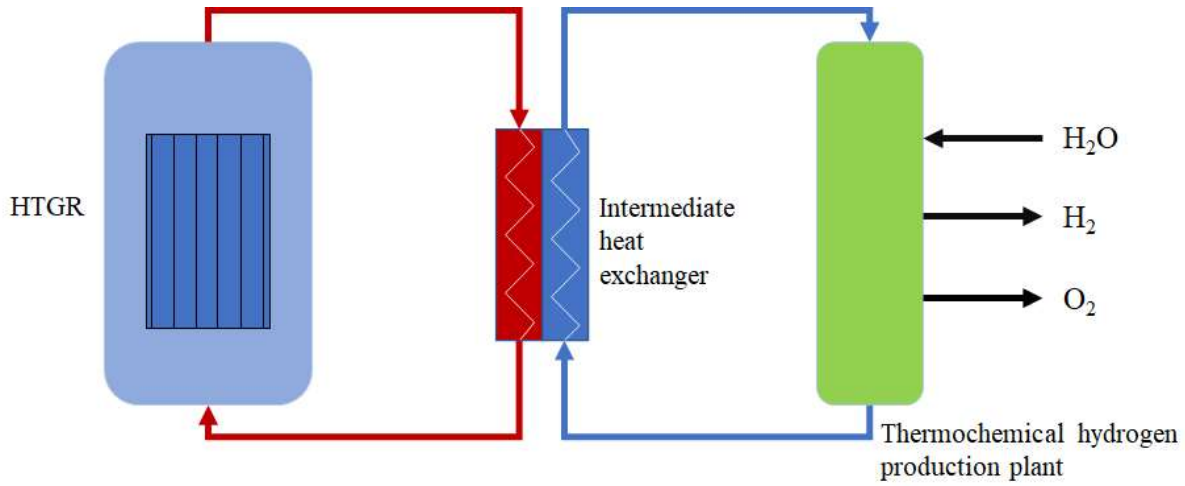

FIG. 7. Heat process and nuclear plant coupling scheme through intermediate heat exchanger.

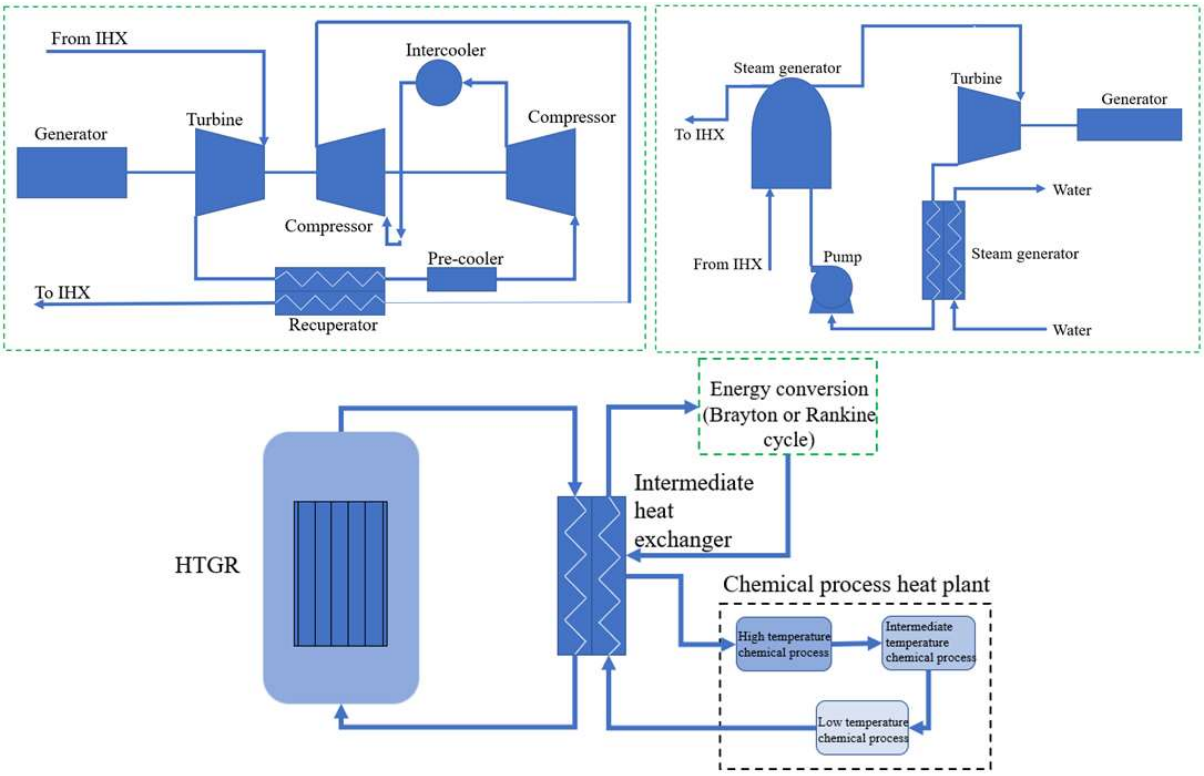

FIG. 8. Nuclear plant coupling scheme with cogeneration of electricity.

2.3.2. Model for integrated high temperature gas cooled reactor with the sulphur-iodine cycle

Regardless of any specific process, such as S-I cycle or HyS cycle, the chemical plants for the hydrogen generation are complex systems. Worldwide considerable efforts on the development of the efficient process flowsheet have been conducted. If the chemical process is connected to a NPP, the problem is much more complex. Reliable and safe NPP operations in normal conditions, plant startup, plant shutdown, and any anticipated operational transients have to be demonstrated. For this purpose, a comprehensive system model is necessary for the coupled nuclear-chemical plant. The model can be used to optimize hydrogen production as a function of key parameters such as reactor outlet temperature, core geometry, heat exchanger efficiency, and mass flow rates.

The simulation model was developed accounting the chemical reactions in each section within the reaction chamber model. The reaction chamber was considered as a control volume and the governing equations were derived to account inlet and outlet flows from each chamber. The governing equations derived included the molar balance, the energy balance, the constant pressure condition, the transient pressure, and the state equations [68], [69]. The reaction segments in the S-I cycle are the following: the Bunsen reaction segment, the sulfuric acid decomposition segment, and the hydroiodic acid decomposition segment. In this model, the recycling of H_2O, I_2, and HI was considered within each chemical plant sections and the separation and concentration were neglected or simplified. The extent of the reaction was defined for each reaction chamber.

The reaction rate equation for the Bunsen reaction segment on the depletion of sulphur dioxide is written with kinetic equation as in Ref. [68]:

$$-\frac{d[SO_2]}{dt} = k_1 \cdot [I_2] \cdot [H_2O] \cdot [SO_2] \tag{12}$$

Thus, the depletion rate of sulphur dioxide is dependent on the reaction rate, as well as the concentration of each of the constituents. For the sulfuric acid decomposition segment, the analysis is carried out in two steps. First, sulfuric acid is assumed to be decomposed into water and sulphur trioxide. Second, oxygen and sulphur dioxide are produced by the decomposition of sulphur trioxide [70]. These steps are:

$$H_2SO_4 \rightarrow H_2O + SO_3$$

$$SO_3 \rightarrow SO_2 + \frac{1}{2}O_2$$

The chemical kinetics indicate that the reaction of H_2SO_4 decomposition, where water and sulphur trioxide are products, has close to 100% conversion rate above 700°C [70]. The overall kinetic equation for the sulfuric acid decomposition segment is written as:

$$-\frac{d[H_2SO_4]}{dt} = -\frac{d[SO_3]}{dt} = k_2 \cdot [SO_3] \tag{13}$$

The determination of HI depletion rate is substantially more complicated because of the significant reverse reaction rate for the hydrogen iodine decomposition segment. Three coupled differential equations for the generation of hydrogen, iodine, and the depletion of hydrogen iodide can be used in the quantification of the reaction:

$$2HI \leftrightarrow H_2 + I_2$$

with k_3 being the kinetic constant for the direct reaction and k_{-3} being the kinetic constant for the reverse reaction. These equations are:

$$\frac{d[H_2]}{dt} = k_3 \cdot [HI]^2 + k_{-3} \cdot [H_2] \cdot [I_2] \tag{14}$$

$$\frac{d[H_2]}{dt} = \frac{d[I_2]}{dt} \tag{15}$$

$$\frac{1}{2}\frac{d[HI]}{dt} = -k_3 \cdot [HI]^2 + k_{-3} \cdot [H_2] \cdot [I_2] \tag{16}$$

The Runge-Kutta method was used to resolve these coupled equations for the hydrogen iodine decomposition segment. These reaction rate constants could be determined by applying the following relationships, presuming that each reaction is elementary:

$$k_1 = A_1 exp\left(-\frac{E_1}{R}\left(\frac{1}{T_1} - \frac{1}{T_0}\right)\right) \tag{17}$$

$$k_2 = A_2 exp\left(-\frac{E_2}{RT_2}\right) \quad (18)$$

$$k_3 = A_3 exp\left(-\frac{E_3}{RT_3}\right) \quad (19)$$

$$k_{-3} = A_{-3} exp\left(-\frac{E_{-3}}{RT_3}\right) \quad (20)$$

A summary of each parameter (for k_n) for the reaction rate is presented below. The steady state and the transient behaviours of each reaction chamber were therefore characterized using a basic chemical model. When combined with an appropriate temperature model, this chemical reaction chamber model created a fully coupled, simplified model of the S-I cycle.

For the Bunsen reaction (liquid phase, 120°C), the pre-exponential factor (A_1) and the activation energy (E_1) were 3×10^{-6} $L^2/(mol^2 \cdot s)$ and 4.187 kJ/mol respectively. For the H_2SO_4 decomposition (gas phase, 850°C), the pre-exponential factor (A_2) was 6.8×10^4 s^{-1}, and the activation energy (E_2) 73.1 kJ/mol. The reaction of HI decomposition (gas phase, 450°C) had the following values for the kinetic parameters: pre-exponential factor (A_3) was 10^{11} L/(mol·s) and activation energy (E_3) was 184 kJ/mol, whereas for the reverse reaction, the A_{-3} was 1.596×10^7 L/(mol·s) and E_{-3} was 108 kJ/mol.

2.3.2.1. Model implementation

It is necessary to complete a thorough steady state computation before applying the transient model. Relying on the reactor coolant and reactant flow rates, and temperatures, a steady state hydrogen generation rate was determined during the steady state analysis. Following the inceptive computation for the steady state, one of the pertinent quantities, like the temperature of the reactor coolant, could be varied, and the resulting transient could be analyzed.

Fixing all but one of the essential quantities could result in reaching a steady state condition. For instance, the required coolant flow rate could be calculated while the appropriate hydrogen generation rate was specified. Optionally, if the coolant flow rate was fixed, the appropriate heat exchanger transfer area could be determined. There could be a diversity of possible steady state outcomes as a result.

A quantity, like the reactor coolant flow rate or the temperature of the reactor coolant, could be tweaked once a steady state solution has been reached. The transient response of the S-I cycle could be observed utilizing the time dependent energy balance, continuity balance, reaction rates, and momentum assumption.

By adding a fluctuation and iterating with a relatively short time step to convergence, the transient was modeled. Figure 9 illustrates the flowchart for the steady state initialization while Fig. 10 shows a flowchart of the suggested transient model process.

A partial loss-of-coolant accident, in which a portion of the reactor coolant is removed from the coolant stream, is one of the most significant transients. This reactor accident has the propensity to be severe. An essential aspect of nuclear safety is comprehending the chemical plant's transient response in such a situation. Hence, in transient analysis, a quick shift in flow rate is a significant deviation. Periodically, an emergency introduction of negative reactivity is

required to stop an uncontrollable nuclear reaction. The temperature of the reactor coolant's outflow would swiftly decrease because of the reactivity reduction. In such a situation, it would be crucial to comprehend how chemical plant reaction rates and hydrogen production rates would shift. The helium inlet temperature and flow rate fluctuations were simulated as transient analyses in the section that follows.

The transient model for the reaction chamber was implemented in a series of MATLAB scripts based on the available thermodynamic and kinetic data. The current version of the model was not coupled with a nuclear reactor.

For the steady state condition, it was assumed that separated helium streams flow through each reaction chamber (the segment for H_2SO_4 decomposition and the segment for HI decomposition) with helium inlet temperature of 900°C (1173.15 K) and helium outlet temperature of 450°C (723.15 K).

The steady state helium flow rate could be determined from the steady state helium inlet and outlet temperatures using the heat exchanger heat load and a hydrogen generation rate of 1 mol/s.

Figures 8 and 9 present the flowchart for the steady state initialization of the variables in the S-I thermochemical cycle and the flowchart for the transient analysis of the S-I thermochemical cycle, respectively.

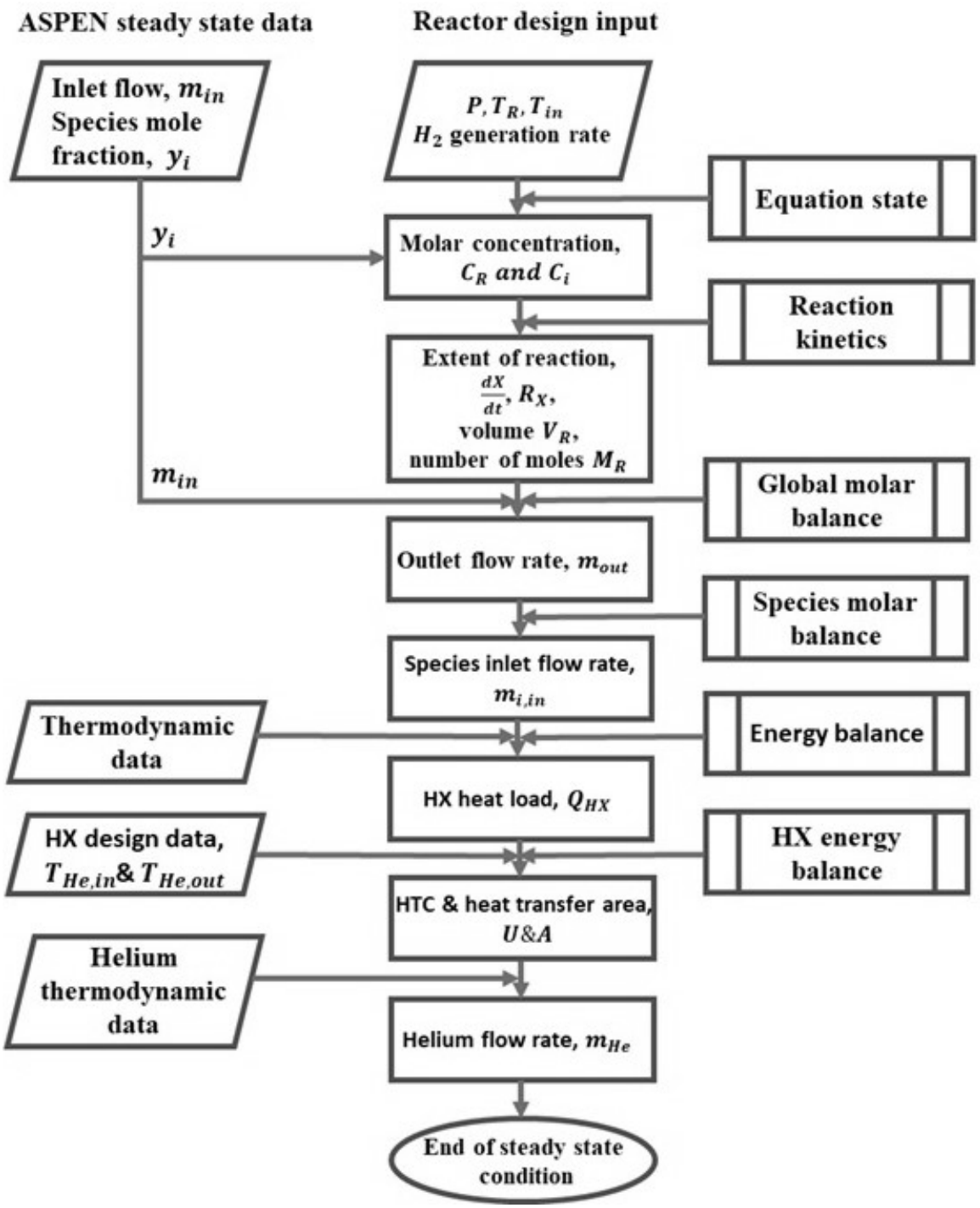

FIG. 9. Flowchart for the steady state initialization of the variables in the S-I thermochemical cycle.

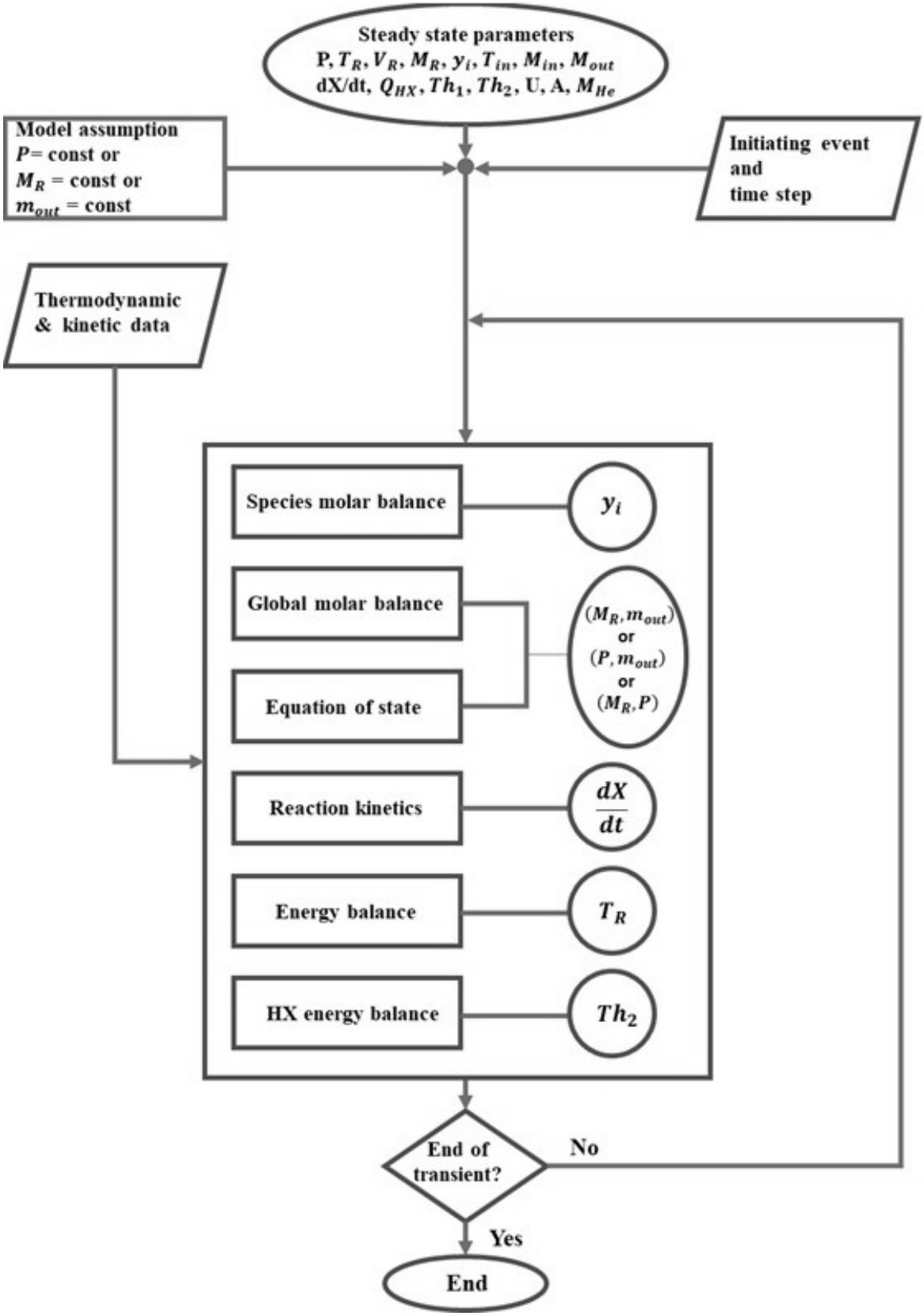

FIG. 10. Flowchart for the transient analysis of the S-I thermochemical cycle.

2.3.2.2. Integration of sulphur-iodine and hybrid sulphur cycle to nuclear heat

In the previous section, a reaction chamber model was presented, demonstrating its capability to simulate transients. However, the reaction chamber model for each reaction should be integrated to simulate a full process such as the entire S-I cycle. The integration scheme is complicated since there are many factors to be considered such as recycling fraction, the operating parameters in the pre-vaporizer, evaporator and preheater, the heat recovery strategy, etc. Furthermore, those factors are also interconnected to each other.

A setup of the process parameters for the fully integrated S-I cycle was developed on the basis of the General Atomics flowsheet [68].

Figure 11 shows the integrated flowsheet of the simplified S-I model. The model includes: the Bunsen reaction (segment 1), the H_2SO_4 decomposition (segment 2), and the HI decomposition (segment 3); i.e., all three of the reactions composing the S-I cycle. Except for the outgoing hydrogen and oxygen streams, and the feeding water, all the streams in the three segments (1, 2, and 3) are interlinked and regenerated.

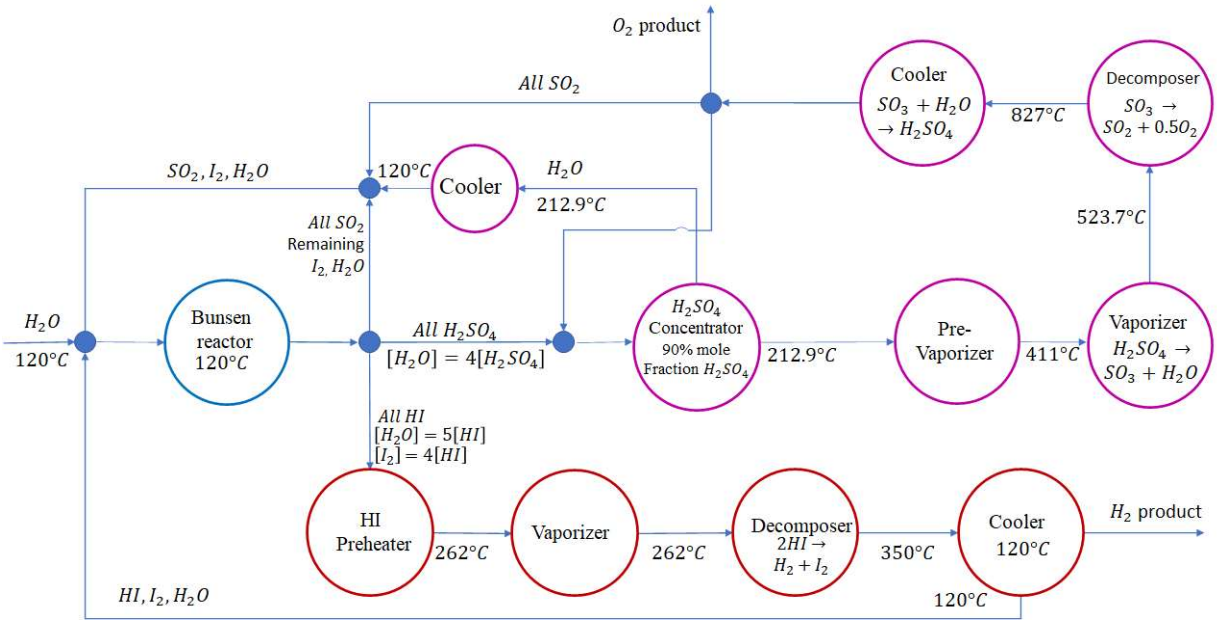

FIG. 11. Flowsheet of the simplified S-I model: integration scheme.

Several assumptions were made in the flowsheet to simplify the S-I cycle model. The summary of these assumptions is listed below:

— Segment 1, Bunsen reactor, 3-Phase separator. All produced sulfuric acid and hydrogen iodide are flowing into segment 2 and 3 respectively. The water flow rate into segment 2 is 4 times that of sulfuric acid molar flow rate, and the water flow rate into segment 3 is 5 times of hydrogen iodide molar flow rate. The unreacted iodine flow rate into segment 3 is four times hydrogen iodide molar flow rate. The unreacted sulphur dioxide, iodine, and remaining water are recycled back to segment 1, Bunsen reactor.
— Segment 2, the sulfuric acid decomposition that includes:
  - The sulfuric acid concentrator, where 90% of the sulfuric acid molar fraction is concentrated and remaining water is returned to segment 1, the Bunsen reactor.

- The vaporizer, where 100% of sulfuric acid is decomposed into water and sulphur trioxide.
- The decomposer, where the decomposition of sulphur trioxide into oxygen and sulphur dioxide occurs as per chemical kinetics equation.
- The cooler, where the reactants are cooled to 120°C. The unreacted sulfuric trioxide from decomposer section recombines with water to form sulfuric acid. All sulfuric acid, and the remaining water are recycled in segment 2 which is then sent to the sulfuric acid concentrator. All sulphur dioxide produced in the decomposer is returned to segment 1 Bunsen reactor. All oxygen is separated and collected as product.

— Segment 3 Hydrogen iodide:

- The decomposer, where the decomposition reaction of hydrogen iodide into iodine and hydrogen occurs.
- The cooler, where the reactants are cooled to 120°C. The hydrogen produced is separated and is collected as product. The unreacted reactants are returned to segment 1, the Bunsen reaction.

— Preheater and vaporizer use the cooling loads heat rejected from segments 2 and 3 coolers.

— The heat produced in the Bunsen reactor (exothermic heat of reaction) is neglected.

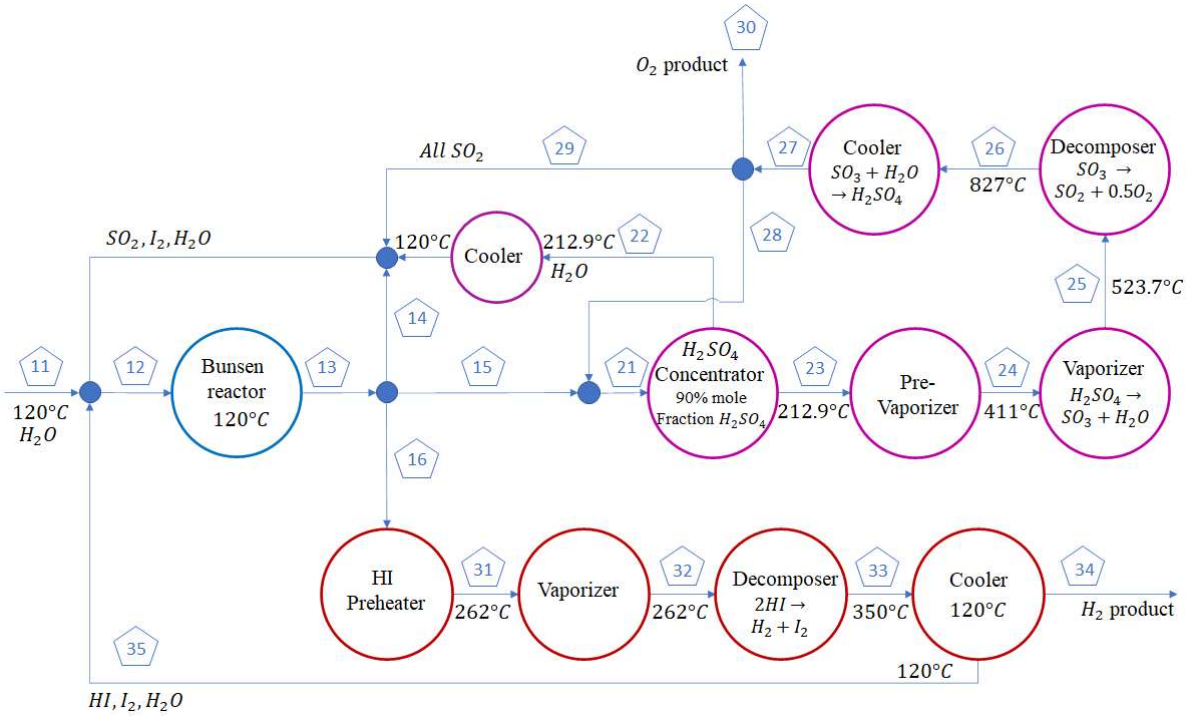

FIG. 12. Flowsheet of the simplified S-I model: stream numbering scheme.

2.3.2.3. Sulphur-iodine cycle: results and discussion

A steady-state solution was obtained for the fully coupled model between three reaction sections for 1 mol of hydrogen generation. The hydrogen iodide decomposition reaction is very slow due to both forward and backward reactions. Hence a large decomposer chamber was required for segment 3, much bigger than the sulphur trioxide decomposer. As a simplification, only the forward reaction was considered to prevent an unrealistic reactor chamber volume in the model. The reactions in the segments 2 and 3 are endothermic reactions. To facilitate the

decomposition of the acids, segments 2 and 3 had heating devices such as preheaters, pre-vaporizer, and vaporizers. The amount of the heat required for these processes was calculated assuming a 100% heat recovery.

The representative results of the steady state analysis are summarized here. Table 11 presents the summary of results for 1 mol of hydrogen generation.

TABLE 11. RESULTS FOR 1 MOL OF HYDROGEN GENERATION

	Segment 1	**Segment 2**	**Segment 3**
Reaction chamber temperature, °C	120	827	450
Reactor volume, m^3	7.60	9.20×10^{-3}	4.14
Heat loads, J	-	6.57×10^{5}	6.08×10^{6}
Cooling loads, J	-	4.35×10^{5}	6.09×10^{6}

The reactor volume was much bigger for segment 3 than for segment 2. This was due to much slower kinetics in segment 3. Heat loads for segment 1 were not considered. Although the reaction heat was less for segment 3 than for segment 2, the heat loads were much bigger for the segment 2 due to a large recycling of H_2O, I_2, and HI. However, much of the heat loads could be supplied by the recuperation of the high temperature stream. Table 12 presents the values of the heat load in the components of segment 2.

TABLE 12. SEGMENT 2 HEAT LOAD.

Component	**Type**	**Heat load, J**
Concentrator	Sensible	6.68×10^{4}
	Latent	1.70×10^{5}
Pre-vaporizer	Sensible	3.39×10^{4}
Vaporizer	Latent	1.01×10^{5}
Recuperator	Sensible	4.04×10^{4}
Decomposer	Sensible	5.86×10^{4}
	Latent	1.86×10^{5}
Total		6.57×10^{5}

The value of the cooling heat load in segment 2 from hot stream to cold stream was 4.346×10^{5} J and the following values were obtained for the net heat load in segment 2:

- 222 kJ, 100% heat recovery of cooling load;
- 266 kJ, 90% heat recovery of cooling load;
- 309 kJ, 80% heat recovery of cooling load;
- 353 kJ, 70% heat recovery of cooling load.

Table 13 presents the values of heat load in the components of segment 3.

TABLE 13. SEGMENT 3 HEAT LOAD

Component	**Type**	**Heat load, J**
Pre-vaporizer	Sensible (liquid)	1.94×10^{5}
Vaporizer	Latent	4.52×10^{6}
Decomposer	Sensible (gas)	1.36×10^{6}
	Latent	1.24×10^{4}
Total		6.08×10^{6}

The value of the cooling heat load in segment 3 from hot stream to cold stream was 4.35×10^5 J and the following values were obtained for the net heat load in segment 3:

- -15 kJ, 100% heat recovery of cooling load;
- 595 kJ, 90% heat recovery of cooling load;
- 1 204 kJ, 80% heat recovery of cooling load;
- 1 814 kJ, 70% heat recovery of cooling load.

A negative net heat load was calculated for segment 3. The reason for this could be an erroneous equation in the reaction heat calculation correlation.

2.3.3. Hydrogen cost analysis with proton exchange membrane electrolysis and grid electricity

In this analysis, hydrogen production from PEM electrolysis was studied. A PWR plant was assumed to provide electricity for the PEM electrolyser through a grid power system. For base case, it was assumed that the PEM electrolyser system is standalone, and the total hydrogen production capacity was 50 t/day or 0.58 kg/s.

2.3.3.1. Proton exchange membrane electrolyser and energy load characteristics

The PEM electrolyser stack shown in Fig. 13 had a series of PEM layers. The inputs for the electrolyser are water and electricity and the outputs are oxygen and hydrogen. The water flows into the anode section where the applied current splits water into hydrogen ion (protons, H^+) and oxygen gas (O_2). The hydrogen ion diffuses through polymer electrolyte to cathode section where it recombines into diatomic hydrogen gas (H_2). The hydrogen gas is collected and is further purified as dry gas product. The oxygen from the anode side of the system is collected after being diluted with air (if a sweep gas is used). The electrolyser typically operates close to atmospheric or higher pressures depending on electrolyser design. For the analysis conducted, no practical use for oxygen gas was considered.

In Table 14, the PEM electrolyser stack and the energy load characteristics are listed.

TABLE 14. REFERENCE PEM STACK AND LOAD CHARACTERISTICS

H_2 outlet pressure		MPa (psi)	3.1 (450)
Stack electrical usage			
	Cell voltage	Volts/cell	1.75
	Voltage efficiency	%	70.3%
	Dryer loss	% of gross H_2	3.0%
	Permeation loss	% of gross H_2	0.7%
	Total stack energy usage per mass net H_2	$kWh_{elec}/kg_{Net\ H2}$	49.23
Balance of plant loads			
	Power inverter efficiency	%	95%
	Inverter electrical load	$kWh_{elec}/kg_{Net\ H2}$	2.59
	Dryer thermal load	$kWh_{therm}/kg_{Net\ H2}$	0.34
	Dryer efficiency	kWh_{elec}/kWh_{therm}	3.67
	Dryer electrical load	$kWh_{elec}/kg_{Net\ H2}$	1.25
	Total balance of plant electrical load	$kWh_{elec}/kg_{Net\ H2}$	5.04
Summary			
	Stack electrical usage	kWh_{elec}/kg_{H2}	49.23
	Balance of plant electrical usage	kWh_{elec}/kg_{H2}	5.04
Total system electricity usage per mass net H_2		$kWh_{elec}/kg_{Net\ H2}$	54.30

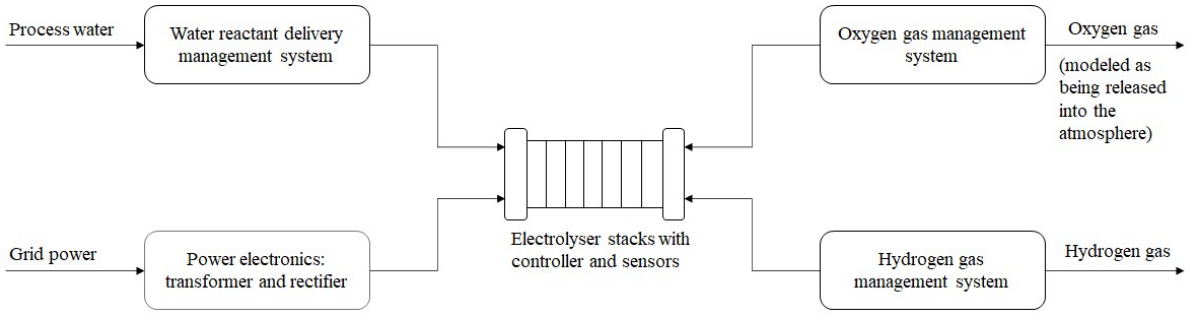

FIG. 13. Process flow diagram for PEM electrolyser (from H2A code Version 3).

2.3.3.2. Operating parameters and capital costs

In Table 15 and Table 16 the plant operating parameters, feedstock and capital cost are given.

TABLE 15. FINANCIAL AND OPERATING SPECIFICATIONS

Technical operating parameters and specifications	
Operating capacity factor (%)	97.0
Plant design capacity (kg of H_2/day)	50 000
Plant output (kg/day)	48 500
Plant output (kg/year)	17 702 500
Financial input values	
Plant construction period (years)	1
Capital spending for construction during 1st year (%)	100
Capital spending for construction during years 2-4 (%)	0
Life of plant and analysis period (years)	40
Depreciation duration (years)	20
Depreciation method	Modified accelerated cost recovery system
Equity financing (%)	40
Debt interest rate (%)	3.70
Fixed operating costs throughout start-up period (%)	100
Revenues during start-up (%)	50
Variable operating costs during start-up (%)	75
Plant decommissioning costs (% of depreciable capital investment)	10
Plant salvage value (% of total capital investment)	10
Rate of inflation (%)	1.9
After-tax real internal rate of return (%)	8.0
State taxes (%)	6.0
Federal taxes (%)	21.0
Total tax rate (%)	25.7
Working capital (% of yearly change in operating costs)	15

TABLE 16. BASE REFERENCE CAPITAL, FEEDSTACK AND OPERATING COSTS

Total capital costs (USD)	165 837 229
Total fixed operating cost per year (USD/year)	8 186 103
Total variable operating costs (USD/year)	66 214 400
Total utility costs per year (USD/year)	200 123
Feedstock - industrial electricity price (USD/kWh)	7×10^{-2}
Feedstock - total cost of electricity per year	67 268 565
Feedstock - deionized water price (USD/gal)- (Usage 4.76 gal/1 kg H2)	2.37×10^{-3}
Feedstock - process water cost per year (USD)	200 123

2.3.3.3. Levelized cost of hydrogen

Table 17 shows the cost distribution and total levelized cost of hydrogen for the base case. It can be seen from this table that the major cost of hydrogen is the feedstock cost derived primarily from the electricity price.

Figure 14 shows the tornado chart depicting the variations in the feedstock consumption and the operating capacity factor.

The price of industrial electricity from an NPP varies in USA from 0.02 USD to 0.08 USD, depending on the time of the day and on the geographical location. Since the electric grids are shared, the price of the nuclear electricity follows the grid price.

The results of the sensitivity analysis of the electricity price on the hydrogen levelized cost are shown in Fig. 15.

TABLE 17. SPECIFIC ITEM AND LEVELIZED COST FOR HYDROGEN FROM PEM ELECTROLYSIS

Cost component	Cost contribution (USD/kg)	% of H_2 cost
Capital costs	0.75	15.0%
Plant decommissioning costs	0.00	0.1%
Fixed operating and maintenance (O&M) costs	0.46	9.2%
Plant feedstock costs	3.80	75.5%
Cost of other raw material costs	0.00	0.0%
Credits for by-products	0.00	0.0%
Costs of utilities and other variables	0.01	0.2%
Total	**5.03**	

FIG. 14. Tornado chart of cost distribution of hydrogen produced using a PEM electrolyser.

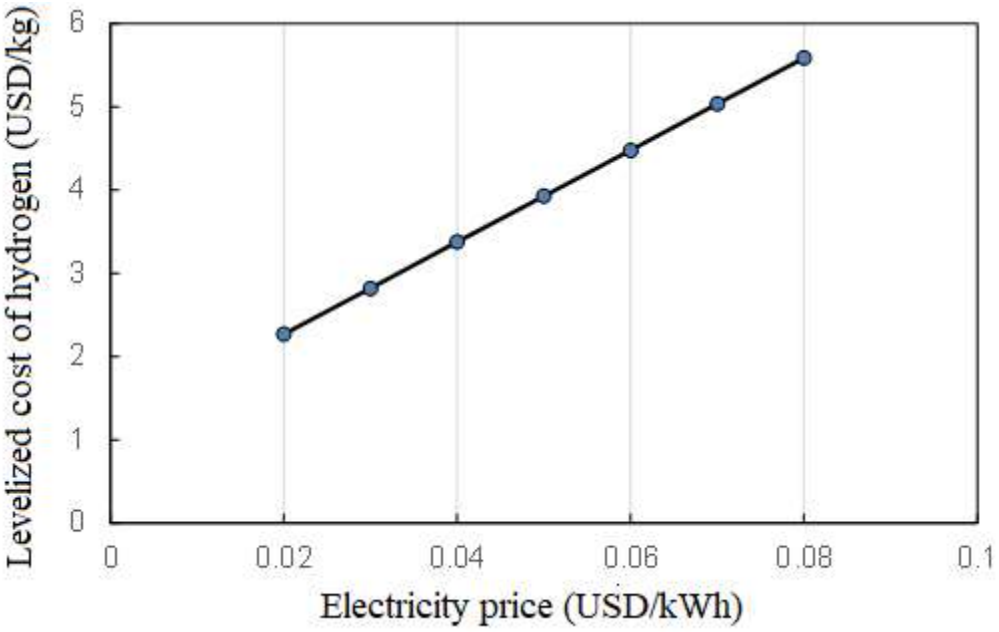

FIG. 15. Levelized cost of hydrogen for various electricity price.

2.3.4. Hydrogen cost analysis with solid oxide electrolysis and high temperature gas cooled reactor

In this analysis, the hydrogen production using a solid oxide electrolyser cell was studied. An HTGR plant was assumed to be integrated with the solid oxide electrolyser to provide electricity and heat.

For the base case, it was assumed that the PEM electrolyser system is standalone, and the total hydrogen production capacity was 815.6 t/day or 9.44 kg/s. The electrolyser units used process water, and heat and electricity from the HTGR.

2.3.4.1. Solid oxide electrolyser and energy load characteristics

As shown in Fig. 16, high temperature steam is introduced into the cathode section of the electrolyser cell, where it is split into hydrogen and oxygen ion driven by the applied current. The oxygen ion diffuses through the solid-state electrolyte from the cathode to anode, where it reforms into diatomic oxygen.

The process stream is shown in Fig. 17.

The corresponding stream summary is given in Table 18TABLE *18*. The hydrogen outlet pressure is 2 MPa. For the analysis conducted, no practical use for the oxygen was considered for HTSE hydrogen production. In Table 18TABLE *18*, the solid oxide electrolyser stack and the energy load characteristics are listed.

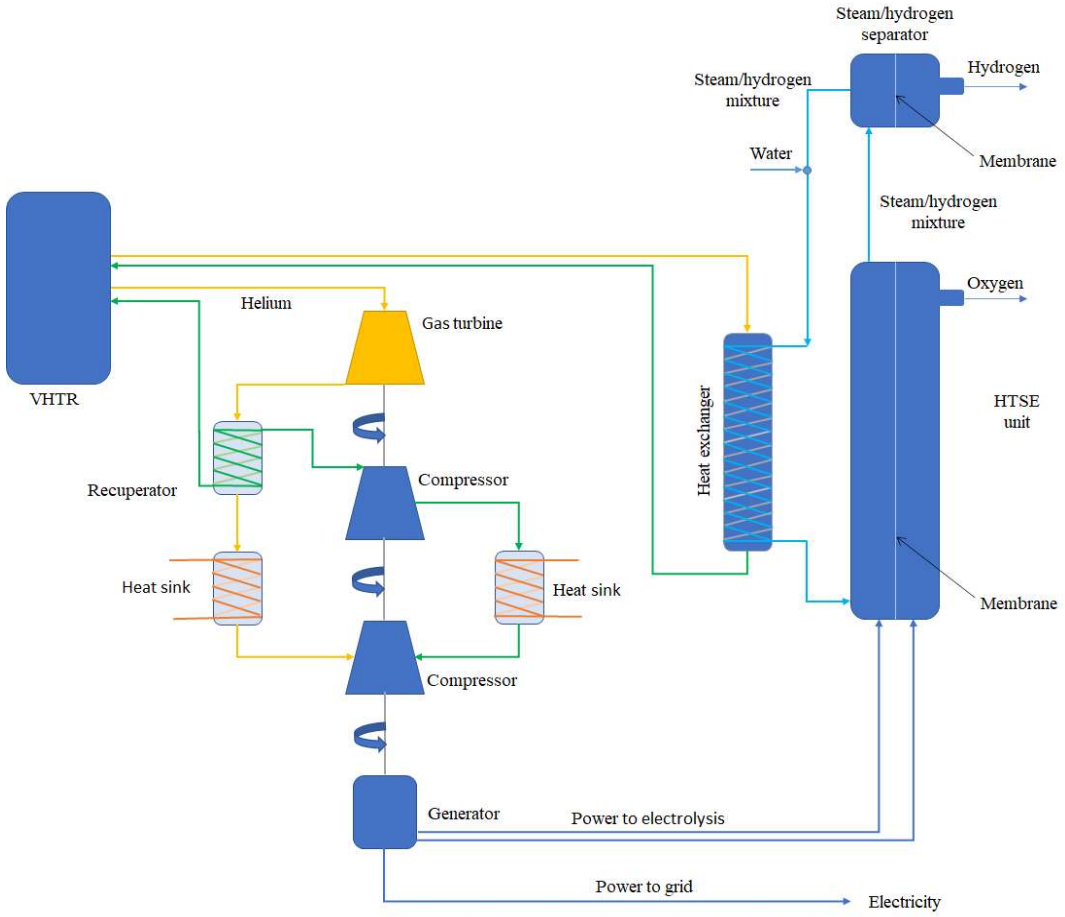

FIG. 16. The schematic diagram of HTGR integrated with solid oxide electrolyser.

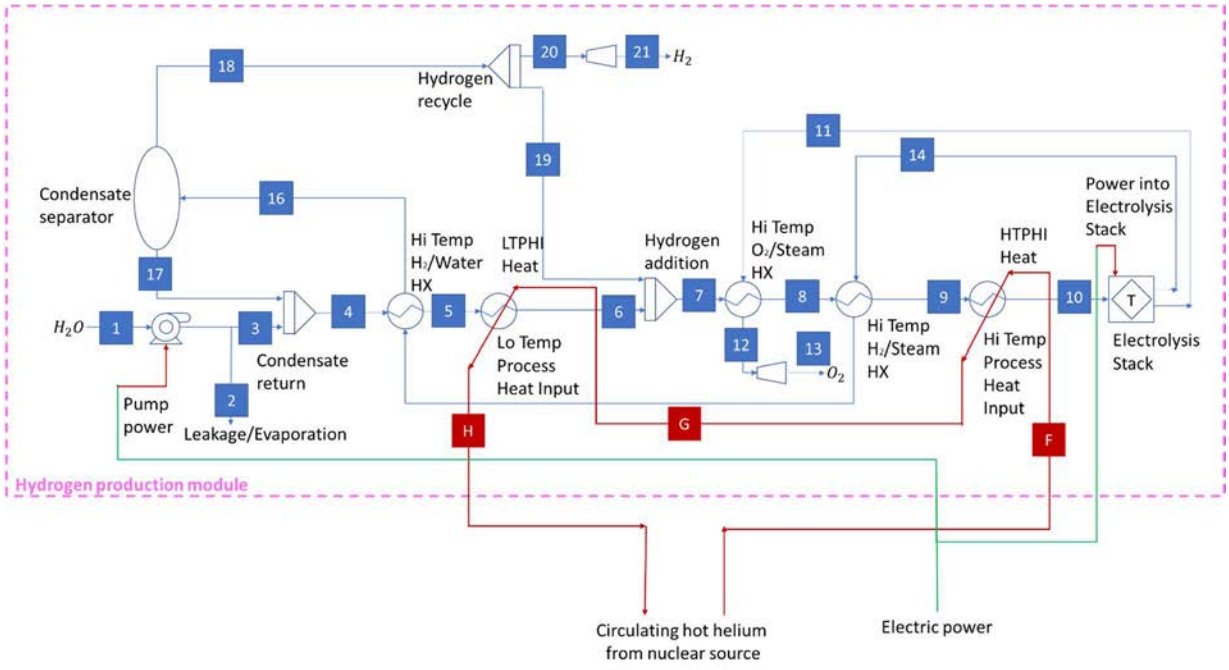

FIG. 17. Process flowsheet for solid oxide electrolyser (from H2A code version 2).

TABLE 18. PROCESS FLOWSHEET STREAM VALUE SUMMARY

Key point in process flowsheet	Mass flow kg/s	Temperature °C	Pressure bar	Composition
1	92.7	20	1	water
2	18.3	20	50	water
3	74.4	20	50	water
4	83.8	37	50	water
5	83.8	200	50	water
6	83.8	285	50	water
7	84.8	276	50	90% water 10% hydrogen
8	84.8	320	50	90% water 10% hydrogen
9	84.8	650	50	90% water 10% hydrogen
10	84.8	850	50	90% water 10% hydrogen
11	66.1	843	50	oxygen
12	66.1	725	50	oxygen
13	66.1	90	1	oxygen
14	18.7	843	50	90% hydrogen 10% water
15	18.7	425	50	90% hydrogen 10% water
16	18.7	175	50	90%hydrogen 10%water
17	9.3	175	50	water
18	9.4	175	50	hydrogen
19	1.0	175	50	hydrogen
20	8.3	175	50	hydrogen
21	8.3	70	20	hydrogen

2.3.4.2. Operating parameters, capital costs

In Table 19 and Table 20, the plant operating parameters, the feedstock and capital cost are given.

TABLE 19. FINANCIAL AND OPERATING SPECIFICATIONS

Technical operating parameters and specifications	
Operating capacity factor (%)	90.0
Plant design capacity (t of H_2/day)	815.61
Plant output (t/day)	734.05
Plant output (t/year)	267 929.85
Financial input values	
Financial data for reference year	2005
Assumed plant start-up year	2030
Plant construction period (years)	3
Capital spending for construction during first year (%)	25
Capital spending for construction during second year (%)	45
Capital spending for construction during third year (%)	30
Plant start-up time (years)	1
Life of plant and analysis period (years)	40
Depreciation duration (years)	20
Depreciation method	Modified accelerated cost recovery system
Equity financing (%)	100
Fixed operating costs throughout start-up period (%)	100
Revenues during start-up (%)	50
Variable operating costs during start-up (%)	50

TABLE 19. FINANCIAL AND OPERATING SPECIFICATIONS (CONT.)

Financial input values	
Plant decommissioning costs (% of depreciable capital investment)	10
Plant salvage value (% of total capital investment)	10
Rate of inflation (%)	1.90
After-tax real internal rate of return (%)	10
State taxes (%)	6
Federal taxes (%)	35
Total tax rate (%)	38.9
Working capital (% of yearly change in operating cost)	15

TABLE 20. BASE REFERENCE CAPITAL, FEEDSTOCK AND OPERATING COSTS

Total capital costs (million USD)	988.84
Total fixed operating cost per year (million USD)	55.94
Total variable operating costs (million USD/a)	730.88
Total utility costs (million USD/year)	3.16
Feedstock - industrial electricity price (USD/kWh)	0.13
Feedstock - total cost of electricity per year (million USD/a)	727.72
Feedstock - deionized water price (USD/gal)- (usage 2.3609 gal/1 kg H_2)	5×10^{-3}
Feedstock - process water cost per year (million USD/a)	3.16

2.3.4.3. Levelized cost of hydrogen

Table 21 shows the cost distribution and the total levelized cost of hydrogen for the base case. It can be seen from this table that the large cost of hydrogen is the feedstock cost, which stems primarily from the electricity price.

Because they make it easier to compare the effects of one variable (or uncertainty) on the output (value) of an independent variable, the tornado charts are frequently used in sensitivity analysis. They can be useful as representations for comparisons.

Figure 18 shows the tornado chart depicting the variations in feedstock consumption and operating capacity factor.

TABLE 21. SPECIFIC ITEM AND LEVELIZED COST FOR HYDROGEN FROM SOEC ELECTROLYSER PLANT

Cost component	**Cost contribution (USD/kg)**	**Percentage of hydrogen cost**
Capital costs	0.77	26.0%
Decommissioning costs	0.00	0.0%
Fixed O&M	0.22	7.4%
Feedstock costs	2.90	66.1%
Other raw material costs	0.00	0.0%
Byproduct credits	0.00	0.0%
Other variable costs (including utilities)	0.01	0.4%
Total	**3.90**	

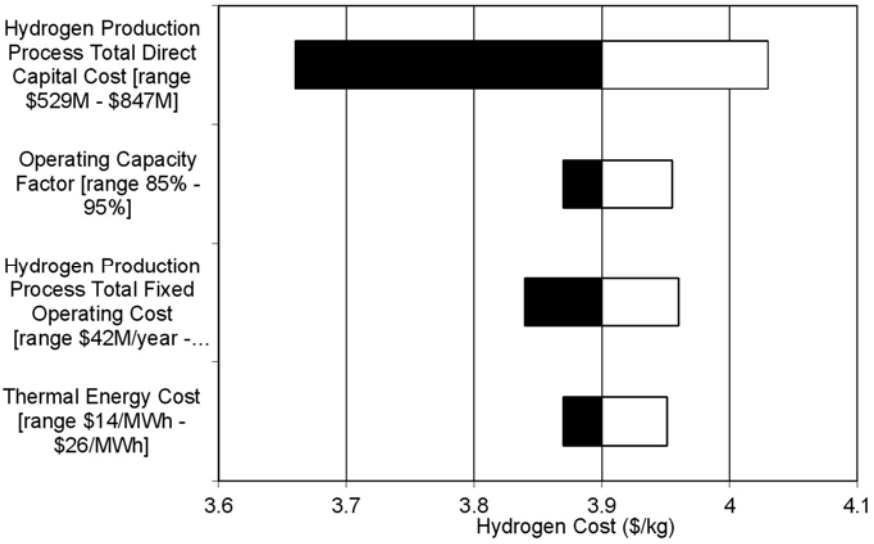

FIG. 18. Tornado chart of cost distribution for hydrogen production using HTSE.

2.3.5. The effects of scaling for hydrogen production cost with nuclear plant

2.3.5.1. Economies of scale for nuclear power plants

Following demonstration reactors, several commercial reactors were built in 1950s and early 1960s. Most of these reactors had capacities ranging from 250–500 MWe each. Similar to conventional power plants, larger sized reactors were built since 1960s in the power range of 1 GWe, assuming large size will be economic. But these large reactors turned out to be more expensive. Several reasons were attributed for this increased cost for large reactors. One was the industry overestimation of the scaling effect, which led to an inefficient over increase in unit size over time. Another reason was related to the increasing of construction durations for large reactors and escalation of costs. Unlike conventional power plants, the NPPs require large capital investment in construction. As large reactors have major site requirements for the containment building and auxiliary systems, any construction delay would result in an escalated cost.

In the case of SMRs, the major components of the reactor such as the pressure vessel, the containment vessel, and the power conversion turbine systems can be factory manufactured and shipped to the site for installation. This is expected to reduce the construction time and to eliminate the construction delays. The scaling of economy for power plants is typically done by considering the ratio of the power for the two sized plants (small and large), and relating it to the ratio of the associated overnight capital costs:

$$\frac{C_S}{C_L} = f(P_S/P_L) \tag{21}$$

where P and C are power and overnight capital costs, subscript S and L refer to small and large reactors. If one assumes that the SMR and large nuclear reactor have similar technology, then the expected cost of the SMR can be related to that of the large reactor. The IAEA has proposed a scaling relation to predict the first-of-a kind cost for an SMR, given by the following equation [71]:

$$\frac{C_{SMR}}{C_{NPP}} = \left(\frac{P_{SMR}}{P_{NPP}}\right)^{n-1} \quad (22)$$

where C_{SMR} and C_{NPP} indicate the cost for the SMR and large NPP respectively, and the power ratings, P_{SMR} and P_{NPP} are related through n, a scale factor. The applicability of the empirical scaling factors to a future SMR design will depend on its similarity to existing technology. Several studies to estimate the scaling factor n for NPPs have been carried out. These studies indicate the scaling factor varied from n=0.25 to n=1, where n=1 implies no scaling effect. One study [71] used n=0.6 as a median value for 250 MWe SMR, and another study [72] used midpoint value of n=0.55 for 10 MWe micro reactor using base large reactor of 1000 MWe.

Figure 19 illustrates the cost of first-of-a-kind SMR as function of the SMR power, based on the large-scale Westinghouse AP1000 reactor with an overnight capital cost of 5500 USD/kW.

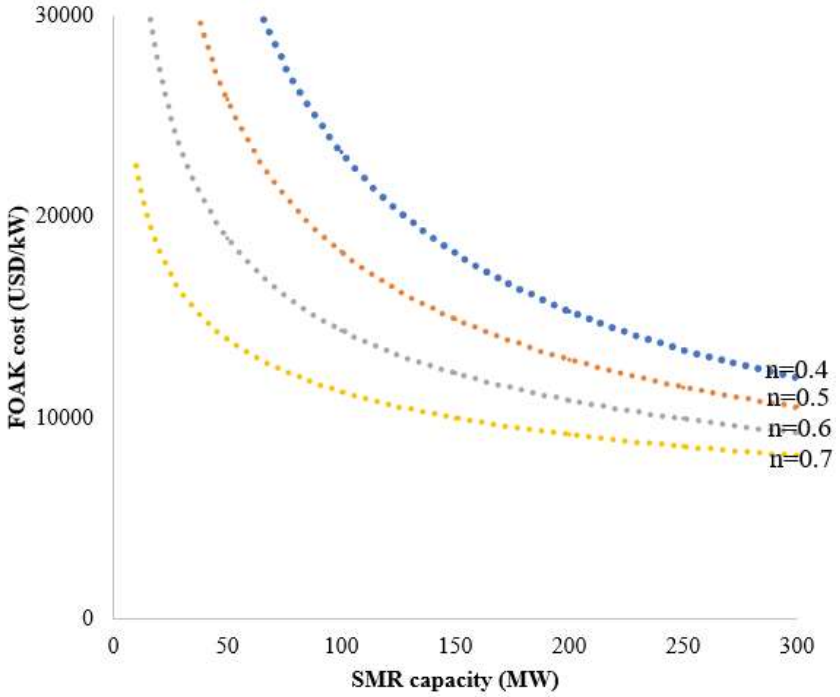

FIG.19. The cost of first-of-a-kind SMR as function of SMR power for different scale factor n.

2.3.5.2. Levelized cost of electricity of SMRs and large nuclear power plants

Conventional nuclear power being large in size has advantage of economies of scale in comparison with SMRs. However, SMRs will enable the manufacture of modular components in a factory setting, thus reducing associated costs. Nuclear power plants are capital cost intensive; fuel, and O&M costs are relatively lower. Typical estimated combined O&M and fuel costs are in the 29 USD/MWh to 42 USD/MWh range. From the experience with the AP1000 plant construction, the conventional large sized power can be a deterrent to the electricity price in a competitive market. This has been found to be due to the large capital cost upfront, resulting in considerable difference in the levelized cost of electricity (LCOE) for the new large scale NPPs [73].

The LCOE ranges between 118 USD/MWh and 192 USD/MWh for the unsubsidized power, and after-tax internal rates of return of 5.4% and 9.2%, respectively. The comparison of the conventional nuclear power cost at the low and high end is provided in Table 22, based on the Lazard data [73]. These costs for new-build NPPs contrast with current operating nuclear reactor costs.

A study conducted by the Nuclear Energy Institute [74] indicated combined costs of O&M and fuel costs ranged between 29 USD/MWh and 42 USD/MWh, with an average of 32 USD/MWh. The fuel cost for large reactors do not have much impact on LCOE. The data from the Nuclear Energy Institute [74] reveal that costs of the fuel are near 6–7 USD/MWh lower than the Lazard values [73], shown in Table 22.

TABLE 22. COST RANGE (USD/MWH) OF LARGE SCALE NPPS FROM THE LAZARD DATA COST

Cost type	**Low end**	**High end**
NPP capital cost (USD/MWh)	91	162
Fixed operations and maintenance costs (USD/MWh)	15	17
Variable operations and maintenance costs (USD/MWh)	4	4
Fuel cost (USD/MWh)	9	9
Electrical energy cost (USD/MWh)	119	192

The study conducted by the Massachusetts Institute of Technology (United States of America) [75] provided an estimate of capital costs in the range of 5.2–6.1 billion USD for advanced reactors, at conceptual and pre-conceptual design stage with power range from 2200 MWt to 3400 MWt as shown in Table 23. The capacity factors were estimated uniformly across reactor types at 90% according to the study.

TABLE 23. CAPITAL COSTS WITH INTEREST FOR ADVANCED REACTORS (BASED ON DATA FROM [75])

Reactor	Size (MWt)	Total Cost (mil. USD)	USD/MWh
HTGR	4 × 600	5200	118
Large fluoride-salt reactor	4 × 840	5600	118
SFR	3400	5200	116
Fluoride-salt reactor with nuclear air-Brayton combined cycle	12 × 242	5400	135
MSR	2275	6100	120

2.3.5.3. Hydrogen production technologies and cost of hydrogen

The nuclear reactor coupled to hydrogen production has the potential for higher overall energy use efficiency and better utilization of capital equipment. The reason for this is that the nuclear power plant can operate at full capacity and at the same time follow the load variation during the day. At night, when the electricity prices are lower or sometimes negative, the coupled NPP can use electricity and heat to generate hydrogen. This hydrogen can be stored and can be used to produce energy during the day when the price of electricity is higher.

In Fig. 20, the routes for nuclear hydrogen generation is dependent on reactor outlet temperature; the maximum temperature of the reactor coolant is also an important consideration.

Nuclear reactors have outlet temperatures that vary from approximately 300 to 950°C, depending on the design.

The current commercial LWRs have maximum temperature of around 330°C. These temperature ranges are not suitable of thermal driven chemical processes that need more than 600°C.

Advanced reactors such as sodium cooled fast reactors and molten salt reactors have higher outlet temperatures, up to 900°C. The hydrogen production scheme is determined by the outlet temperature of the reactor.

Based on studies such as [76], Fig. 21 shows the process diagram for each hydrogen production technology with nuclear heat and electricity, illustrating the energies involved and the reactor type, temperature, and the hydrogen yield from each process.

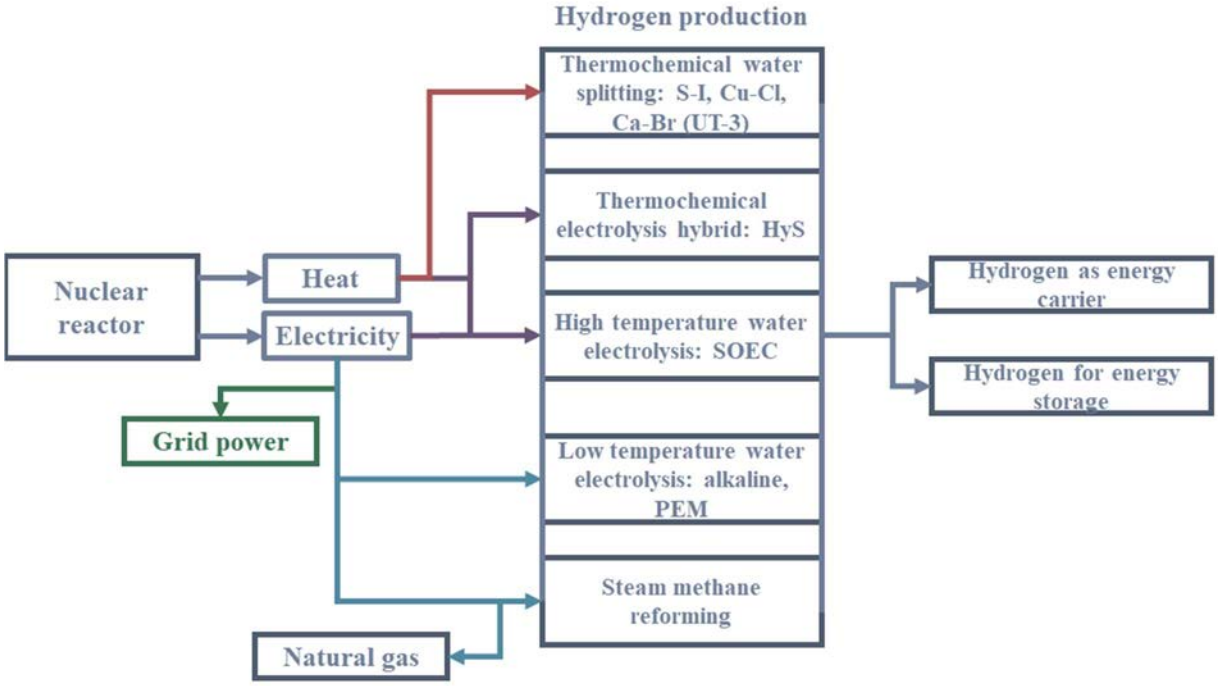

FIG. 20. Nuclear hydrogen production technology.

Table 24 shows a range of cost per unit kg of hydrogen produced based on low or high temperature electrolysis and various thermochemical processes: S-I, calcium bromide (Ca-Br) cycle, HyS, and Cu-Cl cycle. The hydrogen generated form thermochemical processes is expected to be lower than the hydrogen generated from electrolysis because the cost of electricity is higher than the cost of heat.

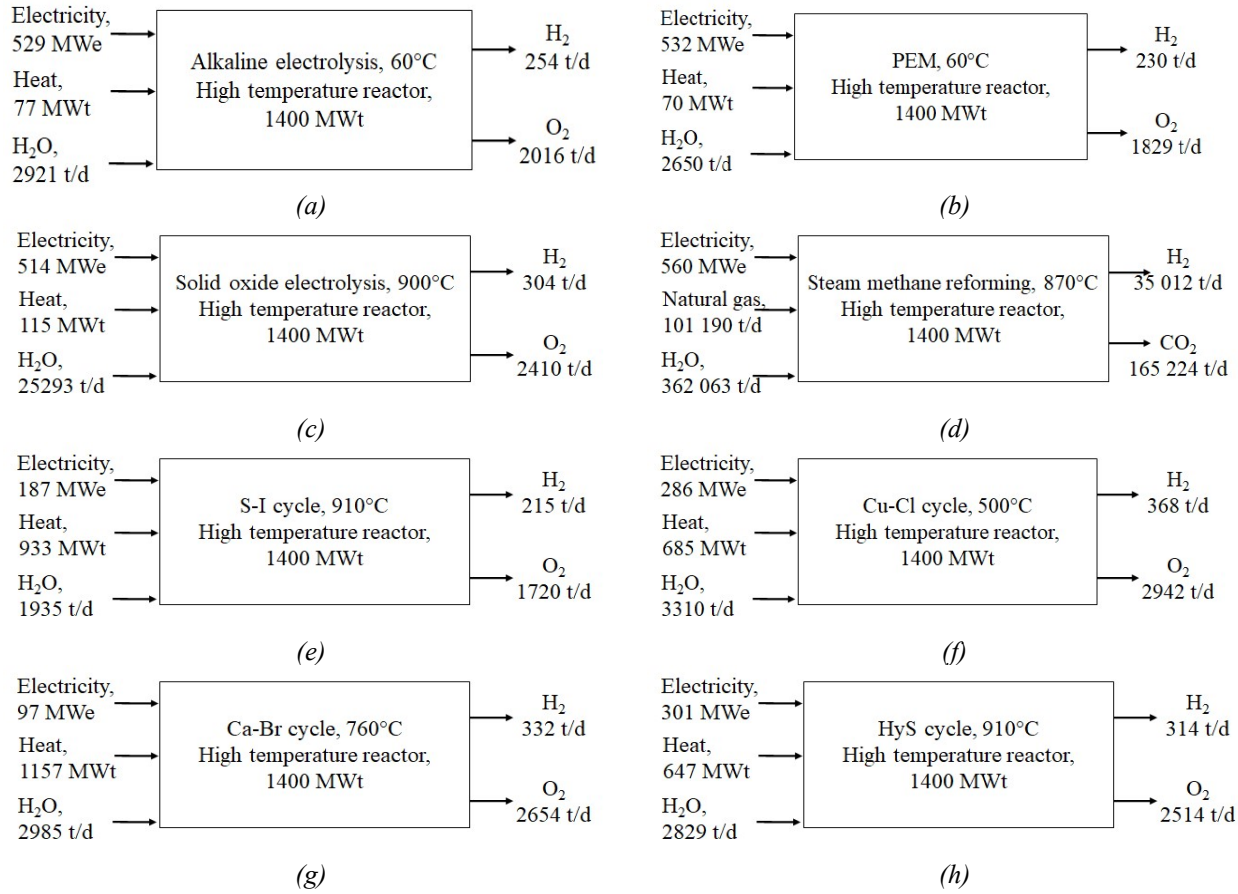

FIG. 21. Process flow diagrams for nuclear hydrogen system.

TABLE 24. UNIT COST FOR VARIOUS NUCLEAR HYDROGEN SYSTEM TECHNOLOGIES

	Alkaline	PEM	SOEC	Steam methane reforming	S-I	Ca-Br	HyS	Cu-Cl
T (°C)	60–80	30–90	700–900	870	710–910	760	710–910	500
H_2 production cost (USD/kg)	5.92	3.56–5.46	2.24–3.73	1.54–2.30	2.18–5.65	7.06	2.29–6.27	2.36–3.86

2.4. TECHNOLOGY READINESS (JAPAN ATOMIC ENERGY AGENCY)

This section details on the state of the art of the technology readiness for the hydrogen production in a hybrid energy system and using direct coupling with the high temperature reactor, based on the research conducted in Japan.

2.4.1. Study of net-zero hybrid energy system including nuclear hydrogen production

The Japan Atomic Energy Agency (JAEA) participates in a national nuclear energy system development project in collaboration with; the University of Tokyo, Institute of Energy Economics Japan, JGC Corporation, and Mitsubishi Heavy Industries. Funded at 1.4 million USD for a period of 2021 to 2024, the project studies a net-zero energy supply and demand system for Japan for the future period of 2030–2100, considering the technology options

including advanced nuclear reactors and production methods to be developed and deployed over the period.

Nuclear reactors of various types and sizes (SMRs and large LWRs) are considered together with renewables (wind, solar, biomass, and hydro) and fossil fuels with carbon capture and utilization. Hydrogen production based on nuclear and from the other sources are investigated.

The goals of the study are as follows:

— Study net-zero best mix scenarios in terms of grid resilience, supply cost, and fuel sustainability of energy technologies (nuclear, solar, wind, hydro, geothermal, and fossil fuels), integrated storage and intermediate products, battery, heat storage, hydrogen production, and synthetic fuel with carbon capture and utilization.
— Understand the roles of various types of nuclear reactors, considering their performance capabilities and limitations of fuel cycle sustainability, flexibility of load following, temperature range, thermal efficiency, and production costs, in the various net-zero best mix scenarios.

The study models the integrated energy system shown in Fig. 22 with electricity grids (including up to 400 transmission lines and 300 substation notes nationwide) and energy demands (for electricity, heat, hydrogen, synfuel) at local, regional, and national levels.

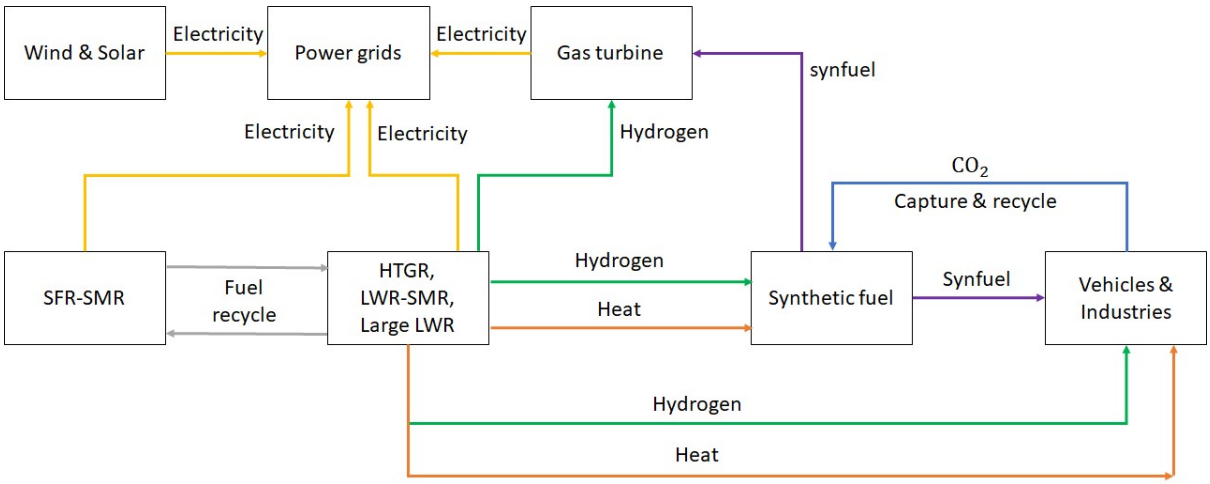

FIG. 22. Modelling of hybrid energy system including nuclear hydrogen production.

While many case studies have been performed by the model simulation and significant findings obtained, only one case study is reported in this publication. The case evaluates the economic values of nuclear power and hydrogen supply over a total of eight energy mix scenarios given in Fig. 23. The large LWRs and SMRs are used for base load power generation, while fast reactors and HTGRs together with fossil fuels and synfuel (ammonia produced from hydrogen) for variable power generation to compensate for intermittent wind and solar. The cases assume various methods of hydrogen supply to meet the hydrogen demands by fuel cell vehicles and hydrogen-based steelmaking. As seen in Fig. 24, the hydrogen is sourced from imported hydrogen, reforming from biomass or natural gas (with carbon capture and storage), and HTGR hydrogen co-generation or HTGR dedicated to hydrogen production.

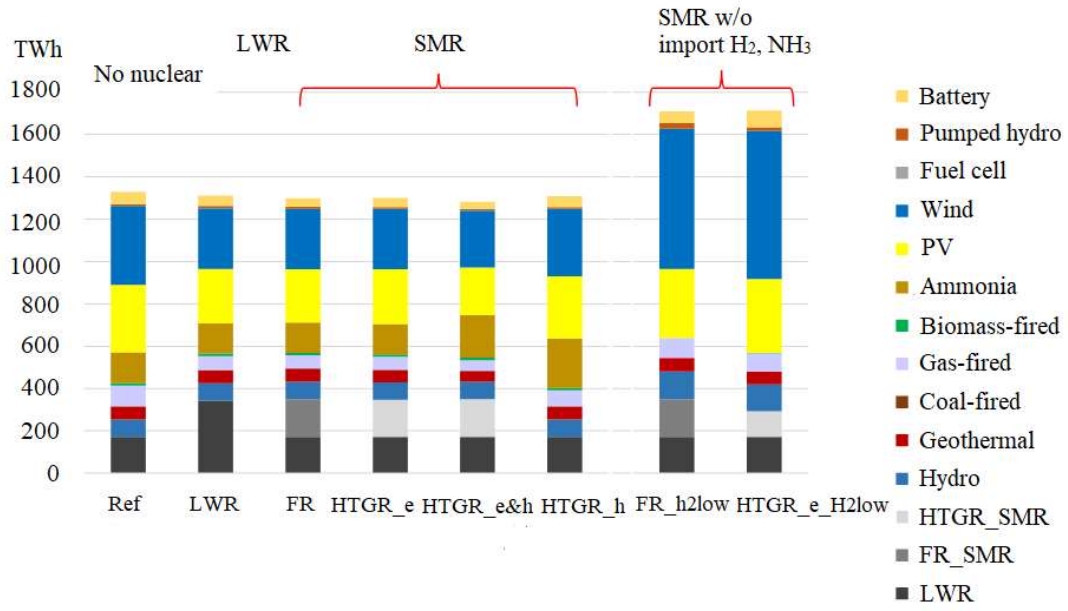

FIG. 23. Scenarios of energy supply mixes including HTGR-produced hydrogen.

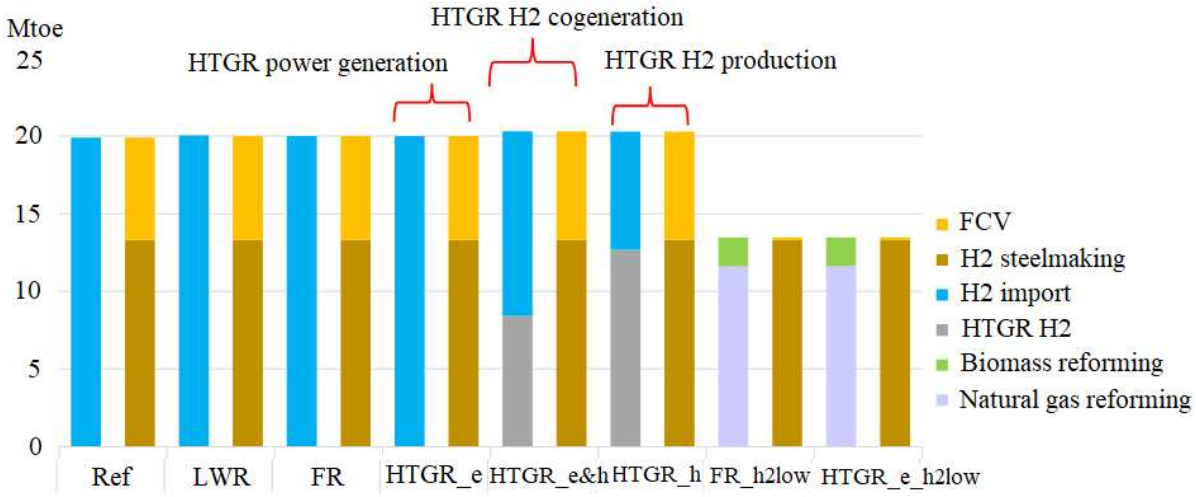

FIG. 24. Hydrogen supply sources (import, fossil and HTGR) and demand (fuel cell vehicles, steelmaking).

The major findings drawn from the case study of the eight scenarios are as follows:

— Nuclear system should be deployed until the upper set limits-as the electricity sales exceed the production costs for all reactor types as seen in the last 3 scenarios from the left of Fig. 25. Suppression of deployment rate for nuclear system would increase the total energy system cost.
— Under the condition of large penetration case of renewables, economic value of SMRs (fast reactor, HTGR) will significantly increase, as seen in the 2 scenarios on the rightmost side of Fig. 25. Deployment of SMR with load following capability will decrease the necessity of batteries.
— HTGR offers comparable economic values when used for standalone power generation and cogeneration of power and hydrogen as shown in Fig. 25.

— Due to the flexibility of cogenerating two variable products of electricity and hydrogen following demands, the economic value of HTGR for cogeneration significantly increases from that of the HTGR dedicated to hydrogen production only.

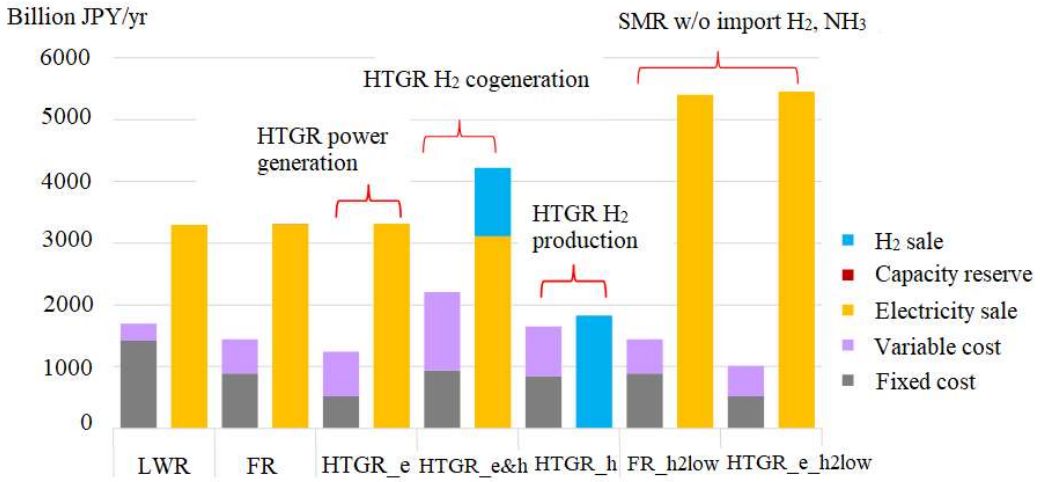

FIG. 25. Economics values of nuclear power and nuclear hydrogen.

2.4.2. Test plant of simulated nuclear hybrid energy system including hydrogen production

JAEA is conducting a national project, in collaboration with Mitsubishi Heavy Industries and JGC Corporation, to develop an electrically heated simulated-nuclear hybrid energy test plant, to demonstrate the integrated energy system and related equipment technologies described in Section 2.4.1. During the first phase funded at 1.5 million USD for a period of 2021–2023, the project will complete the design of the test plant schematically shown in Fig. 26. The plant consists of:

— Nuclear reactor simulator electrically heated at 5 MWt;
— Helium circulation loop with intermediate heat exchanger for hydrogen production and heat storage;
— Helium gas turbine power generator set rated at about 1 MWe;
— Hydrogen and heat production systems;
— Heat storage system (molten salt);
— Renewable energy system.

The first phase will complete the following development:

— Pre-construction plant design.
— System operation dynamics and safety analysis code, which will be validated during the test plant operation and made available to support the design and licensing of future commercial systems.
— High-speed communication and control system consisting of internet of things and digital twin. The system will be developed to be capable of monitoring the safety and assisting in the control of nuclear plant operation, while optimizing the performance and cost of demand and supply among the various subsystems of the hybrid energy system.

The second phase expected to begin in 2024 will construct the test plant and perform the tests.

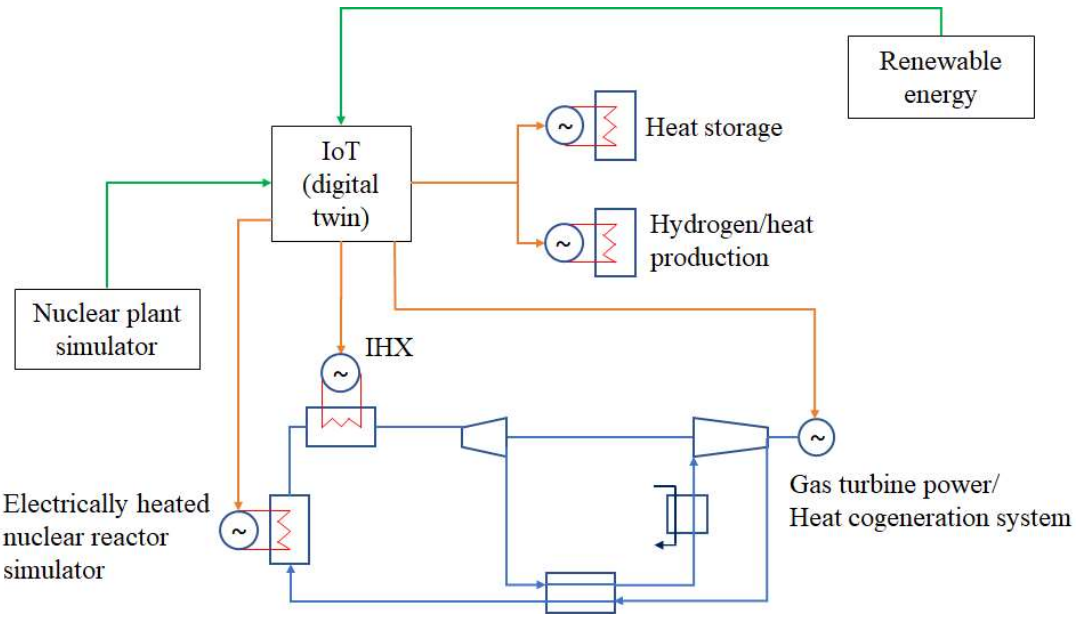

FIG. 26. Test plant of simulated nuclear hybrid energy system.

2.4.3. Nuclear hydrogen production plant coupled to the high temperature test reactor

A third ongoing national project is coupling of a hydrogen production system to the existing high temperature test reactor (HTTR) in JAEA. The project, which runs during 2022–2029 with the 2022 year funding of 9 million USD, will develop the heat transport coupling technologies; including high temperature isolation valve, and helium circulating loop and will license, and demonstrate nuclear hydrogen production using the high temperature heat provided by the HTTR. As illustrated in Fig. 27, a natural gas steam reforming system is connected to the HTTR through a helium circulating loop.

The high-temperature heat of the HTTR primary helium is transferred to the secondary helium gas circulation loop via an intermediate heat exchanger. The secondary helium gas piping penetrates the reactor containment vessel and the reactor building, supplying the nuclear high temperature heat to the steam reformer to produce hydrogen.

The project aims to achieve the following objectives:

- Development of high-temperature isolation technologies as shown in FIG. 28, including isolation valve, helium piping, and helium gas circulator, to provide safety isolation between the reactor and hydrogen production plant in case of emergency.
- Development and validation of a plant simulator to assist in control design and operator training of future commercial HTGR hydrogen production systems.
- Demonstration of licensing application and approval of nuclear hydrogen production with Japan`s Nuclear Regulation Authority.
- Demonstration test of nuclear hydrogen production from the HTTR.

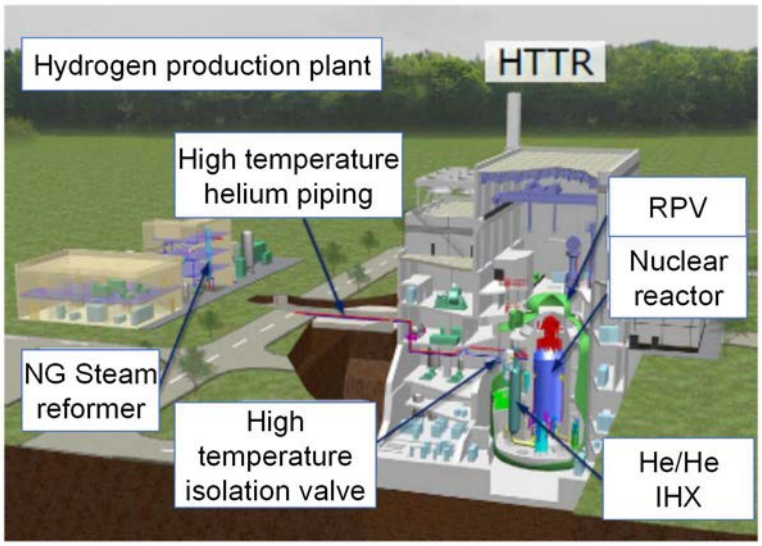

FIG. 27. HTTR nuclear hydrogen production test plant project.

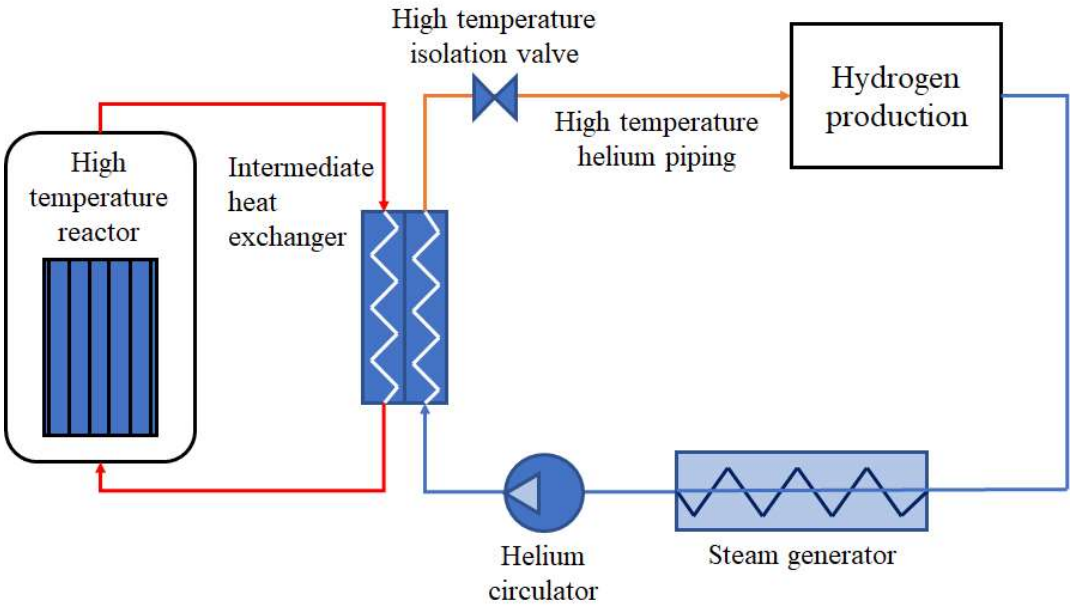

FIG. 28. Coupling scheme of hydrogen production to the HTTR.

2.5. REVIEW OF HIGH-TEMPERATURE REACTOR FACILITIES DESIGNED IN RUSSIAN FEDERATION WITH APPLICATION FOR HYDROGEN PRODUCTION (NATIONAL RESEARCH CENTER KURCHATOV INSTITUTE, RUSSIAN FEDERATION)

Several Russian HTGR designs were reviewed for their potential for hydrogen production. HTGR technology was developed in Russia since 1970's in the frameworks of the hydrogen energy concept. Projects included the small and medium power units with modular principles and fuel technologies based on micro particles dispersed in the pebbles or compacts. Table 25 shows the main features of the HTGR projects developed in the Russian Federation.

TABLE 25. MAIN FEATURES OF HTGR PROJECTS DEVELOPED IN RUSSIAN FEDERATION

Parameter	**VGR-50**	**VG-400**	**VGM**	**VGM-P**	**GT-MHR**	**MHR-T**	**MHR-100**
Thermal power, MWt	136	1060	200	215	600	600	215
Purpose	Electricity generation and radiation modification of materials	Generation of electricity and heat for production processes	Generation of electricity and heat for production processes	Heat generation for oil refinery	Electricity generation	Electricity and hydrogen production	Electricity, hydrogen production, heat supply
Fuel/ Enrichment, %	U/21%	U/6.5%	U/8%	U/8%	U/14%, Pu/93%	U/14.7%	U/14%
Coolant	Helium	Helium	Helium	Helium	Helium	Helium	Helium
Helium temperature at the core outlet, ºC	810	950	950	750	850	950	750-950
Status	Detailed design, 1978	Detailed design, 1987	Detailed design, 1992	Technical proposal, 1996	Preliminary design, 2002	Technical proposal, 2004	Technical proposal, 2008

Two designs, MHR-T with steam methane reforming and HTSE options and MHR-100 with steam methane reforming option, were chosen for further study due to availability of the necessary techno-economic data on them. MHR-T is a reactor design developed by JSC Afrikantov OKBM for an energy-technological complex, consisting of power and chemical-technological parts intended for combined production of electricity in the direct gas-turbine cycle and hydrogen (Fig. 29). The facility provides heat or steam and electricity, respectively.

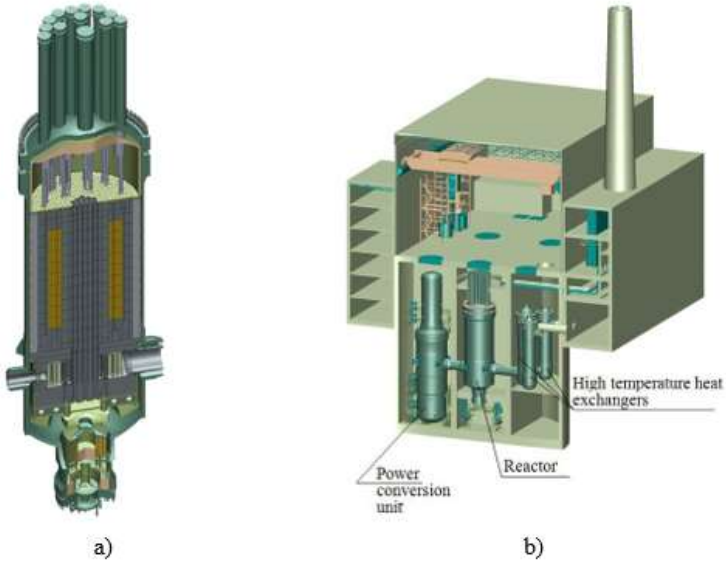

FIG. 29. MHR-T general view. a) the reactor; b) the energy-technological complex [66].

Steam methane reforming and high temperature solid oxide electrochemical processes are considered for hydrogen production as most competitive (Fig. 30). The technological complex consists of 4 units. Each unit includes reactor and chemical part [77].

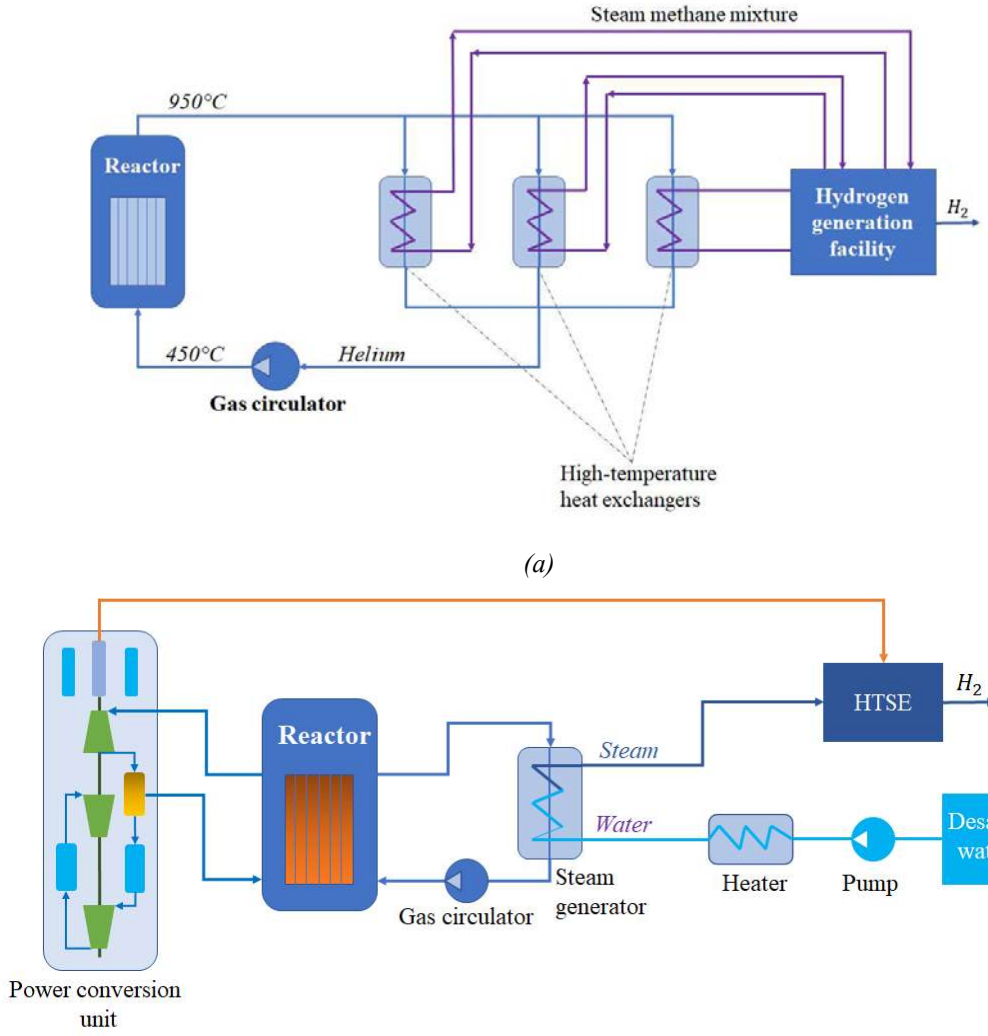

FIG. 30. Steam methane reforming (a) and HTSE (b) schemes of MHR-T options.

Main technical features of MHT-R with steam methane reforming and HTSE options are presented in Table 26 [63].

TABLE 26. TECHNICAL FEATURES OF MHT-R WITH STEAM METHANE REFORMING AND HTSE OPTIONS (ONE UNIT)

Thermal power, MW	600
Electrical power, MW	205.5
Thermal power for H_2 production, MW	160
Electrical power for grid, MW	175.5/0
Hydrogen production, t/year	100 000/54 050
Outlet coolant temperature, °C	950
Helium pressure, MPa	7.5
Fuel element type	Compact
Average fuel enrichment, %	14.7
Fuel lifetime, days	900

HTGR-200 is a latest design, developed by JSC "Afrikantov OKBM" based on MHR-100 design for power generation and technological purposes, including hydrogen production.

HTGR-200 through an intermediate circuit is coupled with a chemical part producing hydrogen by method of steam-methane reforming with oxygen (Fig. 31).

In the selected case, the nuclear facility provides only high-temperature heat for the chemical part. The energy technological complex consists of 4 units. Each block includes reactor and chemical part.

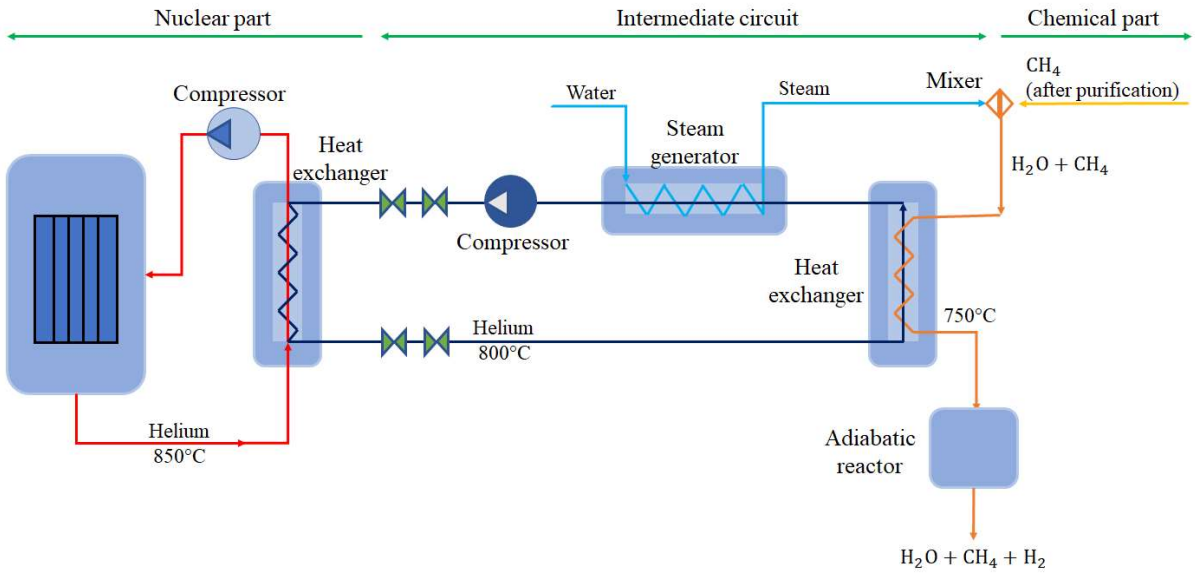

FIG. 31. Scheme of HTGR-200 with steam methane reforming option.

Main technical features of HTGR-200 with steam methane reforming option are presented in Table 27 [62].

TABLE 27. TECHNICAL FEATURES OF HTGR-200 WITH STEAM METHANE REFORMING OPTION (ONE UNIT).

Thermal power, MW	200
Electrical power	Not generated
Hydrogen production, t/year	110 000
Consumed outside electrical power, MW	48
Outlet coolant temperature, °C	850
Helium pressure, MPa	5
Fuel element type	Compact
Average fuel enrichment, %	14
Fuel lifetime, days	800

3. STUDIES OF PROMISING HYDROGEN TECHNOLOGIES FOR UPSCALING

3.1. THERMOCHEMICAL CYCLES TECHNOLOGY (BHABHA ATOMIC RESEARCH CENTRE, INDIA)

This section illustrates the details of the sulphur-iodine thermochemical cycle.

3.1.1. Sulphur-iodine thermochemical technology

The closed loop S-I process is a high temperature heat based pure thermochemical cycle. It is one of the most efficient thermochemical processes [78]. It contains three chemical reactions and is considered suitable for large-scale cost-effective production of clean hydrogen. The S-I thermochemical cycle was developed at General Atomics. Subsequently, researchers focused on studying important features of this cycle, such as catalysts, phase separations, materials, engineering aspects of the cycle, and economics.

In 1977, the United States Department of Energy, through General Atomics, started the design and construction of a bench-scale unit to perform the S-I thermochemical cycle as one continuous operation. The purpose of the bench-scale work was to study the actual processing steps and their interactions by conducting key continuous flow reactions and separation steps. The purpose of the study also included fluid handling, key operation behaviour, and the effects of incomplete physical separations and possible side reactions [79].

The innovative high temperature reactor is under design in India. The 20 MWt molten salt cooled reactor is a pebble bed type and uses graphite as moderator. It is envisaged to be used for hydrogen production using S-I process. A part of the heat from the reactor will be converted to electricity using a high efficiency power conversion system to provide electrical heating to the SO_3 decomposition step, while other sections of the S-I process will be directly heated by the reactor.

The S-I cycle consists of the following reactions:

- Segment 1: Bunsen reaction (exothermic, at 20–120°C):

$$I_2 + SO_2 + 2\ H_2O \rightarrow 2HI + H_2SO_4$$

- Segment 2: Sulfuric acid decomposition (endothermic, at 800–900°C)

$$H_2SO_4 \rightarrow H_2O + SO_2 + 0.5\ O_2$$

- Segment 3: Hydroiodic acid decomposition (endothermic, at 300–450°C)

$$2HI \rightarrow H_2 + I_2$$

The Bunsen reaction generates two products as two phases. Under certain conditions, these phases are immiscible and can be separated readily. Sulfuric acid (H_2SO_4), also known as the top phase, is the lighter phase; and a denser aqueous solution of HI, H_2O, and I_2 (HIx) is the

lower phase. The two immiscible liquid phases are transferred to the succeeding sections for breakdown upon phase separation.

In segment 2, H_2SO_4 is concentrated and decomposes into SO_2, O_2, and H_2O at high temperature. The decomposition reaction is endothermic. Decomposed products are recycled to the Bunsen reaction. In segment 3, HI is distilled from HIx and decomposes into H_2 and I_2 at intermediate temperature. The decomposition reaction is endothermic. Iodine is recycled back to the Bunsen reaction.

There is no waste discharge in the S-I cycle and the components are transportable easily in gaseous or liquid form. All the chemicals utilized are recycled, and the process required only water and heat as an input. The heat sources that can deliver the heat for H_2SO_4 decomposition reaction which is a high-temperature reaction can be: a high temperature nuclear reactor, a solar tower, a coal- and natural gas-fired plant.

3.1.1.1. Sulphur-iodine process flowsheet

The Bunsen reaction is among the three primary reaction steps in the S-I process, and it can be regarded as the key phase since it's essential to the overall process's achievability, stability, and efficacy.

The Bunsen reaction is multiphase, reversible, and exothermic. The Bunsen reaction involves a complex and non-ideal phase and chemical equilibrium. It is challenging to understand the relative role of kinetics and mass transfer. Enhancement of purity of product phases, conversion and yield need a close understanding of the role of operating conditions like temperature, compositions, etc. Phase and chemical equilibria of this highly non-ideal reacting system is another challenging task [80]. Contacting scheme, reactor type, and size also have a severe bearing on reaction and product phase separation.

An enormous amount of flowsheet effort is achieved to describe the reaction environments and process flow details within the S-I cycle, through which determining the material performance can be obtained [81-83]. Developments in materials know-how can redefine the existing flowsheets, as improved materials will drive the reactions to be performed more resourcefully and extend equipment lifespan. Because of this, there will be a rise in the total cycle efficiency and a decrease in the cost of hydrogen produced. The energy details for various processes are discussed in [84].

3.1.1.2. The Bunsen reaction

The Bunsen reaction obtains the sulphur dioxide gas from the decomposition of sulfuric acid, and liquid iodine from segment 2. They are mixed with excess water to carry out a Bunsen reaction. Addition of excess iodine promotes the reaction products to form two immiscible liquid phases that can be divided into two streams through gravity separation. The lighter phase is H_2SO_4, and the denser phase is an HIx (mixture of HI, H_2O, and I_2).

3.1.1.3. Sulfuric acid decomposition

The sulfuric acid segment obtains diluted sulfuric acid from the Bunsen reaction and catalytically decomposes it into O_2, SO_2, and H_2O at highest temperature of the cycle [85]. The product gases from this reaction are then recycled to segment 1 and SO_2 is consumed in the

Bunsen reaction. First, the incoming acid is concentrated from 57 to 86 wt%. The sulfuric acid is initially given heat to raise the temperature up to 475°C for vaporization. At about 500°C, H_2SO_4 gas starts decomposing into H_2O and SO_3. In the next step, decomposition of SO_3 into SO_2 and O_2 is achieved by using a catalytic driven reaction at a temperature of 850°C [85].

3.1.1.4. Hydroiodic acid decomposition

The hydroiodic acid decomposition segment obtains HIx from the Bunsen reaction to produce hydrogen by decomposition of hydroiodic acid. The hydroiodic acid in the HIx feed stream is initially concentrated and decomposed into H_2 and I_2 [86]. There are several possibilities to achieve this concentration but most explored are: extractive distillation, and electro-electro dialysis or reactive distillation. These processes involve different reaction conditions and the chemicals used are different. Membrane separation of hydrogen is also a good option found in the literature [87].

Extractive distillation

Phosphoric acid is used in extractive distillation to separate HI and H_2O from HIx because, except for I_2, they are dissolvable in H_3PO_4. Additionally, H_3PO_4 causes the azeotrope of HI and H_2O to break down, which separates HI from the acid complex before it decomposes. This procedure consists of four steps: (1) iodine elimination, (2) HI distillation, (3) phosphoric acid concentration, and (4) HI breakdown. Phosphoric acid is mixed with the HIx from the Bunsen reaction, and this results in the creation of a liquid mixture of I_2 and HI + H_2O + H_3PO_4 as two separate phases.

The iodine is removed by gravity and recycled to the Bunsen reaction. The lighter HI–H_3PO_4 acid compound is sent to the distillation column for performing HI distillation as shown in Fig. 32. HI gas is removed from the mixture of HI + H_2O + H_3PO_4 and is flowed on to the decomposition reactor for HI decomposition in the existence of a catalyst to produce iodine and hydrogen. Using boilers and vacuum recompression, the phosphoric acid that is water-diluted in the distillation column is concentrated to 96% by weight from 87% by weight.

To restart the extraction process, concentrated phosphoric acid is combined with the inward HIx input.

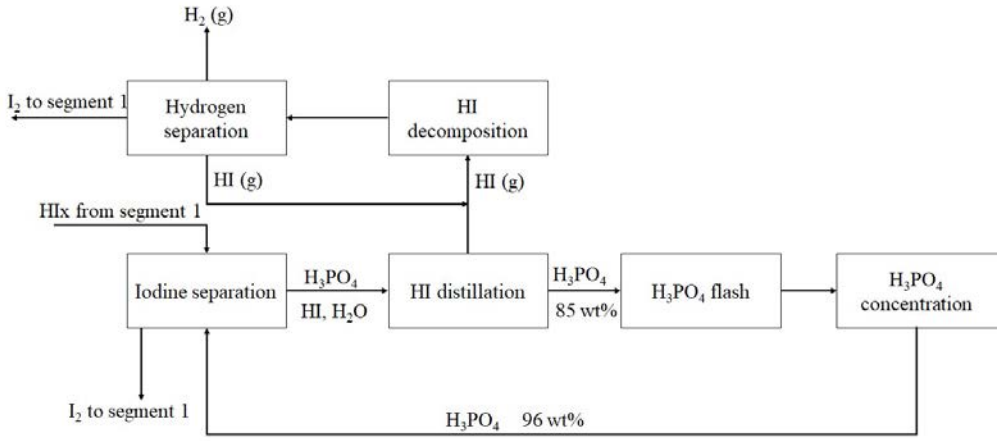

FIG. 32. Extractive distillation flowsheet.

Electro-electro dialysis

Among the processes recommended for the pre-concentration of the HIx solution prior to actual distillation is the electro-electro dialysis operation. A catholyte's HI molality can rise above quasi-azeotropic ones thanks to the electro-electro dialysis process, which includes I_2/I^- redox reaction at the electrodes, and a proton permeation selectivity via cation exchange membrane. The redox process of I_2/I^- happens at both the anode as well as the cathode. The cation exchange membrane allows H^+ to pass from anolyte to catholyte unto carrying an electric charge, while I^-, the counter ion, passes via the opposite way.

Reactive distillation

In principle, reactive distillation is a less complex process than extractive distillation, but it needs to be tested in practice. There are some important distinctions between the distillation types (extractive and reactive). The HIx azeotrope is initially unresolved, unlike the extractive procedure, leading to a similar constitution in the vapor and liquid phases. Next, pressure is required for reactive process. In this process, distillation of azeotropic mixture of HIx is done under pressurized column and the HI decomposition within the HIx vapor stream is achieved catalytically, giving the gas mixture of HI, I_2, H_2, and H_2O. At the reboiler section of the column, the HIx is heated to around 310°C. The distilled HIx (HI, I_2, and H_2O) vapor flows over a catalyst bed at the top of the reactive column as shown in Fig. 33, and HI inside the stream of vapor is converted into H_2 and I_2 gases at 300°C. Unreacted HI, I_2, and H_2O are condensed at the top of the column, and the resulting liquid is refluxed back into the column.

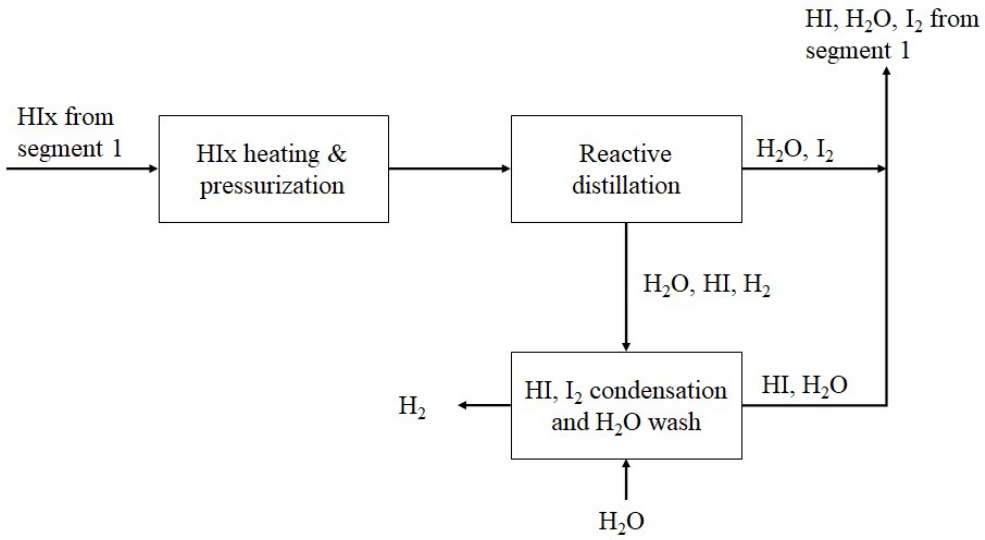

FIG. 33. Reactive distillation flowsheet.

3.1.2. Studies on the sulphur-iodine cycle

In Ref. [88] the analysis of efficiency and entropy production of the Bunsen reaction is described. Theoretical calculations are carried out to study the efficiency of the Bunsen reaction. The study determined that the selection of operating conditions for the Bunsen reaction is integrally connected to the total process flowsheet. But the study is not backed by experiments to assure the calculated efficiencies of Bunsen reaction are correct.

In Ref. [89] the Bunsen reaction at 20°C in a wide range of H_2O, I_2, and HI concentrations at ambient temperature in the bench-scale is described. The study has adopted a lower temperature because of the ease in handling chemicals at room temperature in the apparatus. Experiments are conducted by passing SO_2 along with N_2 gas to the H_2O-I_2-HI mixture which reacts rapidly. The study has discussed the role of the excess of H_2O and iodine in Bunsen reaction on the formation of a homogeneous solution of HI and H_2SO_4 at lower concentrations of the former chemicals. Further, the study has obtained the correlation between the molar fraction of H_2O, for HI-H_2SO_4-H_2O system and density at 20°C under conditions of iodine saturation. The conclusion of the study was that, at a molar fraction of feed water below 0.92, two phase separation occurs. Decreasing the amount of water in the feed had led to an increase in HIx phase density. However, the density of the sulfuric acid phase remained constant at 1.4 g/cm^3.

In Ref. [90] a conceptual design of the Bunsen reactor is discussed. The design of the Bunsen reactor has incorporated reaction cum separation in a single counter-current reactor. The design has considered the separation of SO_2 and O_2 before the introduction into the Bunsen reactor.

Reference [91] presents basic experimental studies carried out using a glass reactor to characterize the Bunsen reaction between temperatures of 30–120°C and different initial compositions. Apart from the Bunsen reaction, purification of the HIx phase by removal of H_2SO_4 and residual SO_2 is also discussed in their work. Also, iodine removal from the sulfuric acid stream is studied. A continuous lab-scale setup to study the Bunsen reaction and subsequent purification of the product acids is carried out.

Variations in temperature and iodine concentration were used in the study presented in Ref. [92] to perform the Bunsen reaction. By saturating HI-I_2-H_2O solutions with gaseous SO_2, the operation temperatures in the research were adjusted from 30°C to 120°C, and the iodine composition altered within 0.22 and 0.57 mole fraction.

The purpose of the study is to scrutinize the iodine concentration effect and the temperature on the Bunsen reaction. Temperature and dissolved iodine are dependent, as the solubility of iodine depends on temperature. The solubility of iodine defines the occurrences of side reactions below a lower bound. It is observed in the study that at temperatures lower than 35°C, the separation of the two phases is quite slow unless a great excess of water is adopted. Besides that, an increase in temperature and iodine concentration leads to a decrease in the solubility of the sulphur dioxide and reaction conversion but leads to a decrease in contamination of sulphates in the HIx phase, and thus improving the purification of acid.

Reference [93] presents the study of the characteristics of the Bunsen reaction with the reactor shape and temperature, by using a counter-current continuous reactor. Experiments were carried out at ~90°C, with the molar ratio of I_2/HO varying from 0.250 to 0.450. The length to diameter ratios of a reactor was set at three different conditions those are 9.25, 13.71, and 21.67. The author studied the semi-batch Bunsen reaction initially, and then conducted the continuous Bunsen reaction at the same conditions of semi-batch experiments.

In Ref. [94] the Bunsen reaction is conducted using a continuous counter-current reactor at the pressurized condition to investigate the characteristics of phase separation of Bunsen reaction. The results of the study indicated a steady-state operation. This is inferred from the constant composition of Bunsen products at the outlet. The conversion of the reactant increased at the pressurized condition because of increased SO_2 solubility in water with pressure.

Reference [95] presents a study of the Bunsen reaction to obtain the effect of O_2 on the Bunsen reaction by supplying SO_2–O_2 mixture gases in the presence of HIx solution. The experiments have been conducted at I_2 saturation points of respective temperature with SO_2 and SO_2–O_2 mixture gases. The study completed a series of the experiment at 60°C with O_2/SO_2 molar ratios in the range of 0.2–0.5, to find the role of the amount of O_2 in SO_2–O_2 mixture gases. The important conclusion of the study is that; the amount of impurities in each phase produced from the Bunsen reaction with the HIx solution was barely influenced by the O_2/SO_2 molar ratios.

In Ref. [96] the Bunsen reaction is studied using a counter-current continuous reactor; the Bunsen reaction and product separation steps are performed simultaneously, and the composition difference of each phase settled at the top and bottom of the reactor was examined. The process parameters are the molar ratio of I_2/H_2O, SO_2 feed flow, operating temperature. The study found that by maintaining steady feed flow and continuous product outflow, the concentrations remained steady even after 120 min of reaction time, demonstrating a steady-state process.

In Ref. [97] the effect of the initial HI amount in the feed solution and the operating temperature on the thermodynamics and kinetics of the Bunsen reaction are studied. The author found that increasing the initial HI concentration in the feed or temperature (30–85°C) resulted in amplification of the reaction kinetic rate, and this led to the faster formation of liquid-liquid separation as well as a short time to attain the thermodynamic equilibrium. The study obtained an over-azeotropic HI concentration in the HIx phase with feeding HI. The conversion of SO_2 lowered as the initial HI content and the temperature was increased.

Reference [98] presents a series of experiments conducted by charging the mixture of SO_2/N_2 in an iodine-water mixture in the temperature range of 63–85°C to study the kinetics and thermodynamics of the Bunsen reaction. The role of different operating parameters such as temperature, SO_2 flow rate, I_2 content, and H_2O content on the efficiency of SO_2 conversion and kinetic rate are reported.

Reference [99] describes the studies carried out on the Bunsen reaction to investigate the flow of SO_2, ratio of iodine and water in the feed. The study projected the Bunsen reaction mechanism given the kinetic characteristics. The results of the study showed that an increase in iodine amount and a decrease in water amount enhanced liquid–liquid equilibrium separation characteristics. The H_2S formation reaction has happened with the rise in water content and reduction in iodine content. The study has projected the ideal operating condition for the inlet SO_2 mole fraction >0.12 and initial I_2/H_2O molar ratio >0.284 on the experimental results, with a focus on improving the separation characteristics and preventing side reactions.

Reference [100] presents a study on a semi-batch Bunsen reaction. The study involves a parametric study of Bunsen reaction. Experiments are conducted in a Bunsen reactor of tubular construction at various pressures and temperatures with sulphur dioxide. The study detected that there is an increase in the overall reaction rate with pressure. The overall reaction decreases with an increase in temperature. Later studies have been performed with N_2 and SO_2, to comprehend the influence of gas film resistance on the conversion and overall reaction rate [101]. It was found that the Bunsen reaction rate has increased with an increase in operating pressure at a specific temperature, and the reaction rate has decreased with an increase in temperature for a specified operating pressure. The study concluded that the role of temperature

on reaction length or reaction rate is more dominant in comparison to the role of pressure on reaction rate.

Reference [102] presents the studies on the features of the Bunsen reaction with the usage of the HIx solution in a co-current continuous mode operation. The role of the operating variables such as feed flow rates of reactants, H_2O and I_2 feed compositions, temperature, and reaction volume on the Bunsen reaction is studied. The results of the study indicated that decreasing the I_2 feed concentration and increasing the H_2O feed concentration improved the extent of the Bunsen reaction. When the temperature increases, the purity of the Bunsen products is enhanced, but the SO_2 conversion is decreased.

Reference [103] presents the studies on the features of the Bunsen reaction at different operating conditions such as pressure, temperature, I_2, and H_2O feed concentrations. In the study, a mixture of HI, I_2, and H_2O is used as the reactant. The results of the study show that, when the pressure is increased, the degree of Bunsen reaction is improved.

The Bunsen reaction kinetics is explored in ref. [104] by comparing the pressure decrease of SO_2 gas with progress of reaction. The results of the study showed that the absorption amount of SO_2 in HI solution increases with the HI acid concentration and pressure of the SO_2, while the role of temperature on SO_2 absorption in HI solution is complex.

Reference [105] details on the study performed on a Bunsen reaction to determine kinetic parameters using the initial rate approach. By tracking the change in SO_2 pressure as the reaction progresses, the study carefully examined the impact of key parameters such as SO_2 partial pressure, I_2 concentration, agitation speed, as well as reaction temperature on reaction rate. The Bunsen reaction rates are found to be in 0.23 and 0.77 order with respect to SO_2 pressure and I_2 concentration using the initial rate analysis technique. A value of 5.86 kJ/mol was found for the activation energy, and a formula for the rate of the Bunsen reaction is also derived.

The Bunsen reaction was studied in Ref. [106] to identify the role of different operating conditions on purity of Bunsen reaction product phases. In order to determine the impact of various conditions of operation on the concentrations of the Bunsen reaction product mix, the Bunsen reaction was studied in a co-current reactor [107]. Tantalum tube and a stainless-steel jacket make up the tubular reactor, which has been used for Bunsen reaction experiments in the 50–80°C temperatures and 2–6 bar (g) pressure bands. Elevated mole fractions of HI in the HIx phase and H_2SO_4 in the sulfuric acid phase have been seen when SO_2 feed flow rate and pressure was raised. The mole fraction of HI in the HIx phase rose with temperature, whereas the mole fraction of H_2SO_4 in the sulfuric acid phase dropped; amount fraction of HI in the HIx phase was reduced by an increase in feed I_2/H_2O ratio and HIx feed flow rate; and the conversion of Bunsen reactants into products was enhanced by higher pressure.

3.1.3. Safety considerations on the coupling of the sulphur-iodine cycle with high temperature reactor

The following areas that are significant for safety were identified for coupling of the S-I cycle with the innovative high temperature reactor:

— Ni-Mo-Cr-Ti is the proposed material for a major portion of the heat transfer circuit. This material is not covered under the American Society of Mechanical Engineers

Boiler and Pressure Vessel Code[2]. Generation of high temperature mechanical strength data is required for this material, while considering the variability of heat, as well as the variations due to fabrication processes.

— Purification of both fluoride and chloride salts especially for removal of oxide and moisture impurities is essential to ensure corrosion free operation. In addition, development of online molten salt chemistry monitoring instruments is required.
— Effect of sudden load rejection arising out of unavailability of any of the heat exchangers, especially on the safety of the nuclear reactor needs to be investigated.
— The S-I plant contains hazardous chemicals such as SO_2, SO_3, H_2SO_4, HI, and I_2. During abnormal operations, these chemicals would leak from piping/components of process into atmosphere. The impact assessment of such leakages needs to be quantified during normal operation of the innovative high temperature reactor.
— The S-I plant produces hydrogen. The deflagration/detonation of hydrogen leaks needs to be quantified and further impact assessment to be done. Safety systems must be in place for safe shutdown of the innovative high temperature reactor and S-I plant.
— Coolants used in the reactor can be radioactive. Any leakages from the reactor system in the heat exchanger circuit results in activity spread in S-I process. Quantitative risk assessment needs to be carried out during such scenarios.

During emergency shutdown of the reactor the heat supply system gets affected in the S-I process. Under such scenarios, S-I process plant needs to be shutdown safely. Safe operation procedures need to be developed under such scenarios.

3.1.4. Sulphur-iodine thermochemical technology in Japan

This section details on the sulphur-iodine technology in Japan.

3.1.4.1. The sulphur-iodine process test facility

A closed cycle loop hydrogen production test facility seen in Fig. 34, interconnecting the production and decomposition processes of the three chemical reaction subsections of the S-I process has been constructed of off-the-shelf industrial materials – lining materials, metals and ceramics, and high temperature heat and corrosion-resistant components as shown in Table 28.

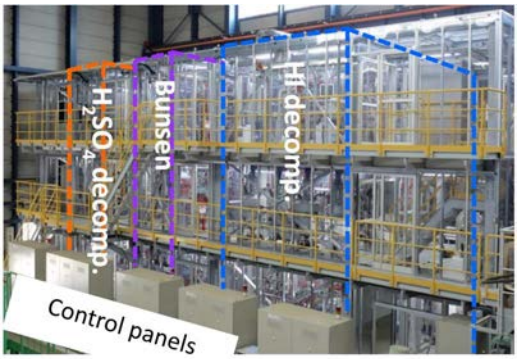

FIG. 34. Sulphur-iodine process test operational facility in JAEA (100 L/h).

[2] https://www.asme.org/codes-standards/bpvc-standards.

TABLE 28. STRUCTURAL MATERIALS OF THE HYDROGEN PRODUCTION FACILITY

H_2SO_4 decomposer	SiC ceramics
Heater tube of towers	SiC ceramics
HI decomposer and pipes	Nickle base alloy (Hastelloy® C-276)
HI concentrator (electro-electrodialysis cell, phenol resin impregnated)	Impervious graphite
Heat exchangers (polytetrafluorethylene impregnated)	Impervious graphite
Vessels and pipes (>100°C, gaskets: fluorine resin)	Glass-lined steel
Prevention of gas (H_2, SO_2) permeation	Glass-lined steel
Cooler	Glass-lined steel
Vessels, pipes and valves (<100°C, gaskets: fluorine resin)	Fluororesin-lined steel
Metering pump	Alumina ceramics
Pressure gauge (diaphragm)	Tantalum
HI concentrator (electro-electrodialysis cell)	Cation-exchanger membrane (Nafion®)
Pipes (N_2 and H_2O supply, H_2 and O_2 outlet)	

JAEA has achieved a closed loop automated continuous hydrogen production experiment at rates of up to about 100 L/h and for time periods of up to 150 h, not simultaneously. The facility dimensions are 18.5 m × 5 m × 8.1 m. The designed maximum temperature is 950°C while the maximum pressure is 0.5 MPa. The heating is done electrically. Important test data and knowhow obtained are being applied to improve the design and performance reliability of the components and to develop fluid and reaction control techniques necessary to achieve longer term operations.

At the trial runs, major technical issues such as fluid leakages through penetration of the process equipment and pipe clogging were identified [108]. As a countermeasure, the design of the HI solution pump has been revised to add a shaft sealing system to prevent the solidification of iodine. The revised design is shown to enable the stable delivery of the HI solution by the pump. In addition, the manufacturing quality of the thermocouple has been improved to prevent the leakage of the HI solution through the glass-lined sheath. Furthermore, a water removal mechanism of the HI section has been installed to adjust the HIx solution concentration during operation to suppress pipe clogging due to iodine precipitation. These countermeasure technologies are instrumental to continuously extend the operation of hydrogen production to 150 h at 30 L/h from 30 h at 20 L/h. Having performed these hydrogen production tests, the facility is inspected to assess the structural integrity, manufacture quality, and performance function of the chemical reactors, other equipment, and piping. The inspection has confirmed the prospect for practical use of the components made from industrial materials. Currently, improvement is being made on automatic process measuring and control system. This is being conducted through simulation. When completed, future tests will aim to ramp hydrogen production rates up to the rated hydrogen production capacity (100 L/h) of the facility.

3.1.4.2. Improved design for sulfuric acid decomposer

The improved design for the H_2SO_4 decomposer – a key equipment that carries about 60% thermal duty for the S-I process - has been performed by JAEA. The study is focused on two efforts. One is, development of a metal to replace the SiC, that is the choice of material for this equipment installed in the test facility. The availability of metal with acceptable corrosion resistant performance would significantly reduce the material and manufacturing cost for the equipment. The second effort is the conceptual study of commercial-scale design based on the new metal developed.

Corrosion resistance of several stainless steels and Ni-based alloys whose chemical compositions are modified from their existing ones were evaluated in the SO_3 decomposition gas environment simulated of the S-I process [109]. Their corrosion films were also analysed for better understanding of the corrosion behaviour. Based on the results of 100 h corrosion test, a Ni-based alloy containing 2.4% Si shows good corrosion resistance, whereas a ferritic stainless steel containing 3% Al (3Al-Ferrite) shows a greater performance with the corrosion rate being less than the 0.1 mm/a of the SiC performance.

As the relative corrosion film of 3Al-Ferrite, a Ni-based alloy that has already been pre-filmed with Al_2O_3 is made. Compared to 3Al-Ferrite, it had a considerably higher rate of corrosion. The long-term corrosion test had an Ni-based alloy having 2.4% Si form a Si oxide film that had some cracks, as per the studies of the oxide films using the electron probe microanalyzer. S consequently passed through the oxide layer and into the matrix's grain boundaries. The penetration of S into the grain boundaries of 3Al-thin ferrite and uniform Al_2O_3 layer was not seen. Because the Al_2O_3 pre-film initially contained numerous tiny flaws, it also demonstrated S penetration in the matrix. Alpha-Al_2O_3 comprised the entire corrosion oxide layer on 3Al-Ferrite, whereas alpha as well as gamma-Al_2O_3 made up the Al_2O_3 pre-film. These findings indicate that the superior corrosion resistance of 3Al-Ferrite is an outcome of the early, ubiquitous formation of a dense alpha-Al_2O_3 film.

Based on the corrosion performance data obtained of the metal, during 2019–2020 period, JAEA has initiated a joint conceptual design study with a major Japanese chemical process maker of commercial scale sulfuric acid decomposer for the 170 MWt class S-I process plant. The manufacturing feasibility of the materials selected, structural design consisting of biomaterial and thermal expansion joints are reviewed and confirmed in this study.

3.2. HYBRID TERMOCHEMICAL TECHNOLOGIES (KARABUK UNIVERSITY, TÜRKIYE)

Electrochemical hydrogen production requires costly electricity to produce hydrogen. Considering a 70% efficiency electrical energy consumption for producing hydrogen can be as high as 56 kWh. A simple assumption of 50 USD/MWh cost of electricity makes the operational expenses above 2.8 USD/kg H_2 excluding capital expenses. Thermochemical cycles are proposed to replace the electrical energy consumption with thermal energy, which is over four times less expensive, and can potentially decrease the hydrogen costs to levels that can compete with fossil driven technologies. However, thermal energy requirement of pure thermochemical cycles is at high temperatures with difficult to handle reactions.

Hybrid thermochemical cycles have been proposed to decrease the thermal energy grade of pure thermochemical cycles by using electrical energy at one of the reactions through the cycle. Some attempts for hybrid thermochemical cycles are ISPRA's Mark 11 (Westinghouse-HyS) at 1120 K and 0.16 V, Cu-Cl cycle at 800 K and 0.6–0.8 V, Ca-Br cycle at 1020 K and 0.8 V, and magnesium-chloride (Mg-Cl) cycle at 730 K and 0.99 V [23]. Electrical energy consumption is lower than pure electrochemical hydrogen splitting (1.23 V) generally to accomplish cost effective and efficient hydrogen production [110]. The HyS cycle has attracted interest due to its very low electrical energy requirement while many attempts failed in the electrochemical step due to complexity of overpotentials and cell poisoning [111]. As a modification of the pure S-I cycle SO_2 electrolysis is used in a PEM electrolyser [112]. Research is mainly focused on the electrochemical step by oxidizing SO_2 to sulfuric acid and decomposition of sulfuric acid is present at 1020 K. The cycle is meant to be integrated to

advanced next generation reactors and concentrated solar energy [113]. Research on HyS cycle is paused due to complexities in the electrochemical step of the cycle, however, it shows great potential for cost competitive hydrogen production with enhanced electrochemical cell [3]. HyS cycle, by concept, is the most efficient and cost-effective hydrogen production system among other hybrid cycles with one of the highest amounts of research conducted. Overcoming challenges through the electrochemical step is the key point for successful operation of the cycle [114]. The HyS cycle OPEX is very low compared to pure electrochemical process. A 0.16 V electrochemical process corresponds to 11 kWh/kg H_2 and its thermal energy requirement is 35 kWh/kg H_2. Compared to given cost of thermal and electrical energy, OPEX from HyS is around 0.55 USD/kg H_2 electrical and 0.43 USD/kg H_2 thermal making it 65% more cost effective than that of electrochemical water splitting.

Various configurations of the hybrid Cu-Cl cycle were proposed starting with the work of the US Institute of Gas Technology as reported in [115]. Three, four, and five-step configurations are available in pure and hybrid form, where CuCl oxidation leads to copper production in the main hybrid variant which is the five-step one as shown in Fig 38. Chlorination reaction is the leading reaction for hydrogen production while oxygen production step is where thermolysis occurs [23]. The four-step configuration includes an electrochemical step producing hydrogen along with a separation unit for $CuCl_2$ crystallization in aqueous media. Cu-Cl cycle has been one of the most researched thermochemical cycles with its high efficiency and relatively lower maximum temperature requirement, compared to SI and Hys cycles with the potential to be integrated to advanced next generation reactors especially to the Canada Deuterium Uranium (CANDU) reactor. Atomic Energy Canada Limited takes the initiative to further investigate the cycle; specifically, the electrochemical step and certain problems in the drying process; the research is still ongoing [116]. Compared to pure electrochemical technologies, hydrogen production from Cu-Cl cycle is expected to be cost effective due to its low power consumption through electrolysis [117]. Power consumption of the cycle is below 20 kWh/kg H_2 while the rest is compensated by thermal energy at a rate of 44 kWh/kg H_2. Making the same assumption as above, hydrogen production OPEX expense for the Cu-Cl cycle results in roughly 1 USD/kg H_2 from the electrical energy requirement and 0.55 USD/kg H_2 from the thermal energy requirement. Comparing only the OPEX, Cu-Cl cycle is 45% more cost effective. Knowing that OPEX for hydrogen production systems generally covers over 80% of all hydrogen cost from a plant, this is a significant enhancement in terms of cost-effective hydrogen production. Cu-Cl cycle is still under research, while reactor integration with further development on the electrochemical process is on the way by AECL and Ontario Tech University.

The Mg-Cl cycle is based on the Reverse Deacon cycle where HCl electrolysis process is used for Chlorine recovery [118]. To decrease the recovery temperature from over 1000 K to around 750 K, a three-step configuration is developed for hydrogen generation where hydrolysis occurs through an endothermic reaction, reaction of steam with $MgCl_2$ leading to HCl production. MgO produced from hydrolysis reaction and Cl_2 gas from the electrochemical step reacts at the chlorination (oxygen production) step [119]. For better reaction rate of hydrolysis, steam to Mg ratios need to be higher, resulting in aqueous HCl production that increases the overpotentials in the electrochemical step. Therefore a four-step configuration is developed to prevent half of the HCl from being aqueous and to increase the reaction kinetics at the oxygen production step [120]. Compared to Cu-Cl and HyS cycles, this cycle has not been intensively researched yet, but deserves to be further investigated since the reaction steps are mature and already available at industrial level. In terms of its cost with a practical approach, power consumption of the cycle is 27 kWh/kg H_2 and its thermal energy consumption is 22 kWh/kg, resulting in electrical and thermal energy OPEX to be 1.35 USD/kg and 0.28 USD/kg,

respectively. Overall OPEX saving compared to electrochemical process in this case is potentially equal to or higher than 40%.

The Ca-Br cycle has four-steps, where an electrochemical step for decomposition of HBr via electrolysis decreases the maximum temperature requirement to around 1020 K and the complexity of high temperature reactions [121].

Less than half of the electrical energy requirement (0.6 V) of a pure electrochemical water splitting can be accomplished that can potentially provide lower OPEX through hydrogen production [122]. In this case the electrical energy requirement is as low as 16 kWh/kg H_2 and the thermal energy requirement is 39 kWh/kg hydrogen. Considering a 50 USD/MWh electricity cost and 12.5 USD/MWh thermal energy cost, OPEX cost of Ca-Br cycle is 0.8 USD/kg H_2 for electricity and 0.48 USD/kg H_2 for thermal energy. This results in a 55% decrease of OPEX in hydrogen production.

Overall, hybrid cycles are cost effective options for hydrogen production in replacing pure electrolysis and deserve further investigations to achieve ambitious low-cost hydrogen production targets in next decades.

Capacity of processes and electricity cost are significant factors in hydrogen production; therefore, source selection and cleanliness are of critical importance. Nuclear sources are green options to energize hybrid thermochemical cycles with high capacities that can provide both electrical and thermal energy. Detailed reactions through steps of selected hybrid thermochemical processes are provided in Figs. 35–38.

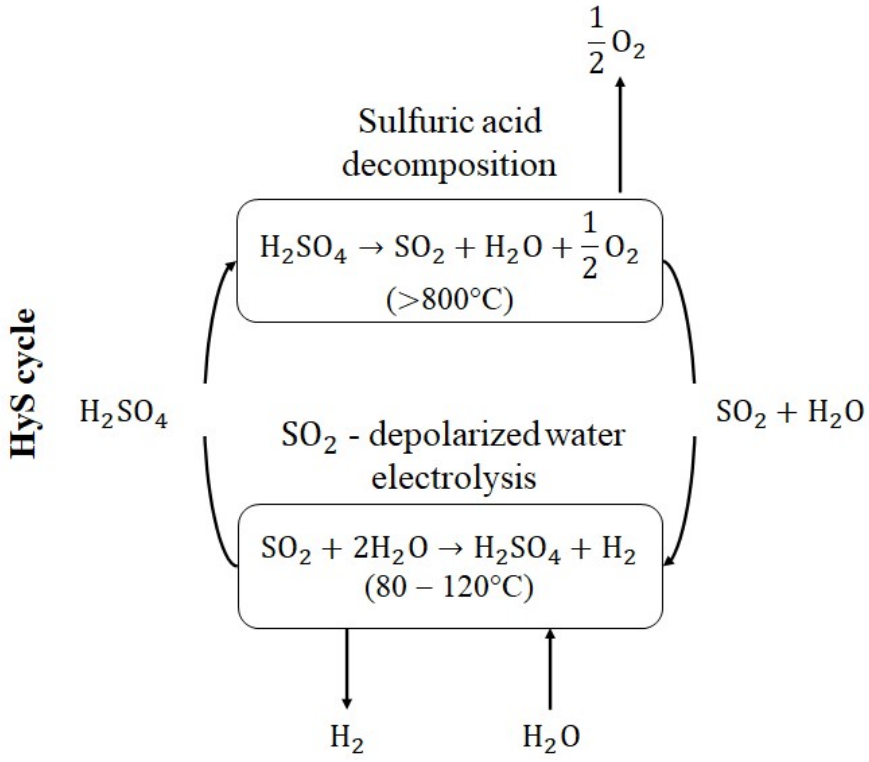

FIG. 35. Schematics of HyS cycle.

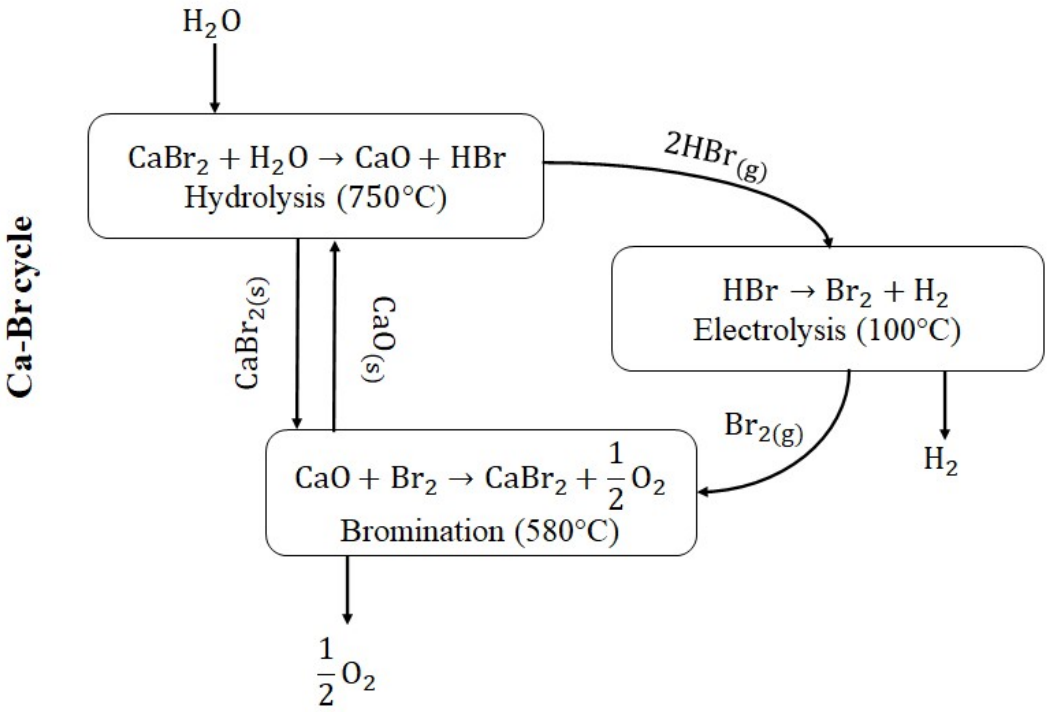

FIG. 36. Schematics of Ca-Br cycle.

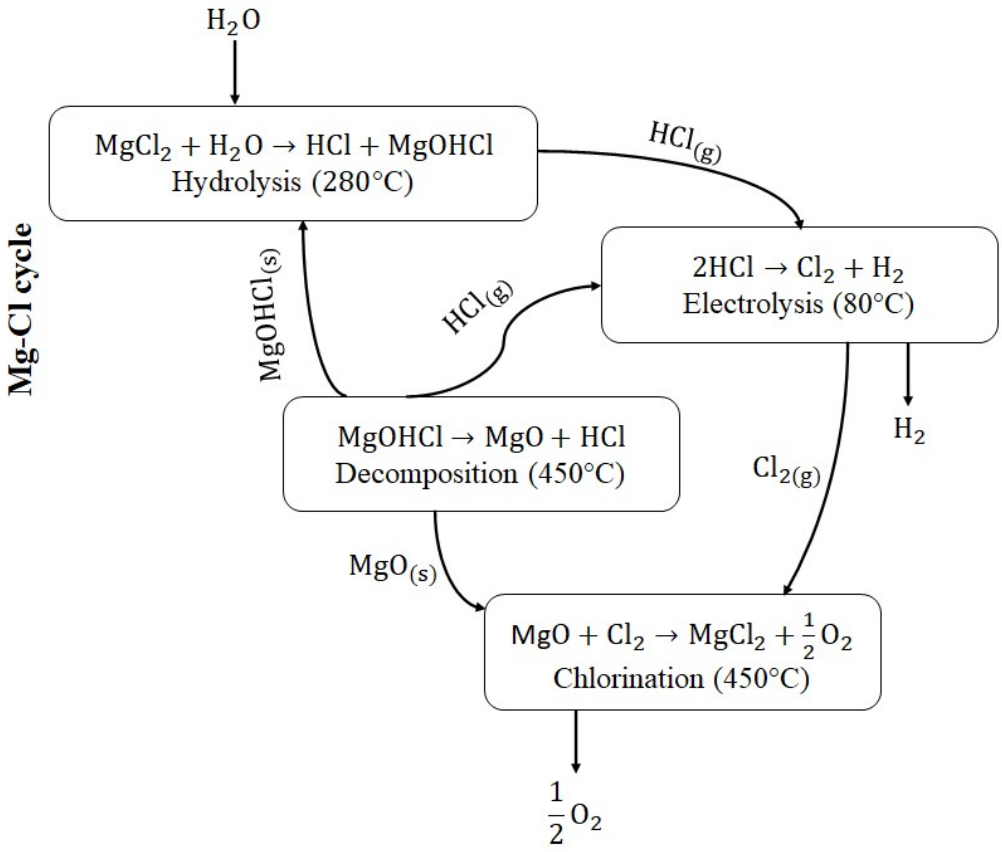

FIG. 37. Schematics of Mg-Cl cycle.

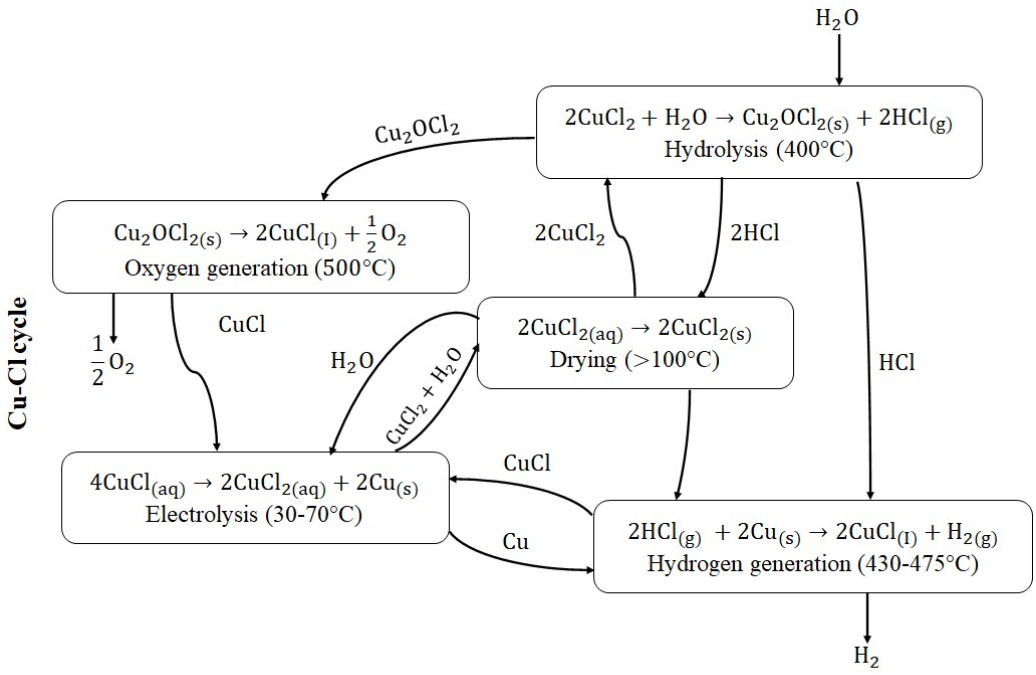

FIG. 38. Schematics of Cu-Cl cycle.

Figure 39 provides information on operational temperatures of hydrogen production options and potential energy sources that can provide high temperature energy for these options [110].

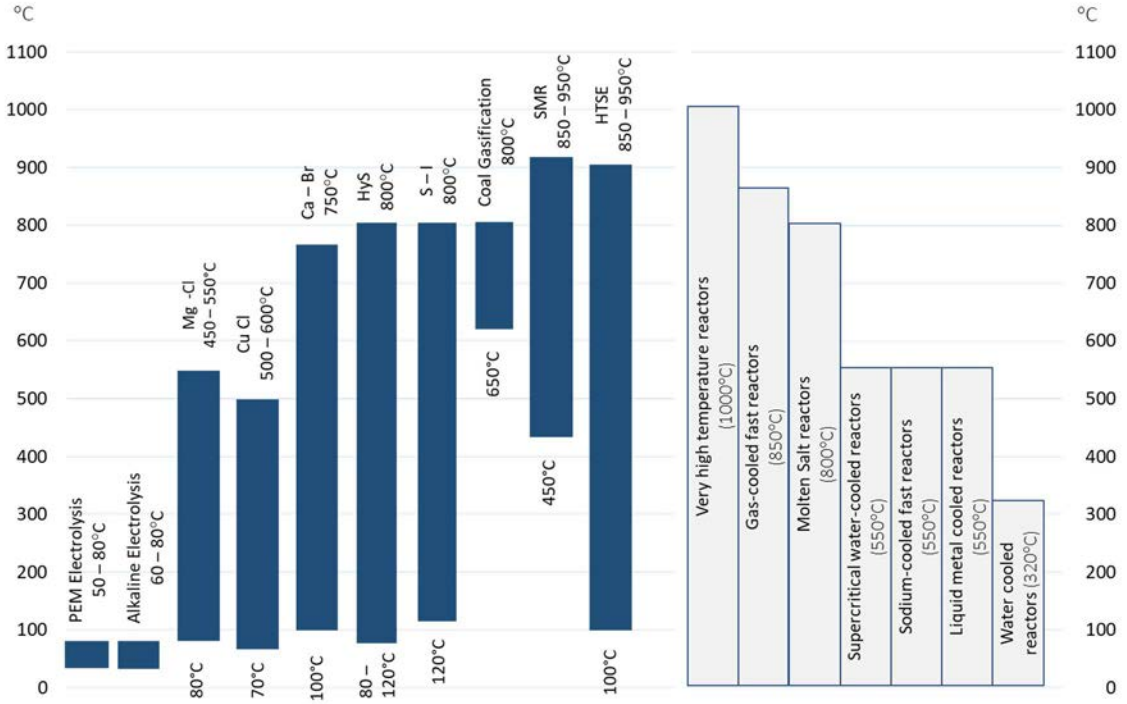

FIG. 39. Potential of nuclear reactor technologies for integration with hydrogen production technologies based on ranges of operating temperature [110].

There have been several cases considering the temperature requirement and the technology where best- and worst- case scenarios are considered. Table 29 summarizes selected hydrogen production configurations, their electrical and thermal energy requirements, and their efficiency range. Mg-Cl cycle is the only thermochemical hydrogen production option below 500ºC. The ΔG and ΔH values show the required heat for a mole of hydrogen generation [123]. Based on the literature information, the lowest electricity consumption belongs to the HyS cycle, amounting to 30% of PEM electrolysis. This shows significant advantage for less use of electricity to favour lower hydrogen generation cost followed by Cu-Cl, Ca-Br and Mg-Cl cycles. Here, the lowest temperature cycles are Cu-Cl and Mg-Cl cycles that have the potential to be integrated into next generation medium temperature reactors such as CANDU-SCWR.

TABLE 29. REQUIRED TEMPERATURE, HEAT AND POWER FOR SELECTED HYDROGEN PRODUCTION PROCESSES (THEORETICAL BASIS)

Power system	Power system efficiency range (%)	Hydrogen system	Hydrogen system efficiency range	Hydrogen system ΔG (kJ/mol H_2)	Hydrogen system ΔH (kJ/mol H_2)	Hydrogen system heat/work ratio
Temperature range: 100–200°C						
Organic Rankine cycle/ Kalina cycle/ Absorption power cycle	8–14	-	-	-	-	-
	8–14	PEM	75–85	237.4	4	0.017
	8–14	Alkaline	60–90	237.4	50	0.210
Temperature range: 200–300°C						
Organic Rankine cycle	18–25	-	-	-	-	-
	18–25	PEM	75–85	237.4	4	0.017
	18–25	Alkaline	60–90	237.4	50	0.210
Temperature range: 300–400°C						
Organic Rankine cycle / Steam turbine	24–30	-	-	-	-	-
	24–30	PEM	75–85	237.4	4	0.017
	24–30	Alkaline	60–90	237.4	50	0.210
Temperature range: 400–500°C						
Steam turbine	26–34	-	-	-	-	-
	26–34	PEME	75–85	237.4	4	0.017
	26–34	Alkaline	60–90	237.4	50	0.210
	26–34	Mg-Cl	42–51	191.0	152	0.793
Temperature range: 500–1000°C						
Steam turbine/ Gas turbine	33–45	-	-	-	-	-
	33–45	PEM	75–85	237.4	4	0.017
	33–45	HTSE	52–75	191.0	75	0.393
	33–45	Mg-Cl	42–51	191.0	152	0.793
	33–45	Cu-Cl	37–54	133.1	308	2.313
	33–45	Ca-Br	33–46	115.8	282	2.435
	33–45	HyS	35–55	77.2	249	3.220

3.3. GASIFICATION OF SOLID FUELS (COMISIÓN NACIONAL DE ENERGÍA ATÓMICA, ARGENTINA)

3.3.1. Overview

One of the possible routes for using nuclear reactors in non-electric applications is the hydrogen production through the steam gasification of solid carbonaceous fuels in indirect-heating gasification reactors, in which the nuclear heat is supplied to the gasification process as the thermal energy needed to drive the endothermic gasification reactions. The hydrogen

production using nuclear energy as primary energy source has two essential components of the long-term global energy supply systems: it does not generate greenhouse gases, and it has the potential to produce hydrogen at scales large enough to replace substantial uses of fossil resources.

Coal gasification technologies have generated a renewed interest in the last years, since they offer the potential of a clean and efficient energy, together with the possibility of cogeneration of electricity, hydrogen, liquid fuels, and high value chemicals in integrated power generation complexes [124, 125]. In a conventional coal gasification reactor, 60% of the coal feed is used as raw material for producing the synthesis gas, while the remaining 40% is combusted inside the gasification reactor for providing the heat needed to drive the endothermic gasification reactions. Alternatively, a nuclear assisted gasification reactor uses thermal energy to provide indirect heating to the gasification process, replacing the partial combustion of the coal feed material. The idea is then to replace this 40% of coal input by nuclear heat at temperatures in the order of 900–950ºC. The advantages of this idea compared with the conventional gasification processes in countries with high price rates for coal are; lower costs, saving of coal reserves, and the production of smaller amounts of CO_2 in the coal gasification plants [126].

Comprehensive R&D activities were conducted in Germany during 1970s and 1980s, addressed to evaluate the use of nuclear reactors coupled with coal gasification plants for the large-scale generation of hydrogen, synthetic natural gas, and liquid fuels. During that time, different processes of nuclear-assisted gasification for the two types of domestic German coals were investigated and developed, i.e. steam gasification of hard coal and hydrogasification of lignite [127]. Those activities were based on the use of a pebble bed HTGR as nuclear heat source. For more than 50 years, the pebble bed HTGR has been under development in Germany, involving public institutions like the Forschungszentrum Juelich and the Aachen University, industrial companies, and other organizations. From the beginning, the interest in developing HTGR was focused on providing nuclear process heat at temperatures above 600°C that cannot be reached by water-cooled nuclear reactor designs, with the final objective of achieving a safer and more balanced energy supply in Germany, reducing its historic dependence on imports of oil and natural gas. In this context, nuclear-assisted coal gasification and subsequent production of synthetic natural gas was considered a reasonable first step, but anticipating numerous more potential applications [128].

For such purpose, the German Prototype Nuclear Process (PNP) Heat Project was created as a cooperation between the HTGR industries, the coal industries, and the Forschungszentrum Juelich. The PNP Heat Project was addressed to develop and construct a nuclear heat generation system based on an HTGR design coupled with a gasification reactor for German coals processing. It included the development and testing of a demonstration plant operating at 950ºC gas outlet temperature, intermediate circuit, heat extraction, coal gasification processes, and nuclear energy transport [129]. The concept selected for the PNP heat project was a pebble bed HTGR design with thermal power sizes of 500 MW (PR-500) and 3000 MW (PNP-3000) [130]. As most of chemical processes are performed at lower pressures, some adaptation of the nuclear reactor design to the chemical process plants was necessary and the nuclear reactor pressure was reduced from 7 MPa for electricity-generating plants to 4 MPa for the PNP Project [31]. However, the basic lessons learnt from the former experience on the HTGR operation were that medium- and large-sized gas cooled reactors are highly complex in their operation, and this is due to multiple technical problems as demonstrated in the case of the German 300 MWe THTR-300 steam cycle plant, that had to be shut down after only 16410 operation hours, or 423 days of equivalent full power operation [128].

Certainly, influenced by that unsuccessful experience, a new trend towards small sized and modular HTGRs emerged during the eighties, which was characterized by reduced reactor thermal powers and a much higher degree of inherent safety in comparison with the larger predecessors. The SMRs of HTGR type were designed with the concept that, under the most critical accidental conditions involving the failure of all active cooling systems, the decay heat can be removed in a passive way by heat conduction, radiation and convection [131–133]. Safety criteria for modular HTGRs are based on temperature limitation of fuel elements under 1600ºC to keep the coated fuel particles intact, even under the severe accident conditions like a loss of forced convection in the depressurized reactor with residual heat removal through the reactor vessel to the reactor cavity cooling system. The HTGR cores are quite large and, therefore, their core power density is appreciably low. With their low power densities, the HTGRs can accommodate the decay heat removal passively from the reactor core through a large graphite volume without causing any radioactivity release. On the other hand, the maximum fuel temperatures under normal operating conditions are extremely low, typically below 1250ºC, and according to that, a significant fuel failure rate of coated particles can be excluded [134]. At present, there are two types of well-known modern HTGR designs based on the modular concept: one has a core with block type fuel elements, and the other has a pebble bed core with spherical fuel elements. Power sizes with a pebble bed of spherical fuel and prismatic block type fuel and with annular active core geometry are limited to about 400 MWt and 600 MWt, respectively. These limit values are determined by the maximum allowable fuel temperature that has to be less than 1600ºC in the case of loss of forced convection [129]. Some of the main characteristics of the modern HTGR designs with block-type core and pebble bed type core are compared in Table 30 (extracted from [129]).

In the case of a block type core, the gas outlet temperature of 850ºC has been selected for power generation reactor designs [135–137], and of 900–950ºC for process heat reactor designs [138–140]. In the case of a pebble bed core, the higher gas outlet temperature of 900ºC can be achieved easily during normal operation, even the maximum fuel temperature at a depressurization accident is most critical.

TABLE 30. MAIN CHARACTERISTICS OF MODERN HTGR DESIGNS WITH BLOCK TYPE CORE AND PEBBLE BED CORE

Reactor type	**Block core**	**Pebble bed core**
Power and efficiency		
Thermal power (MWt)	600	200–500
Electric power (MWe)	274–284	80–200
Cycle/net thermal efficiency (%)	47.2–48.4/45.6–46.2	44–49.5/45.5
Main gas conditions		
Reactor inlet/outlet temperature (°C)	460–587/850	280–550/750–950
Helium gas pressure (MPa)	7–7.15	5.5–9
Mass flow rate (kg/s)	296.4–440	-203
Fuel		
Fuel element	Monolithic pin-in-block	60 mm diameter sphere
Average enrichment (%)	15	10
Packing fraction	29–35	4–11
Average burnup (GWd/t U)	110–120	100
Fuel cycle (days)	450–730	903
Fuel exchange working time (days)	33–82 (incl. reflector exchange)	On power loading

TABLE 30. MAIN CHARACTERISTICS OF MODERN HTGR DESIGNS WITH BLOCK TYPE CORE AND PEBBLE BED CORE (CONT.).

Reactor type	Block core	Pebble bed core
Core		
Equivalent diameter (m) cylindrical annular	3.70/5.48 (inner/outer)	≤3.0 2.70/4.50 (inner/outer)
Effective height (m)	8.1–8.4	9.4
Average power density (MW/m^3)	5.44–5.77	4.2
Pressure drop (%)	0.65–1.42	3.3
Maximum fuel temperature during normal operation (°C)	1108–1286	1130
Maximum fuel temperature during normal operation in accident (°C)	1546–1575	1520
Reactor vessel		
Inner diameter (m)	7.62–7.89	≤7.3
Height (m)	23.4–24.4	≤32.4
Weight upper/lower part (t)	285–398/838-923	134/975
Material	9Cr-1Mo-V or SA533/SA508 steel	SA 533
Dose rate due to fission product plate out on the turbine rotor (mSv/h)	160	5440

To fulfil the new safety criteria for fuel temperature limitations in HTGRs, two different concepts of pebble bed HTGRs for nuclear process heat applications are being developed in Germany:

- The HTR-Module, with a cylindrical reactor core generating a thermal power of 200 MW for a gas outlet temperature of 700ºC, and 170 MW for a gas outlet temperature of 950ºC. The 200 MWt version of the HTR-Module is designed to produce electricity through a steam cycle, while the 170 MWt version is designed to be coupled with a chemical plant requiring process heat temperatures above 850ºC.
- The PNP-500, which is an evolutionary version of the original PNP Heat Project with an annular reactor core generating a thermal power of 500 MW.

The HTR-Module consists of a compact reactor core of about 3 m in diameter and 10 m of overall height, with a power density not exceeding 3 MW/m^3. The helium pressure in the primary system depends on the process-related application of the heat source; since a high primary system pressure has a favourable effect on the normal and accidental operating conditions of the nuclear reactor, but is not desirable in chemical processes like gasification where the reaction kinetics is more favourable at lower pressures [141].

One of the main applications of the HTR-Module with 950ºC of gas outlet temperature is the direct use of the nuclear heat for coal gasification. In addition, the HTR-Module with a steam generator can be used to produce electrical power and process steam in industrial plants, or for the generation of electrical power and steam for district heating purposes in the municipal sector. On the other hand, the PNP-500 is designed to avoid the restrictions on maximum core temperatures, i.e. 1600ºC under severe accidental conditions, and then on the core power density, by adopting an annular core design with a central graphite column that allows increase of the thermal power of the reactor up to 500 MW. With this arrangement, it is possible to satisfy the safety criteria of temperature limitation without requiring a further reduction of the thermal power of the HTGRs. A power core density of 2 MW/m^3 is taken as basis for design,

and accordingly, the fuel temperatures are well below 1250ºC under normal operating conditions [133, 142].

Based on former experiences on HTGRs developed worldwide, two small-sized engineering and test HTGRs are presently in operation: one in Japan and the other in China. In Japan, the Japanese Atomic Energy Research Institute have designed and constructed the 30 MWt HTTR with the objective of developing the technology foundations for non-electrical nuclear applications that require process heat at temperatures above 700ºC [143–146]. The 30 MWt HTTR is a helium-cooled and graphite-moderated HTGR with a block-type core design that reached the first criticality in November 1998. In December 2001, the operating outlet coolant temperature was increased from 750ºC to 850ºC, and since 2002, safety demonstration tests have been carried out by simulating anticipated operational events to ensure the safe reactor operation under off-normal conditions. From 2005, several irradiation tests on fuels and materials have been also performed. Presently, a first-of-class hydrogen production facility using S-I thermochemical cycle is being coupled with the HTTR to produce hydrogen.

On the other hand, in 1986 China and Germany signed a cooperation project aimed to evaluate the use of HTGRs for application in enhanced oil recovery [149]. Within the framework of that joint venture, in 1988 an agreement between industries and R&D institutes was achieved for the cooperative design and construction of a small pebble bed reactor close to the German HTR-Module concept. That agreement resulted in the conceptual design of the so-called HTR-10 test reactor with a thermal power of 10 MW [147–149]. Construction of this test reactor was approved by the Chinese Government in 1992, reached first criticality in 2000, and full operating conditions in 2003.

The HTR-10 is a pebble bed core reactor that operates with a mean power density of 2 MW/m^3. The main purpose of the HTR-10 is to demonstrate the basic and safety related features of small size modular HTGRs, in particular, the 1600°C integrity limit of the ceramic fuel elements [148], and to jointly incorporate knowledge in the field of reactor components and systems like hot helium gas and fuel element technologies.

Considering the successful experience with these two small-sized test HTGRs, Japan and China are presently involved in the design, development, and construction of an HTGR demonstration power plant. The Japanese Atomic Energy Research Institute launched an applied program of design and development for the Gas Turbine High Temperature Reactor (GTHTR300) power plant in 2001. The reactor module is rated at 600 MWt and 587/850ºC of inlet/outlet gas temperature, and it relies on inherent and passive safety system [139, 150, 151].

Based on the design principles of the HTR-10 test reactor, the Chinese Institute of Nuclear and New Energy Technology of the Tsinghua University developed and designed an HTGR Demonstration Plant called the High Temperature Gas Cooled Reactor Pebble Bed Module (HTR-PM), in collaboration with industrial partners from China and experts worldwide.

The HTR-PM plant started construction in 2012 and consists of two pebble bed modular HTGRs with a thermal power of 250 MW each, coupled with a single steam turbine that generates a net electrical power of 210 MW. The plant was connected to the grid at the end of 2021. The project addressed to demonstrate both the economic competitiveness and the operational safety of the HTR-PM commercial plants that should not require accident management procedures and off-site emergency measures [152, 153].

R&D activities on HTGR designs, manufacturing and testing of coated fuel particles for fuel elements, and development of high-temperature resistant materials have continued during many years all around the world. In this sense, former HTGR plants, and small-sized engineering and test reactors presently in operation in Japan and China have provided an extensive database on the behaviour of materials and components operating under high temperatures and high neutron fluxes.

As a consequence of this hard work, the HTGRs are considered at present as one of the leading candidates for future nuclear power plants for high-temperature process heat applications like coal gasification, on the basis of the following intrinsic advantages [129]:

— Higher thermodynamic efficiency.
— Lower waste quantity.
— Higher safety margins.
— High burnup of fuels (~100 GWd/t U).

Unfortunately, the former construction program of the German PNP demonstration plant for the nuclear-assisted steam coal gasification process was abandoned during the nineties, when the production of nuclear synthetic natural gas from the expensive German coals was demonstrated to be economically non-competitive compared with cheap oil and natural gas available on fuel markets at that time [127]. At that point, the commercial-size gasification reactor with indirect heating for the nuclear-assisted coal gasification had not been constructed or tested and then, its technical feasibility could not be demonstrated.

With the focus on the major milestones achieved at that time and with currently open research issues to be solved, the experience developed during seventies and eighties on nuclear-assisted coal gasification process is critically re-evaluated in this part of this publication, under the current technology and fuel market conditions. The following technical, economical, and safety-related aspects are analysed:

— Definition of main requirements to be fulfilled by the HTGRs used as heat source.
— Evaluation of different HTGR designs to be potentially used for the nuclear-assisted coal gasification process.
— Selection of the gasification technology to be implemented for processing coals in an indirectly heated gasification reactor.
— Heat balance analysis of an indirect-heating coal gasification reactor, and critical evaluation of technical alternatives for upscaling the coal gasification reactors with indirect heating to a more commercial phase under the present state of technology.
— Development of a possible plant layout for the safe coupling between HTGR and a demonstration gasification plant for hydrogen production from coal processing.
— Evaluation of the most critical safety issues for the coupling between HTGR and an indirect-heating coal gasification reactor for hydrogen production.
— Calculations with the IAEA HEEP software for a quick estimate of the levelized cost of hydrogen produced by processing the Argentine Rio Turbio coal through the coupling of HTGR of 170 MWt and 950ºC gas outlet temperature, with a nuclear assisted gasification/hydrogen generation plant of 10 MWt.

3.3.2. Technical consideration and development

This section illustrates the technical details of the high temperature reactors that can be used potentially for coal gasification.

3.3.2.1. Main requirements on the high temperature gas cooled reactors used as process heat source for the nuclear assisted coal gasification

Firstly, the HTGRs for nuclear heat applications have to be able to deliver the process heat at temperature and pressure conditions that match the chemical process requirements. In the case of the coal gasification process, it is well-known that the global kinetics of gasification reactions depends strongly on temperature. That is the coal reactivity in the presence of gasifying agents increases exponentially with increasing temperature. Then, for all chemical reactions involved in the coal gasification process, nuclear heat has to be supplied at temperature levels above about 850ºC to get a minimum efficiency in the process. A further increase of the HTGR gas outlet temperature to about 950ºC or even 1000ºC would have a very positive influence on the overall velocity of such thermo-chemical reactions. Moreover, the proper partition of the heat provided by the HTGRs for heating processes and for steam production requires a particular attention. Temperatures above 800ºC are needed for the direct heating of the heat consuming processes such as coal gasification, while temperatures below this value are adequate for steam production aimed at the electricity generation with a steam turbine cycle. On the other hand, a reduction of the HTGR primary system pressure to 4 MPa or less is beneficial from the chemical reaction kinetics point of view in the gasification process, but this reduction requires a larger volume of the reactor primary loop that can be achieved by a non-integrated design of the HTGR primary loop. As the non-integrated design of the reactor primary loop allows more flexibility in arranging heat consuming components in the primary circuit, a variety of process heat consuming applications may be introduced simultaneously in the primary circuit.

In the case of the nuclear assisted coal gasification process, the heat produced by the HTGR is delivered from the reactor core through a primary helium circuit to a secondary helium circuit, via an intermediate helium-helium heat exchanger. The secondary helium gas enters the gasification reactor to drive the high-temperature gasification reactions. That is the helium gas passes through a heat exchanger immersed in a fluidized bed of coal and steam like an immersion heater, and provides the heat needed for endothermic gasification reactions.

An intermediate helium circuit is required for separating the nuclear island from the coal gasification plant. Thus, it involves a higher degree of safety of the whole plant for inhibiting the permeation of hydrogen from the gasification reactor into the nuclear reactor core, as well as the tritium from the nuclear island into the gasification plant. Furthermore, the possibility of an easier replacement of components of the gasification plant is given. For these reasons, it is felt that an intermediate circuit is necessary to make the coupling between an HTGR and a nuclear-assisted coal gasification plant feasible and safe.

Finally, an HTGR plant for process heat applications should fulfil the same inherent safety requirements as a nuclear power plant for electricity generation. As the average operating core temperatures are higher and the overall system pressure is lower for process heat applications compared to the electricity generation, a further optimization of the reactor core design is required. Two options to satisfy these operational conditions are generally applied: to reduce the total reactor thermal power, and to lower power density of the reactor core. While a small

total reactor thermal power is financially non-attractive, a lower power density leads to a larger core volume, and it can be better realized with non-integrated primary system designs. In addition to the proper selection of the HTGR, the two main issues that have to be solved before the nuclear-assisted coal gasification process proves to be technically feasible are the following:

— The efficient transfer of heat from the HTGR into the coal gasification plant.
— The design, construction, and operation of an indirect heating gasification reactor under the aspects of gasification reaction kinetics, efficient heat transfer, and proper performance of the heat exchanger materials.

3.3.2.2. Evaluation of different HTGR designs to be potentially used for the nuclear assisted coal gasification process

Based on past experiences developed worldwide, present status of the HTGR developments, and considering the main requirements to be fulfilled for assisting the coal gasification process. The following four HTGR designs were evaluated in their respective strengths and weaknesses for this possible route of nuclear hydrogen generation:

— German designs of the HTR-Module with cylindrical core and the PNP-500 with annular core, both having a pebble bed core design and thermal outputs of 170 MW and 500 MW, respectively.
— Japanese design of the GTHTR300 with a pin-in-block core design and a thermal power of 600 MW. At present, there is a baseline reactor design with a gas outlet temperature of 850ºC and an upgraded reactor design with a gas outlet temperature of 950ºC.
— Chinese HTR-PM modular reactor with a pebble bed core design and a thermal power of 250 MW.

Most of these reactor designs are still under development, but the Chinese HTR-PM has already been connected to the grid. For comparative purposes, the main technical characteristics of the four HTGR designs, relevant for assisting the coal gasification process, are summarized in Table 31.

TABLE 31. MAIN TECHNICAL CHARACTERISTICS OF THE HTGRS CONSIDERED FOR ASSISTING THE INDIRECT HEATING COAL GASIFICATION PROCESS

Parameter	**HTR-Module**	**PNP-500**	**GTHTR300 Baseline**	**GTHTR300 Upgraded**	**HTR-PM**
Country	Germany	Germany	Japan	Japan	China
Status	Development	Development	Development	Development	Operating
Thermal/electrical power (MWt/MWe)	170/-	500/-	600/274	600/302	2 × 250/210
Average power density (MW/m^3)	3	3	5.4	5.4	3.22
He inlet/outlet temperature (ºC)	250/950	300/950	587/850	666/950	250/750
Primary helium pressure (MPa)	4	3.9	6.9	6.4	7
Fuel element type	Spherical	Spherical	Prismatic	Prismatic	Spherical
Fuel type	TRISO (UO_2)	TRISO (UO_2)	TRISO (UO_2)	TRISO (UO_2)	TRISO (UO_2)

The considerations derived for each of these designs were the following:

- German HTR-Module and PNP-500, The main advantage of the German reactor designs is clearly the fact that both were developed specifically for nuclear heat applications, particularly for the steam gasification process applied to their domestic coals. For this reason, both reactor designs are theoretically able to deliver the nuclear process heat at temperature and pressure conditions that match very well with the requirements imposed by the coal gasification process, i.e., gas outlet temperature of 950ºC and primary system pressure of 4 MPa. The main drawback of the German reactor designs is the fact that both reactors were designed long time ago (during seventies and beginning of eighties) and it is not clear if they have incorporated all technical advances and experiences obtained from the operation of HTGR test reactors of present generation, i.e., the Japanese HTTR and the Chinese HTR-10.
- Japanese GTHTR300, As shown in TABLE 31, the baseline design is able to reach a gas outlet temperature of 850ºC, which is too low for achieving an efficient kinetics of the nuclear-assisted coal gasification process that requires a minimum reaction temperature of 700–800ºC. On the opposite, the upgraded design with a gas outlet temperature of 950ºC seems to be appropriate for this purpose. Nevertheless, it would be convenient that the primary system pressure of the GTHTR300 upgraded reactor is reduced to match with the pressure requirement of the coal gasification process, i.e., from 6.4 MPa to 4 MPa, and it is not clear how this major design change would affect the overall performance and cost of the plant.
- Chinese HTR-PM, The reactor began the commercial operation and is designed to reach a gas outlet temperature of 750ºC, which is appropriate for generating electricity with a steam turbine cycle but not for supporting efficiently a nuclear assisted coal gasification process, for the technical reasons explained before.

3.3.2.3. Selection of the gasification technology for processing coals in an indirectly heated gasification reactor

In an indirectly heated gasification reactor (allothermal process), thermo-chemical reaction temperatures are limited by the maximum core outlet temperature that can be achieved in the present generation of HTGRs (950ºC or less), as well as by the thermal resistances along the heat transfer pathway from the nuclear reactor core to the gasification reactor. Accordingly, the gasification technology to be implemented in nuclear-assisted coal gasification reactors is limited to the fluidized-bed type reactors, which operate at moderate temperatures, below the softening and melting points of the coal ashes (typically, between 900 and 1200ºC).

Among the commercial options available in the gasification reactors market, the so-called High Temperature Winkler (HTW) gasification process appears to be the most convenient alternative for the nuclear-assisted coal gasification. It uses a circulating fluidized-bed gasification reactor with the necessary modifications to allow the indirect nuclear heating of the feedstock through an intermediate helium circuit. The R&D activities related with the HTW technology are presently complete, a demonstration plant was constructed and successfully operated for methanol production in Berrenrath, Germany, for more than 12 years [154–157].

The HTW gasification process (schematically shown in Fig. 40) involves a gasification unit consisting of the coal feeding system, the gasification vessel, the ash removal system located below the gasifier, and the synthesis gas exit pipe in the head of the gasifier. The crude synthesis gas produced by thermochemical gasification reactions leaves the reactor at the top

and passes through a cyclone for removing the particles of coal that is not gasified and ash, which are then returned to the fluidized bed through a down comer with a loop seal. The cyclone separates approximately 95% of the entrained solids from the product gas and returns them to the fluidized bed, thus increasing the overall carbon conversion rate.

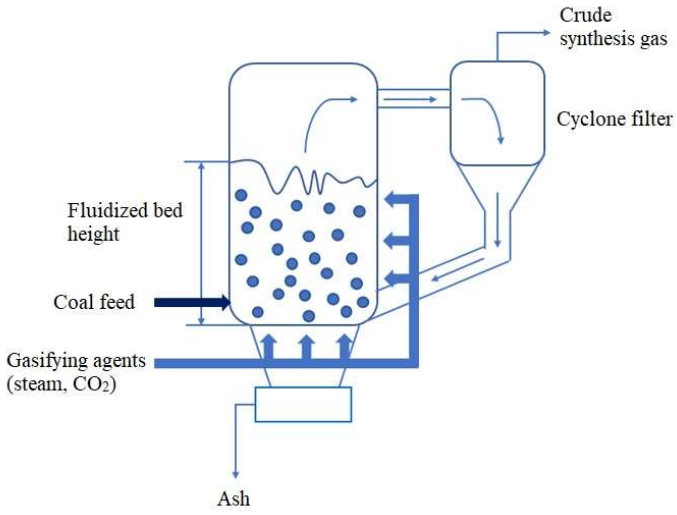

FIG. 40. Schematic view of the HTW fluidized bed coal gasification process.

Downstream of the gasification reactor (not shown in Fig. 40), the crude synthesis gas is cooled, and the recovered heat is used to produce saturated steam that can be exported to external steam consumers. After crude gas cooling, the remaining fine ash particles are removed from the synthesis gas in a ceramic filter. Subsequently, the synthesis gas is conducted to the scrubbing system, where it is quenched with water to remove chlorides, and then further treated in agreement to the needs of the downstream processes such as hydrogen production. Screw conveyors supply the dry coal feedstock to the gasification reactor, and due to the pressure of the system, feeding and bottom ash removal operations have to be performed by lock-hopper systems. The superheated steam used as gasifying and fluidizing agent is injected into the gasification reactor via nozzles that are arranged at several levels. As high material circulation and heat transfer rates are achieved in the fluidized bed reactors, the temperature distribution throughout the gasification reactor is almost uniform. On the other hand, the maximum temperature in the gasification reactor has to be maintained below the softening point of the coal ashes always, to avoid the formation of particle agglomerates.

3.3.2.4. Heat balance analysis of the coal gasification process with indirect heating

The main parameters of the coal gasification process with indirect heating at the equilibrium conditions, i.e., mean gasification temperature, heat involved per unit time, and expected coal input, can be obtained by performing a heat balance analysis of the gasification plant. The gasification power in an allothermal process is determined from the heat balance between the heat transferred from the helium intermediate circuit into the fluidized bed, and the heat consumed by the thermochemical gasification reactions, i.e., the transferred heat equals the consumed heat. This heat balance finally determines the mean reaction temperature at which the gasification process occurs and the coal input to be expected for a given reactor dimensions, this being the fluidized bed volume and density, and the surface area of the immersion heat exchanger.

To solve the heat balance equation, it is necessary to have information on the gasification kinetics of the solid carbonaceous material used as feedstock. This essentially influence the right-hand of the equation, and on the heat transfer data that participate in the left-hand of the equation, such as the heat transfer coefficients and surfaces. In the following, the equations and data used for performing the heat balance analysis of a coal gasification reactor with indirect heating, are described in more detail.

Heat transferred into the gasification reactor through the helium intermediate circuit

At the present state-of-art, the best alternative for coal gasification reactors with indirect heating is to use tube-type heat exchangers, where the secondary helium flows through the cylindrical tubes and transfers the nuclear heat into the fluidized bed composed by a dense mixture of coal and steam.

With this arrangement, the total power of the gasification reactor is finally defined by the heat that can be coupled per unit time to the fluidized bed, since the thermochemical gasification reactions can only occur to the point where the nuclear reaction heat is made available by heat transfer of the immersion heater. The amount of transferred heat per unit time (in kJ/s) is given by:

$$Q_1 = h \times F \times \theta_m(T_1, T_2, T) \tag{23}$$

where:
h – the overall heat transfer coefficient between the secondary helium and the coal/steam fluidized bed (kJ/m^2·s·K)
F – the heat exchanger area (m^2)
θ_m – the logarithmic temperature difference (K).
θ_m is given by the following well-known relationship:

$$\theta_m = \frac{(T_1 - T) - (T_2 - T)}{\ln\left[\frac{T_1 - T}{T_2 - T}\right]} \tag{24}$$

where:
T_1 – helium temperature at inlet of the immersion heater (K)
T_2 – the helium temperature at outlet of the immersion heater (K)
T – mean gasification temperature (K), assumed to be constant in the whole volume of the fluidized bed.

The overall heat transfer coefficient, h, is determined as the sum of the thermal resistances connected in series from the inner of the heat exchanger tube into the fluidized bed, as shown in Fig. 41:

$$h = \frac{1}{\frac{1}{\alpha_1} + \frac{\Delta}{\lambda} + \frac{1}{\alpha_2}} \tag{25}$$

where:
α_1 – the heat transfer coefficient in the interface He-tube (kJ/m^2·s·K)
Δ – the tube wall thickness (m)
λ – the thermal conductivity of the tube material (kJ/m·s·K)
α_2 – the heat transfer coefficient in the interface tube/fluidized bed (kJ/m^2·s·K).

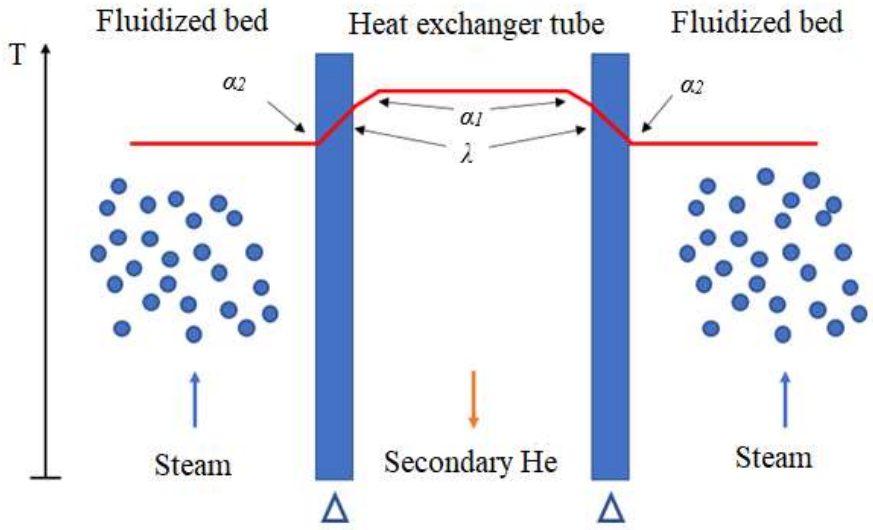

FIG. 41. Heat transfer mechanisms for transporting the nuclear heat from the secondary helium into the fluidized bed.

Heat consumed by the thermochemical gasification reactions

The heat consumed per unit time by the thermochemical gasification reactions (in kJ/s) can be estimated with the following equation:

$$Q_2 = q \times k(T) \times \gamma \times V \tag{26}$$

where:
q – the reaction heat of carbon conversion (kJ/kg coal)
k – the reaction velocity constant as a function of the mean gasification temperature T (s^{-1})
γ – the density of the fluidized bed (kg coal/m^3)
V – the volume of the fluidized bed (m^3).

The temperature dependence of the reaction velocity constant can be described to a good approximation according to an Arrhenius type equation:

$$k = k_0 \times \exp\left(-\frac{E_a}{RT}\right) \tag{27}$$

where:
k_0 – the frequency factor (s^{-1})
E_a – the activation energy (kJ/mol)
R – the general gas constant (kJ/mol·K)
T – the absolute temperature (K).

As an example of the heat balance analysis of the coal gasification process with indirect heating, a theoretical simulation comparing the gasification behaviour of German hard coals and the Argentine Rio Turbio coal was carried out. The two coals are considered to be processed in the only gasification reactor with indirect heating that was constructed and operated successfully in the past: the semi-technical gasification pilot plant, commissioned in Germany in 1976 [158–160]. The German semi-technical pilot plant was a cut out version of the full-scale gas generator to be installed in an industrial-scale nuclear-assisted coal gasification plant, in which the height of the fluidized bed, and the length and arrangement of heat exchanger tubes corresponded to the full-scale design. The gas generator was designed as a fluidized-bed gasification reactor of about 1 m^2 base area and a height of up to 4 m, laid out for a coal input of about 200–250 kg of hard coal per hour [130]. It was constructed as a vertically cylindrical vessel with outer dimensions of 7.75 m diameter (max) and 21.13 m height, prepared to operate at a pressure of 4 MPa. The helium gas was electrically heated up to 950ºC and the total thermal power of the facility was 1.2 MW.

Input data required for the heat balance analysis of the Rio Turbio coal processing is described below. This information was obtained from both theoretical calculations and steam gasification experiments at laboratory scale.

The heat demand for the gasification process or reaction heat for carbon conversion, q in Eq. (26), was estimated in 5860 kJ/kg for the Rio Turbio coal. This heat demand was theoretically calculated with the HSC software [161] and comprises the endothermal chemical reaction between C(s) and H_2O(g), the exothermal formation of CH_4, and the exothermal water-shift reaction, all of which occur simultaneously in a gasification reactor. Kinetic parameters of the overall reaction velocity constant given by Eq. (27) were determined for the Rio Turbio coal by steam gasification tests at laboratory scale [162]. They are presented in Table 32 along with the corresponding values of the German hard coal tested in the semi-technical facility during the seventies [163].

TABLE 32. KINETIC PARAMETERS OF THE OVERALL REACTION VELOCITY CONSTANT, *k(T)*, FOR THE RIO TURBIO COAL AND GERMAN HARD COAL

	***Ea* (kJ/mol)**	***k₀* (s^{-1})**
Argentine Rio Turbio coal	165	2.0×10^5
German hard coal	133.1	8.0×10^2

Figure 42 shows the overall reaction velocity constant for the two coals, as a function of the mean gasification temperature. It is seen that the Rio Turbio coal is most reactive than the German hard coal in the presence of steam, and it is due mainly to its lower ranking (less content of fixed carbon) and its higher content of volatile matter.

Based on dimensions of the German semi-technical pilot plant [160], the following input data were assumed for the heat balance analysis:

- Heat exchanger area (F) = 33 m^2
- Density of the fluidized bed (γ) = 344 kg coal/m^3
- Volume of the fluidized bed (V) = 3.77 m^3.

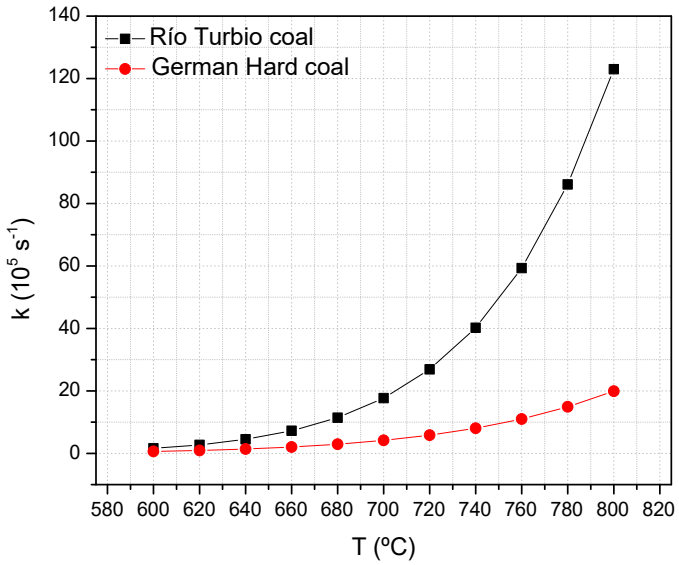

FIG. 42. Overall reaction velocity constant as a function of the mean gasification temperature for Rio Turbio coal and German hard coal.

To estimate the overall heat transfer coefficient (h) given by Eq. (25), the following values were adopted:

- Heat transfer coefficient in the interface helium/tube (α_1) = 1.16 kJ/m^2·s·ºC
- Thickness of the heat exchanger tube (Δ) = 20 mm
- Thermal conductivity of the heat exchanger tube material (λ) =0.012 kJ/m·s·ºC
- Heat transfer coefficient in the interface tube/fluidized bed (α_2) = 0.58 kJ/m^2·s·C.

Using these values that can be considered as conservative and pessimistic, the overall heat transfer coefficient h resulted in 0.235 kJ/m^2·s·ºC or 846 kJ/m^2·h·ºC.

Finally, for the calculation of the logarithmic temperature difference (θ_m) given by Eq. (24), it was assumed that the helium temperature at the heat exchanger outlet (T_2) is higher by 50ºC than that of the fluidized bed ($T_2 = T + 50$ºC).

As it was said before, the thermochemical gasification reactions in the fluidized bed can only occur when the heat provided by the heat transfer mechanisms through the immersion heater reaches the heat needed for producing the endothermic reactions. In this thermal balance conditions, the Eq. (23) and (26) are equal and the following global equation results:

$$h \times F \times \theta_m(T_1, T_2, T) = q \times k_0 \times \exp\left(-\frac{E_a}{RT}\right) \times \gamma \times V \qquad (28)$$

Equation (28) was evaluated numerically by using a computer program for different helium temperatures at the inlet of the heat exchanger (T_1), varying from 850 to 1050ºC with increments of 50ºC. As seen, the consumed heat given by the right-hand of Eq. (28) increases exponentially with the mean gasification temperature T, while the transferred heat given by the

left-hand of Eq. (28) decreases slightly with *T*. The intersection of both curves allows obtain the mean gasification temperature for the corresponding helium inlet temperature, gas generator dimensions and coal feedstock properties, as shown below in Fig. 43 for the hypothetical case of the steam gasification of Rio Turbio coal in the historic German semi-technical pilot plant.

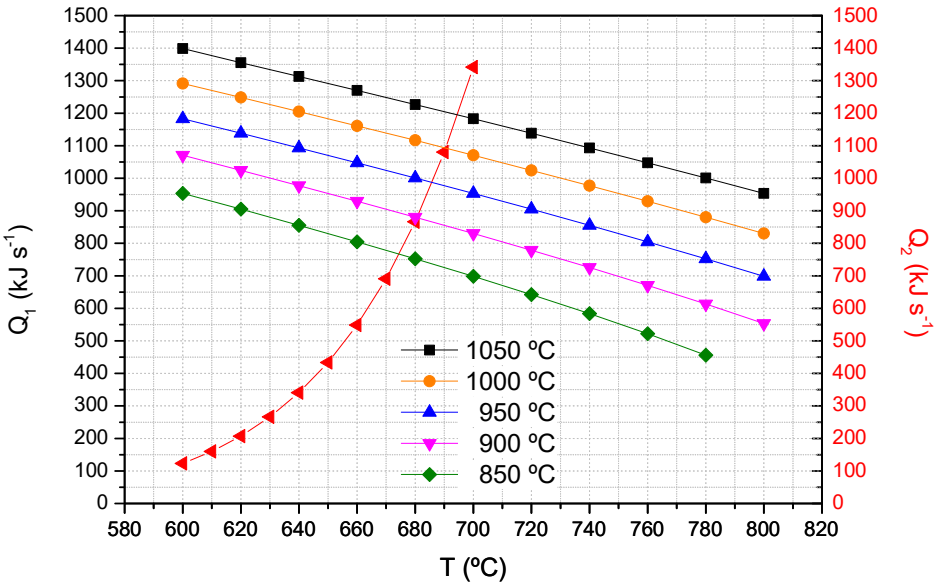

FIG. 43. Q_1 and Q_2 curves as a function of the mean gasification temperature for the steam gasification of Rio Turbio coal in the German semi-technical pilot plant.

In Table 33, results of the heat balance analysis are presented in terms of the main parameters at the equilibrium conditions, i.e., mean gasification temperature, heat involved per unit time, and expected coal input. The expected coal input is obtained by dividing the heat transferred/consumed at the equilibrium by the reaction heat *q* of the coal.

TABLE 33. MAIN RESULTS OF HEAT BALANCE ANALYSIS FOR THE SIMULATED STEAM GASIFICATION OF RIO TURBIO COAL IN THE GERMAN SEMI-TECHNICAL PILOT PLANT

	He inlet temperature				
	850ºC	**900ºC**	**950ºC**	**1000ºC**	**1050ºC**
Mean gasification temperature (ºC)	674	680	686	690	695
Heat transferred/ consumed per unit time (kJ/s)	762	873	988	1086	1198
Expected coal input (kg coal/h)	468	536	607	667	736

The German semi-technical pilot plant had been designed for steam gasification of hard coals at the following steady state conditions: helium inlet temperature of 950ºC, gasification temperature between 700 and 850ºC, and coal input between 200 and 250 kg coal/h [130]. By comparing these values with the theoretical ones obtained by the simulation analysis performed, it can be concluded that the steam gasification of Rio Turbio coal for a helium inlet temperature of 950ºC, is predicted to occur at a lower temperature (686ºC instead of 700–850ºC), with a much higher coal input (607 kg coal/h instead of 200–250 kg coal/h). This

encouraging behaviour can be explained by the higher reactivity of the Rio Turbio coal in presence of steam compared to the tested German coal (Fig. 42).

3.3.2.5. Evaluation of technical alternatives for upscaling the coal gasification reactors with indirect heating

If thermal power and coal input of the indirect-heating coal gasification reactors are desired to upscale to a more commercial application, the following operating parameters should be increased in a significant way compared to those of the historic German semi-technical pilot plant:

- The mean gasification temperature, that depends on several parameters such as the maximum gas outlet temperature of the HTGR used as process heat source (presently 950ºC or less), the heat transfer efficiency at the intermediate helium-helium heat exchanger, and the transfer efficiency of heat between the secondary helium circuit and the steam/coal fluidized bed.
- The dimensions of the gasification reactor where, in particular, the heat transfer surface area and the volume of the fluidized bed that have to be increased significantly.
- The density of the fluidized bed, which is limited in practice by the requirement to avoid agglomerations of fuel particles and to achieve efficient heat and mass transfer between fuel particles and gasifying agents.

Moreover, the use of catalysts of chemical reaction like potassium carbonate (K_2CO_3) can enhance the kinetics of the thermochemical gasification reactions. The essential advantage of using catalysts for accelerating the gasification reactions is that the reaction temperature can be lowered which in turn means that more nuclear heat can be introduced to the gasification process. In the following, a critical analysis on the possible ways to upscale the nuclear-assisted gasification reactors is presented. In this analysis, the use of catalysts for accelerating the gasification reactions was not considered due to the material corrosion problems found in the historic German semi-technical pilot plant with the addition of 4 wt% of K_2CO_3 as catalyst [129]. To explore the possible alternatives for upsizing the indirect-heating gasification reactors to a more commercial phase, a heat balance analysis for an upgraded design of the historic German semi-technical pilot plant was carried out. In this upgraded design, the following assumptions and input data were used:

- The same concept of an immersion heater with tube-type heat exchanger was adopted.
- The height of the fluidized bed was fixed in 4 m as in the historic German semi-technical plant. This value was selected due to a reduction in the gasification reaction rates that was observed experimentally with the fluidized bed height, being attributed to the inhibiting effect of the product gases whose concentration increases with the fluidized-bed height [31].
- The diameter of the fluidized bed was increased up to the maximum diameter used presently in fluidized bed gasification reactors operating with the HTW process, fixing it in 2.75 m that corresponds to the inner diameter of the HTW gasification reactor of Berrenrath, Germany [154]. Accordingly, the cross-section area of the fluidized bed in the upgraded design, could be increased by a factor or 9.3 with respect to that of the historic German semi-technical plant.
- The heat transfer area F was assumed to increase by the same factor of the fluidized bed cross-section area. It means that the increased cross-section area of the upgraded design is considered to be fully packed with tubular heat exchanger bundles. By this

way, the heat transfer area in the upgraded design of the semi-technical pilot plant increases from 33 m^2 to 307 m^2 (33 × 9.3).

With these theoretical dimensions of the upgraded gasification reactor design, the thermal power was determined by a heat balance analysis for a helium inlet temperature at the immersion heater of 900ºC, which corresponds to a HTGR gas outlet temperature of 950ºC. The thermal output of the upgraded design resulted in about 10 MWt compared with 1.2 MWt of the historic German semi-technical plant. It has to be marked that this thermal power represents only 6% of thermal output of the German HTR-Module reactor and 2% of thermal power of the Japanese GTHTR300 and German PNP-500 reactors. If higher thermal powers and coal inputs for the coal gasification process with indirect heating are required, different approaches should be considered in the case of using HTGRs as process heat source:

— Replacement of the tube-type immersion heater by a more compact arrangement that allows increase the heat transfer area in the same volume available (for instance a plate-type heat exchanger). This solution seems to be not possible in the near future due to the lack of knowledge and expertise on performance of this type of heat exchangers in the very harsh environment of a coal gasification reactor, i.e. high temperatures and pressures, corrosive atmosphere and so on.
— Change of the vertical cylindrical vessel arrangement by a horizontal cylindrical vessel where the fluidized bed volume can be enlarged by increasing the length of the horizontal cylinder. This solution had been proposed by German researchers during seventies [164], but the gas generator model could not be tested in the field due to the early closure of the project.
— Splitting of the total thermal power required for a given coal input in several gasification reactors connected in parallel, with the dimensions of the upgraded design and powered at 10 MWt each.
— Implementation of a hybrid system where part of the gasification power required to drive the process is provided by a fraction of the HTGR thermal power (not above 10 MWt). The remaining gasification power is supplied by the combustion of part of the feedstock, as occurs in the conventional gasification reactors. For implementing this design solution, a possible arrangement would consist of locating the immersion heater in the post-gasification zone (above the fluidized bed level); for providing the heat needed for the secondary gasification reactions among gaseous products (volatiles, tar, hydrocarbons). In this case, the injection of oxygen/air as oxidizing agent into the gasification reactor would be required along with the introduction of steam.

3.3.2.6. Layout of a nuclear cogeneration plant for electricity and hydrogen production through the coal gasification process

Based on past experiences developed in Germany during seventies and eighties, the present trend towards more sustainable and cleaner energy systems to mitigate the climate change effects, and the technical feasibility study presented above, a possible layout of a nuclear cogeneration plant for electricity and hydrogen production through the coal gasification process is presented in Fig. 44.

The nuclear cogeneration plant comprises the coupling between HTGR with 950ºC of helium outlet temperature and a coal gasification reactor with indirect heating rated at 10 MWt for hydrogen production. The coupling between the nuclear reactor and the gasification/hydrogen generation plant is through a helium intermediate circuit where the secondary helium gas is

heated at 900ºC by a fraction of the primary helium gas that flows along the shell side of a helium-helium heat exchanger (He-He IHX). Two isolation valves on the secondary helium circuit allow isolate promptly the nuclear island from the gasification/H_2 generation plant in case of emergencies.

Since the nuclear thermal power used for providing the process heat required for the steam coal gasification is a small fraction of the total thermal power of the HTGR (2–6%), the remaining fraction of the nuclear heat is applied to electricity generation through a gas turbine cycle. Additionally, electricity is also generated by a steam turbine cycle by taking advantage of the residual heat contained in the secondary helium gas after leaving the gasification reactor.

The crude synthesis gas that leaves the coal gasification reactor, is composed by a mixture of H_2, CO, CO_2 and small amounts of CH_4. After cooling and cleaning steps to remove the acid gases, the synthesis gas is finally treated in a separation unit to separate the hydrogen from the gaseous stream. The concentration of hydrogen in the treated synthesis gas is expected to reach 65% in volume.

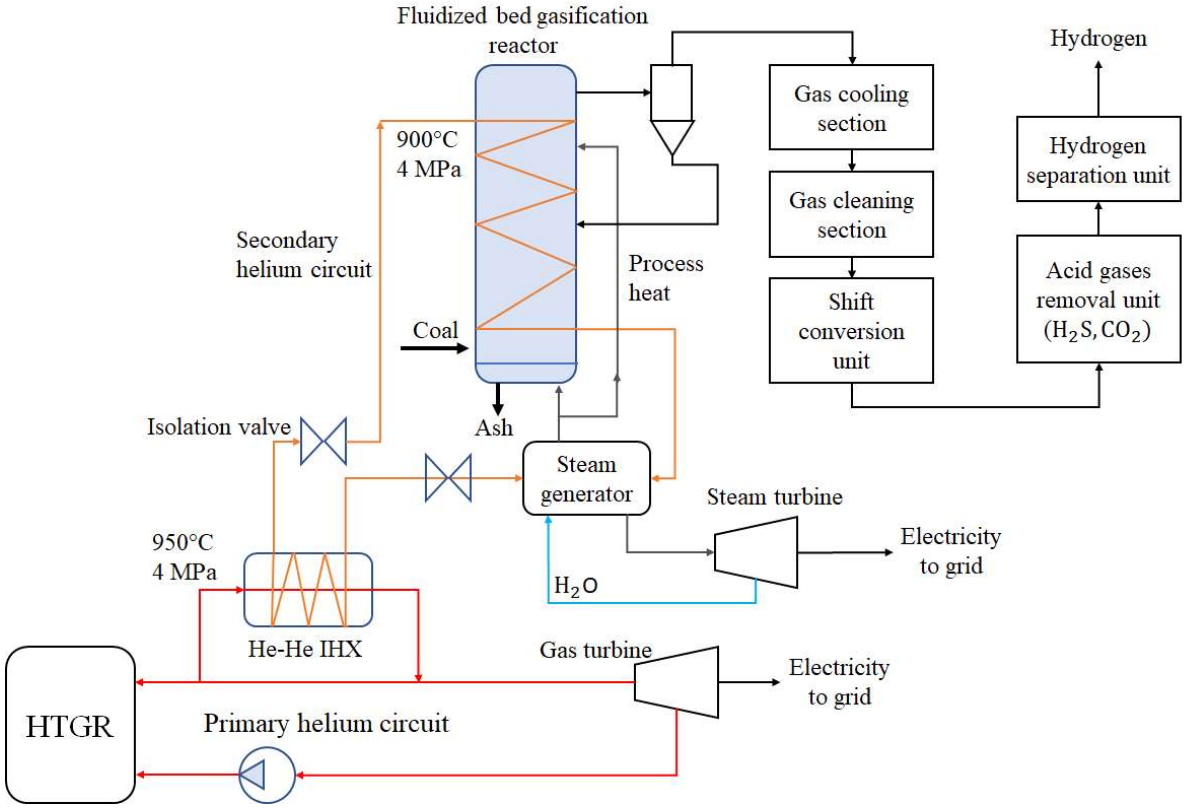

FIG. 44. Layout of the nuclear cogeneration plant for electricity and hydrogen production through the coal gasification process.

3.3.3. Safety considerations of coupling, deployment, and operation

As was said before, in a nuclear/gasification/hydrogen generation energy complex, a fraction of the HTGR thermal energy is transferred to the secondary helium circuit via an intermediate heat exchanger, which is pressurized up to 4 MPa in order to prevent release of radioactivity from the nuclear core in case of an accident. The secondary helium circulates through the inner tubes of an immersion heater submerged into a coal/steam fluidized bed and transfers the

thermal energy required to drive the high-temperature endothermic gasification reactions. The helium gas temperature at the inlet of the immersion heater is assumed to be around 900ºC and the mean gasification temperature to be achieved in such condition is expected to be 700–750ºC.

A relevant issue related with the safety of a nuclear coal gasification for hydrogen production complex is the operability of the gasification plant during a nuclear reactor scram. Present nuclear safety regulations establish that the ultimate heat sink of the nuclear power reactors is limited to water and/or air and cannot be electricity or chemical energy as the result of a conversion process. According to that, the coal gasification process cannot be designed to assume safety functions for the nuclear system as they are exclusively based on the proper functioning of the nuclear reactor cooling system. As the nuclear reactor has to be shut down immediately and remain in a subcritical state in case of a nuclear reactor scram, the abrupt interruption of the nuclear heat input into the gasification plant requires an immediate disconnection of the coal feeding system to the gasification reactor.

A more realistic situation to be expected in the operation of the nuclear/coal gasification/hydrogen production complex is the malfunction or failure of the coal gasification plant instead of the nuclear power reactor. In that sense, a non-expected change of the flow rate of either coal feed or steam induces a thermal disturbance of the helium temperature at the outlet of the immersion heater due to the change of the amount of heat input for the thermochemical gasification reactions. If temperature of the helium returning to the He-He IHX exceeds the allowable limit, the nuclear reactor has to be designed to scram. Potential disturbances that result from a malfunction or failure in the coal gasification process have to be mitigated, and safety measures are then required to allow for a continuous nuclear reactor operation without scram events. If the nuclear reactor scram is unavoidable, the safety measures should be addressed to stop the propagation of thermal disturbances in the secondary helium circuit.

Fire and explosion events inside the nuclear reactor building are also dangerous for the safety-related systems since they are able to produce severe damages to them. According to that, the probability of the ingress into the nuclear reactor building and further ignition of flammable gases like H_2, CO, and CH_4, which are present in the coal gasification reactor, should be as low as possible. An eventual sequence of this kind of accident is a pipe failure in the secondary helium circuit that connects the HTGR with the gasification plant, as a consequence of a strong earthquake. Then, both the secondary circuit pipeline and the gasification reactor should be designed in accordance with the highest seismic safety level. Moreover, a combination of the containment vessel isolation valves in the secondary helium pipeline and the emergency shutoff valve in the coal feed line of the gasification reactor should be provided; to isolate safely the pipe failure and limit the mass of the flammable gas leakage.

Finally, the danger of possible detonations or deflagrations of explosive gas clouds, which can be released from the gasification reactor system is another issue of most interest. In that sense, a safety distance should be adopted between them to avoid the effects of thermal loads arising from fire and blast overpressure due to explosions. It is well known that the safety distance depends on the radioactive inventory present in the nuclear reactor, and it can vary from 100 m to 300 m for most of the nuclear reactors designed for process heat applications.

3.3.4. Economic feasibility evaluation

Preliminary calculations with the IAEA HEEP software were carried out for a quick estimate of the levelized cost of hydrogen (in USD/kg hydrogen) to be produced by processing the Argentine Rio Turbio coal in a nuclear-assisted gasification/hydrogen generation plant.

For the HEEP analysis, the gasification/hydrogen generation plant is considered to be coupled with the HTR-Module reactor of 170 MWt and 950ºC gas outlet temperature. Part of the HTR-Module thermal power (10 MWt) is used as process heat input to drive the high-temperature endothermic gasification reactions. The remaining thermal energy is applied to electricity generation through a steam turbine cycle (producing 48 MWe).

HEEP input data for the HTR-Module were obtained from a State Case Study developed during the former IAEA CRP 17211 "Examining the Techno-Economics of Nuclear Hydrogen Production and Benchmark Analysis of the IAEA HEEP Software".

The Case C of technology based case studies was supplied by Germany and it corresponds to an energy complex where two HTR-Module reactors of 170 MWt/unit are coupled with two hydrogen generation plants for producing hydrogen by steam methane reforming at a total generation rate of 4.2 kg H_2/s [33].

In this study case, part of the HTR-Module thermal output is used as heat input for the steam methane reforming process while the remaining thermal energy produces a fraction of the electricity required for the hydrogen generation plant. Main HEEP input data for the nuclear power plant coupled with the gasification/hydrogen generation plant for processing the Rio Turbio coal are presented in Table 34.

TABLE 34. NUCLEAR POWER PLANT DETAILS

HEEP input data for the HTR-Module of 170 MWt	
Thermal rating (MWt/unit):	170
Heat for the hydrogen generation plant (MWt/unit):	10
Electricity rating (MWe/unit):	48
Initial fuel load (kg fuel/unit):	2396
Annual fuel feed (kg fuel/unit year):	767
Fuel cost (USD/kg fuel):	22937
Capital cost (USD/unit):	6×10^8
Capital cost fraction for infrastructure (%):	10
O&M cost (%):	4
Decommissioning cost (%):	2.5
Construction period (years):	5
Operation period (years):	40

On the other hand, main technical data of the 10 MWt gasification/hydrogen generation plant was obtained from projected values and results of a technical feasibility study based on an upgraded design of the German semi-technical gasification pilot plant. They are summarised in Table 35.

.

TABLE 35. MAIN TECHNICAL DATA OF THE GASIFICATION/H_2 GENERATION PLANT

Main input data of the gasification/hydrogen generation plant	
Thermal rating (MWt/unit):	10
Rio Turbio coal input (kg coal/s):	1.55
Coal conversion rate (%):	80
Effective coal input converted to syngas (kg coal/s):	1.24
Synthesis gas production rate (m^3 syngas/s at standard temperature and pressure):	5.50
Content of hydrogen in the syngas (% in volume):	65
Volume hydrogen production rate (m^3 H_2/s at standard temperature and pressure):	3.60
Mass hydrogen production rate (kg H_2/s):	0.36
Capacity factor of the gasification/H_2 production plant (%):	90
Availability factor of the gasification/H_2 production plant (%):	100
Annual hydrogen production (kg H_2/year):	1.02×10^7

Finally, HEEP input data for the gasification/hydrogen generation plant are presented in Table 36, while the nominal finance values used in the HEEP calculations are given in Table 37.

TABLE 36. HEEP INPUT DATA OF THE HYDROGEN GENERATION PLANT

HEEP input data for the hydrogen generation plant	
Annual hydrogen production (kg H_2/year):	1.02×10^7
Heat consumption (MWt/unit):	10
Electricity required (MWe/unit):	0
Capital cost (USD/unit):	2.00×10^8
Energy usage cost (USD):	0
Other O&M cost (% of capital cost):	8
Decommissioning cost (% of capital cost):	10

TABLE 37. FINANCE PARAMETERS USED FOR HEEP CALCULATIONS

Discount rate	10%
Inflation rate	2.1%
Equity / debt	50% / 50%
Borrowing interest	3.85%
Tax rate	23.8%
Depreciation period	20 years

Using these input data, the levelized cost of nuclear hydrogen production through the coupling between an HTR-Module and a nuclear-assisted gasification/hydrogen generation plant was estimated in 3.88 USD/kg hydrogen. That looks quite promising since it is in the order of other alternatives that are being evaluated for the hydrogen production in Argentina.

Effectively, a research group from Argentina made an economic analysis on the hydrogen production by using conventional low temperature electrolysis, and wind power for the electricity generation in Argentine areas with capacity factors greater than 35% [165]. The evaluation could determine the annual energy available in each area studied, using the information contained in the national wind map. From that, an estimate of the threshold cost of wind power generation such that a project does not have negative returns was done, establishing a relationship between the unit cost in USD/MWh and the capacity factor value. From these analysis results, the levelized cost of hydrogen production for each area under study was evaluated using the H2A software [166].

The levelized cost of hydrogen production by low temperature electrolysis process powered by wind energy was estimated in the range between 2.8 and 3.9 USD/kg hydrogen, without considering costs of hydrogen storage and transport (as in our calculations). As expected, in areas with high-capacity factor values the cost of hydrogen production from wind power was predicted to decrease with increasing the capacity factor. For a conventional electrolysis system with an efficiency of 75%, the lowest cost of hydrogen production was obtained in the provinces of Chubut and Santa Cruz, in the south of the country.

Similar results were obtained for the same research group in another economic evaluation in which the hydrogen was produced by using solar energy instead of wind power to generate the electricity needed for the conventional low temperature electrolysis process. As a result of this analysis, the levelized cost of hydrogen production was predicted to be 3.8 USD/kg hydrogen for the sunnier places located in the mountains of the northern of Argentina [167].

3.3.5. Summary and conclusions

An extensive bibliographic review on past experiences developed worldwide on the use of HTGRs for the nuclear-assisted coal gasification process aimed to cogeneration of electricity and chemicals (synthetic natural gas, liquid fuels, methanol), was carried out. Historic activities, successfully developed during seventies and eighties in Germany, were particularly analysed in depth and critically re-evaluated under the current technology and fuel market conditions. After defining the main technical requirements to be fulfilled by the HTGRs used as nuclear process heat source, and evaluating the different HTGR designs that are being developed all around the world, three HTGR designs were considered to be appropriate for assisting the coal gasification process:

- German designs of the cylindrical core HTR-Modul and the annular core PNP-500, both having a pebble bed core and thermal outputs of 170 MW and 500 MW, respectively, and gas outlet temperature of 950ºC.
- Japanese design of the GTHTR300 with a pin-in-block core and a thermal power of 600 MW, in its upgraded reactor design version with a gas outlet temperature of 950ºC.

The gasification technology for processing coals in a gasification reactor with indirect heating was also defined. As the effective gasification temperature is limited by the maximum core outlet temperature that can be achieved in the present generation of HTGRs (950ºC or less), the gasification technology to be applied is through fluidized bed gasification reactors that operate at moderate temperatures, below the softening and melting points of the coal ashes.

By performing a heat balance analysis of the gasification reactor with indirect heating, it could be concluded that, for the present state-of-art of technology in heat exchangers, the maximum thermal output of the gasification reactor is in the order of 10 MW. This thermal power represents only 6% of thermal output of the German HTR-Module, and 2% of thermal power of the Japanese GTHTR300 and German PNP-500. According to that, the most fraction of the HTGR thermal power has to be applied to electricity generation through a gas turbine cycle and/or a steam turbine cycle.

A critical evaluation of the technical alternatives for upscaling the indirect heating gasification reactors to a more commercial phase was carried out, and the most promising alternatives appear to be:

— Replacement of the tube-type immersion heat exchangers by a more compact arrangement that allows increase the heat transfer area in the same volume available (plate type heat exchangers).
— Change of the vertical cylindrical vessel arrangement by a horizontal cylindrical vessel where the fluidized bed volume can be enlarged by increasing the length of the horizontal cylinder.
— Splitting of the total thermal power required for a given coal input in several gasification reactors connected in parallel and powered at 10 MWt each.
— Implementation of a hybrid system where part of the gasification power required to drive the process is provided by a fraction of the HTGR thermal power (not above 10 MWt), and the remaining gasification power is supplied by the combustion of part of the feedstock, as occurs in the conventional coal gasification reactors.

Main safety considerations about the coupling between a HTGR and a nuclear assisted coal gasification plant for hydrogen production were analysed and based on them, a possible layout of the nuclear cogeneration plant was presented. Since the nuclear thermal power used for providing the heat process required for the coal gasification is a small fraction of the total thermal power of the HTGR, the remaining fraction of the nuclear heat is applied to electricity generation through a gas turbine cycle. Additionally, electricity is also generated by a steam turbine cycle by taking advantage of the residual heat contained in the secondary helium gas after leaving the gasification reactor.

Finally, preliminary calculations with the IAEA HEEP software were carried out for a quick estimate of the levelized cost of hydrogen (in USD/kg H_2) produced by processing the Argentine Rio Turbio coal in a gasification/hydrogen generation plant of 10 MWt that is coupled with an HTR-Module reactor of 170 MWt and 950ºC gas outlet temperature. HEEP calculation results were quite promising, since the estimated levelized cost of nuclear hydrogen production (3.88 USD/kg H_2) is in the order of other alternatives that are being evaluated for the hydrogen production in Argentina. In effect, the cost of the hydrogen production using wind power and solar energy for electricity generation in a conventional low temperature electrolysis process was estimated in the range between 2.8 USD/kg H_2 and 3.9 USD/kg H_2.

3.4. RECOVERY AND UPGRADE OF WASTE HEAT FROM WATER COOLED REACTORS FOR ELECTROLYSIS (UMM AL-QURA UNIVERSITY, SAUDI ARABIA)

Nuclear power plants produce a significant share of the world's electricity demand. According to the IAEA [168], the nuclear electricity share reached 2553.21 TWh as of 2020. Water cooled reactors, including PWR and BWR, are making over 95% of the nuclear plants operating worldwide. For instance, the number of PWR units reached 307, out of which 264 units with capacities of 600 MWe or more. While the number of BWR units was 75, out of which 70 units each produce over 600 MWe [168]. Therefore, what may be seen as a trivial gain in the efficiency or energy unitization of these plants can present a promising opportunity at the global scale. The water-cooled reactors operate in a temperature range below 350°C and over 40°C, considering the heat rejected in the condenser of the secondary circuit (Rankine cycle). This heat is commonly rejected through cooling water into a river or a nearby waterbody. In some plants, the heat rejected is used for district heating which shows more promising economic feasibility in locations with cold weather conditions where heating is required for most of the year. Therefore, what may be seen as a trivial gain in the efficiency or energy unitization of these plants can present a promising opportunity at the global scale. The water-cooled reactors operate in a temperature range below 350°C and over 40°C, considering the

heat rejected in the condenser of the secondary circuit (Rankine cycle). This heat is commonly rejected through cooling water into a river or a nearby waterbody. In some plants, the heat rejected is used for district heating which shows more promising economic feasibility in locations with cold weather conditions where heating is required for most of the year. The concept of waste heat recovery has been investigated by many researchers for various applications, including the production of cooling effects through an absorption system, space heating, seawater desalination, industrial processes, and agricultural applications. Nevertheless, it was rarely proposed for electrolysis hydrogen production. A recent study [169] investigated the use of a gas hydrate heat cycle for waste heat recovery, considering a 1180 MWe PWR plant and reporting an efficiency improvement of 8.7%. The utilization of nuclear waste heat in agricultural applications in the United States was reviewed in Ref. [170]. A novel waste heat upgrading and utilization method was proposed in Ref. [171], studying a vapor compression heat pump with a cascade cycle to utilize the moderator heat and produce hydrogen in the thermochemical Cu-Cl cycle. The proposed system is reported to achieve a 4% energy efficiency improvement.

In order to provide heat at a temperature of about 130°C, a dedicated plant system must be designed to meet such requirements with minimum efficiency penalty. However, the low temperature electrolysers require heat at a temperature of about 90°C, which can be easily by the reactor waste heat with minimum reduction produced power and optimum overall efficiency. The heat rejected by the condenser at about 45°C can be upgraded to 90°C using an external energy source, thereby, a considerable share of the energy required for heat from the ambient condition, e.g., 25°C, is freely supplied by the waste heat. Considering the water specific heat capacity, C_p = 4186 J/kg·°C, the total energy required for heating m = 1 kg of water to T = 90°C, Q, can be calculated according to:

$$Q = m\, C_p(T - T_a) \tag{29}$$

Assuming the ambient temperature is T_a = 25°C, the total energy required to heat 1 kg of water is 272.1 kJ/kg. If nuclear plant heat is utilized to provide water at 45°C, the heat required reduces to 188.1 kJ/kg, this represents an energy reduction of 83.6 kJ/kg, i.e., 30.7% of the total energy required. Furthermore, another alternative is to slightly increase the condenser pressure resulting in an increase in the condensation temperature and thus upgrading the rejected heat to the desired temperature. For example, the advanced power reactor, type APR1400, operates at a condenser pressure of about 5–9 kPa, and the corresponding temperature ranges from 33–44°C. However, if the condenser pressure is raised to 65 kPa, the condenser temperature will automatically rise to 88°C. It is to be noted that the latter option would reduce the plant's energy efficiency. However, it may be worth the consideration to fully utilize the rejected heat and avoid the cost of external heat supply.

In conclusion, the wise utilization of all energy resources leading to the reduction of carbon emissions and energy costs is a primary objective that mandates a critical assessment of current energy systems to look for opportunities to limit environmental impact. The waste heat may be considered low-grade heat with limited useful applications, but the magnitude of this energy can create a momentum of many interesting applications, such as electrolysis hydrogen production.

4. POTENTIAL FOR SMALL MODULAR REACTORS FOR NEAR-TERM HYDROGEN PRODUCTION

4.1. SMALL MODULAR REACTOR TECHNOLOGIES FOR COGENERATION (NATIONAL CENTER OF SCIENTIFIC RESEARCH DEMOKRITOS, GREECE)

This section investigates the possibility of producing hydrogen using energy delivered by SMRs of various designs and types. In principle, any SMR that produces electricity is capable of producing hydrogen, for example by electrolysis, diverting for this purpose part or all of the electrical power it produces.

A quasi exhaustive compilation [172] of SMRs at various stages of achievement that explicitly include the production of hydrogen in their booklet follows:

Light water small modular reactors

— SMR-160 (Holtec International, USA) is a 525 MWt/160 MWe reactor with core inlet/outlet temperature 209/321°C and a system pressure of 15.5 MPa. Its primary application is electricity production with optional cogeneration, including hydrogen production. The reactor is at the Phase 1 of vendor design review with the Canadian Nuclear Safety Commission.

High temperature small modular reactors

— HTR-PM (Tsinghua University, China) with core inlet/outlet temperature 250/750°C, is considered for implementation with 2 or 6 modules and is designed for cogeneration (electricity and hydrogen production). Existing versions include 2× (or 6×) 250 MWt which allow to produce 200 (or 600) MWe and steam at 560°C and 13.24 MPa for high temperature steam electrolysis. The basic version (2×250 MWt driving a single 210 MWe steam turbine) is already in operation (first module connected to the grid on December 20, 2021, full-power operation and control of the dual reactors achieved) whereas the design has been finished for a 650 MWe multi-module plant.
— GTHTR300 (Japan Atomic Energy Agency, Japan) is a <600 MWt/100–300 MWe reactor with core inlet/outlet temperature 587–633/850–950°C and a system pressure of 7 MPa. Apart from electricity generation, the reactor aims at producing hydrogen using thermochemical process with a maximum rate of 120 t/d per reactor module. Its pre-licensing basic design has been completed and commercialization is planned in the 2030s.
— GT-MHR (OKBM Afrikantov, Russian Federation) is a 600 MWt/288 MWe Reactor with core inlet/outlet temperature 490/850°C and a system pressure of 7.2 MPa. Apart from electricity generation, the reactor aims at producing hydrogen using high temperature electrolysis or thermochemical water splitting. Its preliminary design has been completed. GT-MHR modules can be implemented in a hydrogen production plant activating steam methane reforming process or high temperature solid oxide electro-chemical process.
— MHR-100 (OKBM Afrikantov, Russian Federation) comprises helium-cooled reactor models using graphite as moderator. Depending on the model, their capacity is of 215 MWt/25–87 MWe, the range of core inlet/outlet temperature is 490–553/795–950°C and the system pressure is 4–5 MPa. Two of the studied configurations are oriented

towards hydrogen production, namely MHR-100 using high temperature steam electrolysis and MHR-100 using the steam methane reforming method. The reactor is at the conceptual design stage.

— VHTR is a helium cooled and graphite moderated thermal reactor with a capacity of 600 MWt/275 MWe. Coolant outlet temperatures of 900–1000°C are suited for large scale hydrogen production.

Fast small modular reactors

— 4S (Toshiba Energy Systems & Solutions Corporation, Japan) is a pool type, sodium cooled reactor with 30 MWt/10 MWe capacity and core inlet/outlet temperature 355/510°C. A hydrogen and oxygen production system can be incorporated in the 4S reactor with a 3000 m^3/h hydrogen production rate. An enhanced capacity 4S model (50 MWe) can deliver hydrogen at a rate of 15000 m^3/h. The reactor is at the detailed design stage.
— Westinghouse LFR (Westinghouse Electric Company, LLC-USA) is a pool-type, lead-cooled reactor with a 950 MWt/450 MWe capacity. The reactor is working at nearly atmospheric pressure and indicative core inlet/outlet temperatures are 420/600°C. While conceived to deliver baseload electricity, the reactor has the capability of implementing hybrid heat/electricity methods for cost-effective hydrogen generation. The reactor is at the conceptual design stage.
— GFR with a high outlet temperature of the helium coolant of 850°C can deliver electricity and process heat with high conversion efficiency. Its capacity is 600 MWt/275 MWe. The GFR uses a direct Brayton cycle helium turbine for electricity and can provide process heat for the hydrogen production.
— SFR offers the option of electricity production, which may be extended later to hydrogen production and cogeneration, although interest in process heat applications with liquid metal cooled reactors is relatively new.

Molten salt small modular reactors

— CMSR (Seaborg Technologies, Denmark) uses a sodium-actinide fluoride molten salt as fuel. Its capacity is 250 MWt/100–115 MWe and core inlet/outlet temperatures are 600/700 or 700/900°C, depending on the configuration. CMSR is conceived to generate electricity but can co-produce hydrogen, synthetic fuels, ammonia etc. The reactor is at the conceptual design stage.
— FUJI-U3 (International Thorium Molten-Salt Forum, Japan) uses a fluoride molten salt as fuel and coolant and graphite as moderator. Its capacity is 450 MWt/200 MWe and core inlet/outlet temperatures are 565/704°C. FUJI-U3 can be used as heat source for hydrogen production. The reactor's detailed design is not started.
— smTMSR-400 (SINAP, CAS, China) uses a fluoride molten salt as fuel and coolant and graphite as moderator. Its capacity is 400 MWt/168 MWe and core inlet/outlet temperatures are 650/700°C. smTMSR-400 can be used as heat source for hydrogen production. The reactor is at a pre-conceptual design stage.

As far as the near-term deployment of nuclear hydrogen production using SMRs is concerned, it is noticed that the only reactor in the above compilation that is already operational is the

Chinese HTR-PM[3]. All other models are found to be at various design phases from the conceptual to the final one.

4.2. STORAGE AND TRANSPORTATION OF HYDROGEN PRODUCED USING SMALL MODULAR REACTORS (GREECE)

Hydrogen has the potential to be a renewable energy storage solution due to its ability to deliver or store large amounts of energy, provided it is produced in an environmentally friendly manner. A complete energy storage system can be composed of hydrogen production through a hybrid SMR-renewable energy system, hydrogen compression and storage, and hydrogen transportation, making it suitable for a broad range of applications across virtually all sectors.

The importance of hydrogen storage and transportation operations is equal to that of production processes and plays a significant role in the hydrogen economy. The primary objective of storing hydrogen energy is to ensure that it is safe and efficient for use anytime and anywhere [173].

Just like any other product, hydrogen must be packaged, transported, stored, and transferred from production to final use. The main technological challenge facing a viable hydrogen economy is its storage, and so far, a cost-effective method of storing hydrogen has proven to be an insurmountable challenge. To make hydrogen useful for transportation, it must be made more energy dense [174].

Achieving high-density hydrogen storage is a significant challenge for stationary, portable, and transportation applications. Currently available storage options typically involve large-volume systems that store hydrogen in its gaseous form. This is less of a concern for stationary applications where the size of compressed gas tanks is less critical.

Compression is a crucial aspect of almost all storage methods for hydrogen and its subsequent usage. Although hydrogen compression is only part of the hydrogen value chain, it is essential for overcoming the entry barriers to a hydrogen economy. It is widely recognized that significant improvements in the efficiency, durability, and reliability of hydrogen compressors, as well as cost reductions, are needed, especially if the end-use is intended for vehicles or fuelling stations and involves high hydrogen purity requirements for transportation and other industrial applications [175–178].

Efficient hydrogen compression is a crucial element in various applications across the hydrogen supply chain, including onsite storage, transport, and dispensing. Moreover, the development of lightweight high pressure hydrogen storage vessels has resulted in much higher working pressures than before. Currently, diaphragm or reciprocating compressors are typically used at hydrogen fuelling stations. However, poor reliability remains a persistent issue, as current design standards assume prolonged operation at peak pressure, which is not representative of forecourt hydrogen compressors' operating conditions. On/off cycling of compressors due to a lack of station demand exacerbates the operating and maintenance costs of in-service compressors. Additionally, the capital cost of commercial hardware remains high due to low production volumes.

[3] https://www.world-nuclear-news.org/Articles/Demonstration-HTR-PM-connected-to-grid.

Activities to reduce the cost of hydrogen compression at the forecourt include R&D activities to develop design standards and tests that accurately reflect operating conditions. There is also a need for the development of high-temperature polymers and composites that are compatible with hydrogen, as well as the identification of high-strength metallic materials that are resistant to hydrogen embrittlement. Improving compressor efficiency and collecting data on compressor durability and reliability to better understand the current mean time between failures and failure modes are also important steps in reducing costs.

The need for efficient, safe, and cost-effective hydrogen compressors is becoming increasingly apparent. Non-mechanical hydrogen compressors have several benefits over mechanical compressors, including smaller size, lower noise levels, and reduced operating and maintenance costs. Metal hydride compressors are thermally powered systems that rely on the reversible nature of metal hydrides to compress hydrogen without contamination. They can be connected to the outlet of electrolysers and can also use excess renewable energy or waste heat to improve overall system efficiency [175–179].

4.2.1. Hydrogen storage

Hydrogen storage is a vital technology for the development of hydrogen and fuel cell applications in stationary power, portable power, and transportation. Although hydrogen has the highest energy per mass of any fuel, its low ambient temperature density results in low energy per unit volume. Therefore, advanced storage methods with the potential for higher energy density are necessary.

Hydrogen can be stored physically as either a gas or a liquid. Storing hydrogen as a gas typically requires high-pressure tanks (350–700 bar). Storing hydrogen as a liquid requires cryogenic temperatures because the boiling point of hydrogen at one atmosphere pressure is −252.8°C. Materials-based hydrogen storage technologies, including sorbents, chemical hydrogen storage materials, and metal hydrides, can also be used to store hydrogen. The capture and release of hydrogen on materials involve molecular adsorption, diffusion, chemical bonding, Van der Waals attraction, and dissociation. Hydrogen can also be adsorbed in molecular/ionic form on suitable surfaces using pressure, temperature, and electro-chemical potential to control its surface structure and bonding strength.

4.2.1.1. Compressed hydrogen

The compressed hydrogen storage method involves storing hydrogen gas in high-pressure tanks, which can reach pressures of up to 703 kg/cm^2. This storage method is advantageous for fuel purposes because it allows hydrogen to be stored in a smaller space while keeping its energy effectiveness [180]. Increasing the pressure of the gas improves its energy density by volume. However, while the technology behind compressed hydrogen storage is simple, the process itself is inefficient in terms of both volume and weight [181].

4.2.1.2. Liquid hydrogen

At a temperature of 20 K, liquid hydrogen, also known as slush hydrogen, is colourless and non-corrosive. This method of hydrogen storage is commonly used to achieve high concentration of hydrogen storage. Cryogenic storage is required for liquid hydrogen, which allows for higher energy density per volume compared to compressed gas tanks, with a storage capacity of 0.070 kg/L versus 0.030 kg/L. Proper insulation is necessary to maintain the sub-

zero temperature of the storage tanks [180]. Hydrogen atoms or molecules are tightly bound to other elements during the process of liquefaction. Current research is focused on developing composite tank materials that would result in lighter and stronger tanks. While this storage technology appears to be promising in terms of efficiency, more research is needed to address issues such as hydrogen uptake and release, high hydrogen liquefaction rates that cause large energy loss, hydrogen boil-off, and tank costs [182].

4.2.1.3. Chemical storage

Chemical storage involves the use of technologies that rely on chemical reactions to generate hydrogen. Various materials are used for storing hydrogen through chemical storage, including metal hydrides, ammonia, carbohydrates, formic acid, synthetic hydrocarbons, and liquid organic hydrogen carriers [174].

Ammonia

Ammonia, when derived from renewable sources, can be a zero-carbon emissions fuel and a viable option for storing renewable energy. It can be utilized in fuel cells and internal combustion engines. However, ammonia's high nitrogen content leads to increased nitrogen oxides emissions when combusted in high temperatures [183]. Ammonia is a widely traded commodity produced in large quantities by the chemical industry, primarily for fertilizers. This means that there is an existing transportation and distribution network, as well as available port loading infrastructure and experience in handling, making it a more viable option than pure hydrogen. The development of safe ammonia storage is progressing in the form of metal ammine complexes [184].

Metal hydrides

Metal hydrides are known for their ability to absorb and release hydrogen, depending on their temperature (Fig. 45). Although metal hydrides have a hydrogen storage capacity of 5–7 wt%, they require temperatures of 2500°C or higher to achieve this. Releasing hydrogen from metal hydrides also requires high temperatures of around 120–200°C due to the strong binding between hydrides and hydrogen. Metal hydrides used for storage applications offer high hydrogen storage densities and low reactivity for increased safety.

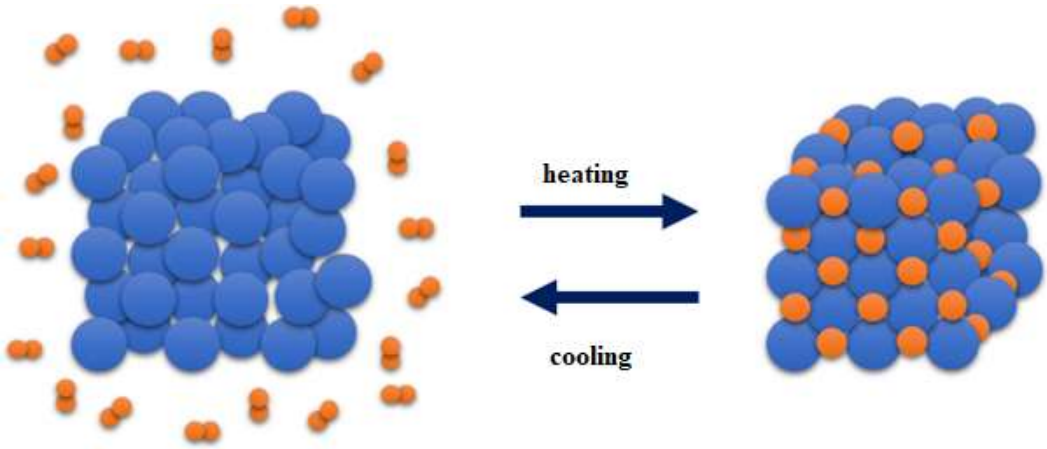

FIG. 45. Schematic representation of hydrogen storage on metal hydrides.

In recent years, a vast number of new intermetallic and partially covalent hydrogen absorbing compounds have been identified and characterized to improve the volumetric and gravimetric capacities, hydrogen absorption/desorption kinetics, and reaction thermodynamics of potential material candidates. Additionally, long-term cycling effects have to be considered for the development of hydrogen-based technologies [185].

Moreover, metal hydrides offer the opportunity to develop a new hydrogen compression technology based on their thermodynamic properties. This technology enables the direct conversion of thermal energy into hydrogen gas compression without the need for any moving parts (see Section 4.4.2 for more information).

Formic acid

Formic acid, also known as methanoic acid, is a simple carboxylic acid used as an important intermediate in chemical synthesis. It is found naturally in bee and ant venom. Researchers are interested in using formic acid as a hydrogen storage material as the hydrogen produced during the reaction is free from carbon monoxide. The reaction involves the use of water-soluble ruthenium catalysts that selectively decompose HCOOH into H_2 and CO_2 in aqueous solution (Fig. 46) [186]. By providing pressure (1–600 bar), stability and catalytic lifetime get improved, along with the removal of CO, making it a viable hydrogen storage material. Carbon dioxide, the co-product during the decomposition process, can be used as a hydrogen vector by hydrogenating it back to formic acid. At room temperature and atmospheric pressure, formic acid contains 53 g/L hydrogen with a gravimetric density of 4.3 wt%.

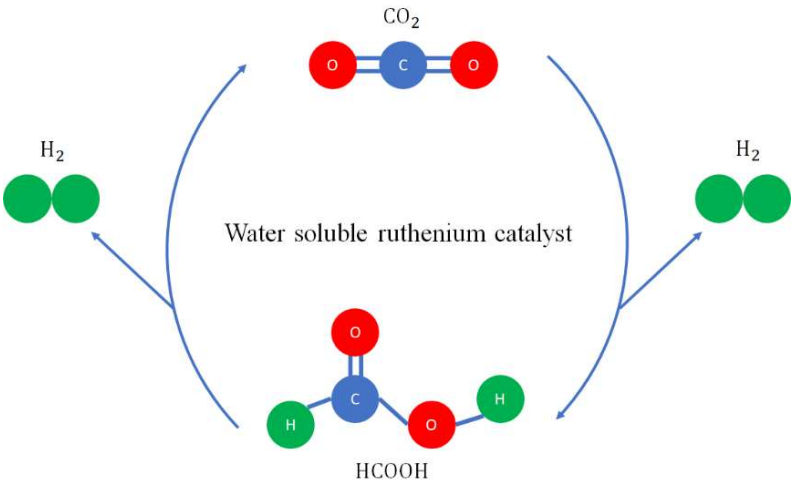

FIG. 46. Schematic representation of homogeneous catalytic system based on water soluble ruthenium catalyst that selectively decomposes HCOOH into H_2 and CO_2 in aqueous solution.

Carbohydrate

Carbohydrates (polymeric $C_6H_{10}O_5$) are the most abundant renewable bioresource available and possess high hydrogen storage densities as a liquid with lower pressurization and cryogenic constraints. They can also be stored as a solid powder. Recently, researchers have been successful in producing nearly 12 mol of hydrogen per glucose unit from cellulosic materials and water. Due to complete conversion and modest reaction conditions, carbohydrates can act as a high energy density hydrogen carrier (14.8 wt%) [187].

Liquid organic hydrogen carriers

Liquid organic hydrogen carriers are unsaturated organic compounds capable of storing large amounts of hydrogen, with gravimetric storage densities of about 6 wt%. The liquid organic hydrogen carriers, such as N-ethylcarbazole, can be hydrogenated/dehydrogenated when energy is needed. The sequence of endothermal dehydrogenation followed by hydrogen purification is considered the main drawback limiting the overall efficiency of the storage cycle. In 2020, Japan built the world's first international hydrogen supply chain between Brunei and Kawasaki City utilizing toluene-based liquid organic hydrogen carriers technology [188]. Figure 47 shows an example of advanced hydrogen storage in liquid organic hydrogen carriers.

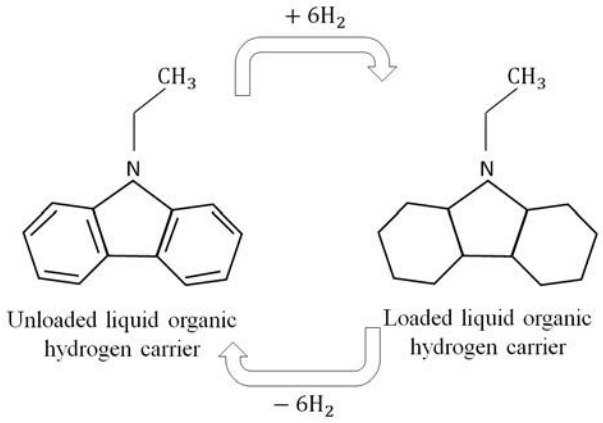

FIG. 47. Advanced hydrogen storage in liquid organic hydrogen carriers.

4.2.1.4. Physisorption

Physisorption is a process in which hydrogen molecules are weakly adsorbed on the surface of a material. One way to improve the kinetics of hydrogen storage is to maintain the molecular identity of hydrogen during the process, which is possible through physisorption. Porous materials, such as carbon materials (fullerenes, nanotubes, and graphene), zeolites, metal-organic frameworks - covalent organic frameworks, microporous metal coordination materials clathrates, and organotransition metal complexes, are the most widely studied materials for physisorption. The compressed gas method requires a large initial pressure, which can cause safety issues, while cryogenic storage requires a large amount of energy input for initial hydrogen condensation. Complex hydrides (e.g., Mg_2NiH_4) are costlier, susceptible to impurities, possess low reversible gravimetric capacity, and undergo desorption at higher temperatures (600 K).

Carbon materials

Van der Waals bonding (~6 kJ/mol) causes hydrogen to adhere to carbon surfaces, such as those found in structures like carbon foam, carbon nanotubes, carbon aerogels, and activated carbon. These structures have high surface area but low volumetric density, whereas fullerene requires high surface area to achieve a sufficiently high packing density.

— Fullerene's spherical curvature results from its pentagonal and hexagonal rings. When a metal atom is supported on carbon fullerene, the electronegativity of C_{60} causes the metal ion to become cationic, allowing it to trap molecular hydrogen through charge polarization. However, theoretical calculations suggest that metal atoms coated on C_{60}

remain largely isolated. Clustering titanium atoms on the C_{60} fullerene reduces hydrogen storage weight percentage.

— Carbon nanotubes, with single or multiple walls, can store hydrogen in their microscopic pores or within their tube structures. They possess high packing density and an estimated capacity of 6 wt%. However, nanotubes' variability in results, processing uncertainties, low synthetic purity, metal clustering, and material instability limit their use.
— Graphene's interaction with hydrogen can be adjusted by tuning the distance between adjacent layers, tuning the sheet curvature, or chemically functionalizing the material, enabling controlled adsorption and desorption of hydrogen. Hydrogen can be stored between graphite layers, and release can be achieved when the material is heated to around 450°C. This method is more efficient than carbon nanotubes and is cheap, safe, and easy to prepare.
— Zeolites, with different pore architecture and composition, force hydrogen into their cavities under elevated temperatures and pressure. When cooled to room temperature, the hydrogen becomes trapped inside the cavity, and release can be induced by raising the system temperature. Zeolites have high thermal stability, low cost, and adjustable composition. The zeolites containing sodalite cages showed a hydrogen storage capacity of 9.2 cm^3/g at 573 K and 10.0 MPa.

Clathrate hydrates

Clathrate hydrates are compounds that contain polyhedral cages made up of hydrogen-bonded water molecules, which can trap guest molecules inside. These compounds typically form two cubic structures known as type I, type II, and type H16. Each structure has distinct crystallographic properties and contains cavities of varying shapes and sizes.

— Type I Clathrate contains 46 water molecules that form two pentagonal dodecahedron (512) and six hexagonal truncated trapezohedron (51262) cages in a single unit cell.
— Type II Clathrate comprises 136 water molecules that form sixteen 512 and eight 51264 cages in a unit cell.
— Type H16 Clathrate is made up of 36 water molecules that form three 512, two 435663, and one 51268 cages in a single unit cell.

Computational studies have shown that the clathrate hydrate cage structures 512 and 51262 can accommodate up to 2 H_2 molecules whereas 51268 can store up to 6 H_2 molecules.

Organotransition metal complexes

Organotransition metal complexes are carbon-based structures containing transition metals that enhance the hydrogen storage capacity of the complex. Some well-known hydrogen storing complexes include Ti-polyacetylene, scandium and vanadium-based ethylene and propane complexes, alkane complexes, Sc atoms and Ti-decorated C_{60} and $C_{48}B_{12}$, niobium based ethene complex, TM-doped organosilica complexes, metal-decorated bucky balls, and multidecker organometallic complexes. These complexes possess high binding energy and have fast hydrogen adsorption and desorption cycles [174].

4.2.2. Hydrogen compression technologies

To transition to an emission-free transport system based on hydrogen, large-scale hydrogen refuelling stations are necessary in Europe. These stations need to have capacities of 1 t/day or more and supply pressure levels of 350 bar or 700 bar, i.e., 500 bar or 900 bar internally in the hydrogen refuelling stations. However, the capital and operational costs of these stations can currently represent more than 3 USD/kg H_2. These costs need to be lowered considerably, particularly operational costs, which are the dominating cost factor for large-scale hydrogen refuelling stations.

About 50% of the cost of hydrogen refuelling stations are related to the compression of hydrogen (Fig. 48) [189]. However, mechanical hydrogen compressors are too costly for large scale applications and lack the desired durability, efficiency, and reliability. A US study attributes 17% of unscheduled maintenance hours to mechanical compressors [190]. This results in high operational and maintenance costs due to the large number of moving parts, the challenge of guaranteeing the tightness of high-pressure moving parts, and the lifetime of membranes (~2000 h). Additionally, mechanical compressors are often too noisy to be operated in hydrogen refuelling stations in many city areas. Most compressors used today for gaseous hydrogen compression are either positive displacement compressors or centrifugal compressors, which can be reciprocating or rotary.

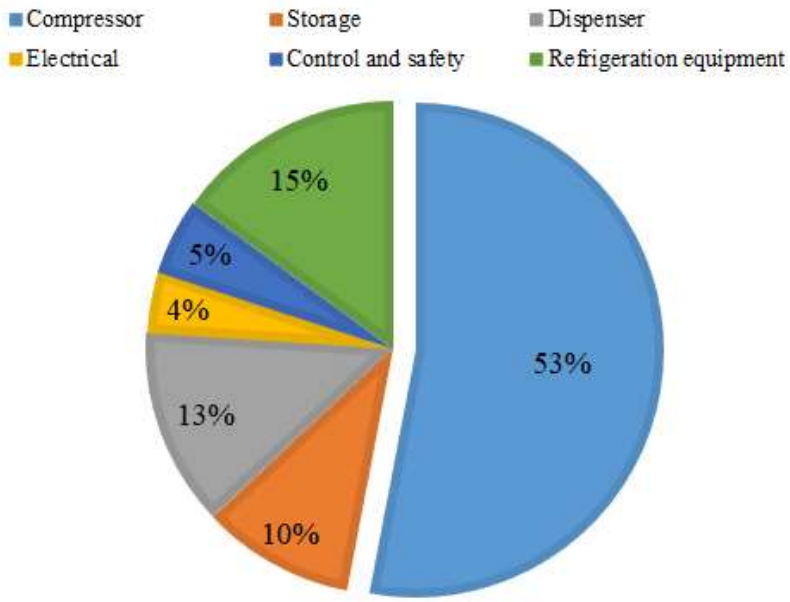

FIG. 48. Contribution of refuelling station components toward the station's levelized cost for a 500 kg/day refuelling capacity (at current low production volume).

Positive displacement compressors and centrifugal compressors are the most commonly used types of compressors for gaseous hydrogen compression.

— Reciprocating compressors use a linear drive motor to move a piston or diaphragm back and forth to compress hydrogen by reducing the volume it occupies.
— Rotary compressors compress hydrogen through the rotation of gears, lobes, screws, vanes, or rollers, but require tight tolerances to prevent leakage.
— Ionic compressors, which use ionic liquids in place of the piston, are a promising

alternative due to their lack of bearings and seals, common sources of failure in reciprocating compressors.
— Centrifugal compressors, on the other hand, are preferred for pipeline applications due to their high throughput and moderate compression ratio.

Other potential compression technologies currently in the research and development stage include electrochemical reactions, metal hydrides, and ionic liquids. Electrochemical compressors use proton exchange membranes, electrodes, and an external power source to drive hydrogen dissociation at the anode and recombination at higher pressures at the cathode. Ionic compressors are hydrogen compressors that use an ionic liquid piston instead of a metal piston. Metal hydride compressors, which use metals that form hydrides via exothermic reactions and then release hydrogen at high pressures when heat is applied, have shown promise in recent studies. An autonomous hybrid system for producing green hydrogen by PV-powered water electrolysis and subsequently compressing it to pressures up to 200 bar with a metal hydride hydrogen compressor has been developed, addressing the integration challenges with the rest of the hydrogen refuelling station system [191].

4.2.2.1. Ionic liquid compressors

An ionic liquid compressor utilizes the unique characteristics of ionic liquids, including their negligible vapor pressures, wide temperature range for the liquid phase, and the low solubility of certain gases like hydrogen. This solubility is used to compress hydrogen up to 1000 bar in hydrogen filling stations by utilizing the body of an ionic liquid. Linde's ionic liquid compressor has significantly reduced the number of moving parts, going from approximately 500 in a typical reciprocating compressor to just 8. The design eliminates many seals and bearings since the ionic liquid does not mix with the gas. Compared to a regular reciprocating compressor, this compressor's service life is approximately ten times longer, and maintenance requirements during use are reduced. Energy costs can be reduced by up to 20%. The heat exchangers used in a standard piston compressor are not needed since the heat is removed in the cylinder itself, where it is generated. Almost 100% of the energy input into the process is utilized, with minimal energy wasted as reject heat.

Furthermore, the conventional metal pistons in Linde's ionic compressor are replaced with a specially designed, nearly incompressible ionic liquid. These organic salts remain in a liquid state within a specified temperature range. Since they do not have a vapor pressure, they do not evaporate or mix with the hydrogen. The unique physical and chemical properties of these liquids make it possible to adjust them to meet virtually any requirement.

4.2.2.2. Electrochemical hydrogen compression

According to insiders, the use of ionic displacement for hydrogen transport was discovered in the 1960s during the development of Nafion®-type membranes for fuel cells. Electrochemical compression of hydrogen works by splitting the hydrogen molecule into protons using a platinum-alloy catalyst on the membrane surface. The protons are then forced through the membrane by an external electric current and recombine on the output side to form hydrogen molecules. Compression is achieved by pumping more hydrogen from input to output while restricting its exit with a back-pressure controller [192].

Figure 49 illustrates the principle of an electrochemical compressor and Fig. 50 indicates the reaction that occur in such a system.

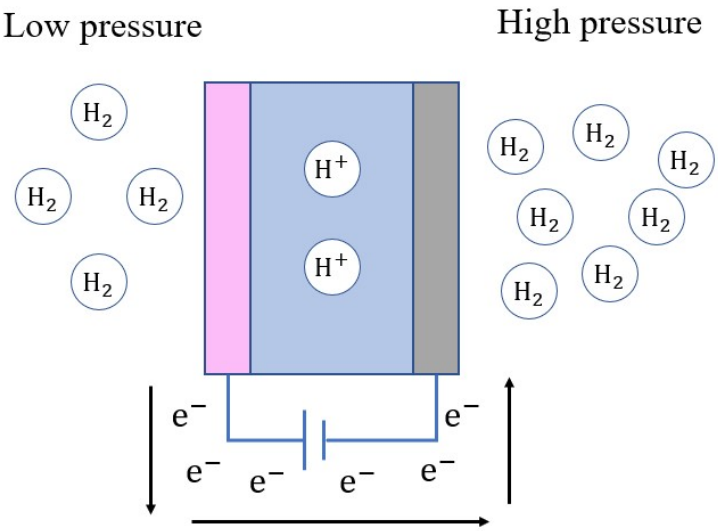

FIG. 49. Electrochemical compressor.

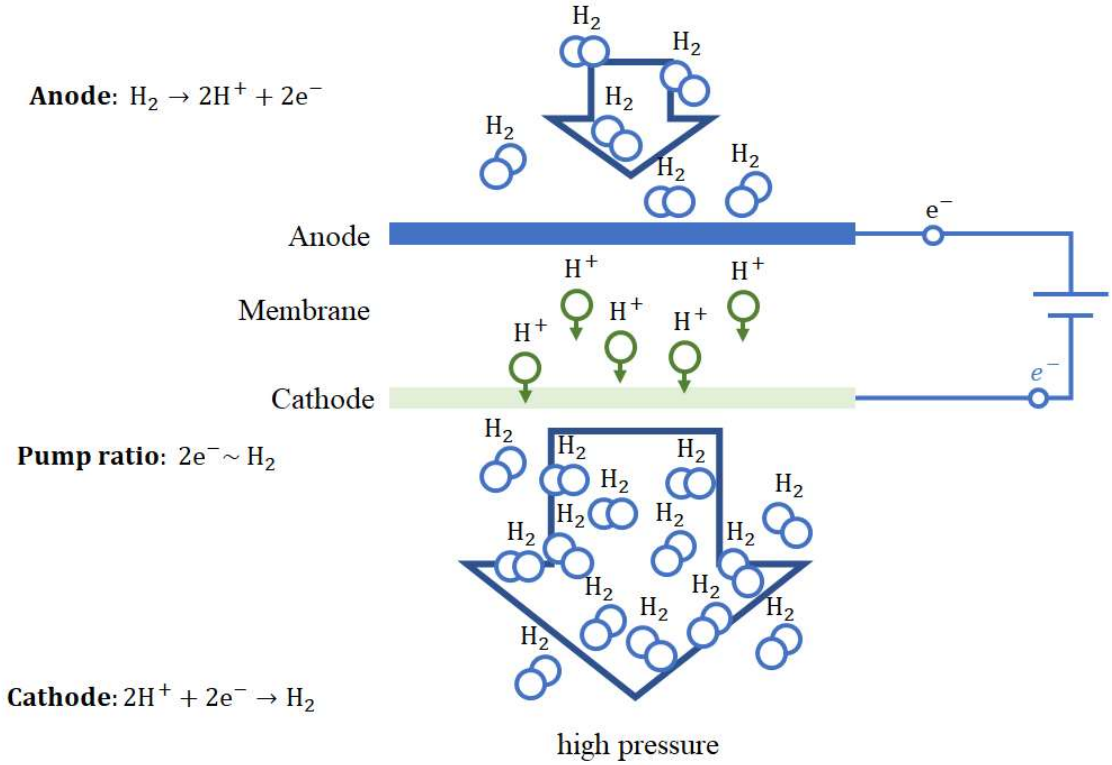

FIG. 50. Electrochemical hydrogen compression uses direct current to pull hydrogen through an impermeable membrane, very efficiently and highly selective for hydrogen.

The limit for pressurized hydrogen depends on the strength of the hydrogen confinement chamber, the permeability of the membrane, and the proton conductivity. Electrochemical hydrogen compression is an efficient and low-maintenance technology that can produce high-pressure hydrogen. The membrane is a crucial component in this process.

Generally speaking, electrochemical hydrogen compression is a potentially high efficient, low-maintenance and silent technology to produce high pressure hydrogen [193].

4.2.2.3. Metal hydride hydrogen compressors

A process to compress hydrogen to high pressure, while avoiding contamination and requiring relatively low energy costs, is based on the reversible hydrogenation/dehydrogenation ability of metal hydrides [194]. This method involves the reversible heat-driven interaction of a hydride-forming metal or alloy or intermetallic compound with hydrogen to form metal hydrides. It is considered an attractive alternative to conventional mechanical and other newly developed electrochemical and ionic liquid piston concepts for hydrogen compression [195, 196]. The advantages of metal hydrides compression include simplicity in design and operation, absence of moving parts, compactness, safety, and reliability. Metal hydrides compression also allows for the utilization of waste industrial heat and/or excess renewable energy for the required heating of the metal hydrides tanks, which can lead to significant operational cost reductions. A metal hydride hydrogen compressor works by absorbing hydrogen at low pressure and temperature and desorbing it at a higher pressure by raising the temperature with an external heat source, such as a heated water bath. Metal hydrides are special alloys like AB5-type or AB2-type, which can chemically store hydrogen in their metallic lattice [197].

This operating principle, called the thermal hydrogen compression system, is based on the equilibrium pressure as a function of temperature and hydrogen content of the hydride. This system can offer an innovative and economical alternative to traditional mechanical hydrogen compressors, in addition to the technical application for hydrogen storage in solid material. The basic principle is depicted in Fig. 51.

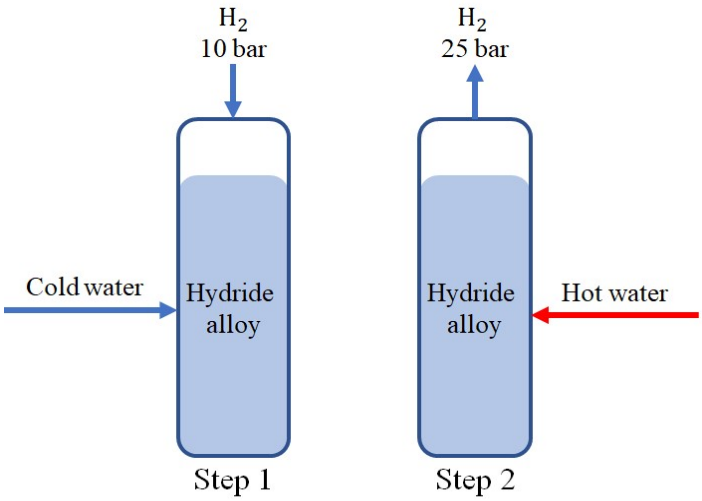

FIG. 51. Metal hydrides based compression principle.

Sufficient information about the metal hydride materials is crucial for designing and developing a metal hydride hydrogen compressor. To predict the level of plateau pressure P, it is necessary to obtain the enthalpy ΔH and entropy ΔS, which are related to the temperature T by van't Hoff's law:

$$ln(P) = \Delta H/RT - \Delta S/R \quad (30)$$

where R is the ideal gas constant.

The pressure increases exponentially with increasing temperature, and moderate temperature changes can result in large pressure values. By selecting appropriate alloys, the metal hydride-based hydrogen compressor can cover a wide range of operating pressures and pressure ratios. For high outlet pressure, multiple hydride units can be connected in series, each with a different alloy and higher operating pressure.

An ideal alloy for hydrogen compression has good hydrogen absorption-desorption rate, fast reaction kinetics, great structural stability during the cycles, and a smaller process enthalpy. Metal hydrides with large pressure to temperature gradients are desirable for compression, especially at low temperatures. FIG. 52 52 illustrates the operation of a three-stage metal hydride hydrogen compressor in a generic Van't Hoff plot.

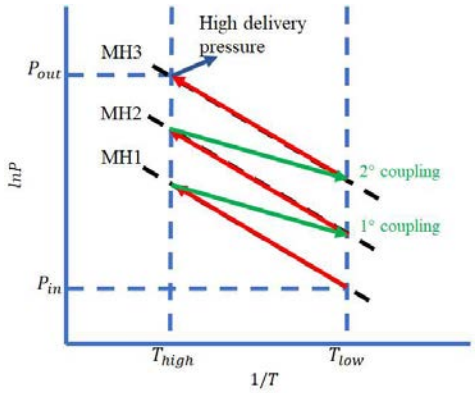

FIG. 52. Generic Van't Hoff plot illustrating the operation of a three-stage metal hydride hydrogen compressor.

Metal hydride hydrogen compression is a promising technology for hydrogen energy systems. It offers advantages over both conventional (mechanical) and newly developed (electrochemical, ionic liquid pistons) hydrogen compression methods. The design is simple, operation is easy, and there are no moving parts, making it compact, safe, and reliable. The use of waste industrial heat or excess renewable energy for heating the metal hydrides containers offers a significant advantage by reducing operational costs. A comparison between metal hydride and mechanical hydrogen compressors is provided in the Table 38 [198].

TABLE 38. COMPARISON OF ADVANCED METAL HYDRIDES COMPRESSORS AND MECHANICAL COMPRESSORS

	Metal hydrides compressor	Mechanical compressor
Hydrogen flow	56.63 Nm^3/h	56.63 Nm^3/h
Inlet pressure	6.89 bar	6.89 bar
Outlet pressure	248.2 bar	248.2 bar
Number of stages	5	3
Weight	1000 kg	3600 kg
Volume	400 L	6000 L
Hot water flow (waste heat)	11.5 m^3/h at 90°C	-
Heat energy required	70 kW	-
Cooling water flow	11.5 m^3/h at 30°C	5.5 m^3/h at 30°C
Electrical power	500 W	20 000 W
Estimated capital cost	€ 130 000	€ 145 000
Annual power cost (2000 h/y, € 0.10/kWh)	€100	€ 4 000
Annual maintenance cost	€ 1 000	€ 8 000

The data presented in Table 38 demonstrates that metal hydrides compressors provide several benefits over mechanical compressors when it comes to large-scale hydrogen production using renewable resources:

- They have considerably lower weight and volume compared to mechanical compressors.
- Their capital cost is slightly lower.
- They have significantly lower operation and maintenance costs.
- They require significantly less energy to operate.
- Waste heat from industry or renewable energy sources can be utilized in metal hydride compressors.
- They are inherently noiseless.

4.2.3. Conclusions

Hydrogen storage plays a crucial role in the advancement of a hydrogen-based economy. Despite its high energy density per unit mass, hydrogen's low volumetric density at ambient temperature and pressure limits its energy density per unit volume. The search for metal hydride materials that can enhance both the gravimetric and volumetric capacities, hydrogen absorption/desorption kinetics, and reaction thermodynamics of potential candidates is ongoing. Additionally, long-term cycling effects have to be considered when developing hydrogen-based technologies.

A noteworthy feature of successful hydrogen storage and transportation systems is simplicity while achieving targets that other alternatives cannot meet. Metal hydrides surpass other storage alternatives in heat storage and provide an opportunity to develop new hydrogen compression technology.

Metal hydride compressors have numerous advantages, including, high purity hydrogen release and heat-based compression rather than work-based compression. Furthermore, these compressors have no moving parts, and pressure only occurs during operation, making them silent and vibration-free. A laboratory-scale compressor is introduced that produces high-pressure hydrogen on demand and automatically refills from the low-pressure hydrogen line when not in use.

Metal hydride hydrogen compressors are highly promising alternatives to conventional technologies for various reasons, as previously mentioned. They rely on thermal energy instead of mechanical energy for compression, resulting in an exergetic efficiency that may exceed that of mechanical compressors. The absence of moving parts ensures a noiseless and vibration-free operation. Metal hydrides allow for hydrogen purification, guaranteeing ultra-pure (99.9999%) hydrogen delivery. Lastly, metal hydride compressors enable hydrogen storage at low pressure, offering a safe buffer while increasing the system's overall flexibility.

4.3. SMALL MODULAR REACTORS-RENEWABLES HYBRID ENERGY SYSTEMS FOR HYDROGEN PRODUCTION (GREECE)

The following paragraphs describe the process of determining the optimal sizing for a hybrid SMR-renewables energy production system for hydrogen production. The island of Crete is considered as a case study, since it has a large enough power consumption for the installation of a SMR to be justified, while being grid connected, thus giving the ability to experiment with

a wider range of potential system setups. The power consumption characteristics of Crete are presented in Table 39.

TABLE 39. POWER CONSUMPTION CHARACTERISTIC OF CRETE

Quantity	Value
Average annual power consumption (GWh)	3198.130
Daily power consumption (GWh)	8.762
Peak load (MW)	700

4.3.1. Grid connected small modular reactor system

First, a system that includes a SMR connected to the grid is examined (Fig. 53).

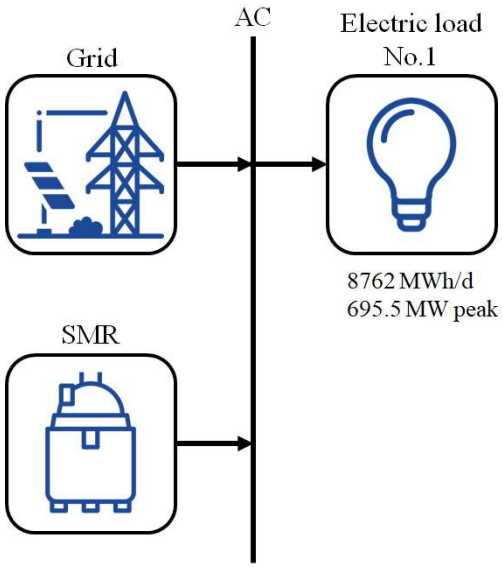

FIG. 53. Schematic of the base system.

The SMR generates enough power for the island's power needs, while selling excess energy to the grid. The system also buys energy from the grid, but only in cases of extreme loads such as the peak load of 650 MW. In this case the sizing of the SMR is dictated by the trade-off between its capital cost and the amount of power that it sells to the grid. This trade-off can be quantified by the LCOE. For the calculation of the CAPEX and OPEX the values that were taken as input are presented in Table 40.

TABLE 40. COST ASSUMPTIONS FOR A SMALL MODULAR REACTOR

Type of cost	USD/kW
CAPEX	3000
OPEX	120 (~4% of CAPEX)

To account for possible reductions in the above costs (stemming from the technological maturity of such systems), the following analysis also includes cases where these values are reduced by 10, 20 and 30%. Also, to account for fluctuations in macro-economic indicators several values for inflation have been taken into consideration.

For the case of a grid connected SMR, the optimization algorithm of HOMER Pro sizes the SMR at 350 MW, which produces the results of Tables 41–43. As seen in TABLE *42* 42, an

SMR of 350 MW can cover 67.8% of the annual electricity needs of the island, with the rest of the energy coming from the grid. Also, the produced energy of the SMR is consumed by the electric load, with excess power sales making up 11.7% of the power consumption (Table 43).

TABLE 41. SMR CHARACTERISTICS

Quantity	Value	Unit
Nominal power	350	MW
Mean output	280	MW
Mean output	6.723	GWh/d
Capacity factor	80	%
Total production	2454	GWh/y

TABLE 42. POWER PRODUCTION OF THE SYSTEM

Production	GWh/a	%
Grid purchases	1167.134	32.2
SMR	2453.850	67.8
Total	3620.984	100

TABLE 43. POWER CONSUMPTION

Consumption	GWh/a	%
Alternative current (AC) primary load	3198.130	88.3
Grid sales	422.854	11.7
Total	3620.984	100

Finally for the base case, which has as inputs the values presented above, the LCOE is calculated as 0.05448 USD/kWh. This value of course is dictated by capital and operating expenditures, which are determined by the level of technical maturity as well as of macroeconomic indicators. For these reasons, Fig. 54 presents their effect on the LCOE. The scenarios examined were the ones with the reduction of CAPEX and OPEX by 10, 20 and 30% respectively.

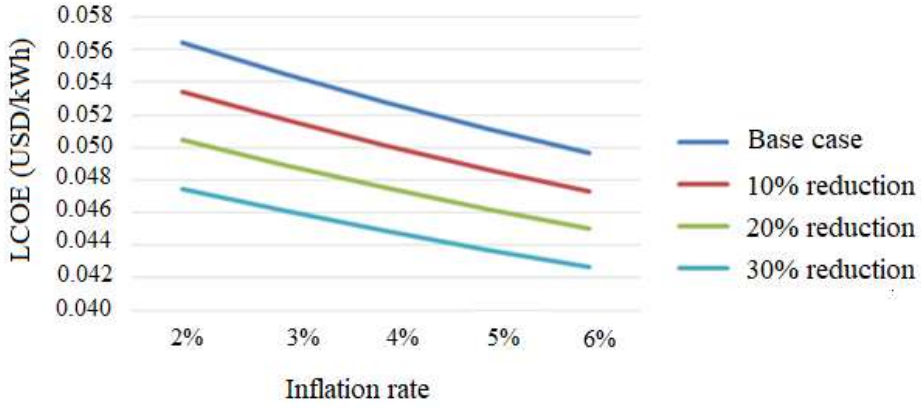

FIG. 54. Inflation effect on LCOE for various CAPEX and OPEX scenarios.

4.3.2. Grid connected small modular reactor/photo-voltaic system

The second part of the analysis considers an additional power source besides the SMR, and more specifically the inclusion of solar panels as a secondary power production system. For this case, the rated capacity of the SMR is considered equal to the one of the previous paragraphs, so the optimization should focus on the optimal sizing of the PV installation. The optimal PV size is determined by the net present value of the system instead of the LCOE, the

reason being that as long as the LCOE value of the PV system is lower than the kWh cost for the energy bought from the grid, the LCOE will be reduced with the increase of the total PV installed capacity. For the following analysis, several different scenarios have been examined, and more specifically the effect of different renewable energy penetration values, as well as potential cost reductions. The assumptions regarding the solar panel costs are presented in Table 44.

TABLE 44. SOLAR PANELS COSTS

Type of cost	USD/kW
Capital expenditures	1500
Operational expenditures (per year)	10

For the case of at least 5% renewable energy penetration, the sizing and details of the PV power generation are shown in Table 45.

TABLE 45. CHARACTERISTICS OF THE PV SYSTEM FOR A MINIMUM 5% RENEWABLE ENERGY PENETRATION

Quantity	Value
Rated capacity (MW)	121.545
Mean output (MW)	23.229
Mean output (MWh/d)	557.486
Total production (GWh/a)	203.482
Capacity factor (%)	19.1
PV penetration (%)	6.36
Max. renewables penetration (%)	31.2

The total power production and consumption of the system are shown in Tables 46–47.

TABLE 46. POWER GENERATION CHARACTERISTICS FOR A MINIMUM 5% RENEWABLE ENERGY PENETRATION

Production	GWh/a	%
Solar panels	203.482	5.4
Grid purchases	1051.876	28.4
Small modular reactor	2453.850	66.2
Total	3709.208	100

TABLE 47. POWER CONSUMPTION CHARACTERISTICS FOR A MINIMUM 5% RENEWABLE ENERGY PENETRATION

Consumption	GWh/a	%
AC primary load	3198.130	86.5
Grid sales	497.763	13.5
Total	3695.893	100

The main economic indicators of the system are shown in Table 48 with the assumption that there is a decrease in the relevant costs for the SMR and the PV.

The cost reductions stem from the level of technical maturity of the used technologies and concern a reduction on CAPEX and OPEX for the SMR by 10, 20 and 30% and a respective reduction on the CAPEX of PV panels by 5, 10 and 15 %.

These cost reductions can be grouped as cases A, B and C, where case A corresponds to a decrease of 10% in SMR and 5% decrease in PV costs, case B corresponds to a 20% decrease

in SMR and a 10% decrease in PV costs, and case C corresponds to a 30% decrease in SMR and 15% decrease in PV costs.

TABLE 48. ECONOMIC INDICATORS FOR A MINIMUM 5% RENEWABLE ENERGY PENETRATION

Indicator	Base case value	Case A	Case B	Case C
Total net present cost (million USD)	3443.787	3256.044	3066.854	2871.631
LCOE (USD/kWh)	0.053	0.050	0.046	0.042
Operating cost (millions USD)	124.252	119.497	110.256	97.935

The exact same methodology as the one described above, is followed in the cases of 10 and 15% renewable energy penetration. The results are presented in Tables 49–56.

TABLE 49. CHARACTERISTICS OF THE PV SYSTEM FOR A MINIMUM 10% RENEWABLE ENERGY PENETRATION

Quantity	Value
Rated capacity (MW)	244.946
Mean output (MW)	46.812
Mean output (GWh/d)	1.123
Total production GWh/a	410.072
Capacity factor (%)	19.1
PV penetration (%)	10.1
Maximum renewables penetration (%)	63

TABLE 50. POWER GENERATION CHARACTERISTICS FOR A MINIMUM 10% RENEWABLE ENERGY PENETRATION

Production	GWh/a	%
Solar panels	410.072	10.7
Grid purchases	985.619	25.6
Small modular reactor	2453.850	63.7
Total	3849.541	100

TABLE 51. POWER CONSUMPTION CHARACTERISTICS FOR A MINIMUM 10% RENEWABLE ENERGY PENETRATION

Consumption	GWh/a	%
AC primary load	3198.130	83.6
Grid sales	628.037	16.4
Total	3826.167	100

TABLE 52. ECONOMIC INDICATORS FOR A MINIMUM 10% RENEWABLE ENERGY PENETRATION

Indicator	Base case value	Case A	Case B	Case C
Total net present cost (million USD)	3464.489	3266.125	3069.166	2871.590
LCOE (USD/kWh)	0.051	0.048	0.045	0.042
Operating cost (million USD)	113.185	109.127	104.677	99.470

TABLE 53. CHARACTERISTICS OF THE PV SYSTEM FOR A MINIMUM 15% RENEWABLE ENERGY PENETRATION

Quantity	Value
Rated capacity (MW)	383.087
Mean output (MW)	73.212
Mean output (GWh/d)	1.757
Total production (GWh/a)	641.340
Capacity factor (%)	19.1
PV penetration (%)	15.1
Maximum renewables penetration (%)	98.5

TABLE 54. POWER GENERATION CHARACTERISTICS FOR A MINIMUM 15% RENEWABLE ENERGY PENETRATION

Production	GWh/a	%
Solar panels	641.340	16
Grid purchases	924.541	23
SMR	2453.850	61
Total	4019.731	100

TABLE 55. POWER CONSUMPTION CHARACTERISTICS FOR A MINIMUM 15% RENEWABLE ENERGY PENETRATION

Consumption	GWh/a	%
AC primary load	3198.130	80.4
Grid sales	781.788	19.6
Total	3979.918	100

TABLE 56. ECONOMIC INDICATORS FOR A MINIMUM 15% RENEWABLE ENERGY PENETRATION

Indicator	Base case value	Case A	Case B	Case C
Total net present cost (million USD)	3496.177	3255.647	3066.854	2871.631
LCOE (USD/kWh)	0.049	0.050	0.046	0.042
Operating cost (million USD)	101.568	121.252	110.256	97.935

4.3.3. Grid connected photo-voltaic/hydrogen systems

The third part of the analysis considers systems that utilize power by a combination of PV panels, SMR and the grid, while also generating hydrogen which covers a daily load for automotive or stationary applications. To do so the system includes an electrolyser and hydrogen tanks. In this instance, the cases that were examined included a daily hydrogen load of 1, 5 and 10 t/ day.

Depending on the size of the hydrogen load, the rest of the system components are sized accordingly as can be seen in the following paragraphs. For each hydrogen load, as in the previous paragraphs, the impact of cost reductions in each component are also examine. The cases which are examined are the reduction by 10, 20 and 30% on capital and operating expenditures for the SMR, and a 5, 10 and 15 % reduction on PV panels and electrolysers.

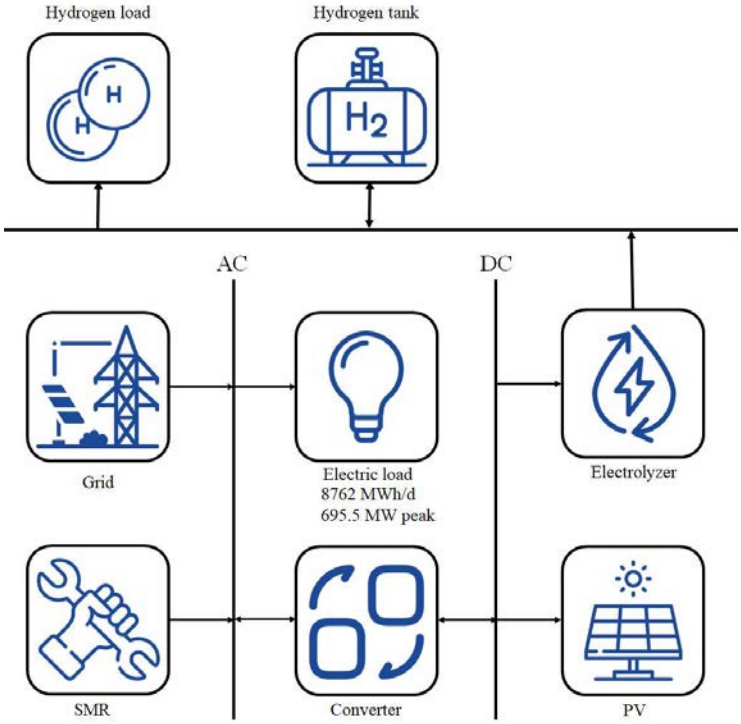

FIG. 55. Schematic of the system.

4.3.3.1. Daily hydrogen demand of one tonne

For 1 tonne daily of hydrogen demand the results from the simulations are presented in Tables 57–61.

TABLE 57. POWER PRODUCTION

Power production	**GWh/a**	**%**
Solar panels	153.113	4.2
Grid purchases	1071.278	29.1
Small modular reactor	2453.850	66.7
Total	3678.242	100

TABLE 58. POWER CONSUMPTION

Power consumption	**GWh/a**	**%**
AC primary load	3198.130	87.2
Grid sales	453.289	12.4
Electrolyser	17.325	0.4
Total	3668.744	100

TABLE 59. CHARACTERISTICS OF THE PV SYSTEM

PV quantity	**Value**
Rated capacity (MW)	91.458
Mean output (MW)	17.479
Mean output (MWh/d)	419.490
Total production (GWh/a)	153.113
Capacity factor (%)	19.1
PV penetration (%)	4.79
Maximum renewables penetration (%)	31.2

TABLE 60. ELECTROLYSER AND HYDROGEN STORAGE CHARACTERISTICS

Hydrogen quantity	Value
Hydrogen production (t/a)	373.351
Rated capacity (MW)	25
Mean input (MW)	1.978
Minimum input (kW)	0
Maximum input (MW)	25
Total input energy (MWh/a)	17.325
Capacity factor (%)	7.91
Mean output (kg/h)	42.6
Minimum output (kg/h)	0
Maximum output (kg/h)	539
Total production (t/a)	373.351
Specific consumption (kWh/kg)	46.4
Amount at end of year (t)	9.351

TABLE 61. ECONOMIC INDICATORS FOR DAILY PRODUCTION OF 1 T OF HYDROGEN

	Base case	Case A	Case B	Case C
Net present cost (million USD)	3496.588	3308.578	3118.406	2920.774
LCOE (USD/kWh)	0.054	0.051	0.047	0.043
Operating cost (million USD)	127.920	121.856	110.374	98.402

4.3.3.2 Daily hydrogen demand of 5 tonnes

For a 5 t daily hydrogen demand the results from the simulations are presented in Tables 62–66.

TABLE 62. POWER PRODUCTION

Power production	GWh/a	%
Solar panels	176.660	4.78
Grid purchases	1063.315	28.8
SMR	2453.850	66.4
Total	3693.826	100

TABLE 63. POWER CONSUMPTION

Power consumption	GWh/a	%
AC primary load	3198.130	86.8
Grid sales	400.891	10.9
Electrolyser	84.711	2.3
Total	3683.732	100

TABLE 64. CHARACTERISTICS OF THE PHOTO VOLTAIC SYSTEM

PV quantity	Value
Rated capacity (MW)	105.524
Mean output (MW)	20.167
Mean output (MWh/d)	484
Total production (GWh/a)	176.660
Capacity factor (%)	19.1
PV penetration (%)	4.79
Maximum renewables penetration (%)	31.2

TABLE 65. ELECTROLYSER AND HYDROGEN STORAGE CHARACTERISTICS

Hydrogen quantity	Value
Hydrogen production (t/a)	1825.471
Rated capacity (MW)	25
Mean input (MW)	9.670
Minimum input (MW)	0
Maximum input (MW)	25
Total input energy (GW/a)	84.711
Capacity factor (%)	38.7
Mean output (kg/h)	208
Minimum output (kg/h)	0
Maximum output (kg/h)	539
Total production (t/a)	1825.471
Specific consumption (kWh/kg)	46.4
Amount at end of year (t)	1.471

TABLE 66. ECONOMIC INDICATORS FOR DAILY PRODUCTION OF 5 T HYDROGEN

	Base case	Case A	Case B	Case C
Net present cost (million USD)	3.552	3 364.344	3 172.509	2 975.457
LCOE (USD/kWh)	0.056	0.052	0.048	0.044
Operating cost (million USD)	129.897	122.360	112.638	99.881

4.3.3.3 Daily hydrogen demand of 10 tonnes

For 10 t daily hydrogen demand the results from the simulations are presented in Tables 67–71.

TABLE 67. POWER PRODUCTION

Power production	GWh/a	%
Solar panels	206.114	5.55
Grid purchases	1056.888	28.4
SMR	2453.850	66
Total	3716.853	100

TABLE 68. POWER CONSUMPTION

Power consumption	GWh/a	%
AC primary load	3198.130	86.3
Grid sales	333.033	8.99
Electrolyser	172.772	4.71
Total	3703.935	100

TABLE 69. CHARACTERISTICS OF THE PV SYSTEM

PV quantity	Value
Rated capacity (MW)	123.117
Mean output (MW)	23.529
Mean output (MWh/d)	564.697
Total production (GWh/a)	206.114
Capacity factor (%)	19.1
PV penetration (%)	6.44
Maximum renewables penetration (%)	31.2

TABLE 70. ELECTROLYSER AND HYDROGEN STORAGE CHARACTERISTICS

Hydrogen quantity	Value
Hydrogen production (t/a)	3723.115
Rated capacity (MW)	50
Mean input (MW)	19.723
Minimum input (MW)	0
Maximum input (MW)	50
Total input energy (GWh/a)	172.772
Capacity factor (%)	39.4
Mean output (kg/h)	0
Minimum output (kg/h)	208
Maximum output (kg/h)	425
Total production (t/a)	3723.115
Specific consumption (kWh/kg)	46.4
Amount at end of year (t)	83.115

TABLE 71. ECONOMIC INDICATORS FOR DAILY PRODUCTION OF 10 T HYDROGEN

	Base case	Case A	Case B	Case C
Net present cost (million USD)	3693.824	3501.286	3306.567	3106.672
LCOE (USD/kWh)	0.059	0.056	0.052	0.048
Operating cost (million USD)	132.796	126.913	118.799	107.666

4.3.4. Conclusions

The results from the simulations which were presented in the previous paragraphs, show that the potential integration of renewable energy sources with SMR for power and hydrogen cogeneration could provide a techno-economically feasible solution in the near future. The LCOE values which are calculated confirm this statement, since not they are found to be within a reasonable range. Also, what would be an additional incentive towards adopting such systems, is the fact that in the above analysis, the income from the potential sales of the remaining hydrogen is not included. Thus, if we assume that the produced hydrogen would be sold, the respective LCOE would be further reduced, meaning that from an economic point of view such an investment would be even more attractive. As a result, such layouts can on the one hand satisfy the respective power demand and on the other, provide a pathway for the large-scale adoption of hydrogen related infrastructure. Thus, what can be deducted is that the use of SMR for hydrogen production, could play a central role in a potential hydrogen economy, since large quantities could be produced by environment friendly methods. Even if hydrogen was not to be sold though, the above analysis leads to the conclusion that it could be an economically viable solution for storing excess energy from solar panels, increasing further the penetration of renewable energy sources.

5. TECHNO-ECONOMIC ASSESSMENT FOR LARGE SCALE AND NEAR-TERM HYDROGEN PRODUCTION

5.1. TECHNO-ECONOMIC ASSESSMENT OF SELECTED OPTIONS OF HYDROGEN PRODUCTION (RUSSIAN FEDERATION)

Techno-economic assessments of hydrogen production were carried out for following options:

- Steam methane reforming and HTSE with MHR-T energy source of heat and electricity;
- Steam methane reforming with HTGR-200 energy source of heat (electricity for own needs is used from grid);
- Steam methane reforming with HTGR-200 energy source of heat and carbon dioxide capture option (electricity for own needs is used from grid);
- Electrolysis using electricity from grid (operating NPP).

The initial conditions for the base calculation are presented in Table 72.

TABLE 72. ECONOMIC INITIAL CONDITIONS FOR THE BASE CALCULATION

Natural uranium price	USD/kg	36.5
Natural gas price	USD/1000 m^3	57
Outside electricity price	USD/MWh	67
USD rate	₽	74.15
Year of assessment		2021

The cost of hydrogen is given by the following expression:

$$Unit\ Cost = \frac{\sum_i \frac{Capital\ Cost_i}{Amortization\ Period_i} + Annual\ O\&M\ Cost}{Annual\ Production} \quad (31)$$

The amortization periods for main equipment of selected options were determined as following:

- Nuclear power plant – 60 years (applied to full capital cost);
- SMR plant (HTGR-200) – 15 years (applied to a cost fraction of main equipment that is 47% of capital cost of SMR plant);
- SMR plant (MHR-T) – 15 years (applied to a cost fraction of main equipment that is 55% of capital cost of SMR plant);
- CO_2 utilization plant – 60 years (applied to full capital cost);
- HTSE plant – 10 years (applied to a cost fraction of main equipment that is 33% of capital cost of HTSE plant;
- PEM electrolyser – 12 years (applied to full capital cost).

Assessments of unit cost of hydrogen were carried out based on developed techno-economic models different to each other for MHR-T, HTGR-200 and electrolysis. Techno-economic parameters and results of assessment of hydrogen cost for MHR-T and HTGR-200 options are presented in Table 73.

TABLE 73. TECHNO-ECONOMIC PARAMETERS OF HTGR-200 AND MHR-T OPTIONS AND RESULTS OF ASSESSMENT OF HYDROGEN COST

Parameter	Unit	HTGR-200 + steam reforming	MHR-T + steam reforming	MHR-T +HTSE
Thermal power	MW	200×4	600×4	600×4
Number of units		4	4	4
Consumption of external electricity (own needs)	MW	192	40	40
Natural gas consumption	Mm^3/year	1770	1269	0
Reactor power for hydrogen production		Full	Part	Full
Hydrogen production	t/year	440 000	400 000	216 200
Nuclear power plant				
Capital cost	Million USD	2 065	2 748	2 748
O&M cost (amortization not included)	Million USD/year	192	324	324
Hydrogen generation plant				
Capital cost	Million USD	1 013	1 496	593
O&M cost (amortization not included)	Million USD/year	296	317	401
Including: energy from NPP	Million USD/year	-	148	370
Including: natural gas	Million USD/year	101.7	72.9	0.0
O&M cost (amortization and energy not included)	Million USD/year	-	169.1	30.8
Cost of hydrogen production	**USD/kg**	**1.28**	**0.96**	**1.98**
CO_2 utilization plant				No CO_2
Own needs	MWe	20	20	0
Capital cost	Million USD	767	767	0
O&M cost (amortization not included)	Million USD/year	62.97	62.97	0.00
Cost addition for CO_2 utilization	USD/kgH_2	0.17	0.19	0.00
Cost of hydrogen (production + CO_2 utilization)	**USD/kgH_2**	**1.45**	**1.15**	**1.98**

Figure 56 presents hydrogen cost dependencies on price of natural uranium and natural gas (with and without CO_2 capture for steam methane reforming option), which were obtained based on the techno-economic model of hydrogen production by MHR-T.

Hydrogen cost for the option of electrolysis using electricity from grid (meaning electricity produced by operating NPP) was calculated based on PEM facility Siemens Sylizer 300[4] (Table 74) using developed techno-economic model.

[4] Silyzer 300 Datasheet (siemens-energy.com).

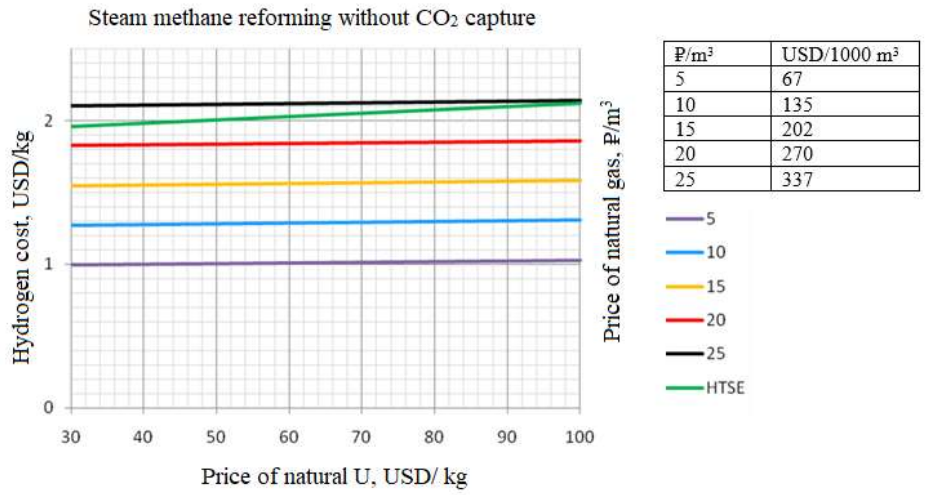

(a)

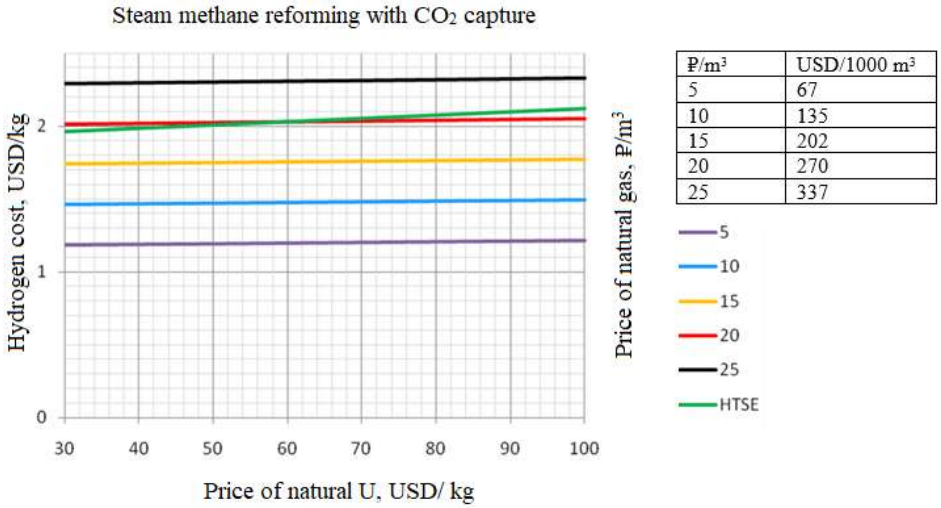

(b)

FIG. 56. Hydrogen cost dependencies on price of natural uranium and natural gas for MHR-T (options steam methane reforming and HTSE). Steam methane reforming (a) without CO_2 capture and (b) with CO_2 capture.

TABLE 74. SILYZER 300 CHARACTERISTICS

Hydrogen production	335 kg/h
Plant efficiency	>75.5%
Power demand	17.5 MW
Start-up time	<1 min
Dynamics in range	10%/s in 0-100%
Minimal load	20% single module
Dimension full mod. array	15.0 × 7.5 × 3.5 m
Array lifetime	>20 years (module ~ 10 y)
Plant availability	~95%
Demin. water consumption	10 L/kg H_2
Dry gas quality	99.9999%
Delivery pressure	Customized

Techno-economic parameters and results of assessment of hydrogen cost for Sylizer 300 are presented in Table 75.

TABLE 75. TECHNO-ECONOMIC PARAMETERS OF SYLIZER 300 AND RESULTS OF ASSESSMENT OF HYDROGEN COST

Type of electrolysis	PEM
Installed capacity, MW	17.5
H_2 production, m^3/h	3728
H_2 production, kg/h	335
Capital cost, millions USD	29.7
O&M cost, millions USD/a	12.8
O&M specific cost (capacity factor=0.9), USD/kgH_2	
- Electricity (~67 USD/MWh)	3.68
- Water	0.01
- Service	0.15
- Salary	0.05
- Other	0.96
Unit cost of hydrogen, USD/kg hydrogen	**5.79**

Based on the calculations performed using the developed economic model of hydrogen production by electrolysis, the unit cost of hydrogen linearly depends, in large degree, on the electricity price (the lower the electricity price, the lower the unit cost of hydrogen).

5.2. HEEP CASE STUDIES (TÜRKIYE, AND RUSSIAN FEDERATION)

5.2.1. HEEP case studies for hydrogen production using thermochemical cycles (Türkiye)

HEEP software is utilized considering various case studies employing some selected hybrid thermochemical cycles for their economic comparisons. Since the HEEP library do not provide information on medium temperature nuclear reactors, certain cases are taken into account as new cases by considering the thermal rating, thermal efficiency, heat-to-power and heat-to-hydrogen plant. The cost assessments of Mg-Cl and Cu-Cl cycles should be conducted utilizing the SCWR or peer nuclear reactors at same thermal load, however they still do not exist in the HEEP database, therefore HTGR is used for the cycles as the heat and power source.

Cu-Cl cycle consumes 133.1 MJ/kmol hydrogen electricity and 308 MJ/kmol hydrogen for a practical plant operation. Here considering the reactor heat to power efficiency at a level close to 50%, the amount of heat for electricity generation corresponds to 270 MJ/ kmol hydrogen and total heat required from the HTGR plant is equals to 580 MJ/kmol hydrogen. Therefore, the reactor condition is established based on the power and heat requirements as shown in Fig. 57(a). Here, when it is considered that power generation system is added to the plant 25% of CAPEX is automatically generated by the HEEP software. For the provided energy to the Cu-Cl cycle it is expected to produce a kmol of hydrogen per second that corresponds to 2 kg/s. Since it is required to enter the hydrogen generation data at an annual level, total annual hydrogen generation corresponds to 53.7 million kg hydrogen with an 85% plant capacity for one unit. Cost of hybrid Cu-Cl cycle is highly dependent on the cost of electrolysers while reactor sizes and other cost contributors also needs to be considered when estimating the plane CAPEX. Here for the large-scale plant cost of Cu-Cl cycle is estimated to be 264 million USD for the aforementioned hydrogen generation as shown in Fig. 57(b). Results of the HTGR-Cu-Cl cycle are summarized in Table 76. The hydrogen cost obtained for this case is 2.99 USD/kg, while most of the cost is due to capital and O&M expenditures.

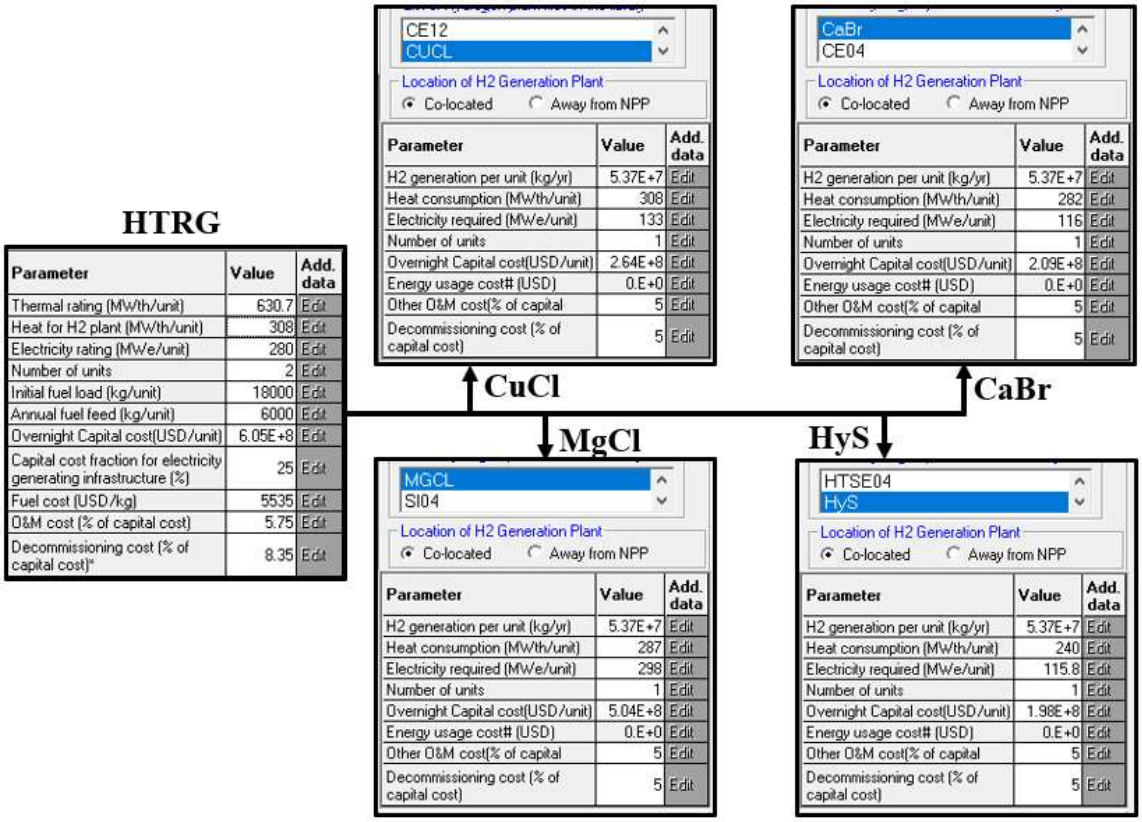

FIG. 57. Thermal rating and economic data of the high temperature gas reactor at HEEP database (a) and corresponding hydrogen generation plants (b) Cu-Cl, (c) Mg-Cl (d) Ca-Br (e) HyS.

TABLE 76. HEEP RESULTS SUMMARY FOR THE HIGH TEMPERATURE REACTOR COUPLED WITH THE COPPER-CHLORINE CYCLE

	Capital cost (debt)	**Capital cost (equity)**	**O&M and refurbishment**	**Consumable cost**	**Decommissioning cost**	**Fuel cost**	**Total of the facility**
NPP	0.38	0.50	0.65	0.00	0.08	0.71	2.32
H_2 plant	0.17	0.22	0.27	0.00	0.02	0.00	0.67
Total	0.55	0.71	0.92	0.00	0.10	0.71	2.99

The three-step Mg-Cl cycle has a theoretical heat and power consumption of 152 MJ and 191 MJ per kg hydrogen generation. However, it is not wise to make such comparison for this case with a Cu-Cl cycle that has been taken into account with more practical results considering reaction yields, higher steam/metal ratio and residence times. Therefore the heat requirement of the Mg-Cl cycle has been taken into account by considering the heat and power requirements as 287 MJ and 298 MJ per kg hydrogen generation as analysed in reference [199]. Under these circumstances cost of the plant significantly increases due to higher electrolysis cells requirement with a resulting CAPEX of 462 million USD for the same amount of hydrogen generation per year. Due to higher CAPEX of the Mg-Cl cycle under more practical operation, cost of hydrogen results in 3.61 USD/kg. This value also is in parallel with a more detailed exergoeconomic study for the enhanced four-step Mg-Cl cycle claiming that the cost of hydrogen is 3.87 USD/kg [200]. Here since higher amount of electricity is generated, cost of electricity is lower compared to Cu-Cl cycle and share of Mg-Cl cycle CAPEX contribution is as high as 30% due to increased electrolysis cell usage. Details for the HEEP results are available in Table 77. The hydrogen cost obtained for this case is 3.61 USD/kg.

TABLE 77. HEEP RESULTS SUMMARY FOR THE HIGH TEMPERATURE REACTOR COUPLED WITH THE MAGNESIUM CHLORIDE CYCLE

	Capital cost (debt)	Capital cost (equity)	O&M and Refurbishment	Consumable cost	Decommissioning cost	Fuel cost	Total of the facility
NPP	0.38	0.50	0.65	0.00	0.08	0.71	2.32
H_2 plant	0.32	0.41	0.52	0.00	0.03	0.00	1.29
Total	0.70	0.91	1.17	0.00	0.12	0.71	3.61

Hybrid Ca-Br cycle, as a modification of the UT-3 cycle has not been studied in detail due to high temperature requirement. However, it is still possible to estimate hydrogen cost from this cycle by considering the heat and power requirements and its maximum temperature being compatible to those of high temperature reactors. In this case Ca-Br cycle has heat and power requirements as high as 116 MJ and 282 MJ of per kmol of hydrogen. For an ideal model, the Ca-Br cycle total estimated CAPEX is around USD 210 million for an annual hydrogen production of 53.7 million kg hydrogen. Therefore, the hydrogen cost from the HTGR coupled with the Ca-Br cycle results in 2.85 USD/kg as shown in Table 78. A rough estimation with high CAPEX due to increased steam/metal ratio and high voltage requirement due to overpotentials could result in around 30% increase and may result in hydrogen cost of 3.03 USD/kg or even higher. For the present reactor-cycle couple Ca-Br cycle covers 20% of overall hydrogen cost while this value may increase at non-ideal conditions.

TABLE 78. HEEP RESULTS SUMMARY FOR THE HIGH TEMPERATURE REACTOR COUPLED WITH THE CALCIUM BROMIDE CYCLE

	Capital cost (debt)	Capital cost (equity)	O&M and refurbishment	Consumable cost	Decommissioning cost	Fuel cost	Total of the facility
NPP	0.38	0.50	0.65	0.00	0.08	0.71	2.32
H_2 plant	0.13	0.17	0.22	0.00	0.01	0.00	0.53
Total	0.51	0.67	0.87	0.00	0.09	0.71	2.85

A final assessment is made based in the HTGR-HyS couple as one of the most matured hybrid thermochemical cycle configurations. HyS cycle has low electrical consumption electrolysis with depolarized SO_2 electrolysis that corresponds to only 15% of water electrolysis, however it is also known that overpotentials may be very significant for the cell operation resulting in an increase 200% more than the theoretical cell voltage which can be beyond 0.6 V in total. Therefore, it is more practical to utilize experimental or zero-dimensional model results to properly estimate the hydrogen cost from the HyS cycle. In this case it is considered that the power consumption of the HyS cycle is considered by considering the overpotentials that corresponds to around 0.4 V. The power requirement increases around 50%, resulting in higher plant power consumption. Here the contribution of the thermal reactor is also lower compared to other hybrid cycles since there is only one reactor present from decomposition while higher temperature operation brings extra cost load to the cycle. CAPEX cost for this case is close to 200 million USD and hydrogen cost from the HTGR-HyS cycle is estimated to be 2.78 USD/kg. even tough realistic input values are taken into account, HyS cycle presents the lowest hydrogen cost among all other cycles.

Table 79 summarizes the cost aspects of the HTGR-HyS plant.

TABLE 79. HEEP RESULTS SUMMARY FOR THE HIGH TEMPERATURE REACTOR COUPLED WITH THE HYBRID SULPHUR CYCLE

	Capital cost (debt)	Capital cost (equity)	O&M and refurbishment	Consumable cost	Decommissioning cost	Fuel cost	Total of the facility
NPP	0.38	0.49	0.64	0.00	0.08	0.70	2.29
H_2 plant	0.12	0.16	0.20	0.00	0.01	0.00	0.49
Total	0.50	0.65	0.84	0.00	0.09	0.70	2.78

Cost comparison of the considered hybrid cycles are represented in Fig. 58. HyS cycle has the lowest hydrogen cost based on results taken from the HEEP software followed by Cu-Cl, Ca-Br and Mg-Cl cycles. Since the main cost contributors are hydrogen plant and cost of thermal and electrical energy it is already expected and well aligned with the reported works in the literature. However, Mg-Cl and Cu-Cl cycles are medium temperature cycles that can be integrated to medium temperature reactors if they were available in the HEEP database. There are many studies in the literature presenting advances in hybrid thermochemical cycles where none of them are ready for market penetration while HyS is the closest one for hydrogen generation in shorter terms. However, it is also reported that challenging electrolysis technologies in the HyS and Cu-Cl cycles are the main issues preventing these cycles to be ready for the market for sustainable hydrogen production. Mg-Cl cycle shows higher hydrogen production cost under realistic conditions with a well-known HCl electrolysis process which has been under operation for different purposes for decades. Under idealistic conditions cost of hydrogen is well below 3 USD/kg while it is not realistic to report such values.

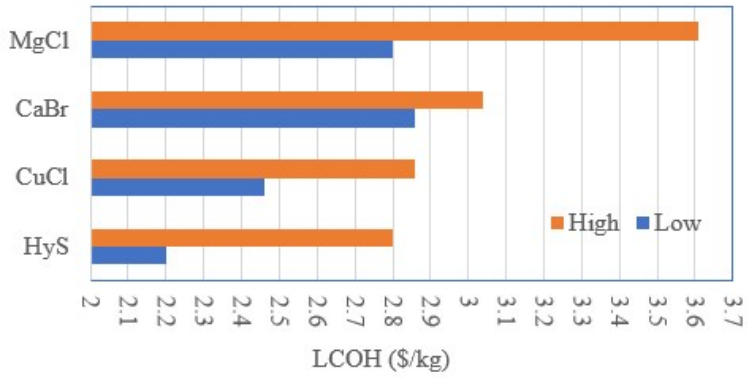

FIG. 58. Cost of hydrogen range from selected nuclear hydrogen generation facilities.

5.2.2. HEEP case studies for hydrogen production using high temperature gas cooled reactors (Russian Federation)

Four options of nuclear hydrogen production have been assessed using HEEP in simplified manner:

- HTGR-200 + steam methane reforming;
- MHR-T + steam methane reforming;
- MHR-T + HTSE;
- Electricity from grid (conditionally PWR) + PEM-electrolysis.

In general, the results obtained using the HEEP are consistent with the results obtained in calculations using the developed models.

Initial data for options and results of HEEP assessments are presented below.

HTGR-200 + steam methane reforming

Capital cost for the hydrogen generation plant of the option HTGR-200 + steam methane reforming has been determined for HEEP, considering to amortization period for main equipment and capital cost fraction of main equipment (Fig. 59). The results are included in Table 80.

Parameter	Value	Add. Data
Thermal rating (MWth/unit)	200	Edit
Heat for H2 plant (MWth/unit)	200	Edit
Electricity rating (MWe/unit)	0	Edit
Number of units	4	Edit
Initial fuel load (kg/unit)	0	Edit
Annual fuel feed (kg/unit)	0	Edit
Overnight Capital cost(USD/unit)	5.16E+08	Edit
Capital cost fraction- electricity generating infrastructure (%)	0	Edit
Fuel cost (USD/kg)	0.00E+00	Edit
O&M cost (% of capital cost)	9.31	Edit
Decommissioning cost (% of capital cost)	0	Edit

Location of H2 Generation Plant: (●) Co-located ( ) Away from NPP

Parameter	Value	Add. Data
H2 generation per unit (kg/yr)	1.10E+08	Edit
Heat consumption (MWth/unit)	200	Edit
Electricity required (MWe/unit)	33	Edit
Number of units	4	Edit
Overnight Capital cost(USD/unit)	6.11E+08	Edit
Energy usage cost# (USD)	0.00E+00	Edit
Other O&M cost(% of capital cost)	12.09	Edit
Decommissioning cost (% of capital cost)	0	Edit

FIG. 59. Data for option: HTGR-200 + steam methane reforming.

TABLE 80. HEEP RESULTS SUMMARY FOR OPTION: HTGR-200 + STEAM METHANE REFORMING

	Capital cost (debt)	**Capital cost (equity)**	**O&M +refurbishment**	**Consumable**	**Decommissioning**	**Fuel**	**Facility total**
NPP	0.00	0.08	0.44	0.00	0.00	0.00	0.51
H_2 plant	0.00	0.09	0.67	0.00	0.00	0.00	0.76
Total	0.00	0.17	1.11	0.00	0.00	0.00	1.28

MHR-T + steam methane reforming

Capital cost for the hydrogen generation plant of the option MHR-T + steam methane reforming has been determined for HEEP, considering to amortization period for main equipment and capital cost fraction of main equipment (Fig. 60). The results are included in Table 81.

Parameter	Value	Add. Data
Thermal rating (MWth/unit)	600	Edit
Heat for H2 plant (MWth/unit)	160	Edit
Electricity rating (MWe/unit)	205.5	Edit
Number of units	4	Edit
Initial fuel load (kg/unit)	0	Edit
Annual fuel feed (kg/unit)	0	Edit
Overnight Capital cost(USD/unit)	6.87E+08	Edit
Capital cost fraction- electricity generating infrastructure (%)	0.001	Edit
Fuel cost (USD/kg)	0.00E+00	Edit
O&M cost (% of capital cost)	11.8	Edit
Decommissioning cost (% of capital cost)	0	Edit

Location of H2 Generation Plant: (●) Co-located ( ) Away from NPP

Parameter	Value	Add. Data
H2 generation per unit (kg/yr)	1.00E+08	Edit
Heat consumption (MWth/unit)	160	Edit
Electricity required (MWe/unit)	30	Edit
Number of units	4	Edit
Overnight Capital cost(USD/unit)	9.87E+08	Edit
Energy usage cost# (USD)	0.00E+00	Edit
Other O&M cost(% of capital cost)	4.28	Edit
Decommissioning cost (% of capital cost)	0	Edit

FIG. 60. Data for option: MHR-T + steam methane reforming.

TABLE 81. HEEP RESULTS SUMMARY FOR OPTION: MHR-T + STEAM METHANE REFORMING

	Capital cost (debt)	**Capital cost (equity)**	**O&M +Refurbishment**	**Consumable**	**Decommissioning**	**Fuel**	**Facility total**
NPP	0.00	0.04	0.30	0.00	0.00	0.00	0.34
H_2 plant	0.00	0.16	0.42	0.00	0.00	0.00	0.58
Total	0.00	0.20	0.72	0.00	0.00	0.00	0.92

MHR-T + HTSE

Capital cost for the hydrogen generation plant of the option *MHR-T + HTSE* has been determined for HEEP, considering to amortization period for main equipment and capital cost fraction of main equipment (Fig. 61). The results are summarized in Table 82.

Parameter	Value	Add. Data
Thermal rating (MWth/unit)	600	Edit
Heat for H2 plant (MWth/unit)	160	Edit
Electricity rating (MWe/unit)	205.5	Edit
Number of units	4	Edit
Initial fuel load (kg/unit)	0	Edit
Annual fuel feed (kg/unit)	0	Edit
Overnight Capital cost(USD/unit)	6.87E+08	Edit
Capital cost fraction- electricity generating infrastructure (%)	0.001	Edit
Fuel cost (USD/kg)	0.00E+00	Edit
O&M cost (% of capital cost)	11.8	Edit
Decommissioning cost (% of capital cost)	0	Edit

Location of H2 Generation Plant: (●) Co-located ( ) Away from NPP

Parameter	Value	Add. Data
H2 generation per unit (kg/yr)	5.41E+07	Edit
Heat consumption (MWth/unit)	160	Edit
Electricity required (MWe/unit)	205.5	Edit
Number of units	4	Edit
Overnight Capital cost(USD/unit)	3.95E+08	Edit
Energy usage cost# (USD)	0.00E+00	Edit
Other O&M cost(% of capital cost)	1.95	Edit
Decommissioning cost (% of capital cost)	0	Edit

FIG. 61. Data for option: MHR-T+HTSE.

TABLE 82. HEEP RESULTS SUMMARY FOR OPTION: MHR-T + HTSE

	Capital cost (debt)	**Capital cost (equity)**	**O&M +Refurbishment**	**Consumable**	**Decommissioning**	**Fuel**	**Facility total**
NPP	0.00	0.21	1.50	0.00	0.00	0.00	1.71
H_2 plant	0.00	0.12	0.14	0.00	0.00	0.00	0.26
Total	0.00	0.34	1.64	0.00	0.00	0.00	1.98

PWR electricity + PEM electrolyser

This option has been modeled in HEEP as away from NPP with including costs for electricity in other O&M costs (Fig. 62), and the results are summarized in TABLE *83* 83.

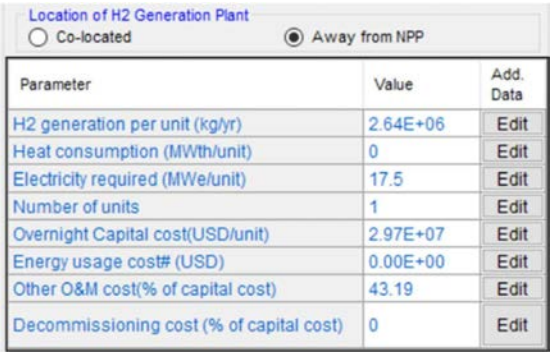

FIG. 62. Data for option: PWR electricity + PEM electrolyser.

TABLE 83. HEEP RESULTS SUMMARY FOR OPTION: PWR ELECTRICITY+PEM ELECTROLYSER

	Capital cost (debt)	**Capital cost (equity)**	**O&M +Refurbishment**	**Consumable**	**Decommissioning**	**Fuel**	**Facility total**
NPP	0.00	0.00	0.00	0.00	0.00	0.00	0.00
H_2 plant	0.00	0.94	4.86	0.00	0.00	0.00	5.80
Total	0.00	0.94	4.86	0.00	0.00	0.00	5.80

5.3. TECHNO-ECONOMIC STUDY OF ELECTROLYTIC HYDROGEN PRODUCTION USING NUCLEAR-SOLAR HYBRID SYSTEM (ALGERIA)

The process considered in the present work is that of hydrogen production using a conventional or low temperature water electrolyser and a high temperature water (steam) electrolyser. For the energy needed to power the process, two different configurations of a nuclear-solar PV hybrid system are considered. The two configurations are explained.

In the first option, a conventional electrolyser is used to produce hydrogen. The electrical energy needed to power the system is provided by both a pressurized water reactor unit and by a solar photovoltaic field.

In the second option, a high temperature electrolyser is used to produce hydrogen. A solar photovoltaic field is used to provide a fraction of the needed electricity for steam electrolysis. A high temperature reactor is also used to provide the needed thermal energy for steam electrolysis and the remaining fraction of the needed electricity for steam electrolysis.

5.3.1. Case of low temperature water electrolysis

As shown in Fig. 63, the system used to produce hydrogen includes a nuclear-based power generation unit, a solar photovoltaic field, a power conditioning unit, and a conventional electrolysis unit. Besides these units, the system includes the auxiliary unit such as the control and regulation unit, and the produced gas separation unit. The main component of the nuclear system is a nuclear reactor for heat generation and a thermodynamic unit that includes a steam generator and an electrical power generator. This system plays an important role in overcoming the intermittency and variability of solar energy. This system produces the part of the nuclear-based electricity that is needed for hydrogen production by electrolysis at low temperature.

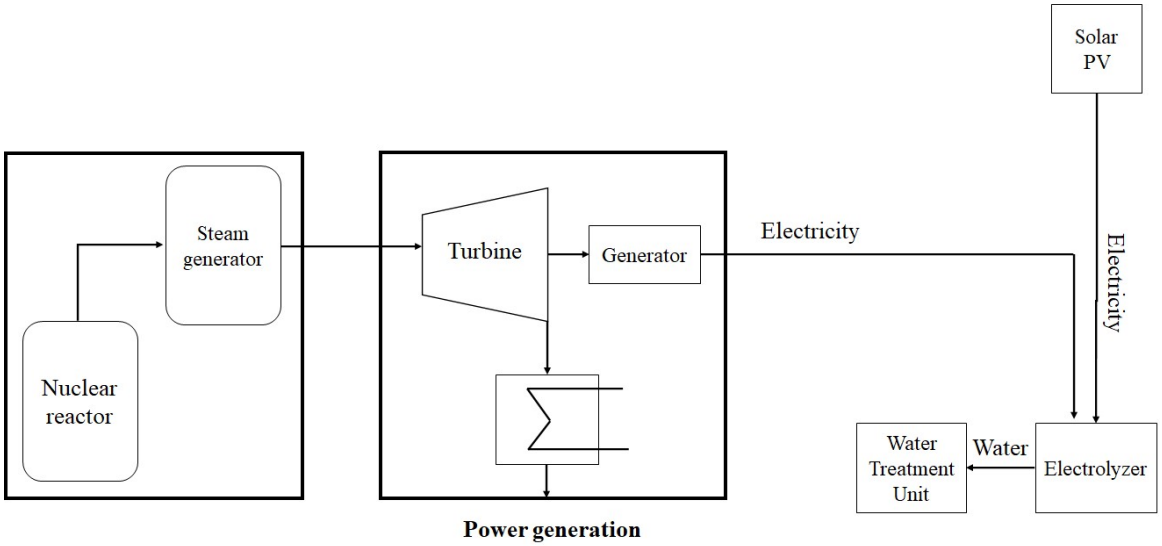

FIG. 63. Hybrid nuclear-solar PV energy system for low temperature hydrogen production.

The nuclear reactor under consideration is a pressurized water reactor. Its role is to provide heat to the steam generator. Its capacity factor is 90%.

Different techno-economic factors and economic models have been reported in the literature, for example [201–204]. In the present study, the main techno-economic factors used in this study are reported in Table 84 [205, 206].

TABLE 84. NUCLEAR TECHNO-ECONOMIC FACTORS

Factor	Value
Type of reactor	PWR
Capacity factor	90%
Capital cost	8776.078 USD/kWe
O&M cost	1.66% of capital cost
Decommissioning cost	2.8% of capital cost
Annual fuel cost	97.75 USD/kWe

5.3.1.1. Solar PV field

The solar photovoltaic field includes mainly the photovoltaic modules for solar radiation collection and conversion into electrical energy. It is assumed that the modules are made of advanced silicon photovoltaic cells of efficiency in the order of 14% –26%.

The solar field is design in such a way that it generates the fraction f_p of the total power of the hybrid system. In this case, the total useful area of the module is given by:

$$A = \frac{EPV}{365\eta_{mod}\eta_T\eta_{op}H_{pv}} \tag{32}$$

where:

EPV – annual electrical energy generated by the PV field
η_{mod} – the solar PV module efficiency
η_T – the temperature effect on the solar photovoltaic module efficiency
η_{op} – the solar photovoltaic module optical efficiency
H_{pv} – solar daily irradiance incident on the inclined photovoltaic modules.

The characteristics of the solar PV system are reported in Table 85 [207].

TABLE 85. CHARACTERISTICS OF THE SOLAR SYSTEM

Parameters	**Values**
Optical efficiency	85%
Cell efficiency	14% –20%
Module efficiency	0.85 × cell efficiency
PV efficiency	85%
Electrolyser efficiency	85%
Temperature effect	75%

The most important parameters needed for the evaluation of electricity generation cost are the solar cell capital cost C_{cel}, the PV capital cost C_{mod}, the cost of the PV balance of system (BOS) $C_{BOS,}$ and the O&M (operational, maintenance, and related costs) C_{OM}. In this model, the cost related to the powering of the balance of system is accounted for by a capital cost C_{BP}.

Different values for these costs have been proposed [206]. In the present work, the costs of the balance of system C_{BOS} and the capital module C_{mod} are taken to be respectively 40 USD/m² and 100 USD/m². The O&M cost C_{OM} is assumed to be 2% of the capital cost while the BOS powering cost is taken to be 1.61 USD/W. It should though be noted that, there are the effects of learning curve and scaling factor that drives these costs down [208]. The relation used to estimate the cost of solar-based electricity generation is given by [209, 210]:

$$C_e = \frac{K\left(C_{BOS} + C_{mod} + C_{BP} I_P \eta_{op} \eta_{mod} \eta_{BOS}\right) + C_{OM}}{31.536 \cdot H_{mod} \eta_{mod} \eta_e \eta_{op} \eta_T} \tag{33}$$

Here I_p = 1 kW/m^2 is the standard solar irradiation. The values of the temperature effect η_T, the module efficiency η_{mod} , the electrolyser efficiency $\eta_{e,}$ and the BOS efficiency η_{BOS} are reported in Table 88.

The economic parameters, i.e., the discount rate, the taxes, the insurances, and the indirect cost are expressed through the factor K. In the present case, its value is estimated to be 0.096.

5.3.1.2. Water electrolysis system

The most important component of the electrolyser unit is the electrolysis cells rack. The electrolyser is a conventional PEM electrolyser. The electrolyser water consumption is assumed to be 0.2 L/kg hydrogen [206]. The most important characteristics of the electrolyser used in this study are given in Table 86.

TABLE 86. CHARACTERISTICS OF THE ELECTROLYSIS SYSTEM

Factor	Value
Electrolyser efficiency	0.85
Coupling efficiency	0.85
Lifetime	20 years
Rated current (mA/cm²)	134
Rated voltage (V)	1.74
Operating current (mA/cm²)	268
Capital cost (USD/kW)	800

Different models have been proposed for the evaluation of the cost of the electrolysis system [211, 212]. In the model considered in this study, the cost of the electrolysis system C_{elec} is given by Ref. [213]:

$$C_{elec} = \frac{K_{el}}{31.536 \cdot n_r CF} C_{em} \left[f_1 + (1 - f_1) \frac{i_r}{i} + \frac{f_2}{2} \left(1 + \frac{i_r}{i} \right) \right] \quad (34)$$

The parameter f_1 *is* the fraction of the electrolyser equipment cost that does not depend on the electrolyser operating and rated current densities i_o and i_r, while f_2 is the fraction of the associated costs, i.e. installation, start up, etc. Values of these parameters are reported in the literature [213-215].

C_{em} and capacity factor are respectively the electrolyser capital cost and the capacity factor. The operation and maintenance cost and the economic related parameters are represented by the factor K_{el} which is found to be 0.128. The other parameters are reported in TABLE 86.

The electrolysis unit is connected to the hybrid nuclear-solar PV system via a converter. This converter is necessary for shaping and conditioning the power issued from the hybrid system. Studies on power conditioning have shown that its efficiency could be as high 97%. In this work, the lifetime of the converter is taken to be 10 years and its capital cost 130 USD/kW [56, 216].

5.3.2. Case of high temperature water electrolysis

5.3.2.1. System description

The system for high temperature water electrolysis powered by a hybrid nuclear-solar PV unit is reported in Fig. 64.

As shown in Fig. 64, the main parts of the hybrid nuclear-solar PV powered high temperature electrolysis system are as follows.

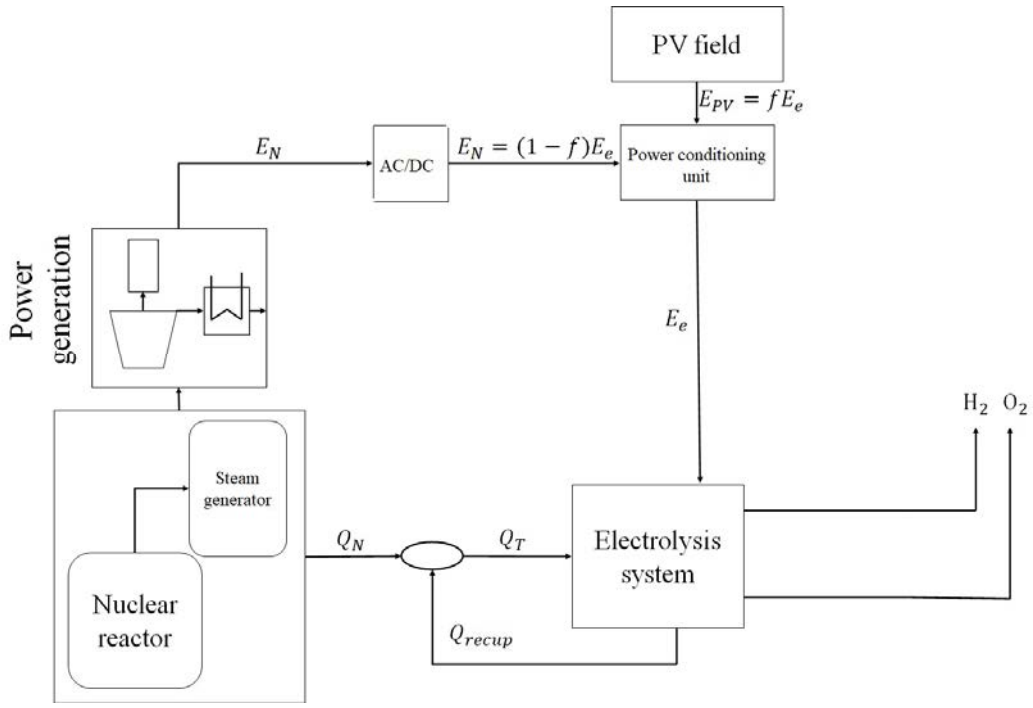

FIG. 64. Hybrid nuclear-solar PV energy system for high temperature hydrogen production.

Solar photovoltaic field

The solar photovoltaic field includes mainly the photovoltaic modules for solar radiation collection and conversion into electrical energy. It is assumed that the modules are made of advanced silicon photovoltaic cells. Details on the physical and economic characteristics of the PV field are already reported in the previous section. They are similar to that of the PV field used in the nuclear-solar PV powered conventional electrolysis system. The solar PV field provides the fraction *f* of the electric energy E_e needed for high temperature water electrolysis.

The nuclear unit

The nuclear unit comprises a nuclear reactor for heat generation, and a thermodynamic unit that includes a steam generator and an electrical power generator. This unit produces the remaining part of the electricity as well as the heat needed for hydrogen production by electrolysis at high temperature. This unit plays an important role in overcoming the intermittency and variability of solar energy. The efficiency of the thermodynamic unit is assumed to be 40%. The nuclear reactor under consideration is a high temperature reactor. The different techno-economic factors of the high temperature reactors are reported in the literature, for example [204, 205]. The main techno-economic factors used in this study are reported in Table 87 [205, 206, 217].

TABLE 87. NUCLEAR TECHNO-ECONOMIC FACTORS

Factor	Value
Type of reactor	PWR
Capacity factor	90%
Capital cost	2500 USD/kW
O&M cost	4% of capital cost
Decommissioning cost	2.8% of capital cost
Annual fuel cost	71 USD/kW

Water electrolysis system

The most important component of the electrolysis unit is the electrolysis cells rack. The electrolyser is a solid oxide electrolyser cell type. The model of this electrolyser is developed below [84, 85] and is used to determine the different parameters such as the operation voltage, the over-potentials, and the over-potential heat. The most important characteristics of the electrolyser used in this study are given in Table 88 [212, 218–222].

TABLE 88. CHARACTERISTICS OF THE ELECTROLYSIS SYSTEM

Parameter	Value
Electrolysis efficiency	0.85
Coupling efficiency	0.85
Capital cost (USD/kW)	661
O&M cost (% of capital cost)	2
Lifetime (years)	20

The system also includes converters and heat exchangers. The economic parameters of these factors are reported in Table 89 [222, 223].

TABLE 89. CHARACTERISTICS OF CONVERTERS

Parameter	Value
Efficiency	0.92
Capital cost (USD/kW)	100
O&M cost (% of capital cost)	2%
Lifetime (years)	20

5.3.2.2. Electrolysis cell modeling

The different parameters characteristics have been determined from existing model [22, 218, 222–224].

The required voltage (V_{op}) for water electrolysis is the sum of the Nernst potential (V_{Nernst}) and the over-potential resulting from losses (V_{ovp}):

$$V_{op} = V_{Nernst} + V_{ovp} \tag{35}$$

The Nernst potential is expressed by the Nernst equation:

$$V_{Nernst} = 1.253 - 2.4516 \cdot 10^{-4} T + \frac{RT}{2F} ln\left(\frac{P_{H_2}\sqrt{P_{O_2}}}{P_{H_2O}}\right) \tag{36}$$

The over-potential, $V_{ovp,}$ resulting from irreversible processes leads to heat generation in the electrolyser. The generated heat, Q_{ovp}, is given by Ref. [222]:

$$Q_{ovp} = 2\ T\ F\ V_{ovp} \tag{37}$$

Moreover, the over-potential (V_{ovp}) is the sum of the activation over-potential (V_{act}), the concentration over-potential (V_{conc}) and the ohmic over-potential (V_{ohm}):

$$V_{ovp} = V_{act} + V_{conc} + V_{ohm} \tag{38}$$

The activation over-potential depends on the activity of the electrodes (γ_a, activity of the anode, and γ_c, activity of the cathode), the current density (J) flowing through the cell and the energy activation of the cathode reaction (E_{ac}), and of the anode reaction (E_{aa}):

$$V_{act} = \frac{RT}{2F}\left(asinh\left(\frac{J}{2\gamma_a} epx\left(-\frac{E_{aa}}{RT}\right)\right) + asinh\left(\frac{J}{2\gamma_c}\exp\left(-\frac{E_{ac}}{RT}\right)\right)\right) \quad (39)$$

The concentration over-potential is related to the impediment to the diffusion of the reactants and products of the electrolysis process. It could be expressed by the following relation:

$$V_{conc} = \frac{RT}{4F} ln\left(\sqrt{1+\frac{JRT\xi d_a}{2FB_g P^2}}\right) + 2ln\left(\frac{1+JRTd_c/2FD_w P_{H2}}{1-JRTd_c/2FD_w P_{H2}}\right) \quad (40)$$

The ohmic over-potential, V_{ohm} results from the resistance to ions flow in the electrolyte and to electrons flow through the electrodes and the metallic contacts in the electrolyser. It can be expressed by:

$$V_{ohm} = \frac{d_a}{\sigma_a} + \frac{d_c}{\sigma_c} + \frac{d_{el}}{\sigma_{el}} exp\left(\frac{-E_a}{kT}\right) \quad (41)$$

The different parameters introduced in the equations with their values used in the present work are reported in Table 90 [18, 212, 221, 225].

TABLE 90. CHARACTERISTICS OF THE SOLID OXIDE ELECTROLYSIS CELL

	Parameters	**Values**
Anode	Thickness (μm)	17.50
	Average pore radius (μm)	1.07
	Average particle diameter (μm)	50
	Porosity	0.48
	Tortuosity	5.40
	Pre-exponential factor (A/m^2)	2.05×10^9
	Activation energy (kJ/mol)	120
	Electrical conductivity (1/(Ω·m))	80000
Cathode	Thickness (μm)	12.50
	Average pore radius (μm)	1.07
	Average particle diameter (μm)	50
	Porosity	0.48
	Tortuosity	5.40
	Pre-exponential factor (A/m^2)	1.344×10^{10}
	Activation energy (kJ/mol)	100
	Electrical conductivity (1/(Ω·m))	8400
Electrolyte	Thickness (μm)	12.50
	Activation energy for electrical resistance (kJ/mol)	85.640
	Pre-exponential factor for electrical conductivity (1/(Ω·m))	33400

For a proper performance of solid oxide electrolysis cell of area *A,* and with a current density *J* flowing through it:

— The hydrogen production rate (n_{H_2}) and the water dissociation rate (n_{H_2O}) are given by:

$$n_{H_2} = n_{H_2O} = \frac{JA}{2F} \quad (42)$$

— The oxygen production rate (n_{O_2}) is given by:

$$n_{O_2} = \frac{JA}{4F} \quad (43)$$

— The electrical power required for hydrogen production (P_E) is given by:

$$P_E = J\,A\,V_{op} \quad (44)$$

— The heat needed for water dissociation is given by:

$$Q_{react} = T\Delta S \quad (45)$$

— Considering the fact that irreversibility generates an over-potential heat Q_{ovp} , then the heat required for electrolysis Q_{we} is:

$$Q_{we} = Q_{react} - Q_{ovp} = T\Delta S - 2\,T\,F\,V_{ovp} \quad (46)$$

5.3.2.3 Operation of the high temperature electrolysis nuclear-solar powered system

The temperature of the high temperature water electrolysis process is assumed to be 1100 K. The hydrogen production rate is 1 kg/s. At the anode flow channel, there is exclusively an oxygen inlet stream flow.

At the cathode flow channel, the inlet stream is a mixture of water and oxygen. A summary of the operation parameters of the system is reported in Table 91.

TABLE 91. SYSTEM OPERATION CHARACTERISTICS

Parameters	**Values**
Inlet steam stream molar composition	10% H_2–90% H_2O
Inlet oxygen stream molar composition	100%
Fraction of steam consumed at electrolyser	80%
SOEC cell area (m^2)	0.04
Current density (A/m^2)	4000

5.3.3. Results

In this study, an analysis and a discussion of the results of the evaluation of hydrogen production using the systems described above, i.e. solar-based system, nuclear based system, hybrid nuclear-solar-based conventional electrolysis system, and hybrid nuclear-solar-based high temperature electrolysis system are carried out. It should be noted that the cost of hydrogen production includes the cost of electricity production and the cost of water electrolysis as well as the cost related to the converters.

For the solar based system, the cost of electricity is the cost of solar electricity generation, while it is the cost of nuclear electricity generation in the case of the nuclear-based hydrogen production system. In the case of the hybrid nuclear-solar system, the cost of electricity is the

sum of the cost of the nuclear-based fraction of electricity and the PV solar based fraction of electricity. The effect of the solar fraction and of the solar irradiance on the costs of electricity and of the hydrogen production as well as on the size of the PV field has been investigated. In the case of high temperature electrolysis, the effect of heat recuperation on the cost of hydrogen is also investigated.

5.3.3.1. Solar photovoltaic–based electrolytic hydrogen production

The evolution of the hydrogen production cost as function of the solar photovoltaic field for two different values of solar irradiance are reported in Fig. 65. In this option, solar PV electricity is used to power a conventional electrolyser for hydrogen production. Besides a water treatment unit and a gas separation unit, the hydrogen production system includes a solar field for solar electricity production, a converter for power conditioning, and a conventional electrolysis unit for hydrogen production.

The estimation of the cost of production has been carried out in two different sites: the site of Annaba with a low solar irradiance value and the site of Adrar with a high irradiance value. From this figure, it is noticed that efficiency of the solar panel plays an important role: there is an exponential decrease in the cost of hydrogen production with an increase in this efficiency. This is an indication that, with the improvement of technology the cost of solar PV-hydrogen production will be cost effective. Moreover, the results show also that an increase in solar irradiance will drastically decrease the cost of hydrogen production. The choice of high irradiance solar sites for hydrogen production units is then highly recommended for cost effective hydrogen production.

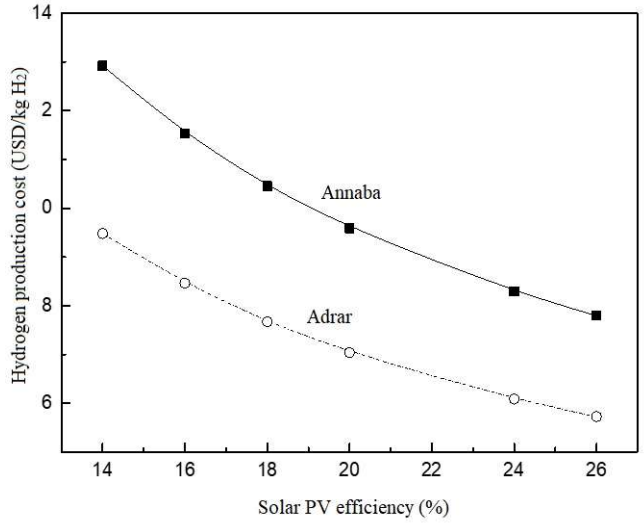

FIG. 65. Evolution of the cost of electricity production with the solar PV efficiency for different values of solar irradiance.

5.3.3.2. Nuclear based electrolytic hydrogen production

In this option, electricity of nuclear origin is used to power a conventional electrolyser for hydrogen production. The nuclear-based electrolytic hydrogen production system includes a nuclear-based power generation unit, more specifically a pressurized water reactor with a power generation system, a power conditioning unit, and a conventional electrolysis unit for hydrogen production. The cost of hydrogen production was evaluated using HEEP, a software

developed by IAEA [33, 203]. The evolution of the cost of hydrogen production for different production rates are reported in Fig. 66.

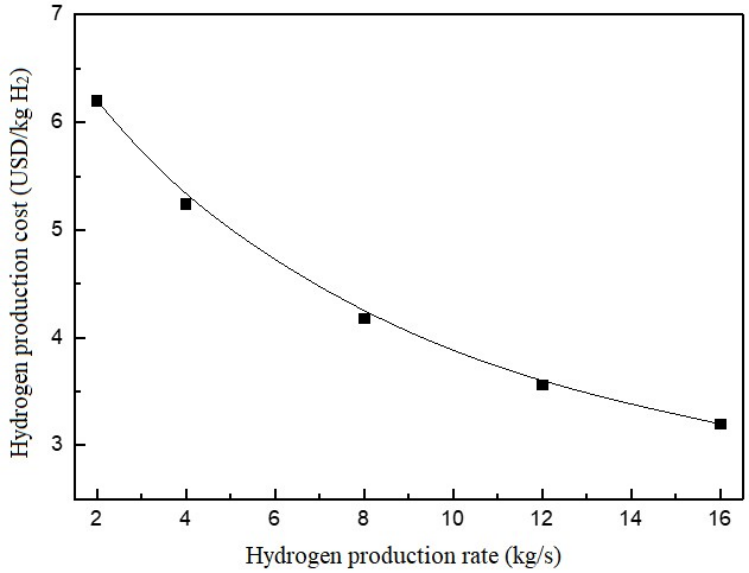

FIG. 66. Evolution of the cost of electricity production with the hydrogen production rate.

Figure 66 indicates the cost depends on the production capacity, i.e., on the size of the production unit. The production is more cost effective for large-scale production unit. Nonetheless, at the actual state of technology, the actual results indicate that nuclear-based hydrogen production technique is more cost effective than the conventional solar PV-based hydrogen production technique. Nuclear-based technique could then be used or combined with solar-based technique to produce hydrogen until solar technologies reach maturity.

5.3.3.3. Hybrid nuclear-solar-based conventional electrolysis system

The evolution of cost of the hybrid system electricity production with the daily solar irradiance incident on the solar PV panels for different solar fractions are reported in Fig. 67. It should be noted that the solar fraction represents, in the present case, the fraction of the total energy of the hybrid system that is of solar energy origin. It can be seen from this figure that the cost of electricity production of the hybrid system increases with increasing solar fraction. That is an indication that the electricity production of nuclear origin is competitive for this range of the daily solar irradiances.

Results have shown that the cost of electricity production of solar origin is higher than the cost of electricity production of nuclear origin in this range of solar irradiance. It should also be noted that the rate of increase depends on the solar irradiance: the higher the solar irradiance the lower the rate of increase in the electricity production cost of the hybrid system.

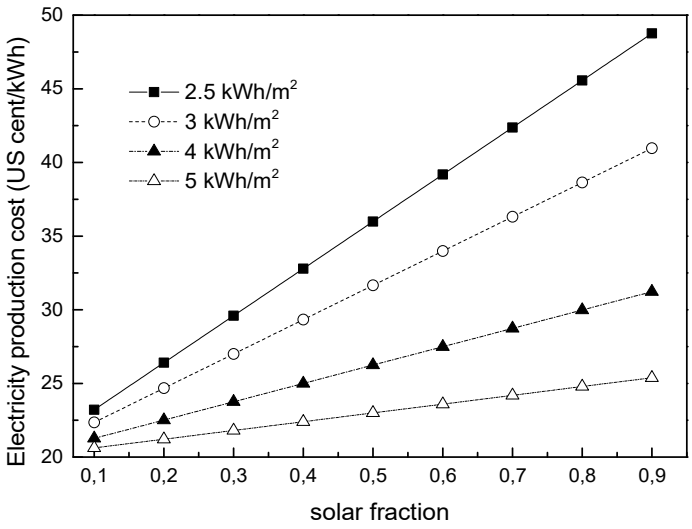

FIG. 67. Evolution of the cost of electricity production with the daily solar irradiance incident on the solar PV panel for different solar fractions: case of low solar irradiance.

However, as reported in Fig. 68, the opposite effect is noticed at high daily solar irradiances.

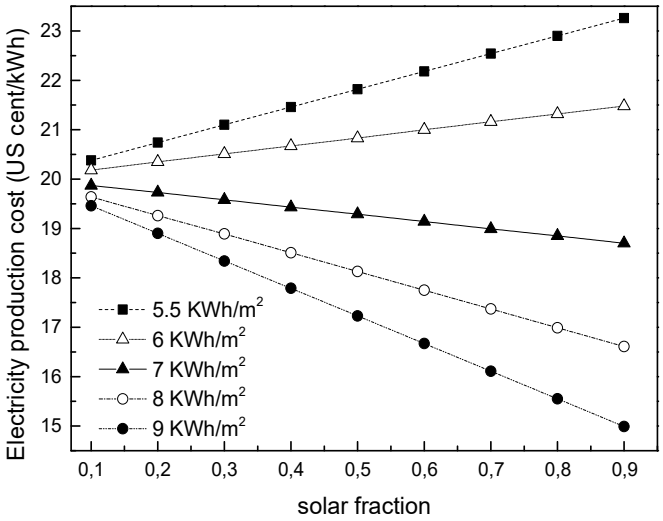

FIG. 68. Evolution of the cost of electricity production with the daily solar irradiance incident on the solar PV panel for different solar fractions: case of low solar irradiance.

Indeed, it can be seen from this figure that above 6.5 kWh/m^2, there is a decrease in the cost of electricity production cost of the hybrid system with an increase in solar fraction.

Figure 69 clearly shows that the rate of decrease increases with increasing solar irradiance. In the present case, electricity production of solar origin is more competitive. The increase in solar fraction leads to an increase in the share of electricity of solar energy origin, and thus a decrease in the overall cost of electricity production of the hybrid system. Figure 69 shows the evolution of the solar PV area with solar fraction at different values of the daily solar irradiance incident on the solar PV panel. The solar PV area is the area necessary for the production of the fraction of the solar based electricity needed for the water electrolysis to produce hydrogen.

It can be noticed from Fig. 69 that the area increases, as expected, with the solar fraction. Indeed, to produce more electricity of solar origin, it is necessary to have more PV cells and then more solar PV panel area. It can though be noticed that the rate of increase in area with the solar fraction decreases with increase in the value of the daily solar radiation incident on the PV panel.

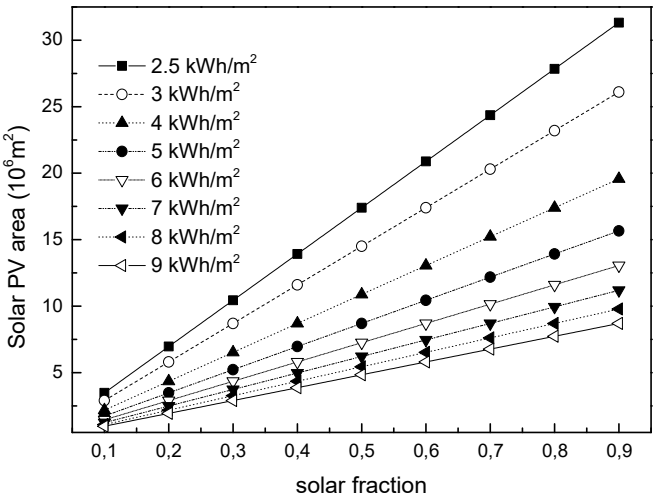

FIG. 69. Solar PV area evolution with solar fraction at different values of the daily solar radiation incident on the solar PV panel.

This rate of increase is 1.22×10^5 m^2 per 1% increase in the solar fraction for a value of the solar radiation of 2.5 kWh/m^2. However, this progression in the rate of increase is only 4.38×10^4 m^2 per 1% increase in the solar fraction for a value of the solar radiation of 7 kWh/m^2, and 3.41×10^4 m^2 per 1% increase in the solar fraction for a value of the solar radiation of 9 kWh/m^2. Moreover, the evolution of the solar PV area with the value of the daily solar radiation incident on the solar PV panel for different values of the solar fraction is reported in Fig. 70. It can be noticed that the solar PV area needed to produce electricity of solar origin drops rapidly to start leveling off at high solar irradiance. It is also seen that the drop in the solar PV area with the solar irradiance increases with the solar fraction.

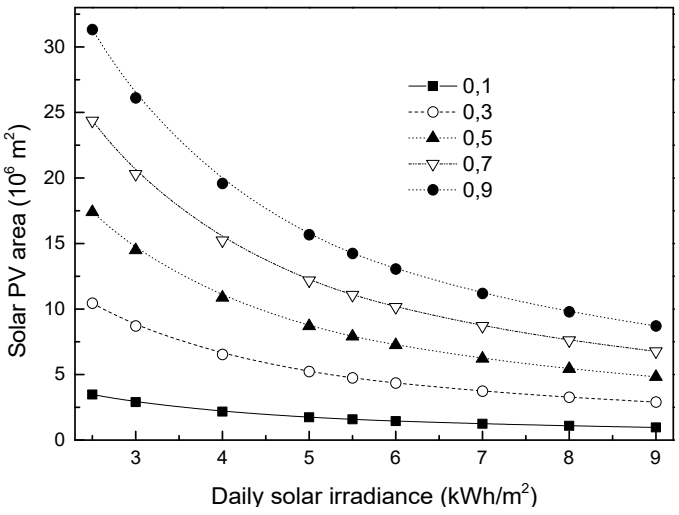

FIG. 70. Solar PV area evolution with daily solar irradiance for different solar fraction.

Hydrogen production cost

Analysis of the hydrogen production cost results have shown that hydrogen production cost is dominated by the cost of production of electricity which, as shown previously, is dependent on the solar fraction and on the site solar irradiance. Figure 71 shows the evolution of the hydrogen production cost with the solar fraction for different values of the solar radiation incident on the PV solar panels.

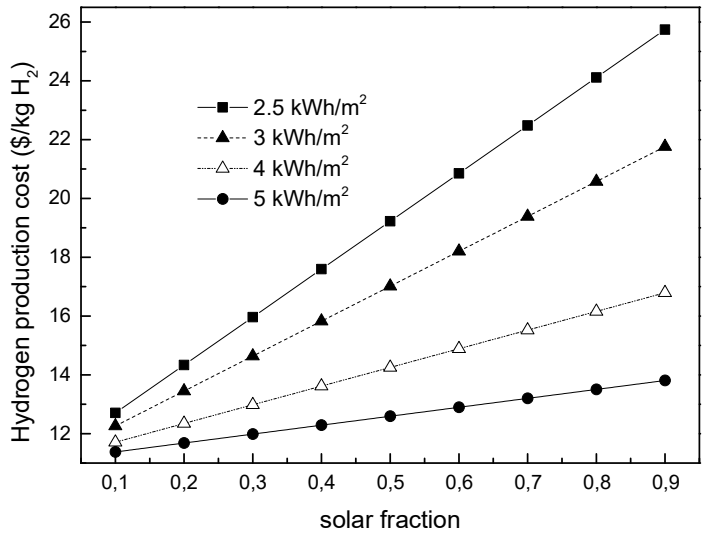

FIG. 71. Evolution of hydrogen production cost with solar fraction at different solar irradiance: case of low solar irradiance.

For this range of values of solar radiation, it can be seen that the cost of production of hydrogen increases with increasing solar fraction. This is because the cost of solar electricity is less competitive and an increase in solar energy increases the cost of hybrid electricity and by that, the cost of hydrogen production. As shown in Fig. 72, the rate of this increase depends on the solar irradiance and the solar fraction.

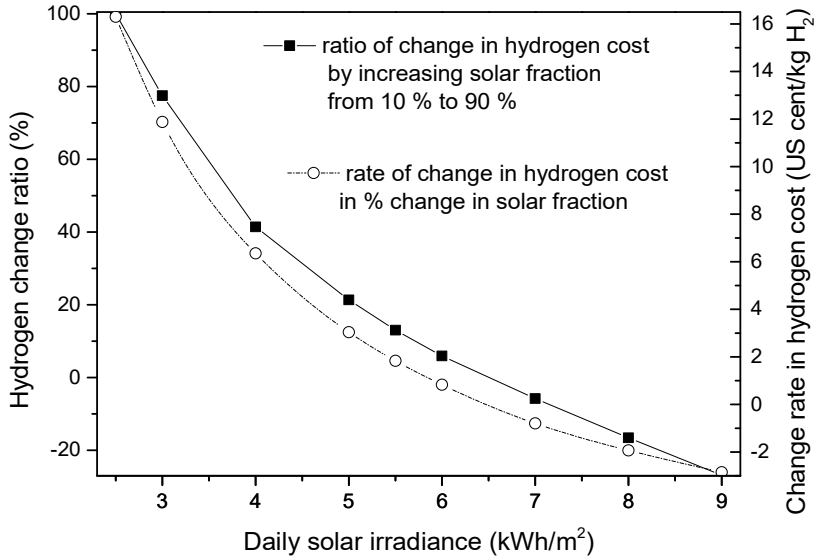

FIG. 72. Evolution of hydrogen production cost change with solar fraction.

The rate of increase has a low value at low irradiation but increases with higher irradiation. It is about 16.30 US cents/kg H_2 by 1% of solar fraction for a solar irradiance of 2.5 kWh/m^2. However, it is only about 0.83 US cents/kg H_2 by 2% of solar fraction for a solar irradiance of 9 kWh/m^2.

As shown in Fig. 73, by raising the value of the solar radiation incident on the solar PV panels, the increase in hydrogen cost diminishes and eventually becomes negative. This is due to the fact, as reported previously, that the solar cost of solar electricity at high solar irradiance is competitive. By introducing more solar electricity, the overall cost of hydrogen production drops.

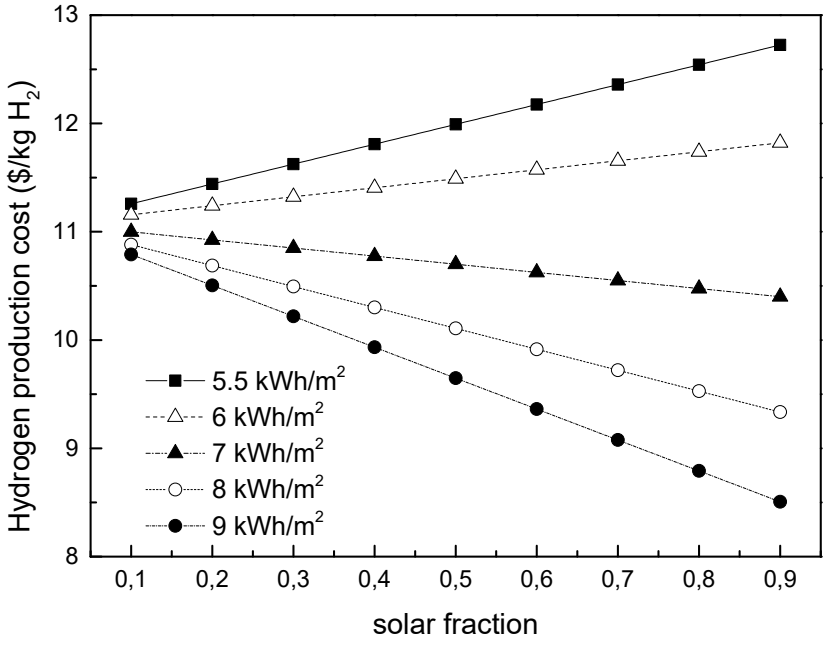

FIG. 73. Evolution of hydrogen production cost with solar fraction at different solar irradiance: case of low solar irradiance.

As seen in Fig. 73, the drop depends on the solar irradiance and the solar fraction. From this figure, it can be seen that the drop is about 0.80 US cents/kg hydrogen by 1% of solar fraction for a solar irradiance of 7 kWh/m^2. However, this drop goes up to about 2.85 US cents/kg H_2 by 1% of solar fraction for a solar irradiance of 9 kWh/m^2. To determine the effect of the solar PV efficiency on the cost of hydrogen production, the evolution of hydrogen production cost with solar PV efficiency at an irradiance of 3 kWh/m^2·day is reported in Fig. 74.

From Fig. 74, it can be noted that cost of hydrogen production decreases exponentially with solar efficiency increase. The cost increases with increasing solar fraction. However, the difference in hydrogen production costs between the different solar fractions decreases with increasing solar PV efficiency. As the value of solar irradiance increases, the evolution of hydrogen production with solar PV efficiency gives some interesting results.

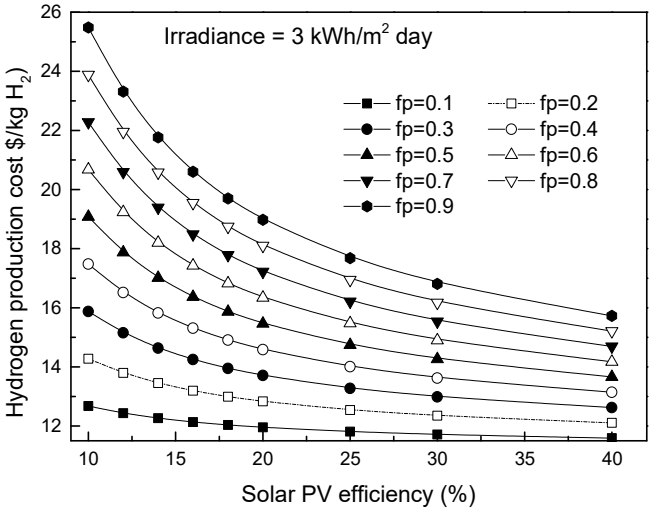

FIG. 74. Evolution of hydrogen production cost with solar PV efficiency for different solar fraction at irradiance of 3 kWh/m² day.

5.3.3.4. Hybrid nuclear-solar based high temperature electrolysis system

Under the conditions set for the system operation, i.e., operation at 1100 K (826.85°C) and production rate of 1 kg/s, the determined values of the different operation variables are reported in Table 92. These variables are the required heat, and electric power for water electrolysis at high temperature and the heat available at the electrolyser outlet. In the present case, the action of heat recuperation is not considered yet.

TABLE 92. ENERGY REQUIRED FOR WATER ELECTROLYSIS AT 1100 K (826.85°C) FOR A PRODUCTION OF 1 KG/S

Variable	Value
Heat required for hydrogen electrolysis (MW)	72.51
Electrical Power required for hydrogen electrolysis (MW)	99.99
Heat available at the electrolyser outlet (MW)	28.70

During the electrolysis process, there is the reaction heat, i.e., the heat necessary for the reaction to take place. However, as the electrolysis process is underway, there is also generation of heat due to the over-potential (over-potential heat). In Fig. 75, the evolutions of the reaction heat and the over-potential heat with the electrolysis temperature are reported.

This figure clearly indicates that the reaction heat increases with increasing temperature while the over-potential heat decreases with increasing temperature. Moreover, it can be noticed from this figure that the over-potential heat generated by the electrolysis process is larger than the reaction heat for electrolysis temperature below about 950 K (676.85°C).

There is then no need for heat to be added, the only need for heat is to keep the electrolysis temperature at the desired level. However, for temperatures above about 950 K (676.85°C), the reaction heat is much larger than the over-potential heat and so there is a need to provide the extra heat for the reaction to take place.

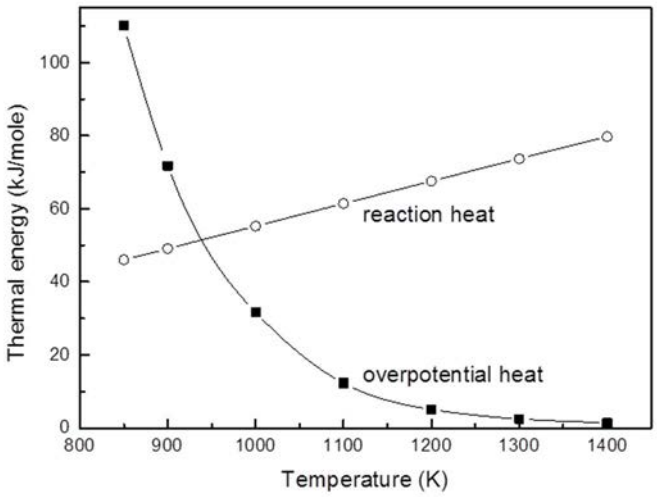

FIG. 75. Evolution of the reaction heat and the over- potential heat with the electrolysis temperature.

The energy needed for water electrolysis at high temperature is made of two parts: the electrical energy and the thermal energy. The evolution of these two forms of energy with the energy available at the outlet of the electrolysis is presented in Fig. 76. As there is heat generation during the electrolysis process, the required heat is on one side the difference between the reaction heat and the heat to keep the electrolysis process at the desired level and on the other side, the heat generated during the electrolysis process and the fraction of the recuperated heat.

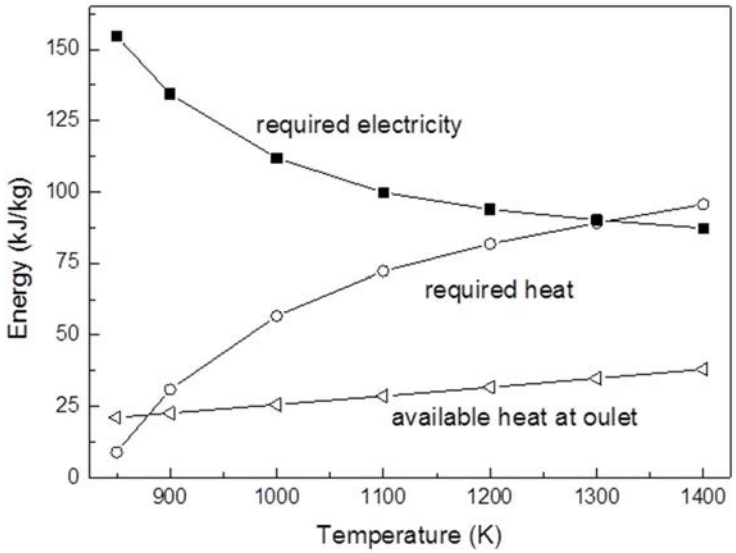

FIG. 76. Evolution of the energy source coming into play during the electrolysis process with the electrolysis temperature.

As expected, there is an increase in required heat and a decrease in required electricity. This increase and decrease are fast at temperatures below 1100 K (826.85°C), but they start leveling off after that. The available heat at the electrolyser outlet steadily increases with increasing electrolysis temperature. Moreover, in the case where the fraction of recuperated heat is 70% and the solar irradiation incident on the PV field is taken to be 5 kWh/m^2, the evolution of the PV specific area as function of PV module efficiency for different values of the solar fraction is given in Fig. 77.

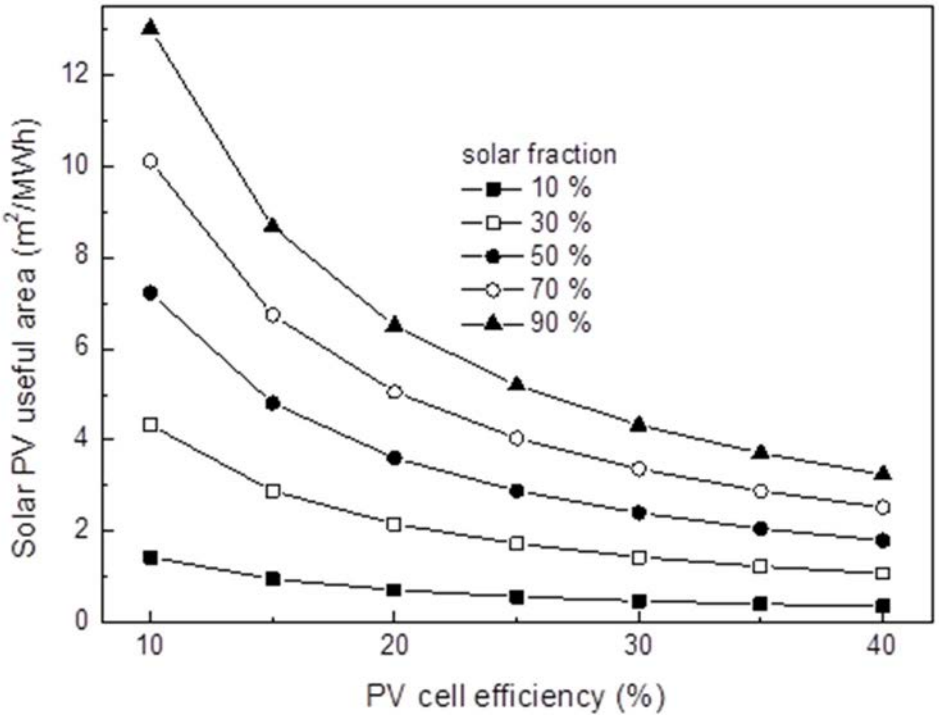

FIG. 77. Evolution of the PV specific area with the PV cell efficiency for different solar fraction.

It can be seen that the PV area decreases with increasing PV cell efficient for the different solar fractions. This decrease is more important at low PV cell efficiency, and it levels off at high efficiency. The rate of decrease drops with increasing PV cell efficiency.

On the other hand, this figure indicates that there is an increase in PV specific area with an increase in solar fraction. This rate of increase with solar fraction is higher at low efficiency.

Hydrogen production cost

The electrolysis of water is carried out at a temperature of 1100 K (826.85°C): for a production rate of 1 kg/s. Many technical as well as economic factors affect the cost of hydrogen production. In this study, we look at the effect of PV cell efficiency, the solar fraction, and the fraction of recuperated heat.

The evolution of hydrogen production cost as function of PV cell efficiency for different values of the solar fraction is reported in Fig. 78. The solar irradiation at the site where the system is mounted is 3.5 kWh/m^{2}·day. The fraction of recuperated heat is 70%.

It can be seen that hydrogen cost decreases with increasing PV cell efficiency for the different solar fraction values. Indeed, the increase in PV cell efficiency increases the production rate of PV solar electricity and so reduces the cost of PV electricity production. This has the effect of reducing the cost of hydrogen production. It should be though noted that the decrease rate of hydrogen production cost is the highest at low PV efficiency and it drops rapidly at high PV efficiency.

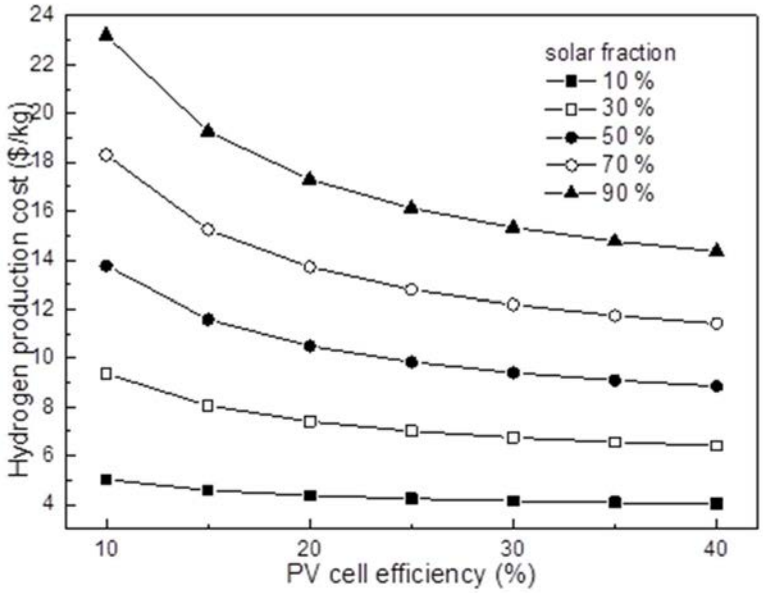

FIG. 78. Evolution of the hydrogen production cost with the PV cell efficiency for different value of the solar fraction.

Concerning the solar fraction, it can be seen from the above figure that the cost of hydrogen production increases with increase in the solar fraction for any PV cell efficiency. The rate of increase of hydrogen production cost with solar fraction is higher at low efficiency, and it diminishes with increase in PV cell efficiency. Indeed, as the cost of solar-based hydrogen production is higher than the nuclear-based cost of hydrogen, any increase in the solar fraction leads then to an increase of hybrid system cost of hydrogen production.

The evolution of hydrogen production cost as a function of solar insolation for different values of the PV cell efficiency is reported in Fig. 79. The fraction of recuperated heat is 70% and the solar fraction is taken to be 30%.

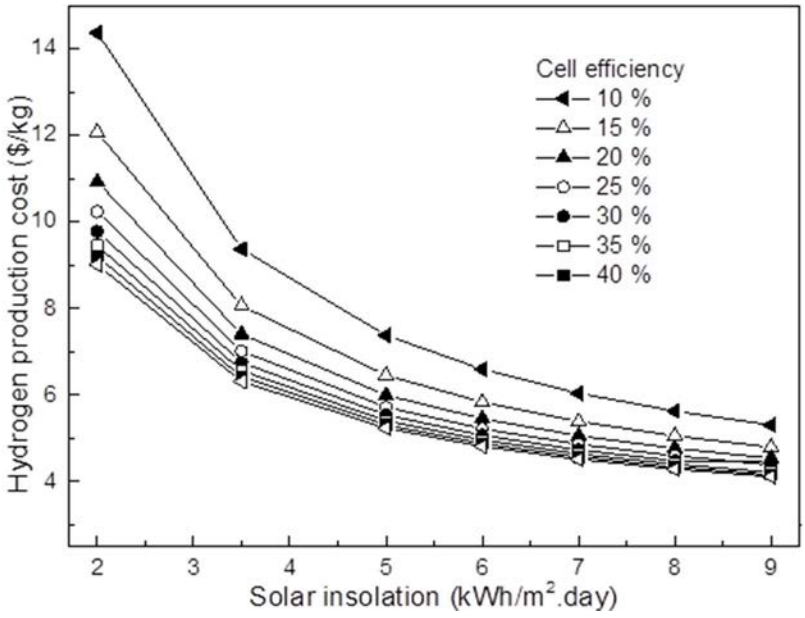

FIG. 79. Evolution of hydrogen production cost with solar irradiation for different values of the PV cell efficiency.

From Fig. 79, it is clearly shown that hydrogen cost decreases with increasing solar insolation at any PV cell efficiency. This is due to the fact that, as the solar insolation incident on the PV field increases, the rate of production of electricity increases, leading to a reduction in the cost of PV electricity production. Through that there is a reduction in the cost of hydrogen production. It should be though noted from this figure that the rate of decrease in hydrogen production cost is high at low solar irradiation, and it levels off at high solar irradiation. Indeed, the difference in hydrogen production cost between PV field with PV efficiency between 30% and 40% is very small. In the same manner, Fig. 79 shows a decrease in hydrogen production cost with increasing PV cell efficient for any value of solar insolation. The decrease is more important at low insolation, and levels off at high efficiency. This situation is, as before, due to the fact that an increase in PV cell efficiency leads to a decrease in PV electricity production cost and so as the overall hydrogen production cost. In this case, the fraction of recuperated heat is 70% and the solar insolation is 5 kWh/m^2.

The evolution of hydrogen production cost as function of solar fraction for different values of the fraction of recuperated heat is reported in Fig. 80.

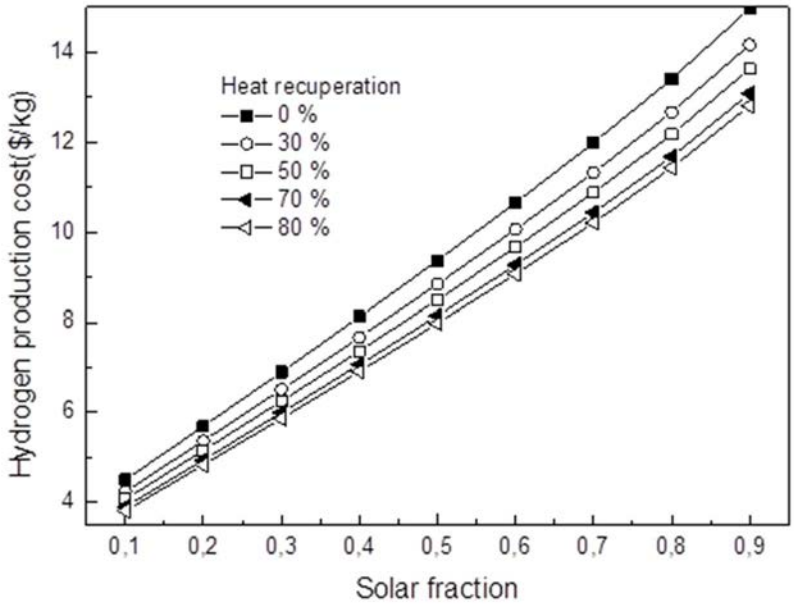

FIG. 80. Evolution of hydrogen production cost with solar fraction for different values of the fraction of recuperated heat.

This figure clearly shows that there is an increase in hydrogen production cost for any value of the fraction of recuperated heat. Once again as, under these conditions, solar hydrogen production cost is higher than hydrogen production cost, an increase in the solar fraction increases the fraction of costly hydrogen and this leads to an overall increase in hydrogen production cost.

The evolution of hydrogen production cost as a function of the fraction of recuperated heat for different values of the solar fraction is reported in Fig. 81. It can be seen that there is a slow decrease in hydrogen cost with increase in heat recuperation for any value of the solar fraction. Indeed, as the fraction of the recuperated heat decreases, the production of heat decreases. This leads to a lower cost in thermal heat and so an overall lower cost of hydrogen.

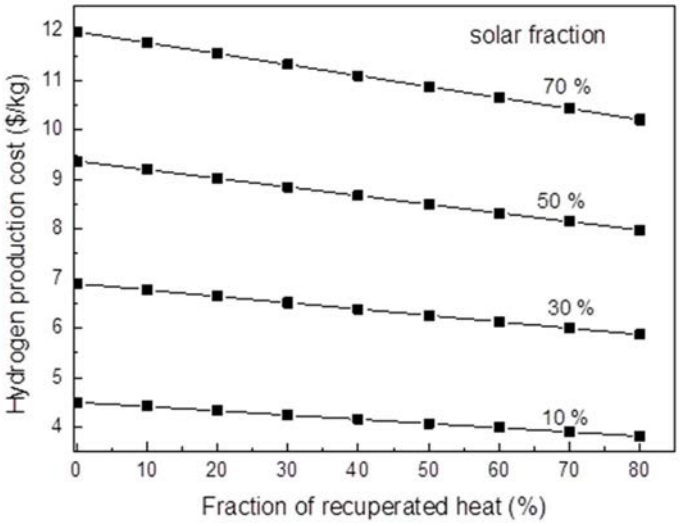

FIG. 81. Evolution of hydrogen production cost with recuperated heat fraction for different values of the solar fraction.

Comparison of hydrogen production cost

The case of an electrolytic hydrogen production unit powered by hybrid nuclear-solar photovoltaic electricity is considered. A comparison of the cost of hydrogen production cost based on the use of a low temperature electrolysis unit to that based on the use of a high temperature electrolysis unit. For the option of high temperature electrolysis, the case with heat recuperation and the case without heat recuperation, are considered respectively.

For the PV field, a PV cell efficiency of 17% is considered. The value of the daily solar irradiation is 5 kWh/m^2 and the fraction of the recuperated heat is 70%. Concerning the solar fraction, the cases of 20% and 40% are considered. The results are reported in Fig. 82. The results indicate that using high temperature electrolysis system is more competitive than using conventional electrolysis system. Indeed, there is a reduction in hydrogen production cost close to 50%. Resorting to heat recuperation with high temperature electrolysis leads to another reduction in the cost of hydrogen production.

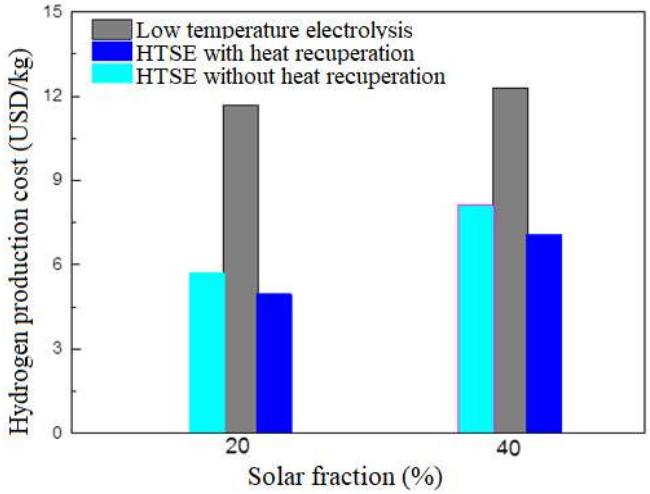

FIG. 82. Comparison of hydrogen production cost between high temperature and conventional electrolysis in the case of a hybrid nuclear-solar PV system.

5.3.4. Conclusions

Hybrid nuclear-solar system, particularly nuclear-solar PV and nuclear-CSP systems are considered for electrolyte hydrogen production for near-term deployment. In the first case, the study of a nuclear-solar PV energy system powering a low temperature electrolyser is carried out. Here both nuclear sub-system and solar PV subsystem provide electricity for low temperature water electrolysis to generate hydrogen.

These results show that the cost of the production of the electricity of solar origin depends strongly on the values of the solar radiation incident on the PV panels. This has, of course, a direct effect on the cost of hydrogen production. Indeed, at high solar irradiance, i.e. for daily solar irradiance equal to or higher than 7 kWh/m^2, the cost of production of electricity of solar origin is more competitive. Use of large fraction of solar PV helps here in bringing down the cost of hydrogen production. In this case, solar PV subsystem assists here in saving nuclear fuel and in bringing down the cost of hydrogen production; while nuclear subsystem provides the means to overcome the intermittency and the variability of solar energy.

In the case where solar irradiance is not high, which is the case in most sites around the world, the cost of the production of electricity of solar PV origin is less competitive with electricity of nuclear origin. To keep down the cost of hydrogen production, the contribution of solar-based electricity to hydrogen production should be low. This means that the solar fraction to be included in the hybrid system should be small. In this case, solar PV offers the opportunity of saving fuel while nuclear energy helps not only overcome the intermittency and the variability of solar energy but also bring down the cost of hydrogen production. In the first case, the study of a nuclear-solar PV energy system powering a high temperature electrolyser is carried out. The nuclear subsystem provides both heat and electricity to the high temperature electrolyser while the solar PV sub-system provides only electricity. The cost of hydrogen production is highly affected by the solar fraction, the solar irradiance incident on the PV panel. The cost of hydrogen increases with increasing solar fraction: The solar system being less competitive than nuclear system, the increase in solar fraction will only bring up the cost of hydrogen production. There are decreases in hydrogen production cost with increase either in PV cell efficiency, solar insolation or recuperation of the heat. However, the rate of decrease depends on the solar fraction. Heat recuperation drastically reduces the cost of hydrogen production. Finally, power by a hybrid nuclear-PV solar system, and a hydrogen production using high temperature electrolysis is economically more competitive than using low temperature electrolysis.

5.4.UPDATES ON THE HEEP TOOL (INDIA)

In the framework of this Coordinated Research Project, the IAEA HEEP software was updated, including the following new features:

- Generation of report in Excel format;
- Capability for sensitivity analysis of specific parameters (discount rate, interest on borrowing, equity, construction period) on hydrogen cost;
- Summary of sensitivity analysis in the form of bar chart as well as tabular form;
- Cost components details of each facility for range of parameter provided by user.

6. CONCLUSIONS

The IAEA CRP on Assessing Technical and Economic Aspects of Nuclear Hydrogen Production for Near-term Deployment was conducted between 2018–2022 and the results achieved by the participant organizations were gathered in this publication. The overall objective of this CRP was to leverage on the gained experience from R&D on nuclear hydrogen production in the participant Member States and to assess the potential near-term deployment of nuclear hydrogen production. This publication gathers the work conducted in the CRP, as reported by the chief scientific investigators responsible for the activities committed.

This section summarizes the conclusions based on the work conducted in the CRP.

6.1.NUCLEAR-SOLAR HYBRID SYSTEMS

Nuclear-solar hybrid systems for hydrogen production benefit from the complementarity of the two clean energy sources: nuclear helps overcome solar intermittency while solar helps save nuclear fuel and increase the time for nuclear fuel replacement. Hybridization gives flexibility and reliability to the hydrogen production system. The conventional water electrolysis process powered by a hybrid solar-nuclear system consisting of a solar PV field, and a pressurized water reactor was studied. The cost of production of hydrogen and the electrical energy as well as the size of the PV field have been investigated for different values of the solar fraction, the incident solar irradiance, and the solar PV efficiency. It has been found that, at low solar irradiance, the cost of hydrogen increases with increasing solar fraction. This is an indication of the low competitivity of solar in this range of solar irradiance: the increase in solar fraction will only bring up the cost of hydrogen production. On the other hand, at high solar irradiation, the cost of hydrogen decreases with increasing solar fraction. This is an indication that the solar system is becoming more competitive than the nuclear system: increasing solar fraction leads to a reduction in the cost of hydrogen production. Similar results are obtained for the PV solar efficiency: an increase in the cost of hydrogen production with an increase in the solar fraction for low PV efficiency and a decrease in its cost with an increase in solar fraction for high PV efficiency. These results are of importance more particularly in the design and the operation of a hybrid nuclear solar system. It could be used for example in the determination of the solar fraction for an optimum operation of the hybrid system that minimizes the costs, helps overcome the solar intermittency, and increase the time for fuel replacement in the nuclear reactor.

Hydrogen production through high temperature steam electrolysis powered by a high temperature nuclear reactor-PV hybrid system was studied. The PV solar system is used to produce part of the electricity needed for the steam electrolysis, while the high temperature nuclear reactor provides the heat and part of the electricity necessary for the steam electrolysis. The evolution of the hydrogen production cost with different factors, such as the PV efficiency, the solar irradiance incident on the PV panel, the size of the reactors and the solar fraction, has been investigated.

6.2. NUCLEAR HYDROGEN PRODUCTION THROUGH GASIFICATION OF SOLID FUELS

A technical feasibility study on nuclear assisted gasification process applied to the Argentine Rio Turbio coal was conducted, including:

— The evaluation of different HTGR designs to be potentially used as heat source for the nuclear-assisted coal gasification process.
— The selection of the gasification technology to be implemented for processing the sub-bituminous Rio Turbio coal.
— The sizing of an indirect-heating gasification reactor to be constructed as a demonstration plant, and the analysis of technical alternatives for upscaling the indirect heating gasification reactor to a more commercial phase.
— The evaluation of most critical safety issues for the coupling between the HTGR and the gasification plant.

The theoretical feasibility study on nuclear assisted gasification process applied to the Rio Turbio coal was of significant importance for Argentina, providing the technical arguments for the decision-making process regarding the nuclear hydrogen production through the gasification of domestic coals. Aspects like the most convenient HTGR design, the maximum size of the gasification plant according to the present state of technologies, and the most critical safety issues to be considered for the coupling of the nuclear reactor and gasification plant, have been clarified through this study.

The experimental activities related with the construction, testing and operation of a bubbling fluidized bed reactor for coal pyrolysis and gasification tests were carried out. The experimental activities planned for pyrolysis and gasification tests at bench-scale are supported in the evaluation of the gasification behaviour of Argentine domestic coal in fluidized bed reactor conditions, as a function of the operational parameters (reaction temperature, partial pressure of reactive gases, and coal particle size). These experimental results also allowed to analyse different performance indices of the gasification process. That includes conversion degree of the raw material, energy and exergy efficiencies, and final composition of the synthesis gas, as well as testing the predictive capability of kinetics models that were previously developed in gasification tests at laboratory scale.

The economic feasibility study on nuclear assisted gasification of the Argentine solid fuels including preliminary cost estimations of the process was performed using the IAEA HEEP software and other predictive tools.

6.3. NUCLEAR HYDROGEN PRODUCTION USING SOLID OXIDE ELECTROLYSER TECHNOLOGY AND THORIUM MOLTEN SALT REACTOR

The research and manufacture of solid oxide electrolysis cell and stack, as well as hydrogen production equipment was achieved. A long-term testing of the 5 kW SOEC stack has been finished with stable performance and a 20 kW hydrogen plant established successfully with high temperature steam electrolysis technology. A MW-scale HTSE plant for hydrogen production driven by wind, solar as well as nuclear power plant is under research. The demonstration project coupling a 200 kW HTSE system with thorium molten salt reactor in Gansu, China, using long-distance molten salt heat transfer circuits in order to achieve large scale hydrogen production, was designed and established by the Shanghai Institute of Applied Physics, in the Chinese Academy of Sciences. Safety considerations were investigated as well. A cost analysis of HTSE hydrogen production using Thorium Molten Salt Reactor was performed with HEEP software.

6.4. SMALL MODULAR REACTOR TECHNOLOGIES FOR HYDROGEN PRODUCTION

Several small modular reactor technologies (operational or at the design phase) have been reviewed and considered for nuclear hydrogen production in Greece based on specific criteria derived from country's needs and specifics, such as: use of proven technologies, capability to fit to a medium-size electric grid, flexibility to smoothly co-operate with growing implementation of renewable energy sources (specifically wind and solar), ability to feed district heating networks, ability to provide electricity for electrolysis-based hydrogen production and process heat for hydrogen compression, and finally, have as long as possible fuel cycle and design life. Since the seismic potential is high in Greece, the selected SMRs need also to withstand horizontal ground accelerations of at least 0.3 g. Based on the study conducted, 2 potential SMR candidates have been selected: the Korean SMART PWR and the Russian KARAT-100 BWR.

Various technological options that are suited to be used for hydrogen compression, storage, transport, and subsequent commercialization have also been reviewed. The selected one is based on the reversible hydrogenation/dehydrogenation ability of metal hydrides. The metal hydride compressor is a device that works by absorbing hydrogen at low pressure (<10 bar) and temperature (≤20°C) and desorbing it at a higher pressure in subsequent steps (stages) by raising the temperature at about 80 °C with an external heat source such as process heat or waste heat produced by a nuclear reactor. By employing successively higher pressure hydride alloys in series, high pressure ratios can be generated. Indeed, using 80°C hot water as the energy source, the multi-stage hydride compressor manages to compress a 10 bar inlet hydrogen to a resulting final pressure of over 300 bar. The compressor is characterized by very low electricity demand. A demonstration version has been operated, based on the use of specially developed metal hydrides and on the availability of thermal energy at low temperature (lower than 100°C).

6.5. USING HIGH TEMPERATURE REACTORS FOR HYDROGEN PRODUCTION

One of the processes that are considered to be coupled with high temperature reactors for hydrogen production is the S-I thermochemical cycle. Only a small fraction (8%) of the heat in an S-I process is needed at temperatures more than 800°C, for the SO_3 decomposition step. Other portions of the S-I process require temperature less than 550°C.

In India, the innovative high temperature reactor, which is currently under design, is envisaged to be used for hydrogen production using the S-I process. A part of the heat from the reactor will be converted to electricity using a high efficiency power conversion system to provide electrical heating to the SO_3 decomposition step, while other sections of the S-I process will be directly heated by the reactor.

The relevant safety considerations of the coupling between the S-I cycle and innovative high temperature reactor were identified.

Japan explores an integrated energy system using small modular reactors for hydrogen production. It is also looking into an HTGR hydrogen cogeneration plant, with a deployment target around year 2040. Tests are planned for non-nuclear (electrically) heated system (with construction target at 2025) and nuclear heated system based on the HTGR (with operation target at 2030).

Russian Federation explored various domestic high temperature reactor designs for hydrogen production using steam methane reforming and high temperature electrolysis. The multi-criteria assessment approach was used for selected nuclear hydrogen production cases, applying different weights of established criteria and several convolution methods. The proposed approach to multi-criteria assessment can be used to compare various cases for nuclear hydrogen production, considering the adequate assignment of weighting factors and determination of criteria values in same manner for all cases investigated.

6.6. HYBRID THERMOCHEMICAL CYCLES FOR HYDROGEN PRODUCTION

Several thermochemical, electrochemical, or hybrid hydrogen generation processes were investigated, in the temperature range of 100°C to 850°C. Among all, HyS with gas turbine (750–1000°C), Cu-Cl with steam turbine (500–1000°C) and Mg-Cl with steam turbine (400–500°C) were found to be the most economically and thermodynamically feasible and carry the potential to be integrated into next generation nuclear reactors. Process flow diagrams for each selected hydrogen plant were developed and comparatively analysed. Thermodynamic and economic assessment of the selected technologies were conducted, and it was found that electric and thermal energy costs are significant contributors to the overall hydrogen generation costs for all studied hybrid systems. Increased cell voltage also increases cost of hydrogen generation in the Mg-Cl cycle by more than 40%, around 30% for Cu-Cl cycle and more than 400% for the HyS cycle. Hydrogen generation costs for down selected technologies were: 2.4 –3.3 USD/kg for Mg-Cl cycle, 1.8–2.2 USD/kg for Cu-Cl cycle, and 0.6–4 USD/kg for HyS cycle. Findings on hydrogen production costs are significantly affected by the electrical energy cost from the nuclear reactor technology. Knowing that thermal energy costs are four times lower than electrical energy costs, decrease in OPEX for Mg-Cl, Cu-Cl, Ca-Br and HyS cycles are potentially 40%, 45%, 55% and 65%, respectively. This significant contribution is unique to hybrid thermochemical cycles. However, further investigation on feasible operation of these systems is critical for cost effective hydrogen production to meet ambitious targets in the next decades, where hydrogen from green sources can compete with fossil driven conventional technologies.

6.7. SYSTEM ANALYSIS OF NUCLEAR HYDROGEN PRODUCTION SCHEMES WITH CURRENT AND FUTURE NUCLEAR REACTOR TECHNOLOGIES

Currently the existing commercial plants are primarily used for electrical power production as a base load supply. However, there is no provision to store the power during low electricity demand. Utilising nuclear power plants for hydrogen production enables storage of the power and hence gives more flexibility in power use. Also, the new reactor designs such as fast breeder reactors, high temperature gas cooled reactors, and supercritical water reactors provide opportunity for more efficient hydrogen production and thus can become commercially attractive. System analysis of various nuclear reactors coupled with hydrogen production plants was performed. Electrolysis (low temperature PEM or alkaline fuel cell and high temperature steam electrolysis) and thermo/electrochemical water splitting below 900°C are viable processes for hydrogen generation with nuclear power plants. The key characteristics of water splitting process and nuclear plants were identified for the coupling schemes, and models were developed for HTSE, S-I, and HyS cycle with HTGR. Both H2A and HEEP software are used in the economic analysis of the hydrogen production schemes. Scaling of production technology was investigated for various sizes of reactor, and associated safety analysis was performed.

6.8. INTEGRATION OF NUCLEAR POWER PLANTS WITH HYDROGEN PRODUCTION FACILITIES

Integration hydrogen production facilities with existing NPPs requires careful planning, design and implementation to ensure that the process is safe, efficient and economically viable. An outline of the steps and considerations for the integration of hydrogen production with existing and future NPPs is provided below, based on the work conducted in the CRP.

- Site analysis:
  - Evaluate the available space and infrastructure at the NPP site to accommodate hydrogen production facilities;
  - Assess the availability of water, which is the primary feedstock for hydrogen production through electrolysis;
  - Evaluate the existing and needed infrastructure to support hydrogen production and generation.
- Feasibility study:
  - Conduct technical and economic feasibility studies to determine the optimal method for hydrogen production to be coupled with a specific NPP (e.g. low temperature electrolysis, HTSE, thermochemical cycles or steam methane reforming, with/without carbon capture and storage/ utilization);
  - Analyse the electrical and thermal output profiles of the NPP to optimize hydrogen production during periods of low electricity demand.
- Safety and risk assessment:
  - Perform a thorough safety assessment to analyse the risks associated with integrating hydrogen production, considering hydrogen's flammability and explosion potential;
  - Ensure that the integration complies with nuclear safety regulations and does not compromise the integrity of the NPP;
  - In the design and engineering phase, prepare the documentation for regulatory reviews and obtain necessary licenses and permits.
- Public and stakeholder engagement:
  - Engage with local communities, stakeholders, and regulatory bodies to explain the benefits and safety measures of the integrated system;
  - Address any concerns and provide transparency throughout the process;
- Performance analysis:
  - Continuously evaluate the performance of the hydrogen production facility to ensure it meets design specifications and production targets;
  - Analyse the operational data to identify areas for improving in efficiency and cost-effectiveness;
  - Use real-world data to refine models and predictions related to maintenance, production optimization and safety;
  - Consider implementing upgrades that could enhance performance or reduce costs;
  - Evaluate the benefits and risks of increasing production capacity, including the potential impact on the NPP and the local grid.

— End-of-life planning:
    - Incorporate end-of-life planning for the hydrogen production facilities as part of the overall lifecycle management of the NPP;
    - Develop strategies for decommissioning the hydrogen infrastructure safely when it reaches its end of service.

Nuclear power plant integration with hydrogen production has the potential to play a pivotal role in the emerging hydrogen economy. As this field evolves, the successful integration of nuclear and hydrogen production will depend on careful planning, stakeholder engagement, compliance with regulatory standards and a forward-looking approach that embraces innovation and sustainability.

Allowing the decarbonisation of present hydrogen usages at a competitive price without compromising other decarbonisation goals is the most stringent challenge facing the hydrogen economy [226]. Aiming for competitive hydrogen production also necessitates taking into account the overall costs at the power system level as well as the costs of hydrogen distribution, transportation, and storage. The comparison of hydrogen production cost by different methods has been conducted in many studies, including the ones developed through the IAEA CRP "Assessing Technical and Economic Aspects of Nuclear Hydrogen Production for Near-term Deployment" and the IAEA CRP "Examining the Techno economics of Nuclear Hydrogen Production and Benchmark Analysis of the IAEA HEEP Software" (2012-2015)[5] [33].

The Nuclear Energy Agency (NEA) along with the International Energy Agency, International Renewable Energy Agency and Lazard developed models to assess the cost of hydrogen production with low carbon sources. An NEA report [226] shows that only long term operation NPPs may compete with current prices for hydrogen production with gas (with carbon capture, utilisation and storage), if gas prices are around 20 USD/MWh (case of the United States). However, the levelized cost of hydrogen and the levelized cost of storage, distribution and transport are obtained with a high level of load factor for the electrolysers which means to dedicate a nuclear unit for hydrogen production. This could generate additional issues for low carbon electrification needs.

Hence, it is necessary to carefully assess the assumptions, data availability, limitations and simplifications of models used to estimate the nuclear hydrogen production cost. It is to be noted that this publication documents the results achieved by the participant organizations in the IAEA "Assessing Technical and Economic Aspects of Nuclear Hydrogen Production for Near-term Deployment" and the results obtained have to be considered in relation to the input parameters, specific technologies, models used and methods considered that are described in this publication.

[5] https://www.iaea.org/projects/crp/i35004

APPENDIX. CONTRIBUTIONS OF THE PARTICIPANTING MEMBER STATES

A-1. Algeria: techno-economical study of hybrid nuclear-solar hydrogen production for near-term deployment

In this work conducted by the Renewable Energy Development Center (Centre de Développement des Energies Renouvelables), Algeria, the main objective was the techno-economic investigation of hydrogen production deployment, using electrolysis as the production process with solar and nuclear energy as the energy to power the production process.

Nuclear-solar hybrid systems for hydrogen production were investigated. Nuclear hydrogen deployment could indeed benefit from hybridization with solar. Nuclear and solar, both clean energy sources complement each other: nuclear helps overcome solar intermittency while solar helps save nuclear fuel and increase the time for nuclear fuel replacement. Hybridization gives flexibility and reliability to the hydrogen production system. Considering different configurations, the objective was to investigate how well nuclear and solar technologies perform together for hydrogen production, concerning particularly efficiency, economic competitiveness, and operation flexibility.

The conventional as well as high temperature water electrolysis process powered by nuclear, solar, and hybrid solar-nuclear systems were considered. The cost of production of hydrogen has been estimated in each case. The evolution of the cost with different factors such as the photovoltaics efficiency, the solar irradiance incident on the photovoltaics panel, the size of the reactors, and the solar fraction, were studied.

A-2. Argentina: upscaling of experimental facilities for nuclear hydrogen production through gasification of Argentine solid fuels

This work was conducted by the National Atomic Energy Commission (Comisión Nacional de Energía Atómica), Argentina. The objective was to support a technical and economic feasibility study on nuclear-assisted steam gasification of Argentine solid fuels for hydrogen production; to conduct gasification tests and specific analyses with selected Argentine solid fuels, with steam as gasifying agent, using the fluidized bed reactor operating in batch mode. Pyrolysis and gasification experiments were carried out at laboratory scale, using specially designed experimental setups like drop tube furnaces, fixed bed furnaces, and thermogravimetric analyzers. Different Argentinian solid fuels were tested using CO_2 and steam as gasifying agents. The effects of solid fuel properties (composition, rank, and content of mineral matter) as well as reaction conditions (temperature, heating rate, partial pressure of gasifying agent, and residence time at high temperature) on the gasification reactivity were extensively investigated, and kinetic models were developed for predicting their behavior under typical gasification conditions.

A critical review on the state-of-the-art in the field of HTGRs for non-electrical applications was conducted with special emphasis on reactors that are in operation or under development worldwide. The objective is of evaluating the technical and economic feasibility of coupling this kind of nuclear reactors with a steam coal gasification plant for producing hydrogen.

The study included an evaluation of the most critical safety issues for the coupling between the HTGR and the gasification/hydrogen production plant.

As a major result of this research contract, a nuclear cogeneration demonstration plant for electricity and hydrogen production was finally proposed for the Rio Turbio site. It comprises the coupling between an HTGR with 950 ºC of helium outlet temperature, and a steam coal gasification reactor with indirect heating rated at 10 MWt for hydrogen production. The coupling between the nuclear reactor and the gasification/hydrogen generation plant is through a helium intermediate circuit, where the secondary helium gas is heated at 900ºC by a fraction of the primary helium gas that flows along the shell side of a helium-helium heat exchanger. Two isolation valves on the secondary helium circuit allow isolate promptly the nuclear island from the gasification/hydrogen generation plant in case of emergencies.

A-3. China: evaluation of nuclear hydrogen production using thorium molten salt reactor coupled with a solid oxide electrolyser

This work was conducted by the Shanghai Institute of Applied Physics, Chinese Academy of Sciences and had the objectives to: (1) set up an MW scale HTSE system; (2) perform system modelling for optimized heat integration technology; (3) couple the MW scale HTSE system with the thorium molten salt reactor; (4) evaluate economic and safety aspects of the thorium molten salt reactor nuclear hydrogen production plant.

A long-term testing of the 5 kW solid oxide stack has been completed with stable performance, and a 20 kW hydrogen plant established successfully with HTSE technology. An MW-scale HTSE plant for hydrogen production driven by wind, solar, as well as nuclear power plant was studied. The demonstration project which coupled a 200 kW HTSE system with thorium molten salt reactor in Gansu, China, using long distance molten salt heat transfer circuits in order to achieve large scale hydrogen production was designed and safety considerations were addressed. A cost analysis of HTSE hydrogen production driven by TMSR was conducted using the HEEP tool.

A-4. Greece: identifying adequate small modular reactor technology for innovative hydrogen production, compression and storage

This work was conducted by the National Center of Scientific Research Demokritos, Greece. Every nuclear power plant has to be implemented in a given socio-economic and industrial environment. Therefore, the decision on the choice of reactor type and consequent construction of a power plant should be taken in accordance with multiple techno-economic criteria. No universal solution exists, since the chosen technological option should be compatible with the conditions prevailing in the region of installation. A common requirement of many regions of the world that are potentially interested by the nuclear hydrogen is that the reactor to be selected should also cover electricity production needs, should be integrated into medium-sized distribution networks, and cooperate with intermittent energy sources. One such example is the Greek region of Western Macedonia, where the shutdown of the existing coal-fired (lignite) power plants has been decided due to the high CO_2 emissions they produce. A rational option could be to replace the polluting old lignite-fired plants with SMRs. The SMRs could fit into the existing medium-size electric grid, are flexible enough to smoothly co-operate with growing implementation of renewable energy sources, feed the existing district heating networks, and also provide electricity used in electrolysis for hydrogen production as well as heat for hydrogen compression. Since the seismic energy annually delivered in the location of

the installation could be high, as is the case in the Western Macedonia region, increased earthquake resistance is an advantage. A review of SMR technologies has been performed and a corresponding quasi-exhaustive compilation has been produced of SMRs that explicitly include hydrogen production in their booklet. Various technological options that are suited to be used for hydrogen compression, storage, transport, and subsequent commercialization have also been reviewed. The selected compression and storage method is based on the reversible hydrogenation/dehydrogenation ability of metal hydrides. Finally, a methodology allowing for the determination of the optimal size of a hybrid SMR – renewables (photovoltaics) energy production system for hydrogen cogeneration has been developed.

A-5. India: technical and safety studies for integration of high temperature reactors with sulphur-iodine process-based hydrogen production plant and upgradation of the HEEP tool for economic assessment of hydrogen production

This work was performed by Bhabha Atomic Research Centre, India. India has an active programme for development of the S-I process. Initially, the closed loop operation of this process was demonstrated in a glass loop at 30 L/h of hydrogen production (in normal conditions). Subsequently, the reactions of S-I process have been studied using facilities constructed with metallic/ceramic materials. Based on this experience, a closed loop metallic system for 150 L/h of hydrogen production was setup. Several new technologies have been developed, including: the multistage counter-current Bunsen reactor in tantalum, the membrane reactor for HI decomposition, the bayonet type SO_3 decomposer in silicon carbide, and an improved surface area catalyst for SO_3 decomposition.

In order to provide the required heat and electricity for the S-I process, the Indian programme envisages use of fluoride salt cooled pebble bed reactor with 665°C as coolant outlet temperature. The nuclear heat will be partially converted to electricity, used to provide electrical heat to the SO_3 decomposition stage of the S-I process, and also to take care of the electricity requirements of various process equipment of the plant. The balance heat from the reactor will be supplied to the other stages of the S-I process. In order to transfer heat from the reactor to the various stages of the S-I process, a cascade of heat transfer loops has been considered. Therefore, the system consists of a number of intermediate heat exchangers. The process designs of these heat exchangers have been completed considering material compatibility, reliability of operation, and design considerations. Issues and technology areas specific to safety have been identified.

Towards upgradation of the software HEEP, a feature of generating report in Microsoft Excel format has been incorporated. Microsoft Excel report echoes the input data used for hydrogen cost calculations including data provided as additional inputs. Features for sensitivity analysis of selected parameters have also been added. This feature allows the values of selected parameters of a reference case to be varied between maximum and minimum values. The effect of this variation on the hydrogen cost is estimated. The results of the sensitivity studies are also exported to Microsoft Excel format.

A-6. Japan: evaluation of nuclear hydrogen production technologies and prospects for deployment

This contribution was provided by Japan Atomic Energy Agency (JAEA) and consisted of review and assessment of nuclear hydrogen production technologies, in particular, those developed in JAEA. That is the HTGR and the S-I process – in terms of development status,

economics, and safety aspects. The assessment targeted to examine the outstanding technical issues (e.g. material performance against corrosion), economic aspects (e.g. equipment cost reduction, scale-up), and safety aspects (e.g. related to reactor and industrial process coupling). JAEA achieved closed loop automated continuous hydrogen production experiments at rates of up to about 100 L/h and for time periods of up to 150 h. Important data have been obtained to investigate material and component performance along with reliability, and to improve fluid and reaction control techniques necessary to achieve longer term operations. During 2019–2020 period, JAEA has initiated a joint conceptual design study with a major Japanese producer of commercial-scale sulfuric acid decomposer – the key equipment for the S-I process. Material selection, scaleup limit, structural design, and manufacture feasibility will be further confirmed in this study. JAEA has also participated in a national project, in collaboration with the University of Tokyo, Institute of Energy Economics Japan, JGC Corporation, and Mitsubishi Heavy Industries; to study distributed electricity, and energy systems and mixes for Japan over the period of 2030–2100. Nuclear reactors of various types and sizes are considered together with renewables (wind and solar) and fossil fuels with carbon capture and utilization.

A-7. Russian Federation: assessing potential of high temperature reactor facilities of Russian design for hydrogen production

This work was conducted by the National Research Center Kurchatov Institute in Russian Federation. It aimed to assess economics of hydrogen production by different energy sources, including the Russian designed HTGRs, and operating LWR, considering steam methane reforming, and electrolysis methods. To fulfill this objective, a review of Russian designed HTGRs was performed, identifying the MHR-T and MHR-100 designs as having most actual economic data available. The characteristic parameters gathered during the review process were used to conduct a technical-economic evaluation of the hydrogen production cost in the following cases: steam methane reforming and HTSE with MHR-T as energy source, steam methane reforming with MHR-100 as energy source, and alkaline electrolysis using electricity from operating NPPs (or from the grid). Comparative assessments using HEEP were carried out and the multi-criteria approach was considered for the assessment of nuclear hydrogen production cases based on a set of evaluation criteria. The approach was tested for the assessed cases of nuclear hydrogen production by applying different weights of criteria and several convolution methods.

A-8. Saudi Arabia: thermo-economic analysis and optimization of a large-scale nuclear hydrogen production utilizing high temperature

This work was conducted by Umm Al-Qura University, Saudi Arabia. It focused on solid oxide electrolysis and advanced reactors, with near-term deployment for large-scale hydrogen production, using relevant data acquired to develop HEEP case studies integrating a solid oxide electrolysis plant with APR100 and HTR-PM, respectively. It also looked at opportunities and challenges associated with nuclear hydrogen production, regarding safety and environmental aspects, in the context of climate change and the future of hydrogen economy. A review of studies and reports available on solid oxide electrolysis technologies, and advanced reactors was accomplished, including relevant key technical and economic data. A model for 1 MWe solid oxide electrolyser was developed and validated with experimental results design, determining the operating parameters for hydrogen production at maximum efficiency.

A-9. Türkiye: economics and integration of hybrid thermochemical cycles to near future nuclear reactors for hydrogen production

This contribution was provided by Karabuk University, Türkiye, and it had the objective to assess the economics and integration of hybrid thermochemical cycles to nuclear reactors with near-term deployment for hydrogen production. Türkiye is still in its early face to investigate the next generation of nuclear reactors including small modular reactors but has a high interest in hydrogen and synthetic fuels to decrease the financial import load of fossil fuels. So far, the contribution to the CRP includes the assessment of technical and economic aspects of different nuclear reactor - hydrogen plant configurations considering CANDU-SCWR and HTGR for the reactor technology, thermochemical and hybrid cycles for hydrogen generation, and the effects of scaling of hybrid cycle configurations on hydrogen production costs. Heat and electricity load of all new cycles are now determined, and size flexible models are already developed. Adaptation of selected thermochemical cycles to the HEEP software are completed. HyS, Ca-Br, Mg-Cl and Cu-Cl cycles cost aspects and scaling has been completed and integrated to the HTGR that is present in the HEEP database. The results indicated that the lowest hydrogen generation costs belong to HyS and CuCl cycles while realistic conditions are not present for the CaBr cycle. MgCl cycle has the highest hydrogen cost range with a well-known electrolysis step.

A-10. United States of America: safety and scaling analysis of nuclear hydrogen production schemes with current and near future nuclear plants

This work was conducted by the Purdue University, USA and had the following objectives:

- To develop integration methods for each hydrogen production scheme; steam methane reforming, low and high temperature electrolysis, the S-I cycle and Cu-Cl cycle with commercial PWRs and BWRs, recently developed small modular reactors, and planned FBR, HTGR, and SCWR,
- To perform scaling analysis for the integrated nuclear hydrogen production systems, techno-economic analysis, and safety and environmental impact for the proposed INHPS.

For the following nuclear reactor types: PWR, BWR, SMR, FBR, HTGR, and SCWR, the characteristics and the key parameters for heat and electrical power transfer were identified. The operating characteristics of the hydrogen production processes considered were identified, i.e. steam methane reforming, low temperature electrolysis, high temperature electrolysis, S-I cycle, Cu-Cl cycle, and Mn-O cycle. The characteristics for each hydrogen production schemes were matched with those of the reactors. Based on appropriate matching of temperatures, heat flux, and power, coupled systems were developed as INHPS. The energy transfer through intermediate heat exchanger or electrical supply units were designed for each INHPS. Operating models were developed for each INHPS, enabling computation of the hydrogen generation as function system parameters. Steady state operation of the INHPS was analyzed.

The cost of hydrogen generation from existing LWR with low temperature electrolysis system was studied; a PEM electrolyser and grid electrical power from LWR was considered. For hydrogen plant, nuclear plant component, and system cost analysis, H2A and HEEP codes were used. A benchmark HEEP-H2A for the system HTGR-HTSE was performed.

The scaling studies on INHPS indicated that the cost of the electricity and heat from nuclear plant largely depends on the capital cost of the nuclear power plant. The SMR and microreactor cost will generally be higher from the historic recent cost estimates for SMRs and microreactors. There is a variation in the estimated capital prices for nuclear reactor plants which should be accounted in economic analysis of hydrogen production.

The study conducted, specifically on analysis of the LWR coupled to low temperature and high temperature electrolysis, was useful in assessing projects carried out by USA nuclear power companies demonstrating hydrogen production with PEM electrolyser, alkaline electrolyser, and high temperature steam splitting with solid oxide electrolyser cell. One of these projects is a pilot integrating a 2 MWe low temperature PEM electrolysis with the 925 MWe Davis-Besse PWR in Ohio. These projects aim to evaluate the economics of hydrogen production with operating reactors. At the Nine Mile Point nuclear power station in New York state, Constellation Energy started running a first-of-its-kind 1 MW demonstration scale nuclear-powered clean hydrogen production facility in March 2023. At its LaSalle Clean Energy Centre in Illinois, the operator plans to construct the largest nuclear-powered clean hydrogen production facility in the world by using some of the funds allocated for the seven US hydrogen hubs under the H2Hubs project. The preparatory studies and lessons learned from the operational experience emerged from the pilot projects may be captured as case studies in future topical IAEA CRPs for the benefit of international community.

REFERENCES

[1] BOUDRIES, R., DIZENE, R., KHELLAF, A., BELHAMEL, M., Hydrogen as an energy carrier. In: Harris Aiden M, editor. Clean energy: resources, production and developments. Nova Science Publishers, Inc., (2010) 147-184.

[2] TOGHYANI, S., et al., Optimization of operating parameters of a polymer exchange membrane electrolyzer, International Journal of Hydrogen Energy **44** 13 (2019) 6403-6414.

[3] TOGHYANI, S., AFSHARI, E., BANIASADI, E., Three-dimensional computational fluid dynamics modeling of proton exchange membrane electrolyzer with new flow field pattern, Journal of Thermal Analysis and Calorimetry **135** 3 (2019) 1911-1919.

[4] KOPONEN, J., et al., Control and energy efficiency of PEM water electrolyzers in renewable energy systems, International Journal of Hydrogen Energy **42** 50 (2017) 29648-29660.

[5] GARCÍA-VALVERDE, R., ESPINOSA, N., URBINA, A., Simple PEM water electrolyser model and experimental validation, International Journal of Hydrogen Energy **37** 2 (2012) 1927-1938.

[6] NOUICER, I., et al., Solar hydrogen production using direct coupling of SO2 depolarized electrolyser to a solar photovoltaic system, International Journal of Hydrogen Energy **44** (2019) 22408-22418.

[7] SMOLINKA, T., GUNTHER, M., GARCHE, J., NOW-Studie: Stand und Entwicklungspotenzial der Wasserelektrolyse zur Herstellung von Wasserstoff aus regenerativen Energien, Technical report, Fraunhofer ISE, (2011)

[8] OJONG, E.T., et al., Development of an experimentally validated semi-empirical fully-coupled performance model of a PEM electrolysis cell with a 3-D structured porous transport layer, International Journal of Hydrogen Energy **42** 41 (2017) 25831-25847.

[9] COLBERTALDO, P., GÓMEZ ALÁEZ, S.L., CAMPANARI, S., Zero-dimensional dynamic modeling of PEM electrolyzers, Energy Procedia **142** (2017) 1468-1473.

[10] OLIVIER, P., BOURASSEAU, C., BOUAMAMA, P., Low-temperature electrolysis system modelling: A review, Renewable and Sustainable Energy Reviews **78** (2017) 280-300.

[11] AWASTHI, A., SCOTT, K., BASU, S., Dynamic modeling and simulation of a proton exchange membrane electrolyzer for hydrogen production, International Journal of Hydrogen Energy **36** 22 (2011) 14779-14786.

[12] ATLAM, O., KOLHE, M., Equivalent electrical model for a proton exchange membrane (PEM) electrolyser, Energy Conversion and Management **52** 8 (2011) 2952-2957.

[13] CHOI, P., BESSARABOV, D.G., DATTA, R., A simple model for solid polymer electrolyte (SPE) water electrolysis, Solid State Ionics **175** 1 (2004) 535-539.

[14] CARMO, M., FRITZ, D.L., MERGEL, J., STOLTEN, D., A comprehensive review on PEM water electrolysis, International Journal of Hydrogen Energy **38** 12 (2013) 4901-4934.

[15] ZENG, K., ZHANG, D., Recent progress in alkaline water electrolysis for hydrogen production and applications, Progress in Energy and Combustion Science **36** 3 (2010) 307-326.

[16] SHEN, M., BENNETT, N., DING, Y., SCOTT, K., A concise model for evaluating water electrolysis, International Journal of Hydrogen Energy **36** 22 (2011) 14335-14341.
[17] NI, M., Computational fluid dynamics modeling of a solid oxide electrolyzer cell for hydrogen production, International Journal of Hydrogen Energy **34** 18 (2009) 7795-7806.
[18] ALZAHRANI, A., DINCER, I., Thermodynamic and electrochemical analyses of a solid oxide electrolyzer for hydrogen production, International Journal of Hydrogen Energy **42** (2017)
[19] KLOTZ, D., LEONIDE, A., WEBER, A., IVERS-TIFFÉE, E., Electrochemical model for SOFC and SOEC mode predicting performance and efficiency, International Journal of Hydrogen Energy **39** 35 (2014) 20844-20849.
[20] HINO, R., HAGA, K., AITA, H., SEKITA, K., 38. R&D on hydrogen production by high-temperature electrolysis of steam, Nuclear Engineering and Design **233** 1 (2004) 363-375.
[21] STOOTS, C.M., O'BRIEN, J.E., CONDIE, K.G., HARTVIGSEN, J.J., High-temperature electrolysis for large-scale hydrogen production from nuclear energy – Experimental investigations, International Journal of Hydrogen Energy **35** 10 (2010) 4861-4870.
[22] NI, M., LEUNG, M.K.H., LEUNG, D.Y.C., Parametric study of solid oxide steam electrolyzer for hydrogen production, International Journal of Hydrogen Energy **32** 13 (2007) 2305-2313.
[23] NATERER, G.F., et al., Canada's program on nuclear hydrogen production and the thermochemical Cu–Cl cycle, International Journal of Hydrogen Energy **35** 20 (2010) 10905-10926.
[24] PRINCE-RICHARD, S., WHALE, M., DJILALI, N., A techno-economic analysis of decentralized electrolytic hydrogen production for fuel cell vehicles, International Journal of Hydrogen Energy **30** 11 (2005) 1159-1179.
[25] MORAN, M.J., SHAPIRO, H.N., Fundamentals of engineering thermodynamics. 5th ed. New York: Wiley, Inc., (2004)
[26] MINGYI, L., BO, Y., JINGMING, X., JING, C., Thermodynamic analysis of the efficiency of high-temperature steam electrolysis system for hydrogen production, Journal of Power Sources **177** 2 (2008) 493-499.
[27] PADIN, J., VEZIROGLU, T.N., SHAHIN, A., Hybrid solar high-temperature hydrogen production system, International Journal of Hydrogen Energy **25** (2000) 295-317.
[28] E. FUNK, J., Thermochemical hydrogen production: past and present, International Journal of Hydrogen Energy **26** 3 (2001) 185-190.
[29] VERFONDERN, K., Nuclear Energy for Hydrogen Production, Energy Technology 58, Forschungszentrums Jülich, Germany, (2007)
[30] CHANG, J., et al., A study of a nuclear hydrogen production demonstration plant, Nuclear Engineering and Technology **39** (2007)
[31] YAN, X., RYUTARO, H., Nuclear Hydrogen Production Handbook, CRC Press, Taylor & Francis Group (2011) 547-554.
[32] YAMAWAKI, M., et al., Application of nuclear energy for environmentally friendly hydrogen generation, International Journal of Hydrogen Energy **32** 14 (2007) 2719-2725.
[33] INTERNATIONAL ATOMIC ENERGY AGENCY, Examining the Technoeconomics of Nuclear Hydrogen Production and Benchmark Analysis of the IAEA HEEP Software, IAEA-TECDOC-1859, IAEA, Vienna, Austria, (2018)

[34] GAUTHIER, J.-C., et al., Potential applications for nuclear energy besides electricity generation: A global perspective, Nuclear Engineering and Technology **39** (2007)
[35] INTERNATIONAL ATOMIC ENERGY AGENCY, Hydrogen Production Using Nuclear Energy, Nuclear Energy Series NP-T-4.2, IAEA, Vienna, Austria (2013)
[36] ELDER, R., ALLEN, R., Nuclear heat for hydrogen production: Coupling a very high/high temperature reactor to a hydrogen production plant, Progress in Nuclear Energy **51** 3 (2009) 500-525.
[37] LUIS, E., HERRANZ, J., LINARES, B., MORATILLA, Y., LOPEZ, R., Thermal assessment and second law analysis of indirect brayton power cycles for high-temperature gas-cooled nuclear reactors, 3rd International Topical Meeting on High Temperature Reactor Technology HTR-2006, Sandton (South Africa), 1-4 October 2006, (2006)
[38] GIBSON, T., KELLY, N., Optimization of solar powered hydrogen production using photovoltaic electrolysis devices, International Journal of Hydrogen Energy **33** (2008) 5931-5940.
[39] NGUYEN DUC, T., GOSHOME, K., ENDO, N., MAEDA, T., Optimization strategy for high efficiency 20 kW-class direct coupled photovoltaic-electrolyzer system based on experiment data, International Journal of Hydrogen Energy **44** 49 (2019) 26741-26752.
[40] BOUDRIES, R., DIZENE, R., Potentialities of hydrogen production in Algeria, International Journal of Hydrogen Energy **33** (2008) 4476-4487.
[41] RICHARDS, B., CONIBEER, G., Comparison of hydrogen storage technologies for solar-powered stand-alone power supplies: A photovoltaic system sizing approach, International Journal of Hydrogen Energy **32** (2007) 2712-2718.
[42] HOLLMULLER, P., JOUBERT, J.-M., LACHAL, B., YVON, K., Evaluation of a 5 kWp photovoltaic hydrogen production and storage installation for a residential home in Switzerland, International Journal of Hydrogen Energy **25** 2 (2000) 97-109.
[43] BERNARDO, L.R., PERERS, B., HÅKANSSON, H., KARLSSON, B., Performance evaluation of low concentrating photovoltaic/thermal systems: A case study from Sweden, Solar Energy **85** 7 (2011) 1499-1510.
[44] NILSSON, J., HÅKANSSON, H., KARLSSON, B., Electrical and thermal characterization of a PV-CPC hybrid, Solar Energy **81** 7 (2007) 917-928.
[45] XIE, W.T., DAI, Y.J., WANG, R.Z., SUMATHY, K., Concentrated solar energy applications using Fresnel lenses: A review, Renewable and Sustainable Energy Reviews **15** 6 (2011) 2588-2606.
[46] LI, M., et al., Performance study of solar cell arrays based on a Trough Concentrating Photovoltaic/Thermal system, Applied Energy - APPL ENERG **88** (2011) 3218-3227.
[47] BOUDRIES, R., Techno-economic Assessment of Solar Hydrogen Production Using CPV-electrolysis Systems, Energy Procedia **93** (2016) 96-101.
[48] PÉREZ-HIGUERAS, P., MUÑOZ, E., ALMONACID, G., VIDAL, P.G., High Concentrator PhotoVoltaics efficiencies: Present status and forecast, Renewable and Sustainable Energy Reviews **15** 4 (2011) 1810-1815.
[49] WANG, Z., ROBERTS, R.R., NATERER, G.F., GABRIEL, K.S., Comparison of thermochemical, electrolytic, photoelectrolytic and photochemical solar-to-hydrogen production technologies, International Journal of Hydrogen Energy **37** 21 (2012) 16287-16301.
[50] BOUDRIES, R., Analysis of solar hydrogen production in Algeria: Case of an electrolyzer-concentrating photovoltaic system, International Journal of Hydrogen Energy **38** (2013) 11507-11518.

[51] OUAGUED, M., KHELLAF, A., LOUKARFI, L., Estimation of the temperature, heat gain and heat loss by solar parabolic trough collector under Algerian climate using different thermal oils, Energy Conversion and Management **75** (2013) 191-201.
[52] BENAMMAR, S., KHELLAF, A., MOHAMMEDI, K., Contribution to the modeling and simulation of solar power tower plants using energy analysis, Energy Conversion and Management **78** (2014) 923-930.
[53] MURADOV, N.Z., VEZIROĞLU, T.N., "Green" path from fossil-based to hydrogen economy: An overview of carbon-neutral technologies, International Journal of Hydrogen Energy **33** 23 (2008) 6804-6839.
[54] KODAMA, T., High-temperature solar chemistry for converting solar heat to chemical fuels, Progress in Energy and Combustion Science **29** 6 (2003) 567-597.
[55] BEHAR, O., KHELLAF, A., MOHAMMEDI, K., A review of studies on central receiver solar thermal power plants, Renewable and Sustainable Energy Reviews **23** (2013) 12-39.
[56] BOUDRIES, R., Techno-economic study of hydrogen production using CSP technology, International Journal of Hydrogen Energy **43** 6 (2018) 3406-3417.
[57] RUTH, M.F., ZINAMAN, O.R., ANTKOWIA, M., Nuclear-Renewable Hybrid Energy Systems: Opportunities, Interconnections, and Needs, Idaho National Laboratory, INL/JOU-14-33322, (2014)
[58] BRAGG-SITTON, S.M., et al., Nuclear-Renewable Hybrid Energy Systems: 2016 Technology Development Program Plan, Idaho National Laboratory, INL/EXT-16-38165, (2016)
[59] BORISSOVA, A.V., Analysis and Synthesis of a Hybrid Nuclear-Solar Power Plant, Proc. 2015 (abstract)
[60] RUTH, M.F., et al., Nuclear-renewable hybrid energy systems: Opportunities, interconnections, and needs, Energy Conversion and Management **78** (2014) 684-694.
[61] YELTARENKO, E.A., Evaluation and selection of solutions for many criteria. Moscow, MEPhI, 111c. tutorial., (1995)
[62] ZHURAVLEV, I.B., ZALUZHNY, A.A., PTITSYN, P.B., Feasibility studies (TEI) on the priority area of scientific and technological development, Hydrogen energy, Private Institution Science and Innovation, ISBN 978-5-498-00807-3, (2021)
[63] VNIPIET, Expert technical and economic assessment of the construction of energy technological complexes based on MGR-T reactor plants, Russian Federation, (2004)
[64] WEISSER, D., A guide to life-cycle greenhouse gas (GHG) emissions from electric supply technologies, Energy **32** 9 (2007) 1543-1559.
[65] https://www.energyforum.in
[66] INTERNATIONAL ATOMIC ENERGY AGENCY, Advances in Small Modular Reactor Technology Developments, A Supplement to: IAEA Advanced Reactors Information System (ARIS), 2018 Edition, IAEA, Vienna, Austria, (2018)
[67] TODREAS, N.E., KAZIMI, M.S., Nuclear Systems Volume I: Thermal Hydraulic Fundamentals (3rd ed.). CRC Press., (2021)
[68] BROWN, L.C., et al., High efficiency generation of hydrogen fuels using nuclear power, DE-FG03-99-SF21888, Final technical report for the period August 1, 1999 through September 30, 2002, La Jolla, CA, General Atomics Corp. Report GA-A24285, (2003)
[69] RAWLINGS, J.B., EKERDT, J.G., Chemical Reactor Analysis and Design Fundamentals, Proc. 2002 (abstract)
[70] HUANG, C., T-RAISSI, A., Analysis of sulfur–iodine thermochemical cycle for solar hydrogen production. Part I: decomposition of sulfuric acid, Solar Energy **78** 5 (2005) 632-646.

[71] INTERNATIONAL ATOMIC ENERGY AGENCY, Approaches for Assessing the Economic Competitiveness of Small and Medium Sized Reactors, IAEA Nuclear Energy Series No. NP-T-3, IAEA, Vienna, Austria, (2013)
[72] MOORE, M., The economics of very small modular reactors in the North, Proc. of 4th International Technical Meeting on Small Reactors (ITMSR-4), November 2-4, 2016, Ottawa, Canada, (2016)
[73] LAZARD, Lazard's Levelized Cost of Energy Analysis – Version 13.0. https://www.lazard.com/media/451086/lazards-levelized-cost-of-energy-version-130-vf.pdf, (2019)
[74] NUCLEAR ENERGY INSTITUTE, Industry Finds NRC's New Reactor Reviews Costly. https://www.nei.org/news/2018/nei-finds-nrc-new-reactor-reviews-inefficient, (2018)
[75] BUONGIORNO, J., PARSONS, J., CORRADINI, M., PETTI, D., The Future of Nuclear Energy in a Carbon-Constrained World: An Interdisciplinary MIT Study, Massachusetts Institute of Technology, MIT Energy Initiative, Revision 1, (2018)
[76] PINSKY, R., SABHARWALL, P., HARTVIGSEN, J., O'BRIEN, J., Comparative review of hydrogen production technologies for nuclear hybrid energy systems, Progress in Nuclear Energy **123** (2020) 103317.
[77] PONOMAREV-STEPNOY, N.N., PETRUNIN, V.V., Design of energy-technological complex on the basis of innovative reactor installation with high-temperature reactor, AtomRegion (2009)
[78] GOLDSTEIN, S., BORGARD, J.-M., VITART, X., Upper bound and best estimate of the efficiency of the iodine sulphur cycle, International Journal of Hydrogen Energy **30** 6 (2005) 619-626.
[79] O'KEEFE, D., et al., Preliminary results from bench-scale testing of a sulfur-iodine thermochemical water-splitting cycle, International Journal of Hydrogen Energy **7** 5 (1982) 381-392.
[80] HADJ-KALI, M.K., et al., Bunsen section thermodynamic model for hydrogen production by the sulfur–iodine cycle, International Journal of Hydrogen Energy **34** 16 (2009) 6625-6635.
[81] CHO, W.-C., PARK, C.-S., KANG, K.-S., KIM, C.-H., BAE, K.-K., Conceptual design of sulfur–iodine hydrogen production cycle of Korea Institute of Energy Research, Nuclear Engineering and Design **239** 3 (2009) 501-507.
[82] PROSINI, P.P., CENTO, C., GIACONIA, A., CAPUTO, G., SAU, S., A modified sulphur–iodine cycle for efficient solar hydrogen production, International Journal of Hydrogen Energy **34** 3 (2009) 1218-1225.
[83] TERADA, A., et al., Development of Hydrogen Production Technology by Thermochemical Water Splitting IS Process Pilot Test Plan, Journal of Nuclear Science and Technology **44** 3 (2007) 477-482.
[84] FUNK, J.E., REINSTROM, R.M., Energy Requirements in Production of Hydrogen from Water, Industrial & Engineering Chemistry Process Design and Development **5** 3 (1966) 336-342.
[85] NOGLIK, A., et al., Solar Thermochemical Generation of Hydrogen: Development of a Receiver Reactor for the Decomposition of Sulfuric Acid, Journal of Solar Energy Engineering **131** 1 (2009)
[86] LANCHI, M., et al., S–I thermochemical cycle: A thermodynamic analysis of the HI–H2O–I2 system and design of the HIx decomposition section, International Journal of Hydrogen Energy **34** 5 (2009) 2121-2132.

[87] GOSWAMI, N., et al., DDR zeolite membrane reactor for enhanced HI decomposition in IS thermochemical process, International Journal of Hydrogen Energy **42** 16 (2017) 10867-10879.
[88] DAVIS, M.E., CONGER, W.L., An entropy production and efficiency analysis of the Bunsen reaction in the General Atomic sulfur-iodine thermochemical hydrogen production cycle, International Journal of Hydrogen Energy **5** 5 (1980) 475-485.
[89] SHIMIZU, S., NAKAJIMA, H., ONUKI, K., A Progress report on bench scale studies of the iodine-sulfur process for thermochemical hydrogen production, Proceedings of a Technical Committee meeting held in Oarai, Japan, 19-20 October, 1992, (1992)
[90] LEYBROS, J., CARLES, P., BORGARD, J.-M., Countercurrent reactor design and flowsheet for iodine-sulfur thermochemical water splitting process, International Journal of Hydrogen Energy **34** 22 (2009) 9060-9075.
[91] GIACONIA, A., SAU, S., CAPUTO, G., PARISI, M., STOLTEN, D., Analysis and Development of the Bunsen Section in the Sulphur-Iodine Process, Proc. of 18th World Hydrogen Energy Conference – WHEC 2010, (2010)
[92] PARISI, M., et al., Bunsen reaction and hydriodic phase purification in the sulfur–iodine process: An experimental investigation, International Journal of Hydrogen Energy **36** 3 (2011) 2007-2013.
[93] KIM, Y.H., et al., Bunsen Reaction Using a Counter-Current Flow Reactor in Sulfur-Iodine Hydrogen Production Process: Effects of Reactor Shape and Temperature, Advanced Materials Research **347-353** (2012) 3238-3241.
[94] KIM, Y.H., et al., Phase Separation Characteristics of Pressurized Bunsen Reaction for Sulfur-Iodine Thermochemical Hydrogen Production Process, Advanced Materials Research **550-553** (2012) 554-557.
[95] KIM, Y.H., et al., The Effect of Oxygen on Bunsen Reaction with HIX Solution in Sulfur-Iodine Hydrogen Production Process, Advanced Materials Research **550-553** (2012) 431-434.
[96] KIM, H.S., et al., Continuous Bunsen reaction and simultaneous separation using a counter-current flow reactor for the sulfur–iodine hydrogen production process, International Journal of Hydrogen Energy **38** 14 (2013) 6190-6196.
[97] YING, Z., et al., Influence of the initial HI on the multiphase Bunsen reaction in the sulfur–iodine thermochemical cycle, International Journal of Hydrogen Energy **38** 36 (2013) 15946-15953.
[98] ZHU, Q., et al., Kinetic and thermodynamic studies of the Bunsen reaction in the sulfur–iodine thermochemical process, International Journal of Hydrogen Energy **38** 21 (2013) 8617-8624.
[99] ZHANG, Y., et al., Experimental Investigation on Multiphase Bunsen Reaction in the Thermochemical Sulfur–Iodine Cycle, Industrial & Engineering Chemistry Research **53** 8 (2014) 3021-3028.
[100] RAO, A.S., et al., Study of effect of high pressures and elevated temperatures on Bunsen reaction of Iodine–Sulfur thermo-chemical process, International Journal of Hydrogen Energy **40** 15 (2015) 5025-5033.
[101] RAO, A.S., et al., Study of Bunsen reaction in agitated reactor operating in counter current mode for iodine-sulphur thermo-chemical process, International Journal of Nuclear Hydrogen Production and Applications **3** 1 (2016) 12-31.
[102] KIM, H.S., et al., Characteristics of Bunsen reaction using HIx solution (HI–I2–H2O) in a co-current flow mode for the sulfur-iodine hydrogen production process, International Journal of Hydrogen Energy **41** 25 (2016) 10530-10537.
[103] KIM, H.S., PARK, H.K., KIM, Y.H., PARK, C.S., BAE, K.K., Effects of operating parameters on the pressurized Bunsen reaction for the integrated operation of sulfur–

iodine hydrogen production process, International Journal of Hydrogen Energy **41** 34 (2016) 15133-15140.
[104] ZHOU, C., CHEN, S., WANG, L., ZHANG, P., Absorption behaviors of SO2 in HI acid for the iodine-sulfur thermochemical cycle, International Journal of Hydrogen Energy **42** 47 (2017) 28164-28170.
[105] ZHOU, C., ZHANG, P., WANG, L., CHEN, S., Apparent kinetics of the Bunsen reaction in I2/HI solution for the iodine–sulfur hydrogen production process, International Journal of Hydrogen Energy **42** 22 (2017) 14916-14925.
[106] AHMED, V.N., et al., Role of operating conditions on cross contamination of products of the Bunsen reaction in iodine-sulfur process for production of hydrogen, International Journal of Hydrogen Energy **42** 49 (2017) 29101-29106.
[107] NAFEES, A.V., et al., Evaluation of Bunsen reaction at elevated temperature and high pressure in continuous co-current reactor in iodine-sulfur thermochemical process, International Journal of Hydrogen Energy **43** 17 (2018) 8190-8197.
[108] HIROKI, N., et al., Hydrogen production using thermochemical water-splitting Iodine–Sulfur process test facility made of industrial structural materials: Engineering solutions to prevent iodine precipitation, International Journal of Hydrogen Energy **46** 43 (2021) 22328-22343.
[109] JAPAN ATOMIC ENERGY AGENCY, Toward Metallic Sulfuric Acid Decomposers in the IS Process, JAEA R&D Review 2021-22, (2022)
[110] EL-EMAM, R.S., OZCAN, H., ZAMFIRESCU, C., Updates on promising thermochemical cycles for clean hydrogen production using nuclear energy, Journal of Cleaner Production **262** (2020) 121424.
[111] BRECHER, L.E., WU, K.C., Electrolytic decomposition of water. No. US 3888750, (1975)
[112] KODAMA, T., GOKON, N., Thermochemical Cycles for High-Temperature Solar Hydrogen Production, Chemical Reviews **107** 10 (2007) 4048-4077.
[113] DOKIYA, M., KAMEYAMA, T., FUKUDA, K., KOTERA, Y., The Study of Thermochemical Hydrogen Preparation. III. An Oxygen-evolving Step through the Thermal Splitting of Sulfuric Acid, Bulletin of the Chemical Society of Japan **50** 10 (1977) 2657-2660.
[114] DÍAZ-ABAD, S., MILLÁN, M., RODRIGO, M.A., LOBATO, J., Review of Anodic Catalysts for SO2 Depolarized Electrolysis for "Green Hydrogen" Production, Catalysts **9** 1 (2019)
[115] CARTY, R., Party and parish pump: electoral politics in Ireland. Wilfrid Laurier Univ. Press, (1981)
[116] POPE, K., WANG, Z., NATERER, G.F., Process integration of material flows of copper chlorides in the thermochemical Cu–Cl cycle, Chemical Engineering Research and Design **109** (2016) 273-281.
[117] ZAMFIRESCU, C., NATERER, G.F., ROSEN, M.A., Chemical exergy of electrochemical cell anolytes of cupric/cuprous chlorides, International Journal of Hydrogen Energy **42** 16 (2017) 10911-10924.
[118] SIMPSON, M.F., HERRMANN, S.D., BOYLE, B.D., A hybrid thermochemical electrolytic process for hydrogen production based on the reverse Deacon reaction, International Journal of Hydrogen Energy **31** 9 (2006) 1241-1246.
[119] KASHANI-NEJAD, S., NG, K.W., HARRIS, R., MgOHCl thermal decomposition kinetics, Metallurgical and Materials Transactions B **36** 1 (2005) 153-157.
[120] OZCAN, H., Experimental and theoretical investigations of magnesium-chlorine cycle and its integrated systems, University of Ontario Institute of Technology, Canada, (2015)

[121] SAKURAI, M., BILGEN, E., TSUTSUMI, A., YOSHIDA, K., Solar UT-3 thermochemical cycle for hydrogen production, Solar Energy **57** 1 (1996) 51-58.
[122] SIMPSON, M.F., UTGIKAR, V., SACHDEV, P., MCGRADY, C., A novel method for producing hydrogen based on the Ca–Br cycle, International Journal of Hydrogen Energy **32** 4 (2007) 505-509.
[123] ATES, F., OZCAN, H., Turkey's industrial waste heat recovery potential with power and hydrogen conversion technologies: A techno-economic analysis, International Journal of Hydrogen Energy (2020)
[124] YAMASHITA, K., BARRETO, L., Energyplexes for the 21st century: Coal gasification for co-producing hydrogen, electricity and liquid fuels, Energy **30** (2005) 2453-2473.
[125] VALERO, A., USÓN, S., Oxy-co-gasification of coal and biomass in an integrated gasification combined cycle (IGCC) power plant, Energy **31** (2005) 1643-1655.
[126] KUGELER, K., Possibilities and state of development of nuclear coal gasification processes, Chemical Engineering Science **35** (1980) 2005-2028.
[127] VON LENSA, W., VERFONDERN, K., Coal gasification for hydrogen production using nuclear energy, Proceedings of 18th World Hydrogen Energy Conference (WHEC 2010) (2010) 191-198.
[128] ALLELEIN, H.J., VERFONDERN, K., Major milestones of HTR development in Germany and still open research issues, Annals of Nuclear Energy **116** (2018) 114-127.
[129] INTERNATIONAL ATOMIC ENERGY AGENCY, Advances in nuclear power process heat applications, IAEA-TECDOC-1682, IAEA, Vienna, Austria, (2012) 179-185.
[130] SCHULTEN, R., ET AL., Industriekraftwerk mit Hochtemperaturreaktor PR-500-OTTO Prinzip zur Erzeugung von Prozessdampf, Report Juelich-941-RG (in German), (1973)
[131] SINGH, J., BARNERT, H., Modular design concept for the HTR on the basis of the AVR, Nuclear Energy **23** (1983) 211-215.
[132] REUTLER, H., LOHNERT, G.H., Advantages of going modular in HTRs, Nuclear Engineering and Design **78** (1984) 129-136.
[133] BARNERT, H., SINGH, J., Design evaluation of a small high-temperature reactor for process heat applications, Nuclear Engineering and Design **109** (1988) 245-251.
[134] INTERNATIONAL ATOMIC ENERGY AGENCY, High Temperature Gas Cooled Reactor Fuels and Materials, IAEA-TECDOC-1645, IAEA, Vienna, Austria, (2010)
[135] LABAR, M., The gas turbine modular helium reactor, Nuclear News **46** 11 (2003) 28-37.
[136] GOLOVKO, V.F., KODOCHIGOV, N.G., VASYAEV, A.V., SHENOY, A., BAXI, C.B., Ways to Increase Efficiency of the High-Temperature Gas Reactor Coupled With the Gas-Turbine Power Conversion Unit, Journal of Engineering for Gas Turbines and Power **131** 5 (2009)
[137] YAN, X., KUNITOMI, K., NAKATA, T., SHIOZAWA, S., GTHTR300 design and development, Nuclear Engineering and Design **222** 2 (2003) 247-262.
[138] U.S. IDAHO NATIONAL LABORATORY, Next generation nuclear plant pre-conceptual design report, Report INL/EXT-07-12967 Rev.1, Idaho National Laboratory, Idaho Falls, USA (2007)
[139] KUNITOMI, K., KATANISHI, S., TAKADA, S., TAKIZUKA, T., YAN, X., Japan's future HTR—the GTHTR300, Nuclear Engineering and Design **233** 1 (2004) 309-327.

[140] RICHARDS, M.B., The modular helium reactor for future energy needs", In Poroceedings Int. Congress Reno ICAPP´06, paper 6154, (2006)
[141] JAEGER, W., WEISBRODT, I., HOERNING, H., Nuclear process heat applications for the modular HTR, Nuclear Engineering and Design **78** (1984) 137-145.
[142] NEEF, H.F., WEISBRODT, I., Coal gasification with heat from high temperature reactors, Nuclear Engineering and Design **54** (1979) 157-174.
[143] OGAWA, M., NISHIHARA, T., Present status of energy in Japan and HTTR project, Nuclear Engineering and Design **233** 1 (2004) 5-10.
[144] SHIOZAWA, S., FUJIKAWA, S., IYOKU, T., KUNITOMI, K., TACHIBANA, Y., Overview of HTTR design features, Nuclear Engineering and Design **233** 1 (2004) 11-21.
[145] SAITO, S., Nuclear Energy and Hydrogen Production. The Japanese Situation", In Policy Debate on the Potential Contribution of Nuclear Energy to Production of Hydrogen OECD/NEA, October 15 (2004) 1-11.
[146] TACHIBANA, Y., NAKAGAWA, S., IYOKU, T., Safety Demonstration Tests using High Temperature Engineering Test reactor (HTTR)", In Proceed. of GENES4/ANP2003 Paper 1095, September 15-19, Kyoto, Japan (2003)
[147] LOHNERT, G.H., Technical design features and essential safety-related properties of the HTR-Module, Nuclear Engineering and Design **121** (1990) 259-275.
[148] STEINWARZ, W., Status of design of the HTR test module in China, Nuclear Engineering and Design **121** (1990) 317-324.
[149] WU, Z., LIN, D., ZHONG, D., The design features of the HTR-10, Nuclear Engineering and Design **218** 1 (2002) 25-32.
[150] YAN. X., ET AL., Design and development of GTHTR300, In Proceed. International Topical Meeting on HTR Technology, Petten, Netherlands, April 22-24 (2002)
[151] SAGAYAMA, Y., Status of Japan in development of innovative reactor, In Proceedings of Innovation for Cool Earth Conference, Tokyo, Japan, October 11 (2018)
[152] ZHANG, Z., et al., Current status and technical description of Chinese 2×250MWth HTR-PM demonstration plant, Nuclear Engineering and Design **239** 7 (2009) 1212-1219.
[153] ZHANG, Z., et al., The Shandong Shidao Bay 200 MWe High-Temperature Gas-Cooled Reactor Pebble-Bed Module (HTR-PM) Demonstration Power Plant: An Engineering and Technological Innovation, Engineering **2** 1 (2016) 112-118.
[154] TOPOROV, D., ABRAHAM, R., Gasification of low-rank coal in the High-Temperature Winkler (HTW) process, The Journal of The Southern African Institute of Mining and Metallurgy **2015** (2015) 589-597.
[155] PRABHANSU, P., ET AL., Circulating Fluidized Bed Gasification: Status. Challenges, and Prospects in Indian Perspective, Indian Journal of Science and Technology **9** 48 (2016) 1-14.
[156] BREAULT, R.W., Gasification Processes Old and New: A Basic Review of the Major Technologies, Energies **3** 2 (2010)
[157] BUCKO, Z., ET AL., 400 MWe IGCC Power Plant with HTW Gasification in the Czech Republic, In Proceedings of the 1999 Gasification Technologies Conference, San Francisco, USA, October 17-20 (1999)
[158] KIRCHHOFF, R., ET AL., Operation of a semi-technical pilot plant for nuclear aided steam gasification of coal, Nuclear Engineering and Design **78** (1984) 233-239.
[159] KUBIAK, H., VAN HEEK, K.H., ZIEGLER, A., Nukleare Kohlevergasung-Erreichter Stand, Einschaetzung und Nutzung der Ergebnisse, Fortschritte in der

Energietechnik, Monographien des Forschunszentrum Juelich (in German) **8** (1993) 153.
[160] VAN HEEK, K.H., JUENTGEN, H., PETERS, W., Wasserdampfvergasung von Kohle mit Hilfe von Prozesswaerme aus Hochtemperatur-Kernreaktoren, Atomkernenergie/ Kerntechnik (in German) **40** (1982) 225-246
[161] HSC Software: Outukumpu HSC Chemistry for Windows, Version 6.12. Outukumpu Research Oy. Pori, Finland (2006)
[162] DE MICCO, G., NASJLETI, A., BOHÉ, A.E., Kinetics of the gasification of a Rio Turbio coal under different pyrolysis temperatures, Fuel **95** (2012) 537-543.
[163] FEISTEL, P.P., DUERRFELD, R., VAN HEEK, K.H., JUENTGEN, H., Layout of an internally heated gas generator for the steam gasification of coal, Nuclear Engineering and Design **34** (1975) 147-155.
[164] JUENTGEN, H., VAN HEEK, K.H., Gasification of coal with steam using heat from HTRs, Nuclear Engineering and Design **34** (1975) 59-63.
[165] RODRÍGUEZ, C.R., et al., Analysis of the potential for hydrogen production in the province of Córdoba, Argentina, from wind resources, International Journal of Hydrogen Energy **35** 11 (2010) 5952-5956.
[166] H2A analysis webpage, http://www.hydrogen.energy.gov/h2a_analysis.html (2009)
[167] SIGAL, A., LEIVA, E.P.M., RODRÍGUEZ, C.R., Assessment of the potential for hydrogen production from renewable resources in Argentina, International Journal of Hydrogen Energy **39** 16 (2014) 8204-8214.
[168] INTERNATIONAL ATOMIC ENERGY AGENCY, Nuclear Power Reactors in the World, IAEA-RDS-2/41, Vienna, Austria, (2021)
[169] OBARA, S.Y., TANAKA, R., Waste heat recovery system for nuclear power plants using the gas hydrate heat cycle, Applied Energy **292** (2021) 116667.
[170] MIERNICKI, E.A., HEALD, A.L., HUFF, K.D., BROOKS, C.S., MARGENOT, A.J., Nuclear waste heat use in agriculture: History and opportunities in the United States, Journal of Cleaner Production **267** (2020) 121918.
[171] ZAMFIRESCU, C., NATERER, G.F., DINCER, I., Upgrading of Waste Heat for Combined Power and Hydrogen Production With Nuclear Reactors, Journal of Engineering for Gas Turbines and Power **132** 10 (2010)
[172] INTERNATIONAL ATOMIC ENERGY AGENCY, Advances in Small Modular Reactor Technology Developments, A Supplement to: IAEA Advanced Reactors Information System (ARIS), 2020 Edition, IAEA, Vienna, Austria, (2020)
[173] TARHAN, C., ÇIL, M.A., A study on hydrogen, the clean energy of the future: Hydrogen storage methods, Journal of Energy Storage **40** (2021) 102676.
[174] NIAZ, S., MANZOOR, T., PANDITH, A.H., Hydrogen storage: Materials, methods and perspectives, Renewable and Sustainable Energy Reviews **50** (2015) 457-469.
[175] GOLBEN, M., DACOSTA, D., Advanced Thermal Hydrogen Compression, Proc. SAE International, United States (1999)
[176] TARASOV, B.P., BOCHARNIKOV, M.S., YANENKO, Y.B., FURSIKOV, P.V., LOTOTSKYY, M.V., Cycling stability of RNi5 (R = La, La+Ce) hydrides during the operation of metal hydride hydrogen compressor, International Journal of Hydrogen Energy **43** 9 (2018) 4415-4427.
[177] LÉON, A., Hydrogen Technology, Springer-Verlag, Heidelberg, Berlin, Germany, (2008)
[178] VANHANEN, J.P., HAGSTRÖM, M.T., LUND, P.D., Combined hydrogen compressing and heat transforming through metal hydrides, International Journal of Hydrogen Energy **24** 5 (1999) 441-448.

[179] LAURENCELLE, F., DEHOUCHE, Z., GOYETTE, J., BOSE, T.K., Integrated electrolyser—metal hydride compression system, International Journal of Hydrogen Energy **31** 6 (2006) 762-768.
[180] SCHLAPBACH, L., ZÜTTEL, A., Hydrogen-storage materials for mobile applications, Nature **414** 6861 (2001) 353-358.
[181] LI, Y., YANG, R.T., Significantly Enhanced Hydrogen Storage in Metal−Organic Frameworks via Spillover, Journal of the American Chemical Society **128** 3 (2006) 726-727.
[182] HIRSCHER, M., Handbook of hydrogen storage new materials for future energy storage, Weinheim Wiley-VCH-Verl, (2010)
[183] GKANAS, E.I., et al., Study on the operation and energy demand of dual-stage Metal Hydride Hydrogen Compressors under effective thermal management, International Journal of Hydrogen Energy **46** 57 (2021) 29272-29287.
[184] CHRISTENSEN, C.H., et al., Metal ammine complexes for hydrogen storage, Journal of Materials Chemistry **15** 38 (2005) 4106-4108.
[185] BELLOSTA VON COLBE, J., et al., Application of hydrides in hydrogen storage and compression: Achievements, outlook and perspectives, International Journal of Hydrogen Energy **44** 15 (2019) 7780-7808.
[186] FELLAY, C., DYSON, P., LAURENCZY, G., A Viable Hydrogen-Storage System Based On Selective Formic Acid Decomposition with a Ruthenium Catalyst, Angewandte Chemie (International ed. in English) **47** (2008) 3966-3968.
[187] ZHANG, Y.H.P., A sweet out-of-the-box solution to the hydrogen economy: is the sugar-powered car science fiction?, Energy & Environmental Science **2** 3 (2009) 272-282.
[188] TEICHMANN, D., ARLT, W., WASSERSCHEID, P., FREYMANN, R., A future energy supply based on Liquid Organic Hydrogen Carriers (LOHC), Energy & Environmental Science **4** 8 (2011) 2767-2773.
[189] REDDI, K., ELGOWAINY, A., RUSTAGI, N., GUPTA, E., Impact of hydrogen refueling configurations and market parameters on the refueling cost of hydrogen, International Journal of Hydrogen Energy **42** 34 (2017) 21855-21865.
[190] NREL, Composite Data Products, https://www.nrel.gov/docs/fy18osti/70529.pdf, (2017)
[191] CHALKIADAKIS, N., STUBOS, A., ZOULIAS, E.I., STAMATAKIS, E., Pilot autonomous hybrid hydrogen refueling station utilizing a metal hydride compressor covering local transportation needs, E3S Web Conf. **334** (2022) 06002.
[192] BOUWMAN, P., HyET BV Hydrogen Efficiency Technologies, Fuel Cells Bulletin, (2014)
[193] CATALANO, J., BENTIEN, A., ØSTEDGAARD-MUNCK, D., KJELSTRUP, S., Efficiency of electrochemical gas compression, pumping and power generation in membranes, Journal of Membrane Science **478** (2015)
[194] YARTYS, V.A., et al., Metal hydride hydrogen compression: recent advances and future prospects, Applied Physics A **122** 4 (2016) 415.
[195] LOTOTSKYY, M.V., YARTYS, V.A., POLLET, B.G., BOWMAN, R.C., Metal hydride hydrogen compressors: A review, International Journal of Hydrogen Energy **39** 11 (2014) 5818-5851.
[196] GKANAS, E.I., KHZOUZ, M., Numerical analysis of candidate materials for multi-stage metal hydride hydrogen compression processes, Renewable Energy **111** (2017) 484-493.
[197] BOSSEL, U., Does a Hydrogen Economy Make Sense?, Proceedings of the IEEE **94** 10 (2006) 1826-1837.

[198] STAMATAKIS, E., et al., Metal hydride hydrogen compressors: Current developments & early markets, Renewable Energy **127** (2018) 850-862.
[199] OZCAN, H., DINCER, I., Modeling of a new four-step magnesium–chlorine cycle with dry HCl capture for more efficient hydrogen production, International Journal of Hydrogen Energy **41** 19 (2016) 7792-7801.
[200] OZCAN, H., DINCER, I., Exergoeconomic optimization of a new four-step magnesium–chlorine cycle, International Journal of Hydrogen Energy **42** 4 (2017) 2435-2445.
[201] RUTH, M.F., et al., The Economic Potential of Two Nuclear-Renewable Hybrid Energy Systems, National Renewable Energy Laboratory Technical Report NREL/TP-6A50-66073 (2016)
[202] RUTH, M.F., CUTLER, D., FLORES-ESPINO, F., STARK, G., The Economic Potential of Nuclear-Renewable Hybrid Energy Systems Producing Hydrogen, National Renewable Energy Laboratory Technical Report NREL/TP-6A50-66764 (2017)
[203] EL-EMAM, R.S., KHAMIS, I., International collaboration in the IAEA nuclear hydrogen production program for benchmarking of HEEP, International Journal of Hydrogen Energy **42** 6 (2017) 3566-3571.
[204] HAMPE, J., MADLENER, R., Economic feasibility of high-temperature reactors for industrial cogeneration: an investor's perspective, Journal of Nuclear Science and Technology **53** 11 (2016) 1839-1857.
[205] EL-EMAM, R.S., KHAMIS, I., Advances in nuclear hydrogen production: Results from an IAEA international collaborative research project, International Journal of Hydrogen Energy **44** 35 (2019) 19080-19088.
[206] INTERNATIONAL ENERGY AGENCY, NUCLEAR ENERGY AGENCY OECD, Projected costs generating electricity, (2010)
[207] BOUDRIES, R., Comparative Economic Competitiveness Assessment of Hydrogen as a Fuel in the Transport Sector in Algeria, Chemical Engineering Transactions **42** (2014) 61-66.
[208] YU, C.F., VAN SARK, W.G.J.H.M., ALSEMA, E.A., Unraveling the photovoltaic technology learning curve by incorporation of input price changes and scale effects, Renewable and Sustainable Energy Reviews **15** 1 (2011) 324-337.
[209] OGDEN, J.M., Renewable hydrogen energy system studies. Final Report. US: NREL, DOE Contract No XR-2-11265-1, (1993)
[210] BOUDRIES, R., DIZÈNE, R., Potential of hydrogen production in Algeria, International Journal of Hydrogen Energy **33** (2008) 4476-4487.
[211] BOUDRIES, R., DIZÉNE, R., Analysis of solar hydrogen production potential in Algeria: case of an electrolyser-PV tracking system, Proc. Energy and Materials Research Conference (EMR2012), 20-22 June 2012, Torremolinos, Spain, (2012)
[212] CANY, C., MANSILLA, C., DA COSTA, P., MATHONNIÈRE, G., Adapting the French nuclear fleet to integrate variable renewable energies via the production of hydrogen: Towards massive production of low carbon hydrogen?, International Journal of Hydrogen Energy **42** 19 (2017) 13339-13356.
[213] SCHRATTENHOLTZER, L., Experience curves of photovoltaic technology, Interim Report IR-00-014, International Institute for Applied Analysis, Laxenburg, Austria, (2000)
[214] BOUDRIES, R., DIZENE, R., Technico-economic analysis of renewable hydrogen production in Algeria, Proc. 10th International Conference on Sustainable Energy Technologies, 4 - 7 September 2011, Kumburgaz, İstanbul, Turkey, (2011)

[215] BILGEN, E., Domestic hydrogen production using renewable energy, Solar Energy **77** 1 (2004) 47-55.
[216] NEZAMMAHALLEH, H., FARHADI, F., TANHAEMAMI, M., Conceptual design and techno-economic assessment of Integrated Solar Combined Cycle System with DSG technology, Solar Energy - SOLAR ENERG **84** (2010)
[217] RUTH, M.F., SPITSEN, P., BOARDMAN, R., Opportunities and Challenges for Nuclear-Renewable Hybrid Energy system, NREL/CP-6A20-72004 (2019)
[218] SEITZ, M., VON STORCH, H., NECHACHE, A., BAUER, D., Techno economic design of a solid oxide electrolysis system with solar thermal steam supply and thermal energy storage for the generation of renewable hydrogen, International Journal of Hydrogen Energy **42** 42 (2017) 26192-26202.
[219] BUTTLER, A., SPLIETHOFF, H., Current status of water electrolysis for energy storage, grid balancing and sector coupling via power-to-gas and power-to-liquids: A review, Renewable and Sustainable Energy Reviews **82** (2018) 2440-2454.
[220] EL-EMAM, R.S., ÖZCAN, H., Comprehensive review on the techno-economics of sustainable large-scale clean hydrogen production, Journal of Cleaner Production **220** (2019) 593-609.
[221] ALZAHRANI, A.A., DINCER, I., Exergoeconomic analysis of hydrogen production using a standalone high-temperature electrolyzer, International Journal of Hydrogen Energy **46** 27 (2021) 13899-13907.
[222] YADAV, D., BANERJEE, R., Economic assessment of hydrogen production from solar driven high-temperature steam electrolysis process, Journal of Cleaner Production **183** (2018) 1131-1155.
[223] WANG, F., et al., Design and optimization of hydrogen production by solid oxide electrolyzer with marine engine waste heat recovery and ORC cycle, Energy Conversion and Management **229** (2021) 113775.
[224] MEHRPOOYA, M., KARIMI, M., Hydrogen production using solid oxide electrolyzer integrated with linear Fresnel collector, Rankine cycle and thermochemical energy storage tank, Energy Conversion and Management **224** (2020) 113359.
[225] HERNÁNDEZ-PACHECO, E., SINGH, D., HUTTON, P.N., PATEL, N., MANN, M.D., A macro-level model for determining the performance characteristics of solid oxide fuel cells, Journal of Power Sources **138** 1 (2004) 174-186.
[226] OECD, N.E.A., The Role of Nuclear Power in the Hydrogen Economy. Cost and Competitiveness, NEA No. 7630, https://www.oecd-nea.org/upload/docs/application/pdf/2022-09/7630_the_role_of_nuclear_power_in_the_hydrogen_economy.pdf, (2022)

LIST OF ABBREVIATIONS

AC	Alternative current
AECL	Atomic Energy Canada Limited
BWR	Boiling water reactor
CAPEX	Capital expenditures
CANDU	Canada Deuterium Uranium
CNEA	National Atomic Energy Commission
CPV	Concentrated photovoltaic
CRP	Coordinated Research Project
CSP	Concentrated solar power
FBR	Fast breeder reactor
GFR	Gas cooled fast reactor
GHG	Greenhouse gas emissions
HEEP	Hydrogen Economic Evaluation Programme
HTGR	High temperature gas cooled reactor
HTR-PM	High-Temperature Reactor Pebble bed Module
HTTR	High temperature test reactor
HTSE	High temperature steam electrolysis
HTW	High-Temperature Winkler
IAEA	International Atomic Energy Agency
IHX	Intermediate heat exchanger
INHPS	Integrated nuclear hydrogen production systems
JAEA	Japan Atomic Energy Agency
LCOE	Levelized cost of electricity
LFR	Lead cooled fast reactor
LWR	Light Water Reactors
NEA	Nuclear Energy Agency
NPP	Nuclear power plant
O&M	Operations and maintenance

OPEX	Operating expenditures
R&D	Research and development
PEM	Polymer electrolyte membrane/ proton exchange membrane
PNP	Prototype Nuclear Process
PV	Photovoltaic
PWR	Pressurized water-cooled reactor
SCWR	Supercritical water reactor
SFR	Sodium cooled fast reactor
S-I	Sulphur-iodine
SMR	Small modular reactor
SOE	Solid oxide electrolysis
SOEC	Solid oxide electrolysis cell
TMSR	Thorium molten salt reactor
TRL	Technology readiness level
VHTR	Very high temperature gas cooled reactor

CONTRIBUTORS TO DRAFTING AND REVIEW

Alzahrani, A.	Umm Al-Qura University, Saudi Arabia
Balanin, A.	National Research Center Kurchatov Institute, Russian Federation
Bohe, A.	Comisión Nacional de Energia Atómica, Argentina
Boudries, R.	Development Center for Renewable Energies, Algeria
Bradley, E.	International Atomic Energy Agency
Chalkiadakis, N.	National Center of Scientific Research "Demokritos", Greece
Constantin, A.	International Atomic Energy Agency
Dulera, I.	Bhabba Atomic Research Centre, India
El-Emam, R.	International Atomic Energy Agency
Jevremovic, T.	International Atomic Energy Agency
Khamis, I.	International Atomic Energy Agency
Khoroshev, M.	International Atomic Energy Agency
Malshe, U.	Bhabba Atomic Research Centre, India
Ohayon, D.	International Atomic Energy Agency
Ozcan, H.	Karabuk University, Türkye
Revankar, S.	Purdue University, USA
Stamatakis, E.	National Center of Scientific Research "Demokritos", Greece
Varvagianni, M.	National Center of Scientific Research "Demokritos", Greece
Wang, J. Q.	Shanghai Institute of Applied Physics, Chinese Academy of Sciences, China
Yan, X.	Japan Atomic Energy Agency, Japan

Research Coordination Meetings

Vienna, Austria: 03–05 December 2018,

Vienna, Austria: 19–21 October 2020,

Vienna, Austria: 15–17 November 2021

IAEA
International Atomic Energy Agency

No. 27

ORDERING LOCALLY

IAEA priced publications may be purchased from the sources listed below or from major local booksellers.

Orders for unpriced publications should be made directly to the IAEA. The contact details are given at the end of this list.

NORTH AMERICA

Bernan / Rowman & Littlefield

15250 NBN Way, Blue Ridge Summit, PA 17214, USA
Telephone: +1 800 462 6420 • Fax: +1 800 338 4550
Email: orders@rowman.com • Web site: www.rowman.com/bernan

REST OF WORLD

Please contact your preferred local supplier, or our lead distributor:

Eurospan

1 Bedford Row
London
WC1R 4BU
United Kingdom

Trade Orders and Enquiries:

Tel: +44 (0)1235 465576
Email: trade.orders@marston.co.uk

Individual Customers:

Tel: +44 (0)1235 465577
Email: direct.orders@marston.co.uk
www.eurospanbookstore.com/iaea

For further information:

Tel. +44 (0) 207 240 0856
Email: info@eurospan.co.uk
www.eurospan.co.uk

Orders for both priced and unpriced publications may be addressed directly to:

Marketing and Sales Unit
International Atomic Energy Agency
Vienna International Centre, PO Box 100, 1400 Vienna, Austria
Telephone: +43 1 2600 22529 or 22530 • Fax: +43 1 26007 22529
Email: sales.publications@iaea.org • Web site: www.iaea.org/publications

24-04469E

International Atomic Energy Agency
Vienna
www.iaea.org